STRUCTURAL SYSTEMS

RESEARCH PROJECT

Report No.
SSRP-13/02

Structural Health Monitoring of Bridges with Seismic Response Modification Devices

by

Gianmario Benzoni

Noemi Bonessio

Giuseppe Lomiento

Final Report

May 2013

Department of Structural Engineering
University of California, San Diego
La Jolla, California 92093-0085

1. Report No.	2. Government Accession No.	3. Recipient's Catalog No.
4. Title and Subtitle Structural Health Monitoring of Bridges with Seismic Response Modification Devices		5. Report Date MAY 2013
		6. Performing Organization Code
7. Author(s) G. Benzoni- N. Bonessio - G. Lomiento		8. Performing Organization Report No.
9. Performing Organization Name and Address Division of Structural Engineering University of California, San Diego La Jolla, California 92093-0085		10. Work Unit No. (TRAIS) 11. Contract or Grant No. 59A0657
12. Sponsoring Agency Name and Address California Department of Transportation Division of Engineering Services 1801 30th St., West Building MS-9		13. Type of Report and Period Covered Final Report 14. Sponsoring Agency Code

15. Supplementary Notes

Prepared in cooperation with the State of California Department of Transportation.

16. Abstract Long-term performance of Seismic Response Modification Devices (SRMD) installed on bridges under service conditions could be modified by a number of factors such as environmental conditions, undesired structural performance, and even the aging of materials used in the components and assemblies. If monitored, devices with degraded performance can be early identified before they compromise the performance of the whole structure. This report addresses the use of Structural Health Monitoring (SHM) techniques to detect changes in the devices' performance through the periodical observation of bridges under normal operations. Two essential requirements of SHM systems applied to civil structures are (i) the economic convenience and functionality of the monitoring systems, and (ii) the reliability in detecting structural issues that can affect the health status of the whole structure. A review of the technical literature showed that many economic monitoring systems have been installed on bridge structures and tested for functionality in different environmental conditions, but that a SHM procedure developed and tested on bridges equipped with SRMDs was still needed. For this reason, a novel SHM algorithm, activated by accelerometric records from any simple sensor network and specifically developed to detect damage in SRMDs installed on bridges, is here proposed and discussed.

17. Key Words	18. Distribution Statement
Anti-seismic devices, Structural Health Monitoring, Seismic, Bridges, Seismic isolation	No restrictions

19. Security Classification (of this report)	20. Security Classification (of this page)	21. No. of Pages 197	22. Price

University of California, San Diego
Department of Structural Engineering
Structural Systems Research Project

Report No. SSRP-13/02

Structural Health Monitoring of Bridges with Seismic Response Modification Devices

by

Gianmario Benzoni
Research Scientist

Noemi Bonessio
Postdoctoral Researcher

Giuseppe Lomiento
Postdoctoral Researcher

Final Report submitted to Caltrans

Department of Structural Engineering
University of California, San Diego
La Jolla, California 92093-0085
May 2013

DISCLAIMER

This document is disseminated in the interest of information exchange. The content of this report reflect the views of the authors who are responsible for the facts and accuracy of the data presented herein. The content do not necessarily reflect the official views or policies of the State of California or the Federal Highway Administration. This publication does not constitute a standard, specification or regulation. This report does not constitute an endorsement by the Department of any product described herein.

For individuals with sensory disabilities, this document is available in braille, large print, audiocassette, or compact disk. To obtain a copy of this document in one of these alternate formats, please contact: the Division of Research and Innovation, MS-83, California Department of Transportation, P.O. Box 942873, Sacramento, CA 94273-0001.

Abstract

Long-term performance of Seismic Response Modification Devices (SRMD) installed on bridges under service conditions could be modified by a number of factors such as environmental conditions, undesired structural performance, and even the aging of materials used in the components and assemblies. If monitored, devices with degraded performance can be early identified before they compromise the performance of the whole structure. This report addresses the use of Structural Health Monitoring (SHM) techniques to detect changes in the devices' performance through the periodical observation of bridges under normal operations.

Two essential requirements of SHM systems applied to civil structures are (i) the economic convenience and functionality of the monitoring systems, and (ii) the reliability in detecting structural issues that can affect the health status of the whole structure. A review of the technical literature showed that many economic monitoring systems have been installed on bridge structures and tested for functionality in different environmental conditions, but that a SHM procedure developed and tested on bridges equipped with SRMDs was still needed. For this reason, a novel SHM algorithm, activated by accelerometric records from any simple sensor network and specifically developed to detect damage in SRMDs installed on bridges, is here proposed and discussed.

The proposed algorithm provides an assessment of the performance degradation of conventional structural components as well as installed isolators and energy dissipators, from changes in modal characteristic of the structural response. The damage detection follows a two steps procedure, in which the damage is previously localized through a "localization index" that is subsequently converted into a "severity index" for the quantification of the damage severity. The procedure has been first validated through data obtained from numerical models and showed an high level of accuracy in the damage localization and severity assessment also in complex scenarios, with damages in both structural components and SRMDs.

The application of the procedure to existing records from a real bridge structure (Vincent Thomas Bridge) confirmed the validity of the approach. Taking into account a specific request of simplicity of use bye Caltrans engineers, the SHM algorithm has been implemented into the executable program DIIB (Damage Identification in Isolated Bridges), tested with ambient and earthquake induced accelerations, the software appeared suitable to be used for extensive application over a range of different bridges structures.

Acknowledgments

The research described in this report was funded by the California Department of Transportation (Caltrans) under contract No 59A0657.

Many thanks are in order to Dr. Charles Sikorsky and Prof. Norris Stubbs for the valuable contribution to this research effort.

Table of contents

List of figures

List of tables

1. Introduction

The California Department of Transportation (CALTRANS) is responsible for the integrity and safety of over 24000 bridges owned by the State of California and California's local government agencies. The comprehensive program of seismic retrofit started in the mid 1980's was specifically addressed to enhance safety of existing bridges. This program has promoted the implementation of a number of structural rehabilitation measures, including installation of restraining cables on bridges with narrow seat widths, member-by-member replacement of specific assemblies, and jacketing of deficient columns.

For the California's long-span toll bridges the use of these techniques, while technically feasible, would have been cost-prohibitive and would have caused significant long-term traffic disruption. Cost effective innovative strategies were hence implemented through the use of Seismic Response Modification Devices (SRMD), such as isolators and/or energy dissipating devices. Friction isolators, lead-rubber bearings, and viscous dampers are among the devices used to enhance the performance of long-span toll bridges in case of seismic events. The program required the design and construction of a dedicated facility able to perform prototype and proof tests of full-scale devices (Benzoni and Seible, 1998). The Caltrans Seismic Response Modification Devices Testing Facility completed, in three years of operation, the full series of tests for devices to be used on bridges as: Benicia-Martinez, Richmond San Rafael, Coronado, San Francisco- Oakland Bay and many others in the United States and around the World (Benzoni and Seible, 2000), (Benzoni et al. 2003), (Benzoni and Innamorato 2003).

Well known stiffness, strength and dissipative characteristics of SRMDs are essential requirements to achieve structural control of a structure subject to ground shaking. Isolators' stiffness should be sufficiently low to decouple the superstructure from the damaging effects of ground accelerations, while the dissipation capacity of dampers should be sufficient to reduce the transmitted accelerations. In recent years, conformity of SRMDs characteristics to performance requirements is assured through specific testing

protocols required for pre-qualification (prototype) and acceptance (proof) before the use on bridges. For this reason recently installed SRMDs are highly reliable in terms of their conformity to design specifications.

However, the expected level of seismic protection of the bridge is assured only if the device performance will remain unchanged during the service-life of the bridge. Due to aging of materials, a change in the device performance is inevitably expected. For devices installed on bridges, this change can also be accelerated by the exposure to extreme environmental conditions and continuous vibration. For this reason, a long-term plan of maintenance of the bridge must address the possible variations of performance experienced by the devices. In this scenario, It is of paramount importance the monitoring of the devices performance in order to detect any early sign of degradation of the devices functionality when still in service.

When addressing strategies for monitoring the performance of in-service devices, the goal of avoiding the partial or complete interruption of the bridge usage, is critical. In this sense, the option of periodic removal of isolators/dissipators from the bridge, to be tested in a laboratory environment, appears constrained by the economical impact of the approach. Visual inspection and local non destructive tests are less invasive techniques, which however provide only indirect information about the performance of the devices. Furthermore, all these techniques present limitations when the degradation of the device must be expressed in terms of impact on the overall structural behavior. Structural Health Monitoring (SHM) is an alternative approach that ‘interrogates’ the structural response of the bridge in order to localize and quantify global response changes as generated by local degradation of conventional structural elements as well as anti-seismic devices. This approach appears as a valuable instrument for the management of bridges with SRMDs.

The process of implementing a damage detection strategy, referred to as SHM, involves the observation of a structure, over a period of time by using continuous or periodically spaced measurements, the extraction of features from these measurements and the analysis of these features to determine the current state of health of the system. It must be clarified that in what follows the world "damage" will be often used not to indicate a necessarily critical condition but to refer to changes of the "design" performance that should be addressed and further monitored. SHM can be effectively used to provide, at

every instant of the structure life, a diagnosis of the conditions of the constituent materials, of the different parts, and of the structure as a whole. The conditions of the structure must remain in the domain specified in the design, although aging, environmental conditions and accidental events can modify this condition. The use of the database provided with time by a SHM procedure can also provide information about the trend of degradation and the residual life of the structure, allowing to optimize maintenance\repair interventions.

These drastic changes in maintenance philosophy are described in several recent papers for civil infrastructures (Aktan et al., 2000; Frangopol and Liu, 2007; Okasha and Frangopol, 2012). The improvement of safety seems to be a strong motivation, in particular after some spectacular accidents due to unsatisfactory maintenance, as in the collapse of the Mianus River bridge (failure of two pin and hanger assemblies that held the deck in place on the outer side of the bridge (**Figure 1a**) and ill-controlled manufacturing process or for the Injak bridge collapse (**Figure 1b**). In both cases, the problem of aging structures was discovered and subsequent programs were established.

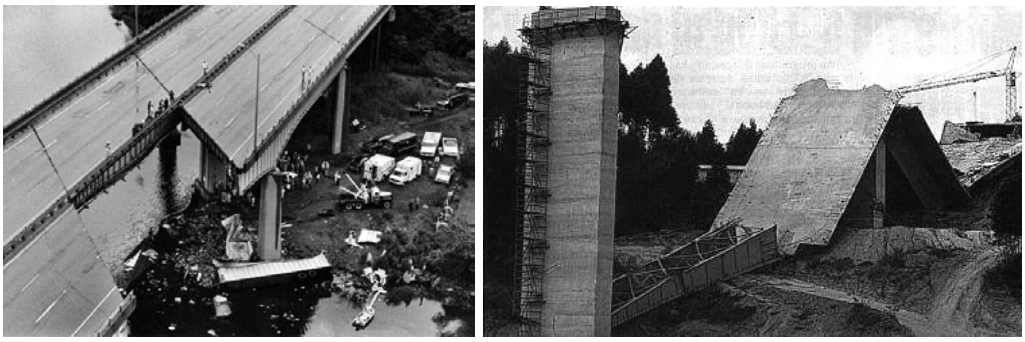

a) b)

Figure 1. a) Mianus River bridge failure, June 1983,; b) Injaka bridge collapse, July 1998.

Aktan et al. (2000) observed that SHM techniques are more likely to be beneficial when able to detect damages in critical members rather than in any generic member of the structure. The authors used the case of the Silver Bridge, which collapsed in 1967, as an example to explain this statement.

This bridge was an eyebar-chain suspension bridge built in 1928, connecting Point Pleasant, West Virginia and, Gallipolis, Ohio, over the Ohio River. The collapse of this bridge was one of the reasons for the current practice of biannual bridge inspections. The bridge failure was due to a defect in a single link, eyebar 330, on the north of the Ohio subsidiary chain, the first link below the top of the Ohio tower. A small crack was formed and grew through internal corrosion. The crack was only about 0.1 inch deep when it became critical with subsequent brittle failure. The growth of the crack was probably exacerbated by residual stress in the eyebar created during the manufacturing process. When the lower side of the eyebar failed (**Figure 2**), the entire load was transferred to the other side of the eyebar, which then failed by ductile overload. The joint was then held together only by three eyebars, and another slipped off the pin at the center of the bearing, so the chain was completely severed. Collapse of the entire structure was inevitable and it took only about a minute for the whole bridge to fall. The authors argue that if the Silver Bridge were in operation today and on the verge of collapse, none of the inspection, innovative experimental, or NDE technologies available would have a

definitive chance of diagnosing its structural condition and predicting its imminent collapse.

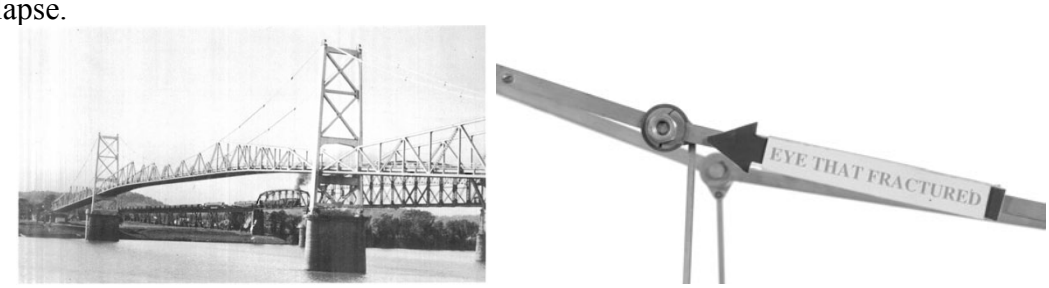

a) b)

Figure 2. a) Silver Bridge; b) Fractured eyebar preserved at the National Institute of Standards and Technology Museum.

Today, a number of bridges have inventory flags indicating fracture-critical members or details. By definition, failure of a fracture-critical member would lead to structural collapse. In this regard, two-girder bridges have been described as fracture critical. However, controlled-damage tests on the I-40 Bridge in New Mexico clearly demonstrated that two-girder bridges that have continuity and sufficient redistribution capacity through the redundancy of their rigidly connected girder-diaphragms-deck system may retain sufficient reserve capacity even after extensive damage to one of the girders (Farrar and Cone, 1995). Clearly, damage to certain structural configurations and details that are deemed fracture critical may not necessarily lead to collapse, whereas many other possibly fracture-critical details may not have been clearly identified.

This consideration affects the whole idea of assessment of the system health, which should not be limited to the purpose of identifying damage in a structure, but also its location, its severity, and its performance impact. This type of approach is defined as Level IV, based on the following classification of performance levels (Rytter, 1993):

Level I Methods that only identify if damage occurred;

Level II Methods that identify damage occurrence and determine the damage location;

Level III Methods that identify if damage has occurred determine damage location and estimate its severity;

Level IV Methods that add to the information provided by Level III also the impact of damage on the structure.

It is unquestionable that malfunctioning SRMDs have an important impact on the performance of a bridge in case of significant seismic events. Any deficiencies in their expected behavior can make the structure significant vulnerable to earthquake loads. It must be noted, in fact, that a significant non-linear capacity of the structure is attributed to the isolators and that their departure from "design" performance can considerably modify the response of the bridge. In this sense induced effects of uplifting, torsion, displacement larger than predicted are among others the likely consequences of isolators performing outside the design boundaries. This issue appears even more crucial if we consider that devices are generally designed with very low structural redundancy, because they operate on the flexibility and the dissipation capacity of the system rather than its strength.

For this reason, SRMDs appear particularly feasible for Level IV SHM assessment. Effects of deficiencies in the performance of these devices can be studied to determine the impact on the structure, in order to identify critical levels of performance degradation. With an SHM system capable of early detection of critical damages in isolators and dissipators, acceptable safety levels for the bridge can be restored through repair and/or replacement of malfunctioning devices.

This report is part of a comprehensive research project on SHM of devices in service on bridges structures. It focuses on a procedure specifically developed to detect response degradation in isolators and dissipators from accelerometric records. The identification of critical levels of damage for a Level IV SHM approach is instead based on forensic investigations of SRMDs removed from existing bridges and on parametric analyses and is the object of additional reports.

In this document, after a literature review about SHM techniques applied to bridges, a damage detection algorithm is proposed and validated first on several numerical models. The algorithm is then tested on real records from the Vincent Thomas Bridge in San Pedro, CA, for the identification of performance deficiencies in the dampers connecting the towers with the deck. The final chapter of the report illustrates the DIIB (Damage Identification for Isolated Bridges) software, an executable code that implements the

damage detection algorithm and can be used as a tool for the application of the SHM to other bridges equipped with SRMDs.

2. Literature review

Bridge monitoring programs have historically been implemented with the aim of understanding and eventually calibrating models of the load–structural response chain. One of the earliest documented systematic bridge monitoring system, by Carder (1937), was conducted on the Golden Gate bridge and the San Francisco-Oakland Bay Bridge in an elaborate program of measuring periods of the various components during their construction in order to learn about the dynamic behaviour and possible consequences of an earthquake. A University of Washington report (1954) describes the monitoring of the first Tacoma Narrows Bridge over its short life before it collapsed due to wind-induced instability, again focusing on vibration measurements, but with an obviously warranted concern for the health of the structure. The Tacoma Narrows experience has far reaching importance since almost all of the long-span suspension bridge monitoring exercises to date have been related to concerns about wind-induced response and possible instability.

In the last decade, permanent bridge monitoring programs have evolved into SHM systems, which have been implemented in major bridge projects in Japan, Hong Kong and, latterly, North America. According to Housner et al. (1997), SHM is a non-destructive in-situ structural sensing and evaluation method that uses a variety of sensors to monitor the structural response, to analyze the structural characteristics for the purpose of estimating the severity of damage/deterioration and to evaluate the consequences thereof on the structure in terms of response, capacity, and service-life. SHM may also include the use of many devices, techniques and systems that are traditionally designated as Non-Destructive Testing (NDT) and Non-Destructive Evaluation (NDE) tools. There is no formal delineation between each approach, but there is a difference between NDT/NDE and SHM. NDT/NDE normally refers to a one-time assessment of the condition of materials and the effect or extent of the deterioration in the structure using equipment external to the structure. The SHM approach instead normally refers to activities focused on a continuous/periodic assessment of the condition of the structure or its key components based on the response under various types of loads. Most importantly,

SHM also involves the interpretation of the recorded data in order to quantify the changes of the structural conditions and assess capacity and remaining service-life.

Structural Health Monitoring (SHM) has become increasingly important as an additional component of maintenance programs and is now being used in a variety of applications including marine, aeronautical and aerospace structures. Among civil structures, off-shore platforms, large dams and highways bridges have received the greatest attention and research effort in the SHM field. Historically, such structures have inspection, monitoring and maintenance programs whose complexity depend on many factors, such as importance, ownership, use, and risk associated to man-made and natural hazards. Active and passive SHM systems, based on acoustic emission, impact detection, strain and accelerations measurements, are currently applied across a range of applications. However, with respect to aerospace and mechanical applications, bridge monitoring presents significant challenges due to environmental and operating condition variability. The physical size of the structure also presents many practical challenges, as well as the difficult of access to possible damage locations for local evaluation (Doherty, 1987). Due to these limitations, NDT methods can detect damage on or near the surface of the structure. The need for quantitative global damage detection methods that can be applied to complex structures has led to the development and continued research on methods that examine changes in the vibration characteristics of the structure. In civil engineering structures, vibration-based damage algorithms have been used since the early 1980s. Modal properties and quantities derived from these properties, such as mode shape curvature and dynamic flexibility matrix indices, have been the primary features used to identify damage in bridge structures. Despite the body of research dedicated to vibration-based damage detection, success is limited to simulations, laboratory studies and well-controlled experiments, and its effectiveness still remains to be proven for operational civil structures. Brownjohn (2007) pointed out that developments of SHM for civil infrastructure may still not be expected to have an inherent capability for damage location and quantification and, while many research teams are progressing in this area, it is still not a reality to recover reliable component-level structural information in real time by system identification. Nevertheless, continuous vibration monitoring can be considered a valuable tool to complement other nondestructive methods in improving reliability and

extending lifetime of bridge structures. Recent applications of SHM are capable of carrying out a minimal level of capacity assessment in real time, but require that a follow-up investigation would be triggered by the SHM system and supported by the evidence it provides.

In the last decades, many SHM systems have been implemented in long-span bridges in Japan, Hong Kong and, latterly, North America. Long-span bridge monitoring systems also provide ideal opportunities to implement and study the SHM approaches. For example, the wind and SHM system (Wong 2003) implemented on the Lantau fixed crossing has stimulated SHM research in Hong Kong, not only concerning the performance of the bridges themselves, but also of SHM methodologies. Being important lifeline structures, modern long-span suspension bridges typically have elaborate inspection and maintenance programs that should visually detect significant damages and signs of deterioration, whereas an SHM system would require a high density of sensors to detect them. Only global changes such as foundation settlement, bearing failure or major defects, such as loss of main cable tension or rupture of deck element, are detectable by global SHM procedures with a minimum of optimally located sensors.

Probably more beneficial is the development of SHM approaches for conventional short-span bridges, documented by research supported through full-scale testing (Salane et al. 1981; Bakht and Jaeger 1990). For smaller bridges, the global response is more sensitive to defects, the visual inspections are less frequent and SHM systems can provide a robust contribution (Alampalli & Fu 1994). It is worth mentioning, for instance, the European research focused on short-span bridges, where the BRIMOS system (Geier & Wenzel 2002) has been used to track the dynamic characteristics of the structure. Studies in Australia have instead focused on the typical very short-span highway and railway bridges, in one case leading to a commercial product named ‘Bridge Health Monitor’ or HMX (Heywood et al . 2000), which is programmed to record selected waveforms of vehicle-induced response while logging statistics of strains due to such events.

As mentioned above, the majority of the SHM approaches are, to date, focused on modal and frequency identification. This is probably because of two main reasons. Firstly, the early literature focused on the modal domain. Secondly, natural frequencies and mode shapes are easily interpreted and so are initially more attractive than other features

extracted in time domains and developed through non-modal based methods, such as statistical patterns and neural networks. A review of modal and frequency based damage analyses and of non-modal based methods is presented in the following paragraphs.

2.1. Modal/frequency based damage analysis

The physically tangible relation between stiffness/mass changes and natural frequency/mode shapes changes suggested the use of modal methods for damage identification. Several authors (Banks et al., 1996; Farrar and Doebling, 1999) questioned the suitability of modal data for damage detection arguing that modal information is a reflection of the global system properties while damage is a local phenomenon. For example the lower natural frequencies, which are those normally measured, are often marginally influenced by local damage. The above position is supported by the work of Alampalli et al. (1997), who investigated the sensitivity of modal characteristics to damage in a laboratory scaled bridge structures, and concluded that a local damage event does not necessarily change mode shapes more significantly at the damage location, or vicinity, than at other locations. A conclusion of an extensive literature survey by Doebling et al. [1996] indicated that there is disagreement among researchers about the suitability of modal parameters for condition monitoring – one body of opinion suggests that they are sufficiently sensitive whereas the other disagrees. To date the opposing arguments have been demonstrated for specific test structures but have not been conclusively proven.

Early studies

Since 1979, numerous studies involving the development and application of damage detection techniques have been reported for bridge structures. Salane, et al. (1981) examined changes in dynamic properties (damping and resonant frequencies) of a 3-span highway bridge during a fatigue test as a possible approach to detect structural deterioration caused by fatigue cracks in the bridge girders. The authors found that changes in damping were inconsistent and could not be used to detect fatigue damage in bridges. Changes in vibration signatures (mechanical impedance plots, Fourier transform of velocity response normalized by the Fourier transform of force input) were also found

to be poor indicators of structural deterioration caused by fatigue. Changes in experimentally determined mode shapes were found to be more sensitive indicators of damage. For these tests sinusoidal excitation was applied with an electro-hydraulic actuator.

Kato and Shimada (1986) performed ambient vibration measurements on an existing prestressed concrete bridge during a test to failure (**Figure 3**). A reduction in natural frequencies could be detected as a statically applied load approached the ultimate load. Significant changes in resonant frequencies were associated with yielding of the prestressing tendons. However, damping values were not affected significantly. The ambient vibration method was used for the system identification.

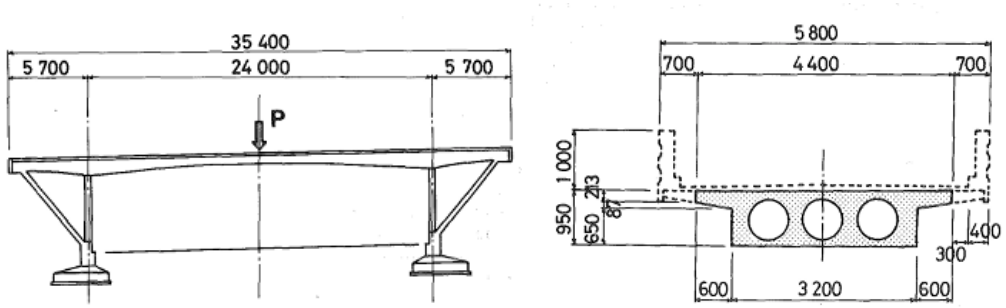

Figure 3. Prestressed concrete test bridge (Kato and Shimada, 1986).

Similar conclusions were carried out by Biswas, et al. (1990) and Jain (199l). The first authors performed modal testing on a 2-span continuous composite bridge in undamaged and damaged condition. The damage consisted of a large fatigue crack simulated by unfastening a set of bolts at a steel girder splice connection. The second one investigated the performance characteristics of a continuously deteriorating railway bridge using a locomotive run at constant speed for the excitation source. Changes in frequency response functions (FRFs, Fourier transform of a response measurement normalized by the Fourier transform of a reference measurement) were found to be detectable and quantifiable. Modal frequencies showed small but consistent drops caused by the presence of the simulated crack. Time histories and their corresponding Fourier spectra showed changes, but these changes were difficult to correlate with damage. Changes in mode shapes as quantified by the modal assurance criteria were found to be the best

indicator of the presence of damage, but not of its local extent or underlying cause. Through experiments on a defective prestressed concrete girder bridge, Tang and Leu (1991) observed that mode shape changes may be a more effective indicator for damage detection in bridges than frequency shifts. They stated that to be effective for damage detection a frequency shift in the order of 0.01 Hz must be detectable.

Mazurek and De Wolf (1990) conducted laboratory tests on the bridge model of **Figure 4** to examine the feasibility of detecting structural deterioration in highway bridges by vibrational signature analysis. Ambient vibration and low-mass vehicular excitation were used to obtain vibrational signature elements of two-span aluminum plate-girder bridge. Data was processed both by curve fitting and by use of a more automatable analytical approach. Two types of damages were investigated: support failures, and crack propagation. Support failure was observed to cause large changes to both resonant frequencies and mode shapes, with also the activation of additional modes. Crack propagation caused slight shifts in resonant frequencies but, as the crack increased, the rate of frequency change also increased. In terms of identification of vibrational characteristics, the authors observed that resonant frequencies and mode shapes were not influenced by vehicle velocity or roadway roughness. However, the intensity of a mode was dependent on velocity, roadway roughness, and vehicle mass. Vehicle mass influence on mode shapes appeared to be minimal. Mode shapes appeared to be heavily influenced by crack propagation, with the greatest changes in the vicinity of the defect. Collectively, the results of this research indicated that the concept of an automated vibration monitoring system was feasible.

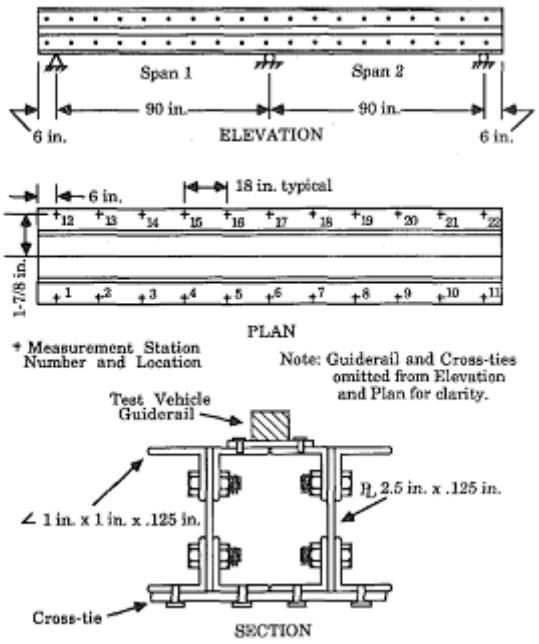

Figure 4. Model bridge girder details (Mazurek and De Wolf, 1990).

Spyrakos, et al. (1990) performed an experimental program on test beams which were designed to respond in a dynamically similar fashion to actual bridges. Each beam was given different damage scenarios (type, location, degree), on which low-level free vibration tests were performed. The authors noted a definite correlation between level of damage and dynamic characteristics of the structure. It was found that frequency change may be insufficient to be a useful indicator of structural safety (less than 5% change in frequency was associated with "critical" damage). However, the study suggested that the method of relating changes in resonant frequencies to damage level may be applicable to more severely damaged structures, and can give an indication of remaining serviceability. The authors stated that mode shapes may be used to locate damage if the input to the structure is measured.

Raghavendrachar and Aktan (1992) performed impact testing on a 3-span reinforced concrete bridge with the goal of detecting local or limited damage, as opposed to severe, global damage (**Figure 5**). The 105-feet long, 40-year old, decommissioned bridge was tested through serviceability and damageability limit states to failure by simulating progressively increasing stationary truck loading with the use of four hydraulic actuators,

reacting against rock anchors. Variations in flexibility of a redundant structure were used as reliable indexes of local damage. The authors concluded that the measured FRF exhibit changes in frequencies (nearly 10%) and damping due to a lack of reciprocity between impact and response locations as well as due to changes in ambient conditions. These nonlinearities are typical in field testing of bridges. Consequently, efforts to identify damage only through changes in frequencies and mode shapes by identifying only a few modes are questionable unless the damage is severe and global in nature. However, changes in flexibility as determined from mode shapes and resonant frequencies were found to be a sensitive indicator of damage, particularly when only a limited number of modes are available. On the same case study, Toksoy and Aktan (1994) observed that unless a bridge structure is completely and accurately characterized and complete baseline information is captured, the possibility to accomplish effective and reliable nondestructive evaluation or health monitoring is questionable.

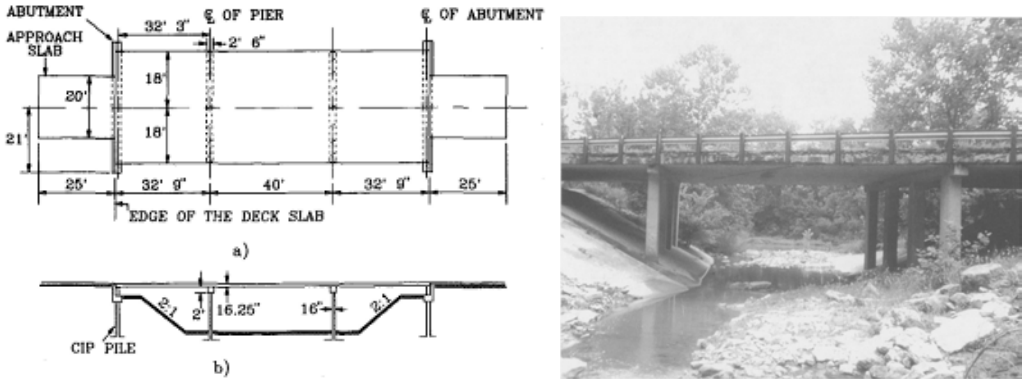

Figure 5. Thee-span reinforced concrete test bridge of Raghavendrachar and Aktan (1992).

The I-40 bridge

The first extensive experimental campaign on vibration damage detection techniques applied to a real bridge was initiated in 1993, on the eastbound side of the I-40 bridge over the Rio Grande. The elevation view and the cross section of the bridge are represented in **Figure 6** and **Figure 7**, respectively. Farrar et al. (1994) were able to introduce simulated fatigue cracks, similar to those observed in the field, into the structure in order to test various damage identification methods and to observe the

changes in load paths through the structure caused by the cracking. Cuts were made in the plate girder to simulate the formation of fatigue cracks that occur under actual field conditions. The cuts were made in four stages and forced vibration tests were repeated after each stage. Variation of resonant frequencies and mode shapes were used to assess the damage. Both the conventional modal analyses and the measurements made with the microwave interferometers showed no change in the global dynamic properties of the bridge until the final stage of damage was introduced. After the final stage of damage had been introduced, changes in the resonant frequencies and their associated mode shapes could be identified. However, the properties of modes that have a node point at the location of damage did not change even after the final stage of damage. These results emphasized the need for more work in the development of damage identification algorithms.

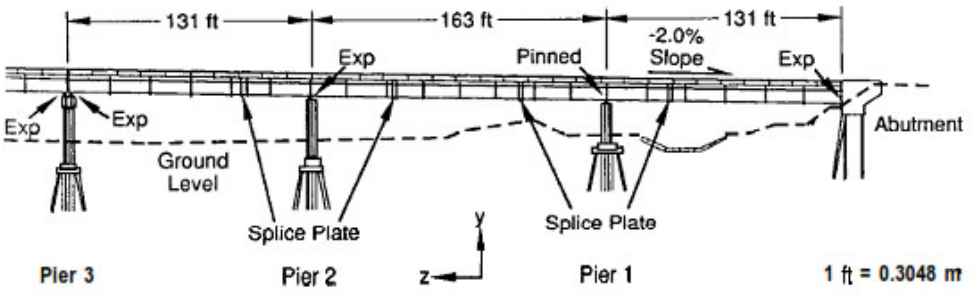

Figure 6. Elevation view of the portion of the eastbound I-40 bridge that was tested (Farrar et al., 1994)

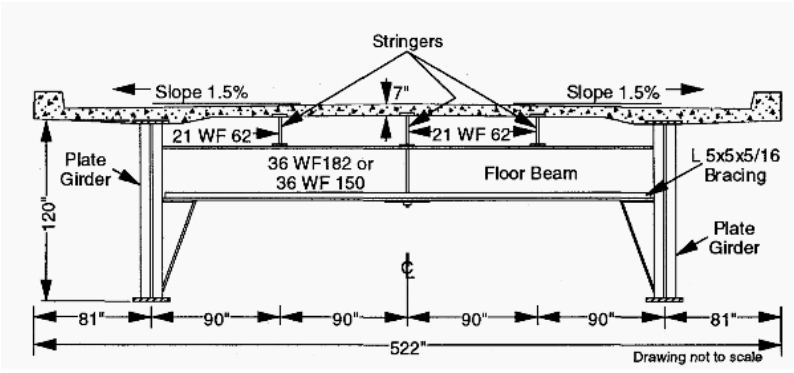

Figure 7. Typical cross section of the I-40 bridge.

In (Farrar and Jauregui, 1996) a direct comparison of five damage identification methods that were applied to the experimental and numerical modal data for the I-40 bridge was presented. The Damage Index Method (Kim and Stubbs, 1993), the Mode Shape Curvature Method (Pandey et al. 1991), the Change in Flexibility Method (Pandey and Biswas, 1994), the Change in Uniform Flexibility Shape Curvature Method (Zghang and Aktan, 1995), and the Change in Stiffness Method (Zimmerman and Kaouk, 1994) were compared. The experimental data were measured on the actual highway bridge. The numerical data were generated from finite element models of the same bridge that had been benchmarked against the measured response. With the numerical models many more damage scenarios could be investigated to further study the relative accuracy of the various damage identification methods. In general, all methods identified the damage location correctly for a cut completely through the bottom flange. However, for several of these methods an inconsistent identification of the location of a less severe damage was noticed. Results of this study show that the Damage Index Method performed the best when the entire set of analyses and experiments were considered. This performance is attributed to the normalization methods for the changes occurring in damage indicators. This method also specifies the criteria to quantify when changes in the monitored parameters are indicative of damage. Such criteria appear critical to be able to determine if damage has occurred at more than one location and to prevent false-positive readings. Farrar and Jauregui (1999a) underlined the sensitivity of modal results to environmental conditions and test procedures such as changes in temperature, traffic loading, wind and excitation methods.

In an extension of this study (Farrar an Jauregui, 1999b), the authors created a finite element model of a continuous three-span portion of the I-40 bridges, correlated with the experimental results. They introduced eight new damage scenarios into the numerical model including a multiple damage case. Results from two undamaged cases were used to study the possibility that the damage identification methods would produce false-positive readings. In all cases analytical modal parameters were extracted from time-history analyses using signal processing techniques similar to those used in the experimental investigation. With the exception of the damage index method, all the

considered methods gave false-positive indications of damage when applied to two undamaged data sets. Although not analytically verified, it was assumed that the false-positive readings could be eliminated with more averages of the data used to obtain the cross-power spectral density function and, in turn, the mode shape amplitudes. Fritzen and Bohle (1999) used a model updating method to identify the damage on the structure. The original Finite Element Model was formulated and updated by means of the FRF data of the undamaged and damaged structure. The adopted method was found able to detect the damage in several conditions, but for other damage scenarios the model inaccuracies led to unreliable or non-unique diagnosis, and in one case the structural change was too small to be identified.

Law et al. (1995a) proposed a model updating method to assess, from the structural modal frequencies and geometric dimensions (**Figure 8**), the structural condition and load-carrying capacity of a T-beam-slab bridge deck. Results indicated that the fundamental frequency of the structure is not sensitive to changes in boundary conditions, the width of the structure, and local damage to the bridge deck. The modulus of elasticity of concrete and the grade of reinforcement were identified as the two most important parameters in the process, and reliable information should be available if the method is to be feasible. In an extension of this work (Law et al. 1995b) a method to estimate the percentage of reinforcement in the main beams of a bridge deck from dynamic testing, was developed. From this particular study of 13 full-scale bridge decks, a maximum error in the estimate of the percentage of reinforcement in the bridge beams was -16.23%. The method can also be used to assess the structural condition of a bridge deck by determining its structural damage factor. The difference between the factor and its upper limit, is proposed as a measure of the cracked condition in the main beams of the deck. Values significantly below 0.5 will suggest that the bridge is in a poor or dangerous condition.

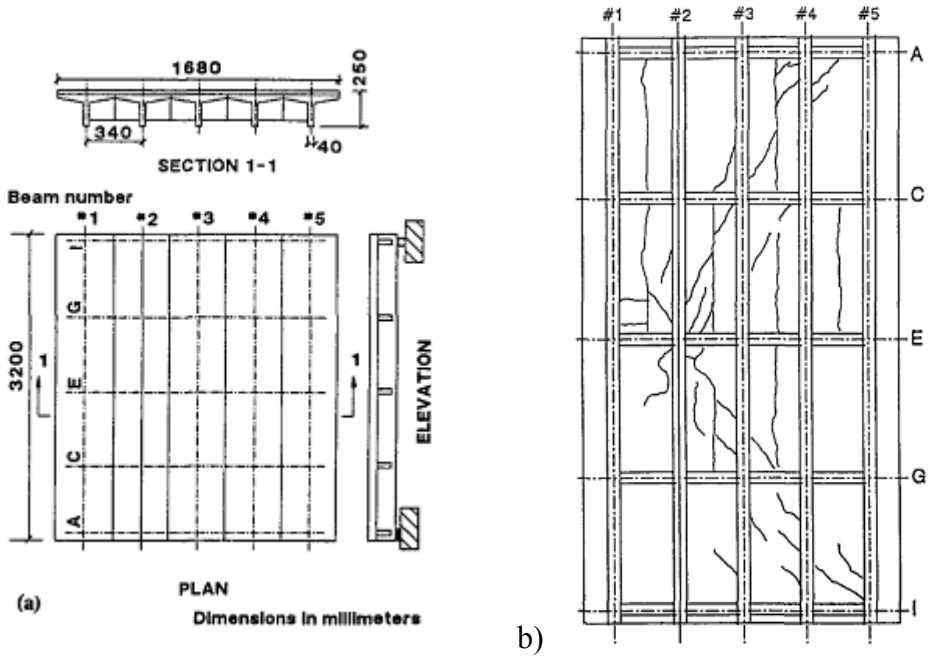

a) b)

Figure 8. Model bridge deck studied by Law et al. (1995): a) plan view, elevation and section; b) underside view of crack pattern of the deck.

Mazurek (1997) examined the sensitivity of selected modal parameters to damage at various locations in the multi-girder model of **Figure 9**. The results showed that the torsional and bending modes identifiable by ambient methods are effective for detecting mid-span and exterior girder damage. However, detectability appeared to become greatly diminished for interior girders at locations removed from mid-span.

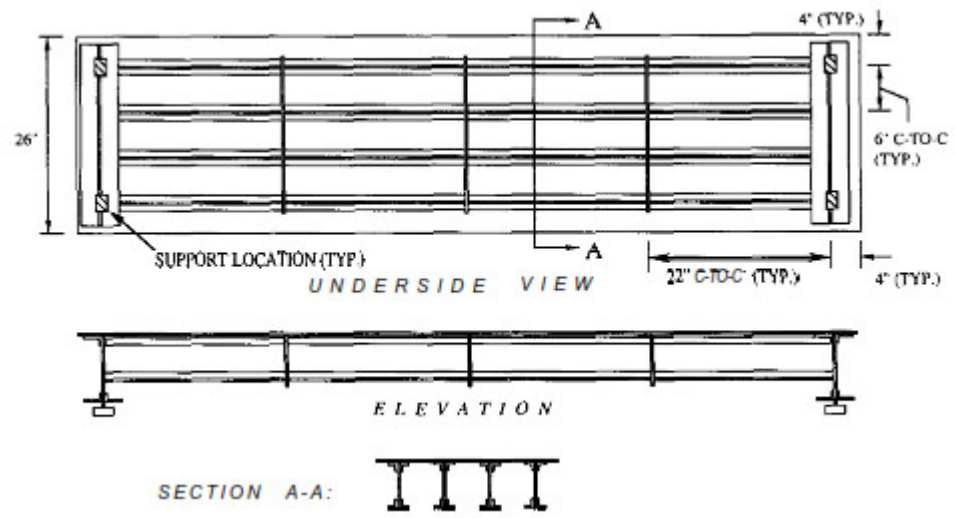

Figure 9. Laboratory model studied by Mazurek (1997).

Liang et al. (1997) measured the modal energy of a 1:6 downscaled model of a 1 span highway bridge, presented in **Figure 10**. For modal testing ambient excitations generated by pulling a model car across the bridge from time to time, were used. Two types of simulated damage conditions were introduced: the removal of one of the bearings of the bridge, and the cutting of the girder at the middle span. Results showed that the location of the damage can be determined by using the change of the modal energy transfer ratio.

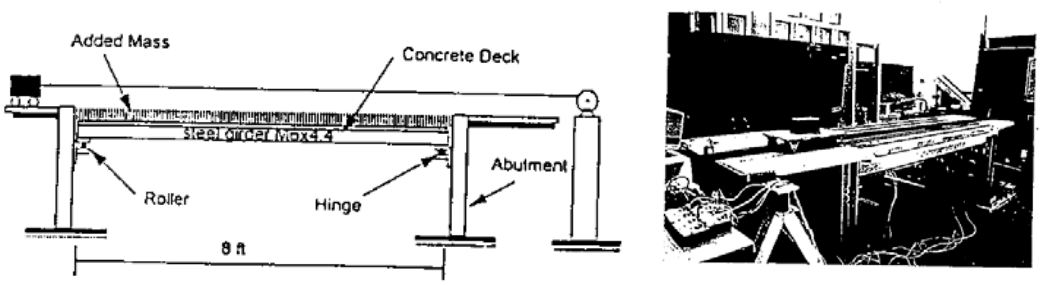

Figure 10. 1/6 scaled bridge studied by Liang et al. (1997).

The Z24 bridge

The bridge Z24, located between the villages Koppigen and Utzenstorf and crosses the highway A1 between Bern and Zurich in Switzerland has also been the object of extensive investigations (**Figure 11**) since 1998. The bridge was used as a full-scale

specimen and subjected to different damage scenarios. Wahab and De Roeck (1999) presented the results for the settlement of a pier. To allow for a settlement, the pier was cut, some part of the concrete was removed and replaced by steel plates and three hydraulic jacks. The settlement scenario was realized in different steps (20, 40, 80 and 95 mm). After each step, dynamic measurements were carried out using ambient vibration due to traffic. The Moment Curvature (MC) technique was applied to detect damage. Due to the irregularities in the measured mode shapes, a curve fitting had to be applied before calculating the MC using the central difference approximation. The results confirmed that the application of the MC method to detect damage in civil engineering structures seemed to be promising. Maeck and De Roeck (1999) presented, for the same structure, results for additional damage scenarios including tilting of foundations, spalling of concrete, landslide, formation of plastic hinges, failure of anchor heads, and rupture of tendons.

Brincker et al. (2001) performed a Level 1 damage detection of the Z24 bridge using frequency, damping and mode shape variations. All three approaches clearly indicated that damage had been introduced, however, the clearest indication was shown by frequency deviation. In practice, if no temperature compensation is used, the mode shape knowledge becomes more important since mode shapes are less sensitive to temperature changes than natural frequencies. If however temperatures are measured, and if a reliable data base is established allowing to filter out the influence of temperature shifts and other environmental changes on the natural frequencies, then it is believed that frequency deviation should be the main tool for health monitoring. The authors stated that the Frequency Domain Decomposition (FDD) technique will come to play an important role in the future as a tool for practical identification of structures. In particular the enhanced FDD and other related techniques that are based on robust identification algorithms, insensitive to user choices, should have high priority for practical use. Even though the Stochastic Subspace Identification (SSI) failed to perform because of practical problems with the large amount of data, this technique proved to be reliable for cases with a limited number of data and recorded channels.

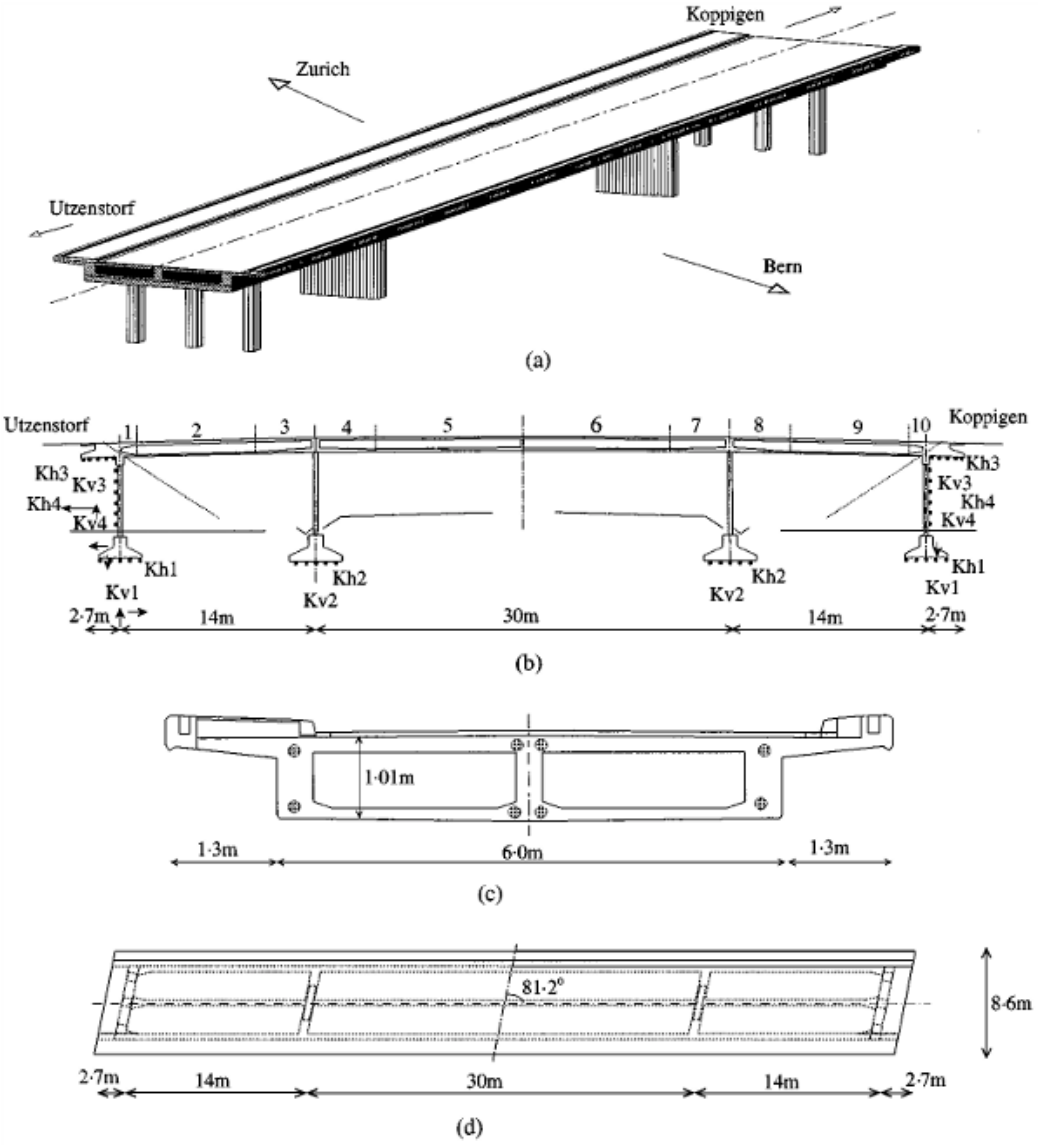

Figure 11. Sketch of bridge Z24. (a), Global view; (b), elevation; (c), cross-section; (d), plan.

Maeck et al. (2001) proposed a damage identification technique based on modal bending moments and curvatures used to assess the bending stiffness at each location. Damage identification results were compared with results from a classical sensitivity-based updating technique. The basic assumption in both techniques is that damage can be directly related to a decrease of stiffness in the structure. For the considered bridge higher

modes seemed to introduce numerical inaccuracies. In order to improve the method, curvatures were suggested to be determined experimentally.

Kullaa (2003) applied control charts for a damage detection procedure. An advantage of control charts is that they can be automated for on-line structural health monitoring. All control charts worked well for the damage detection but appeared sensitive to small shifts and prone to frequent false alarms in an automated monitoring system. Techniques to eliminate false alarms were highlighted as a topic for future research.

In Mevel et al. (2003), a damage detection method, based on the stochastic subspace identification approach, was proposed. The Damage localization is stated as a detection problem. Since the dimension of the physical parameter space is much higher than the modal parameter space, a model reduction problem had to be solved. The idea was to cluster deviations in the physical parameter space. The authors noticed that the overall rise in the test value was slightly hidden by its daily fluctuations originated by variations in environmental variables such as temperature, precise hour of measurements, speed of wind, etc. These changes were found to be potentially larger than the modal variations due to damage.

Most recent studies

Fu and De Wolf (2001) evaluated the behavior of a bridge with partially restrained bearings (**Figure 12**). The work was undertaken based on an early study suggesting that the bearings were not fully free to rotate in colder weather. The results of this study show how vibrational information has been used to verify small changes in structural behavior. A nonlinear dynamic finite-element analysis has been developed to explore the causes of these changes. The experimental results showed that the frequencies increase as the temperature decreases below approximately 60F and that there is little change for temperatures above this level. Nevertheless, the trend provided by the finite-element model explains the relation between temperature and the natural frequencies of the bridge.

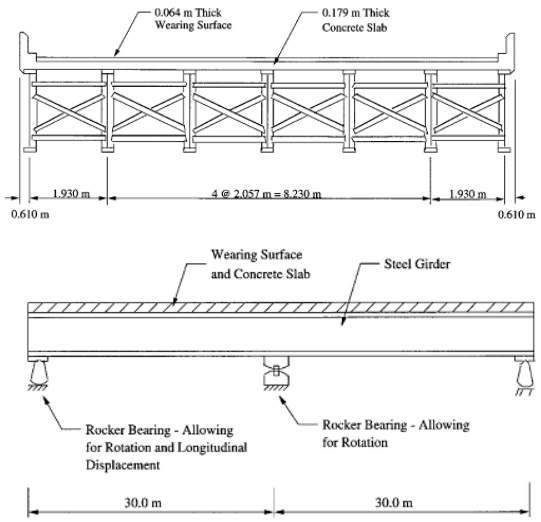

Figure 12. Bridge studied by Fu and Wolf (2001): a) cross section; b) longitudinal view.

Park et al. (2001) detected and localized damages in the superstructure of the concrete box girder bridge shown in **Figure 13**. Numerical and experimental modal parameters were used as input to the damage index method to localize the damage in the bridge superstructure. The results of visual inspections indicated a strong correlation between the predicted damage locations and the observed surface crack pattern. It was however observed that environmental conditions, such as the extreme differences in moisture conditions during the wet winter months and the dry summer months in the region, may significantly affect the accuracy of the damage locations and baseline systems identification.

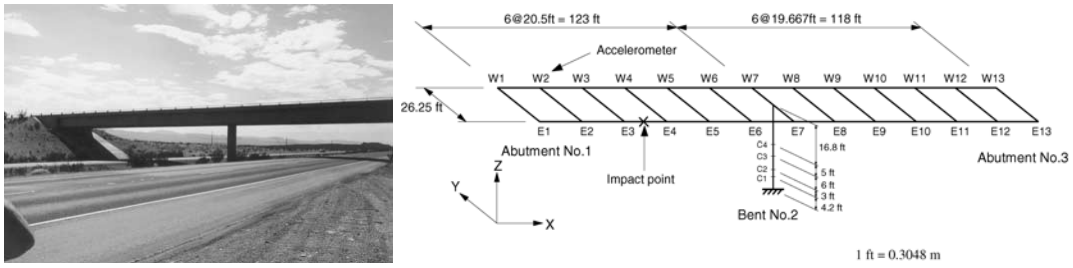

Figure 13. Concrete box girder bridge studied by Park et al. (2001): a) view; b) accelerometer locations.

In an extensive dissertation about monitoring of long span bridges, Fujino (2002) raised issues related to the procedures for the structural identification of bridges subjected to motion-dependent forces, such as wind-induced aerodynamic forces. The author pointed out that ambient sources, such as wind and ground motion, tend to have broadband frequency components that can be used to identify multiple vibration modes. However, monitoring through vibration measurement is known to introduce several difficulties. For instance, reliable measurement and identification of higher vibration modes are usually difficult due to noise and limited density of measurement points. Information about higher modes is considered critical to identify local defects with sufficient resolution.

A small highway bridge was studied by Patjawit and Kanok-Nukulchai in 2005. An index was proposed in this study for inferring the health deterioration of highway bridges, which was named as the Global Flexibility Index (GFI). This index is the spectral norm of the modal flexibility matrix obtained in association with selected reference points sensitive to the deformation of the bridge structure. The modal flexibility matrix can be evaluated from the dynamic responses at these reference points under forced vibration. Results shows that a sharp increase in the index calls for further detailed investigation for appropriate actions.

Li and Chan (2006) used modal parameters for the damage estimation of steel girder bridges using ambient vibration data. The effectiveness of the proposed method was demonstrated by means of a numerical example analysis on a simply supported bridge model with multiple girders, and by a field test on the northernmost span of the old Hannam Grand Bridge over the Han River in Seoul, Korea (**Figure 14**). In the field tests, the first three modes for all of the intact and damaged cases were interpolated into finer mode shapes using a cubic polynomial function to numerically calculate the mode shape curvatures. The damage locations were identified with good accuracy for all damage cases, while there were some false damage alarms at several locations.

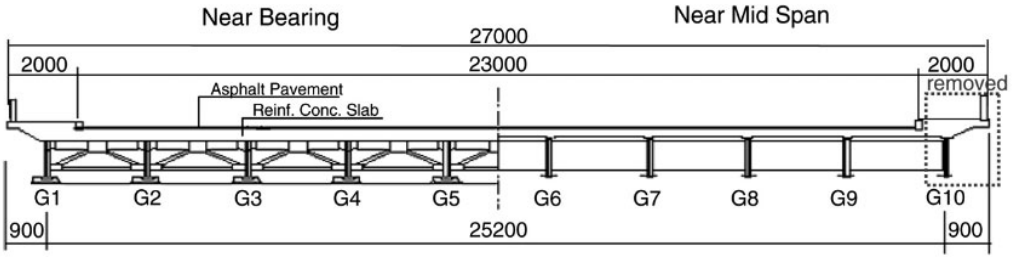

Figure 14. Section view of the Hannam Grand Bridge over the Han River in Seoul, Korea (Li and Chan, 2006)

In (Olund and De Wolf, 2007) a long-term monitoring program, started in 1999 by the University of Connecticut and Connecticut Department of Transportation, is presented. For this investigation, three bridges were considered: a steel-box girder bridge, a cast-in-place concrete box girder bridge, and a steel multi-girder bridge. The program focused on the use of a sparse array of sensors and ambient loading to accurately monitor the real-time health of the structure. Extensive data have been collected using accelerometers, tiltmeters, thermocouples, and strain gauges to observe trends and relationships among data sets. Benchmarks were created for each bridge in order to identify structural changes by use of the vast amount of data, relationships, and statistical trends stored in the database. The early results were published in (Cardini and De Wolf, 2009) for the steel box girder bridge, but were limited to strain data collected from normal truck traffic to determine live load stresses, load distribution factors, and the location of the neutral axis in each girder. The neutral axis shift has been identified as the quantity more sensitive to cracking phenomena occurring in the deck and has been suggested as a potential damage index for reinforced concrete bridges.

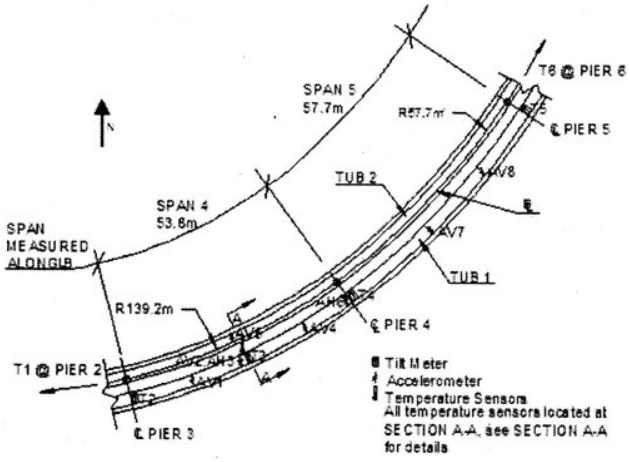

a)

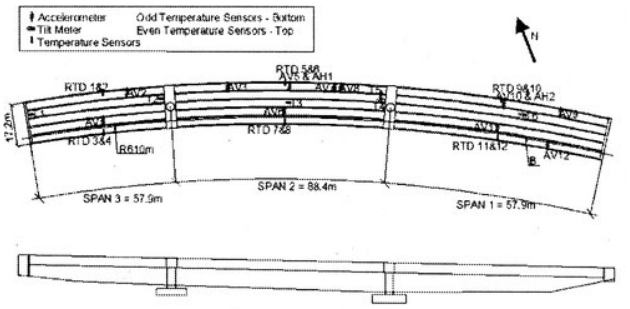

b)

Figure 15. Bridges monitored in the long term monitoring program of the University of Connecticut and Connecticut Department of Transportation (Olund and De Wolf, 2002) a) Sensor locations for steel box-girder bridge; b) plan and elevation views of curved, cast-in-place concrete box-girder bridge with approximate sensor layout.

2.2. Non-modal based methods

Among the non-modal based methods, neural networks and statistical pattern recognition can be mentioned.

Neural networks arose from the study of biological neurons and refer to a computational structure composed of processing units representing neurons. All neurons have multiple inputs and a single output. Neural processing applied to SHM is based on recording the vibrational signature of an undamaged structure and on continuously or periodically monitoring that signature to detect any changes. Respect to vibration based damage

detection, this method provides a self-organizing mapping from inputs to outputs without requiring detailed knowledge of any specific structural dynamics, if these inputs and outputs were known.

Farrar and Doebling (1999) suggested the developments of non-model based patterns to advance the state of the art in vibration based damage detection. For instance, the use of novelty detection is introduced based on the identification of any deviations for data measured under normal operating conditions. Features derived from measurements taken from a structure in its undamaged state will have a distribution with an associated mean and variance. If the structure is damaged, a change in the mean and/or the variance is expected.

Statistical process control provides a framework for monitoring the distribution of these features and identifying new data that is inconsistent with the past – 'outlier analysis'.

In (Spillman and Williams, 1993), tests on an instrumented scale model bridge were carried out in order to investigate the potential for neural processing applied to structural damage detection. The bridge element under investigation was a flexible steel beam 4.58 meters in length as shown in **Figure 16**.

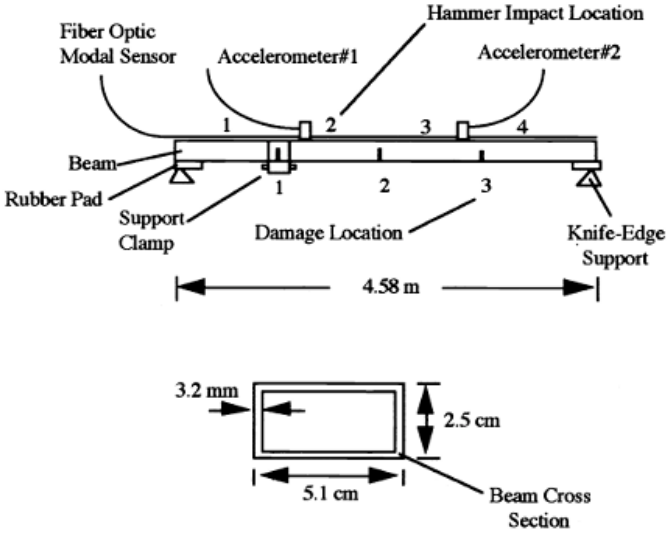

Figure 16. Model bridge girder details (Spillman and Williams, 1993).

The beam was modified so that various states of damage could be introduced by the removal or addition of gusset plates over damaged cross sections. The use of neural processing indicated that with additional training set data and addition sensors, successful damage detection on bridge elements can be performed.

Pandey and Barai (1995) carried out an extensive neural networks investigation on the problem of 21-bar bridge truss as shown in the **Figure 17**, with three distinct zones assumed as damaged. The purpose of the study was to identify the members in the damaged zone and the reduction in their stiffnesses from the response data. It was concluded that neural network are quite appropriate for the structural damage identification. Authors observed that the measured data at only a few locations in the structure is needed to train the network for the identification exercise. The authors compared traditional and time delayed neural network on the same bridge truss configuration (Barai and Pandey, 1997), with the traditional neural network showing less computational/training effort but also less precision with respect to the time delayed neural network.

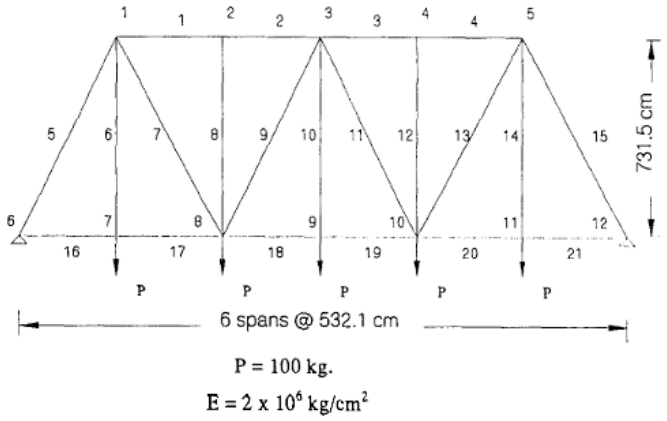

Figure 17. Bridge truss configuration (Pandey and Barai, 1995).

Loh and Yeh (2000) presented artificial neural networks for the identification of bridge structures under earthquake excitation. The procedure was applied to a continuous five-span prestressed box-girder bridge located at the NW coast of Taiwa (New-Lian River Bridge, see **Figure 18**) instrumented with a structural array of 30 strong motion accelerometers located on the deck, the abutments and at a near-by free-field location.

Results showed that the bridge exhibits different behavior due to different level of excitations and that the multi-input characteristic of the bridge makes the responses very complex.

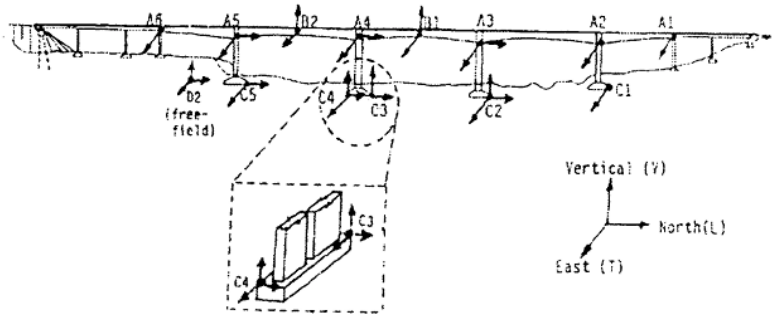

Figure 18. New-Lian Bridge River (Loh and Yeh, 1995).

Liu and Sun (2001) proposed an intelligent inspection system for bridges numerically validated for a simply supported three-span bridge. The longitudinal elongations were used as an indicator of the structural damage. Practical feasibility of the approach needs further validation.

Zhao and Chen (2002) presented a fuzzy rule-based inference system for bridge damage diagnosis and prediction which aims to provide bridge designers with valuable information about the impacts of design factors on bridge deterioration. The validity of these influence parameters is verified by an input variable identification method. Fuzzy logic is utilized to handle uncertainties and imprecision involved. A numerical example showed that the system has a high classification accuracy rate with a small number of rules. However, authors claimed that the reliability of the system should be further investigated with respect to the number of influence parameters, the size of the data points and the number of cluster centers, through techniques such as the sensitivity analysis.

A method for damage assessment for a bridge structure was presented by Lee et al. (2002), based on the use of traffic-induced ambient vibration data. An experimental study was carried out on a bridge model with a composite cross-section subjected to vehicle loadings (**Figure 19**). Vertical accelerations of the bridge deck were measured while

vehicles were running. The modal parameters are identified from the free-decay signals extracted using the random decrement method. The damage assessment is carried out based on the estimated modal parameters using the neural networks technique. As input to the neural networks, the ratios of the resonant frequencies observed before and after the damage occurrence were used together with the mode shapes. Frequency ratios were used due to the evidence that the resonant frequencies of the bridge, extracted from the vibration data, vary depending on the mass of the moving vehicles. Most of the inflicted damages were successfully detected for various vehicle load conditions. The degree of damage severity was however slightly overestimated.

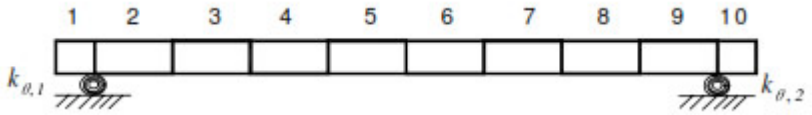

Figure 19. Bridge model studied by Lee et al. (2002).

Ko et al. (2002) developed a multi-stage scheme for damage detection for the cable-stayed Kap Shui Mun Bridge in Hong Kong (**Figure 20**) by using measured modal data from an on-line instrumentation system. A damage-identification simulation was based on a precise three-dimensional finite element model of the bridge. The multi-stage diagnosis strategy aims at successive detections of the occurrence, location and extent of the structural damage. In the first stage, a novelty detection technique based on auto-associative neural networks is proposed for damage alarming. This method needs only a series of measured natural frequencies of the structure in intact and damaged state, and is inherently tolerant of measurement error and uncertainties in ambient conditions. The goal of the second stage is to identify the deck segments or sections that contains damaged member(s). For this purpose normalized index vectors derived from modal curvature and modal flexibility are presented for damage localization. The third stage consists in identifying specific damaged member(s) and damage extent by using a multi-layer perceptron neural network. Only the structural members occurring in the identified segment are considered in the network input, and the combined modal parameters are used as the input vector for damage extent identification. Once the damage segment or section has been determined, the proposed method can identify the damaged member

within the segment by using only a few modal components measured at or near the damage region. Due to very low modal sensitivity of the bridge to damage of a specific deck member, the damage extent can be detected only when a structural member is severely damaged.

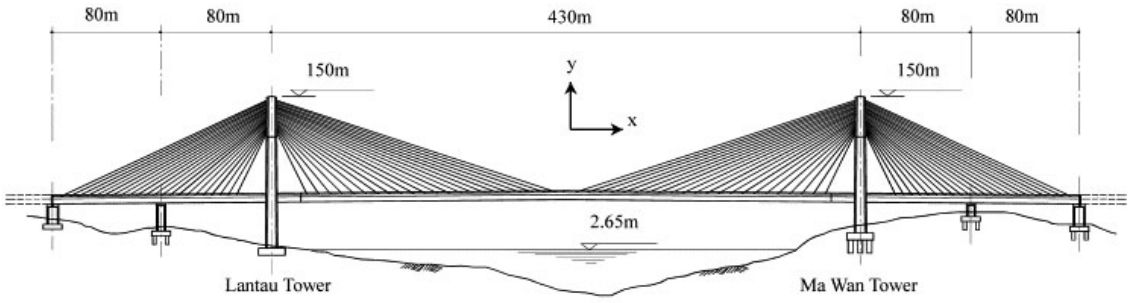

Figure 20. Elevation of Kap Shui Mun Bridge, studied by Ko et al. (2002).

In a recent study (Haritos and Owen, 2004), system identification and statistical pattern recognition approaches were summarized and applied to vibration data collected from three scale-model reinforced concrete bridges. The basic flat slab bridge configuration chosen for the test series consisted of five continuous spans corresponding to the prototype dimensions of 1.6m for the cantilever end spans, 3.65m for the first interior span, and 4.57m for the central span (**Figure 21a**). The cross section variations for the three models are illustrated in **Figure 21b**. Models#1 and #2 possessed three pier columns at each pier-line, while Model#3 possessed four such pier columns per pier-line. The model flat slab bridges simply rested on their truncated piers (column stubs) on top of a 360-mm deep steel beam running the full width of the deck at each pier-line. Results show that the system identification approach provides detailed information on the location and severity of damage. However, it requires more measurement points and the systematic updating of FEA models is not straightforward for civil engineering structures. The use of prior knowledge to inform the model updating process does improve its effectiveness. The pattern recognition approach instead provides less information about the location and severity of damage, but requires less input data and is less sensitive to signal noise.

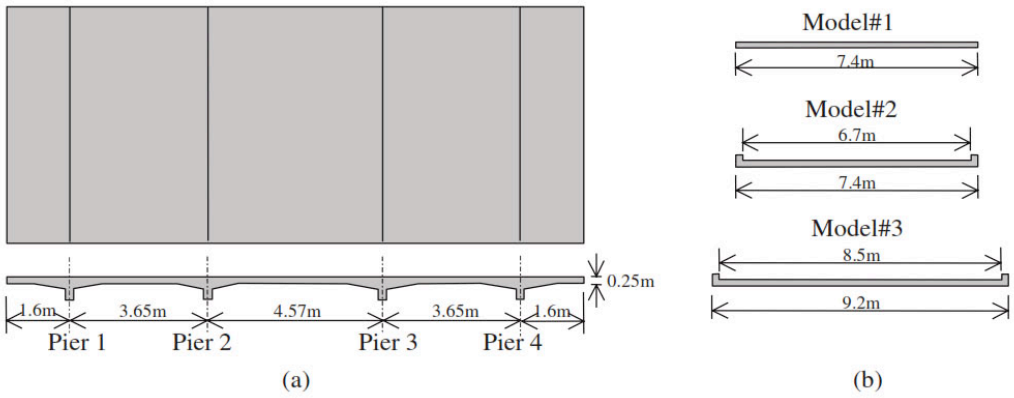

Figure 21. Schematic representation of model flat slab bridges (prototype dimensions): (a) plan and longitudinal; (b) transverse section (Haritos and Owen, 2004).

2.3. Discussion of literature results

The appropriate strategies for monitoring bridges equipped with anti-seismic devices require careful consideration. The fundamental idea for vibration-based damage identification is that the damage-induced changes in the physical properties of the installed devices will likely cause detectable changes in modal properties (natural frequencies, modal damping, and mode shapes) of the protected bridge. Therefore, intuitively damage can be identified by analyzing the changes in vibration features of the structure.

Although in vibration test, the excitation and response are always measured and recorded in the form of time history, it is usually difficult to examine the time and frequency domain data for damage identification. Due to the simpler physical interpretation, when compared with time and frequency domain approaches, the modal domain methods attract more attention and play a dominant role in the state-of-the-art of structural damage identification. During the last three decades, extensive research has been conducted in vibration-based damage identification, and significant progress has been achieved in this highlighted area. A broad range of techniques, algorithms and methods were developed to solve various problems encountered for the analysis of basic structural components (e.g., beams and plates) as well as complex structural systems (e.g., bridges and buildings). The main outcomes from the existing literature are here summarized.

Frequency. The physically tangible relation between stiffness and mass changes and natural frequency changes, coupled with ease of measurement of the natural frequencies (only a single sensor is required in many applications), supported the use of modal methods to identify damage. The greatest success in the use of natural frequency shifts for damage identification, as evidenced by a number of published examples, is limited to simple laboratory structures with only single damage locations. The identification of multiple damage scenarios using frequency shifts, even for simple laboratory experiments, is not as effective as evidenced by the scarcity of examples in this area. Based on the current literature database, the suitability of frequency shifts as single indicator of damage occurrence in full-scale structures appears as unconvincing.

Mode shapes/curvatures. Measurement of the mode shapes of a structure requires either a single excitation point and multiple sensors or a traveling exciter with one or more fixed sensors. Many modal analysis techniques are available for the extraction of mode shapes from the data measured in the time domain. Even though mode shape based methods are well verified with simulated data, significant difficulties when dealing with full-scale structures were encountered. Among them noise and measurement errors as well as mode shape expansion of incomplete measurements should be considered. The use of mode shapes curvatures in damage identification is based on the assumption that the changes in the curvatures of mode shapes are highly localized to the region of damage and that they are more pronounced than modal displacement variations. The use of modal curvature to locate damage in civil engineering structures appears promising.

Modal strain energy. When a particular vibration mode stores a large amount of strain energy in a particular structural load path, the frequency and shape of that mode are highly sensitive to changes in that load path. For this reason changes in modal strain energy might also be considered as a logical indicator of the damage location. In general the modal strain energy method provides a more accurate prediction of the damage location than the frequency/mode shapes based method.

Flexibility matrix. The flexibility matrix is defined as the inverse of the stiffness matrix and, therefore, relates the applied static force to the resulting structural displacement. Authors suggest that monitoring the changes in flexibility can provide information about the location of the damage only in the most severe damage scenario.

Model updating. Research on model updating has provided a rich source of algorithms adaptable to damage identification. Critical aspects of these approaches include, among others, the selection of the measured data to be matched by the model, the accuracy of the initial model, the size and complexity of the model, the number of updating parameters and the non-uniqueness of the resultant model that matches the measured data. The non-uniqueness of updated models is an important concern in damage identification. For the damage identification goal, the lack of knowledge of the damage location leads also to implementation difficulties and increased number of parameters involved. For this reason many authors introduced assumptions about the location and form of damage in order to limit the otherwise required measured data sets.

Non-modal based methods. Neural networks have been applied successfully in many applications including vibration based damage identification. In general, neural networks are particularly applicable to problems where a significant database of information is available and an explicit algorithm is of difficult definition. The algorithms supported by a large number of sensors, such as the residual force vector based methods, were generally successful. The emergence of statistical pattern recognition techniques seems promising when relying on a restricted number of sensors although the ambition of these techniques is still limited to Level 1 identification (damage existence only).

Case studies. In terms of applications, there are a number of real scale bridges that have been investigated, with the most common typologies being reinforced concrete and steel girder bridges. Specific applications of SHM techniques to seismic devices are still missing. The only work with some similarities to this subject has been performed by Liang et al. (1997) that studied simulated damages in the bearings of a 1:6 downscaled model of a highway bridge. Results of this study showed that the modal energy transfer ratio is a parameter able to detect localized damage in the bearings as well as in other portions of the bridge. These results suggest that modal energy based indices are promising for the damage detection in other localized devices of bridges, such as seismic isolators and dampers. The study of Fu and De Wolf (2001) is also oriented to the assessment of bearings' conditions. In this work, the behavior of a bridge with partially restrained bearings has been evaluated. The work was undertaken based on an early study suggesting that the bearings were not fully free to rotate in colder weather. The results of

this study show that vibrational information can be used to verify small changes in structural behavior and that a non linear model is needed to give a physical interpretation of changes in the bearings' behavior.

3. Damage detection algorithm

The assessment of the general structural conditions of bridges equipped with SRMDs represents an excellent example of needed integration between global and local approaches to structural health monitoring (SHM). The SRMDs devices, in fact, tend to concentrate a significant contribution to the non-linear performance of the structure and in this sense to be a possible candidate for degradation during the service life as well as during seismic events. The "local" detection of the device performance changes is, for this reason, of paramount importance. However, this information becomes relevant only if related to the "global" structural conditions. The variability of the device performance characteristics is, in fact, not immediately reflected in a critical change of the structural performance but should be identified through changes of the structural parameters.

In order to verify device performance characteristics, the option of removal from the bridge structure of sample devices is available. However, this solution involves a significant economical effort, particularly if associated to disruption of the regular traffic. It provides also a device response verification difficult to correlate to the structural performance. Health monitoring techniques offer a valuable alternative not requiring the removal of sample bearings from the bridge and maintaining the above-mentioned correlation between global and local responses.

The proposed procedure originates from an algorithm introduced by Stubbs (1985) and extended later by Kim et al. (1993) and Stubbs et al. (2000). The core of the algorithm considers the comparison between the modal energy of the structure in the undamaged and damaged state, as indicative of the degradation experienced on local portions of the overall structural assembly.

The original procedure required a significant level of modifications due to the difficulties introduced by the co-existence of conventional structural elements and anti-seismic devices (Seismic response Modification devices or SRMDs as referred in what follows). The proposed damage detection algorithm in fact uses changes in the modal strain energy to detect levels of degradation in both isolators/dissipators, as well as in structural parts

of the bridge. The presence of isolators requires an high level of accuracy in the localization and severity assessment procedure. Of particular importance appears also the need of a physical interpretation of the damage (degradation) indicator. A generic numerical indication of degradation cannot in fact direct the attention to the phenomena experienced at the device level and so suggest maintenance and retrofit interventions. Special attention was also dedicated, in this work, to the information needed to activate the procedure in order to extend its potential for implementation on existing structures. As a result, only a minimum number of accelerometric records are required for the proposed procedure. This requirement appears in line with the existence of basic sensor networks on most bridge structures.
The conceptual approach is briefly described in what follows.

3.1. Damage localization

A skeletal structure is sub-divided into an arbitrary number of elements N_E. The *i-th* modal stiffness K_i of the overall structure is given by:

$$K_i = \Phi_i^T C \Phi_i \qquad (3.1)$$

where Φ_i is the *i-th* modal vector and C is the stiffness matrix of the overall structure. The contribution of the *j-th* element to the *i-th* modal stiffness $K_{i,j}$ can be expressed as:

$$K_{i,j} = \Phi_i^T C_j \Phi_i \qquad (3.2)$$

where C_j is the contribution of the *j-th* element to the stiffness matrix of the structure and it can be obtained as:

$$C_j = E_j C_{j0} \qquad (3.3)$$

where the scalar E_j represents the material stiffness property and the matrix C_{j0} involves only geometric quantities (and possibly terms containing the Poisson's ratio). The sum of

the modal stiffness contributions $K_{i,j}$ of all the N_E elements provides the overall modal stiffness for the *i-th* mode:

$$K_i = \sum_{j=1}^{N_E} K_{i,j} \tag{4}$$

The fraction of the modal energy for the *i-th* mode that is concentrated in the *j-th* element (i.e., the sensitivity of the *j-th* element to the *i-th* mode) is:

$$F_{i,j} = \frac{K_{i,j}}{K_i} \tag{5}$$

Eq. 4 and Eq. 5 are the basis for the definition of the damage index proposed in the original formulation (Kim and Stubbs, 1993). An alternative approach is proposed here based on the comparison between the modal stiffness $K_{i,j}$ of the *j-th* element and the same quantity $K_{i,k}$ for the *k-th* element, through the sensitivity $F_{i,jk}$ defined as:

$$F_{i,jk} = \frac{K_{i,j}}{K_{i,k}} \tag{6}$$

where *i* represents the mode under consideration. The same term is expressed with asterisks in case of damaged elements:

$$F^*_{i,jk} = \frac{K^*_{i,j}}{K^*_{i,k}} \tag{7}$$

The concept of relating the modal stiffness of a generic element to the corresponding quantity of all other elements represents a major difference with respect to the original formulation of the techniques. The comparison between Eq. 5 and Eq. 6 shows, in fact, the different definition of the sensitivity terms. This modification appeared needed due to the existence of unbalanced contributions of stiffness provided by different structural components. It is in fact evident that the existence of anti-seismic devices, applied to the

structure, provides levels of stiffness of different order of magnitude than the conventional structural elements. This scenario requires a procedure with an higher level of sensitivity to the local conditions, better achieved with the proposed modification. In addition, the new procedure includes the possibility to investigate the degradation of installed anti-seismic devices while introducing a simpler formulation with respect to the original approach. Considering the ratio between the sensitivity terms in the damaged condition $F^{*}_{i,jk}$ to the equivalent term in the original state $F_{i,jk}$ we obtain:

$$\frac{F^{*}_{i,jk}}{F_{i,jk}} = \frac{K^{*}_{i,j}}{K^{*}_{i,k}} \cdot \frac{K_{i,k}}{K_{i,j}} \tag{8}$$

Substituting Eq. 2 and Eq. 3 into Eq. 8:

$$\frac{F^{*}_{i,jk}}{F_{i,jk}} = \frac{E^{*}_{j}E_{k}}{E_{j}E^{*}_{k}} \cdot \frac{\Phi^{*T}_{i} C_{j0} \Phi^{*}_{i}}{\Phi^{T}_{i} C_{j0} \Phi_{i}} \cdot \frac{\Phi^{T}_{i} C_{k0} \Phi_{i}}{\Phi^{*T}_{i} C_{k0} \Phi^{*}_{i}} \tag{9}$$

The relationship between mode shapes in the damage and undamaged state could be approximately expressed, for every generic *j-th* element, as:

$$\Phi^{*}_{i,j} E^{*}_{j} = \Phi_{i,j} E_{j} \tag{10}$$

where $\Phi_{i,j}$ is the *i-th* modal vector component of the *j-th* element. By use of Eq. 10, Eq. 9 may then be organized as:

$$\frac{F^{*}_{i,jk}}{F_{i,jk}} = \frac{E^{*}_{j}E_{k}}{E_{j}E^{*}_{k}} \cdot \frac{\left(E_{j}/E^{*}_{j}\right)^{2} \Phi^{T}_{i,j} c_{j0} \Phi_{i,j}}{\Phi^{T}_{i,j} c_{j0} \Phi_{i,j}} \cdot \frac{\Phi^{T}_{i,k} c_{k0} \Phi_{i,k}}{\left(E_{k}/E^{*}_{k}\right)^{2} \Phi^{T}_{i,k} c_{k0} \Phi_{i,k}} = \frac{E_{j}E^{*}_{k}}{E^{*}_{j}E_{k}} \tag{11}$$

where c_{j0} and c_{k0} are the components of the stiffness matrices, C_{j0} and C_{k0} for the *j-th* and *k-th* elements, respectively. As a consequence, the ratio between the sensitivity terms is expressed only as function of the E terms. From Eq. 9 and Eq. 11, the localization ratio $\beta_{i,jk}$ for the *j-th* element with respect to the *k-th* element is defined as:

$$\beta_{i,jk} = \left(\frac{E_j E_k^*}{E_j^* E_k} \right)^2 = \frac{\Phi_{i,j}^{*T} c_{j0} \Phi_{i,j}^*}{\Phi_{i,j}^T c_{j0} \Phi_{i,j}} \cdot \frac{\Phi_{i,k}^T c_{k0} \Phi_{i,k}}{\Phi_{i,k}^{*T} c_{k0} \Phi_{i,k}^*}$$ (12)

It can be noted that all quantities on the right-hand side can be obtained from modal parameters derived from experimental measurements $\left(\Phi_{i,j}, \Phi_{i,j}, \Phi_{i,k}^*, \Phi_{i,k}^*\right)$ and the geometry $\left(c_{j0}, c_{k0}\right)$ of the elements. Eq. 12 can further be simplified if the following conditions were satisfied:

1. the generic *j-th* element has constant geometrical characteristics along its length;
2. the generic *j-th* element has a predominant behavior (i.e. axial, shear, flexural behavior).

Three main mechanical behaviors were considered: i) the predominant axial behavior, ii) the predominant shear behavior, iii) the predominant flexural behavior (Eulero-Bernoulli beam). For each specific condition, the terms of Eq. 12 can be expressed as:

$$\Phi_{i,j}^T c_{j0} \Phi_{i,j} = \frac{A_j}{L_j} \int_{L_j} \varepsilon_a^2 \, dl$$ (13)

$$\Phi_{i,j}^T c_{j0} \Phi_{i,j} = \frac{A_j}{2(1+\nu) L_j} \int_{L_j} \gamma^2 \, dl$$ (14)

$$\Phi_{i,j}^T c_{j0} \Phi_{i,j} = \frac{I_j}{L_j} \int_{L_j} \Phi''^2 \, dl$$ (15)

where L_j, A_j, and I_j are the length, the cross section area and the second moment of area of the *j-th* element, respectively. The terms ε_a and γ are the axial and shear deformations and Φ'' is the curvature of the element under consideration. The Poisson ratio is expressed as ν. In general terms Eq. 13, Eq. 14 and Eq. 15 can be expressed as:

$$\Phi_{i,j}^T c_{j0} \Phi_{i,j} = c_{j0} \int_{L_j} \varepsilon^2 \, dl$$ (16)

where c_{j0} is a constant value associated with the geometry of the element and ε is the predominant strain term for the element. For each behavior, axial and shear deformation, as well as curvature, must be obtained from the appropriate modal shape components. Substituting Eq. 16 into Eq. 12 the following simplified expression can be used for computing the ratio $\beta_{i,jk}$:

$$\beta_{i,jk} = \frac{\int_{L_j} \varepsilon^{*2}\, dl}{\int_{L_j} \varepsilon^{2}\, dl} \cdot \frac{\int_{L_k} \varepsilon^{2}\, dl}{\int_{L_k} \varepsilon^{*2}\, dl} \qquad (17)$$

The localization term $\beta_{i,jk}$ relates the conditions of a generic *j-th* element to the status of every other *k-th* element of the structure. For an accurate assessment of the performance changes, the number N_E of elements must be selected in order to allow a descriptive representation of the mode shapes of the structure. It must be noted that only a portion of the structure under consideration can also be analyzed with the procedure, provided that a sufficient number of sensors are available for mode shape identification. In general, as demonstrated in what follows, a limited sensor network providing accelerometric records is required for an accurate monitoring activity with the proposed technique.
The numerical value of the ratio $\beta_{i,jk}$ can be greater than unity (for instance if the *j-th* element experienced a reduction of stiffness and the *k-th* element is undamaged) or lower than unity (for instance if the *j-th* element is undamaged and the *k-th* element suffered a reduction of stiffness). $\beta_{i,jk}$ is equal to 1 for undamaged elements. The ratio $\beta_{i,jk}$ can be computed for multiple vibration modes of the structure, in order to improve the efficiency of the damage identification process. If the structure is subdivided into N_E elements, for each vibration mode N_E x N_E indices $\beta_{i,jk}$ should be calculated. The complete N_E x N_E matrix, however, contains many redundant terms and would require a computationally demanding process to be assembled. The significant terms of the matrix can be maintained while reducing the matrix to a single vector of N_E terms, obtained by selecting an arbitrary element *k* as a 'reference'. The localization ratios $\beta_{i,jk}$ are then calculated for all the *j-th* elements with respect to the reference *k-th* element:

$$\beta_{i,1k} \quad \beta_{i,2k} \quad \dots \quad \beta_{i,N_E k} \tag{18}$$

The minimum value $\beta_{i,k_{\min}}$ of these terms is:

$$\beta_{i,k_{\min}} = \min(\beta_{i,1k},\dots,\beta_{i,jk},\dots,\beta_{i,N_E k}) \tag{19}$$

Considering a realistic damage scenario, characterized by a reduction of the material stiffness properties, the value $\beta_{i,k_{\min}}$, obtained from the Eq. 19, always corresponds to an undamaged element with $E_j/E_j^*=1$. From Eq. 12 the condition of $E_j/E_j^*=1$ results in:

$$\beta_{i,k_{\min}} = \left(\frac{E_k^*}{E_k}\right)^2 \tag{20}$$

and combined with Eq. 12 allows the definition of a normalized term, for the generic *j-th* term and *i-th* mode:

$$\beta_{i,j} = \frac{\beta_{i,jk}}{\beta_{i,k_{\min}}} = \left(\frac{E_j E_k^*}{E_j^* E_k}\right)^2 \left(\frac{E_k}{E_k^*}\right)^2 = \left(\frac{E_j}{E_j^*}\right)^2 \tag{21}$$

The procedure for computing the normalized ratio $\beta_{i,j}$ for the *i-th* mode, can thus be summarized through the following steps:

i. choose the arbitrary reference element along the member (i.e. the *k-th* element)
ii. compute the N_E ratios $\beta_{i,jk}$ as in Eq. 17
iii. determine the minimum value $\beta_{i,k_{\min}}$ as in Eq. 19
iv. compute the N_E normalized ratios $\beta_{i,j}$ as in Eq. 21
v. detect damage at the *j-th* element if $\beta_{i,j} > 1$.

It must be noted that $\beta_{i,j} > 1$ can produce a false positive due to the approximation introduced by Eq. 10. The assumption can in fact result in the numerical indication of damage existence in elements in undamaged state. This effect is particularly pronounced for modes that are slightly correlated to the actual damage. When instead the degradation is strongly contributed by a single mode, the damaged element presents a normalized

index significantly greater than one and better localized. This possible error associated with the limitations of Eq. 10 is however of systematic nature and can be mitigated by the use of a reliability index in the modal combination rule and by statistical criteria. For this reason, in order to combine the contribution of different modes, a modal mean error q_i was introduced, expressed as the average of the deviation of the normalized terms $\beta_{i,j}$ from the value 1:

$$q_i = \frac{\sum_{j=1}^{N_E} \left(\beta_{i,j} - 1\right)}{N_E} \tag{22}$$

A reliability parameter for each mode can then be defined as:

$$\gamma_i = \frac{\left(1/q_i\right)^a}{\sum_{i=1}^{n} \left(1/q_i\right)^a} \tag{23}$$

with:

$$\sum_{i=1}^{n} \gamma_i = 1 \tag{24}$$

where n is the number of vibration modes taken into account and a is an exponent based on engineering judgment. For values $a>>1$ the reliability criterion becomes extremely selective and only the mode with the lower value of q_i is considered reliable in the assessment of $\beta_{i,j}$. In general higher values of a are suggested in case of limited availability of sensors and thus questionable dependability of higher mode shapes. A value of a=6 proved to be effective for the case studies taken into consideration.

A multi-modal localization term for the *j-th* element was defined by combination of the modal components:

$$\beta_j = \sum_{i=1}^{n} \gamma_i \beta_{i,j} \tag{25}$$

and utilized for the definition of a damage localization index calculated as:

$$Z_j = \left| \frac{\beta_j - \overline{\beta}}{\sigma_\beta} \right| \tag{26}$$

where the parameters $\overline{\beta}$ and σ_β represent the mean and the standard deviation of β_j, respectively. The damaged condition, for the *j-th* element, is indicated by a value of $Z_j \geq 2$ if a probability of 98% is required.

3.2. Damage severity assessment

The proposed algorithm allows also the assessment of the level of severity of the damage expressed through the index α_j that represents the fractional change in stiffness of the *j-th* element:

$$\alpha_j = \left(\beta_j\right)^{-0.5} - 1 \qquad \alpha_j \geq -1 \tag{27}$$

The current value of the modified stiffness can then be obtained as:

$$E_j^* = E_j\left(1 + \alpha_j\right) \tag{28}$$

It must be noted that the predicted stiffness variation, measured by α_j, can be directly compared with the severity of the simulated damage only for the traditional structural elements. In this case, in fact, the definition of the severity index allows a direct interpretation of this parameter as variation in terms of stiffness. For the SRMD devices instead, in order to physically interpret the significance of the α_j values an additional level of information is required. To describe the nature of the needed information it must be preliminary clarified that two types of devices, commonly used for bridge

applications, were considered.

The first type belongs to the family of the Friction Pendulum Systems (Zayas et al., 1987).

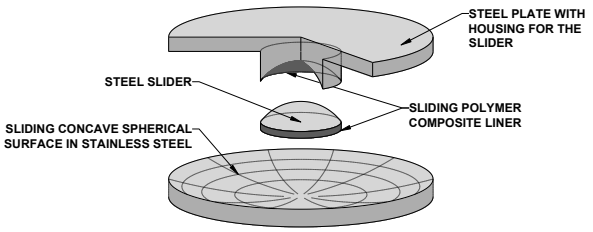

Figure 22. Schematic of Friction Pendulum device

The force equilibrium on the articulated slider of the device results in the following force-displacement relationship (Almazan et al., 1998):

$$F_b = U_b \frac{W}{R} + \mu W Z \qquad (29)$$

where F_b is the lateral force at the isolator level, U_b is the bearing displacement, W is the supported weight, R is the radius of curvature of the bearing, μ is the coefficient of friction mobilized during sliding and Z=sgn($\dot{U}_b$), with $\dot{U}_b$ the bearing sliding velocity.

The second type belongs to the family of the Viscous Dampers (Symans and Constantinou, 1998) were the overall force introduced by the device is expressed as:

$$F_d = c\left|\dot{U}_d\right|^N \operatorname{sgn}\left(\dot{U}_d\right) \qquad (30)$$

where F_d is the axial force of the damper, $\dot{U}_d$ is the relative velocity across the damper, c is the viscous coefficient and N is a real positive exponent with typical values in the range of 0.5 to 2.

Due to the non-linear behavior of the friction isolators and the velocity-dependent behavior of the dampers, modifications of their stiffness can also be detected when a change of the relative displacement across the isolator and/or of the relative velocity

across the dampers are experienced. This modifications cause values $\alpha_j \neq 0$ also in undamaged devices introducing false-positive damage detection. For instance, a damaged condition affecting one isolator can involve a reduction of the relative displacement for all the isolators. This reduction corresponds to an apparent stiffness increment and a consequent higher value of α in all the isolators including the undamaged ones.

For this reason the fractional change in relative displacements δ_j is needed as additional information:

$$\delta_j = \frac{\Delta\sigma_j}{\sigma_j} = \frac{\sigma_j^* - \sigma_j}{\sigma_j} \tag{31}$$

where σ_j and σ_j^* are the standard deviation of the relative displacement between the top and the bottom of the isolators, measured in the undamaged condition and in the damaged condition, respectively. Given the characteristic response of the friction devices, reported in Eq. (29), the fractional variation $\Delta\mu_j/\mu_j$ of the friction coefficient is obtained as:

$$\frac{\Delta\mu_j}{\mu_j} = (1+\delta_j)\left[\alpha_j\left(\frac{\sigma_j}{\mu_j R_j}+1\right)+1\right]-1 \tag{32}$$

where R_j is the radius of the sliding surface, and μ_j is the original friction coefficient of the devices assumed, for simplicity, as known. The current value of the friction coefficient of the *j-th* isolator can then be expressed as:

$$\mu_j^* = \mu_j\left(1+\frac{\Delta\mu_j}{\mu_j}\right) \tag{33}$$

In a similar manner, expressing the energy dissipated by viscous dampers with N=1 using Eq. 20, the fractional variation $\Delta\xi_j/\xi_j$ of their damping ratio is obtained as:

$$\frac{\Delta\xi_j}{\xi_j} = \alpha_j \frac{\dot{\sigma}_j}{\sigma_j}\frac{\sigma_j^*}{\dot{\sigma}_j^*} - 1 \tag{34}$$

being σ_j, σ_j^* and the $\dot{\sigma}_j$, $\dot{\sigma}_j^*$ standard deviation of the relative displacement and velocity, respectively, across the dampers measured in the undamaged and damaged condition.

4. Numerical algorithm validation

In order to evaluate the capability of the proposed algorithm to localize and estimate the severity of a local damage, four numerical models, with increasing level of complexity, were considered:

1. a two span continuous beam
2. a simplified isolated bridge model
3. a multispan bridge with friction isolator
4. a suspension bridge with viscous dampers

The application of the algorithm to numerical models benefits from several simplifications that make them significantly different from in-field case studies. The numerical models have, in fact, a linear to slightly non-linear behavior. Non-linearities are generally concentrated in specific portions of the structure. There are no environmental effects, which can produce variations of the vibration mode shapes and frequencies that can affect the effectiveness of the damage detection procedure. However, the quality of the data from numerical analysis allows investigating in details the characteristics of the proposed algorithm, and showing critical aspects for further applications.

4.1. Two-span continuous beam

The first test structure consists in a two span continuous beam, previously used for the validation of the original approach (Kim and Stubbs, 2002). As shown in **Figure 23**, the simple structure is divided in three components: (1) 50 beam elements modeling the two-span continuous beam; (2) two linear axial springs (Spring 1) modeling two outside supports; and (3) a linear axial spring (Spring 2) modeling a middle support. In this example we assumed that only the vertical component of motion was measured at each nodal point. Values for the material properties of the beam elements and springs were selected as: E=70 Gpa, Poisson's ratio ν=0.33 and the linear mass density r=2710 kg/m^3.

The beam has a cross-section area $A=1.05x10^{-3}$ m^2 and a second moment of area $I=7.23x10^{-7}$ m^4. Springs are modeled as axially stiff element with areas of $A=4.96x10^{-6}$ m^2 and $A=8.4x10^{-6}$ m^2 for Spring 1 and 2, respectively.

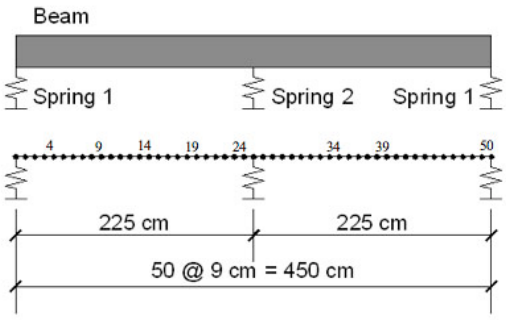

Figure 23. Schematic of two-span continuous beam.

Ten damage configurations were simulated and compared with the un-damaged case. The location and severity of each case are reported in **Table 1**, together with the first 3 natural frequencies of the system. The first eight damage cases represent a damage limited to a single location. Cases 6-8 focus on element 39, approximately at mid span of the right portion of the beam, in which three increasing levels of damage are simulated. The last two damage cases (Case 9 and 10) consider damage localized in two locations. In all cases, damage was simulated in the structure by reducing the elastic modulus of the appropriate elements.

The results of the damage detection algorithm in his original formulation are compared with the results of the proposed method in **Table 2**. It must be noted that Kim and Stubbs (2002) introduced three different methods of damage assessment (A, B and C) of increasing level of complexity and accuracy. The severity index from methods A and B, as well as for the proposed definition of Eq. 27 are computed from the structural mode shapes. Severity index for method C instead is function of mode shapes, geometry, modal masses and eigenvalues. The proposed procedure appears very accurate both in the localization of the damage as well as in the assessment of the damage severity significantly improving even the more elaborate technique of method C. In **Figure 24** to **Figure 33** the localization ratios $\beta_{i,j}$ and the multi-modal localization term β_j, are

graphically reported for each element of the damage case. The multi-modal localization term β_j is the combination of the modal localization ratios $\beta_{i,j}$ according to Eq. 25.

Table 1. Damage scenarios and natural frequencies of two-span continuous beam.

Damage case:	Simulated damage		Natural frequency (Hz)		
	Location	Severity[+]	Mode 1	Mode 2	Mode 3
Undamaged	-	-	32.381	46.377	118.77
1	4	-10	32.368	46.356	118.66
2	9	-10	32.328	46.309	118.69
3	14	-10	32.314	46.331	118.74
4	19	-10	32.346	46.376	118.58
5	24	-10	32.379	46.282	118.75
6	39	-1	32.361	46.358	118.77
7	39	-10	31.179	46.188	118.77
8	39	-50	31.371	45.432	118.77
9	9, 34	-10, -10	32.276	46.297	118.52
10	14, 39	-10, -10	32.247	46.266	118.74

[+]Severity (%) = (E*-E)/E x 100

Table 2. Damage prediction results of two-span continuous beam.

Damage case	Simulated damage		Predicted damage (Method A)		Predicted damage (Method B)		Predicted damage (Method C)		Predicted damage (Proposed method)	
	Location	Severity[+]	Location	Severity[+]	Location	Severity[+]	Location	Severity[+]	Location	Severity[+]
1	4	-10	1,4, 25,26	-12.8,-18.9, -8.6, -23.5	4	-3.8	4	-11.9	4	-10.0
2	9	-10	1,9,26	-11.6, -18.7, -20.9	9	-1.3	9	-10.7	9	-10.2
3	14	-10	14,26	-18.3, -31.4	14	-1.4	14	-9.4	14	-11.9
4	19	-10	19,26	-18.1, -16.8	19	-0.8	19	-9.5	19	-10.0
5	24	-10	24,25,26	-15.7, -18.7, -7.6	24	-0.5	24	-9.3	24	-10.1
6	39	-1	25,26, 49	-11.1, -7.3, -5.2	39	-0.1	39	-1.0	39	-1.0
7	39	-10	25,39	-29.0, -18.5	39	-1.5	39	-9.6	39	-10.0
8	39	-50	25,39	-6.72, -72.7	39	-14.8	39	-46.4	39	-50.2
9	9,34	-10, -10	9,34,50	-18.3, -17.5, -7.7	9, 34	-1.3, -1.1	9,34	-11.1,-8.0	9,34	-12.6,-10.3
10	14,39	-10, -10	14,26,39	-17.4, -11.3, -17.7	14, 39	-1.4, -1.4	14,39	-10.3,-10.9	14,39	-10.7,-10.0

[+]Severity (%) = (E*-E)/E x 100

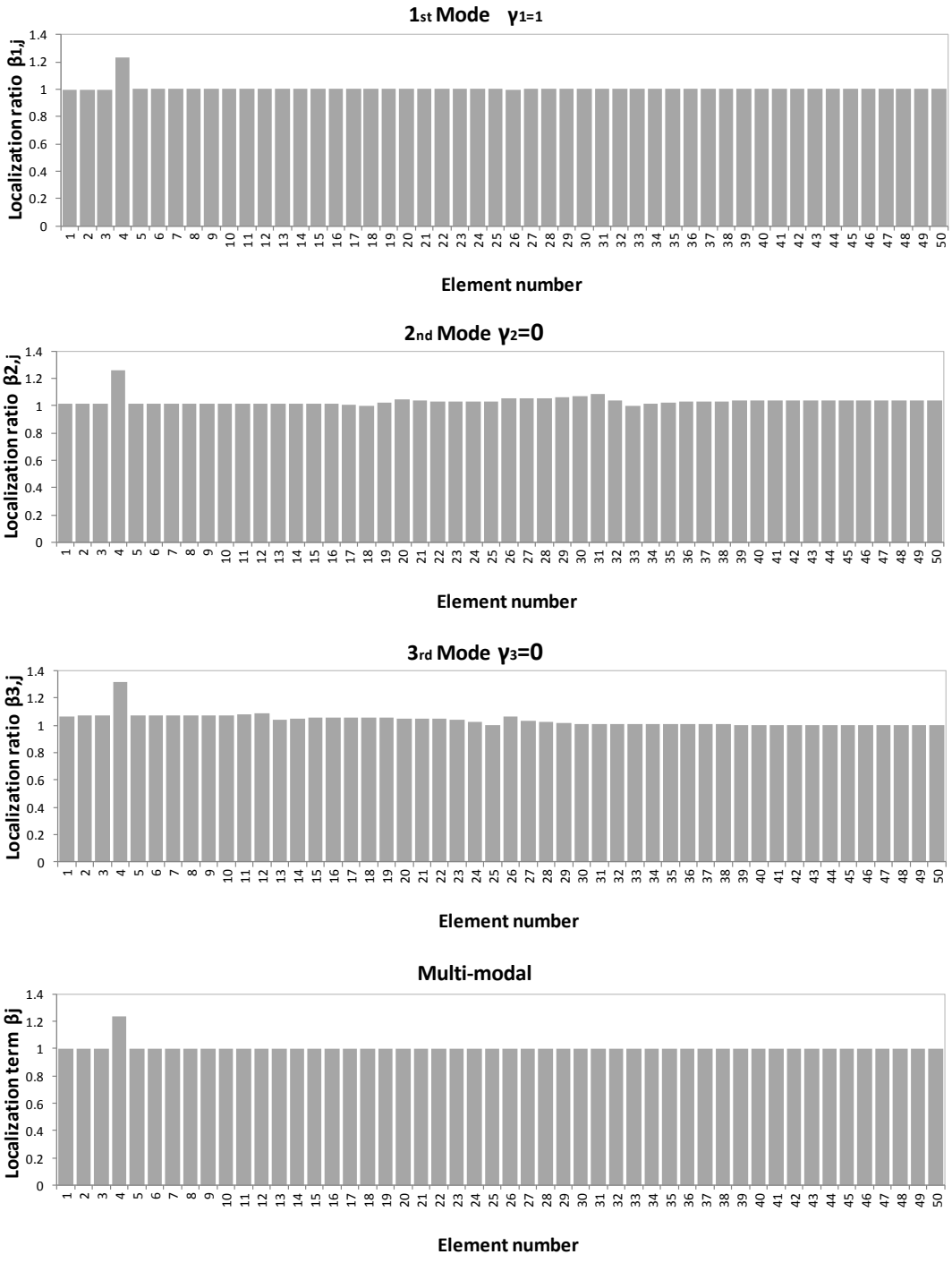

Figure 24. Localization ratios and multi-modal localization term for case no.1.

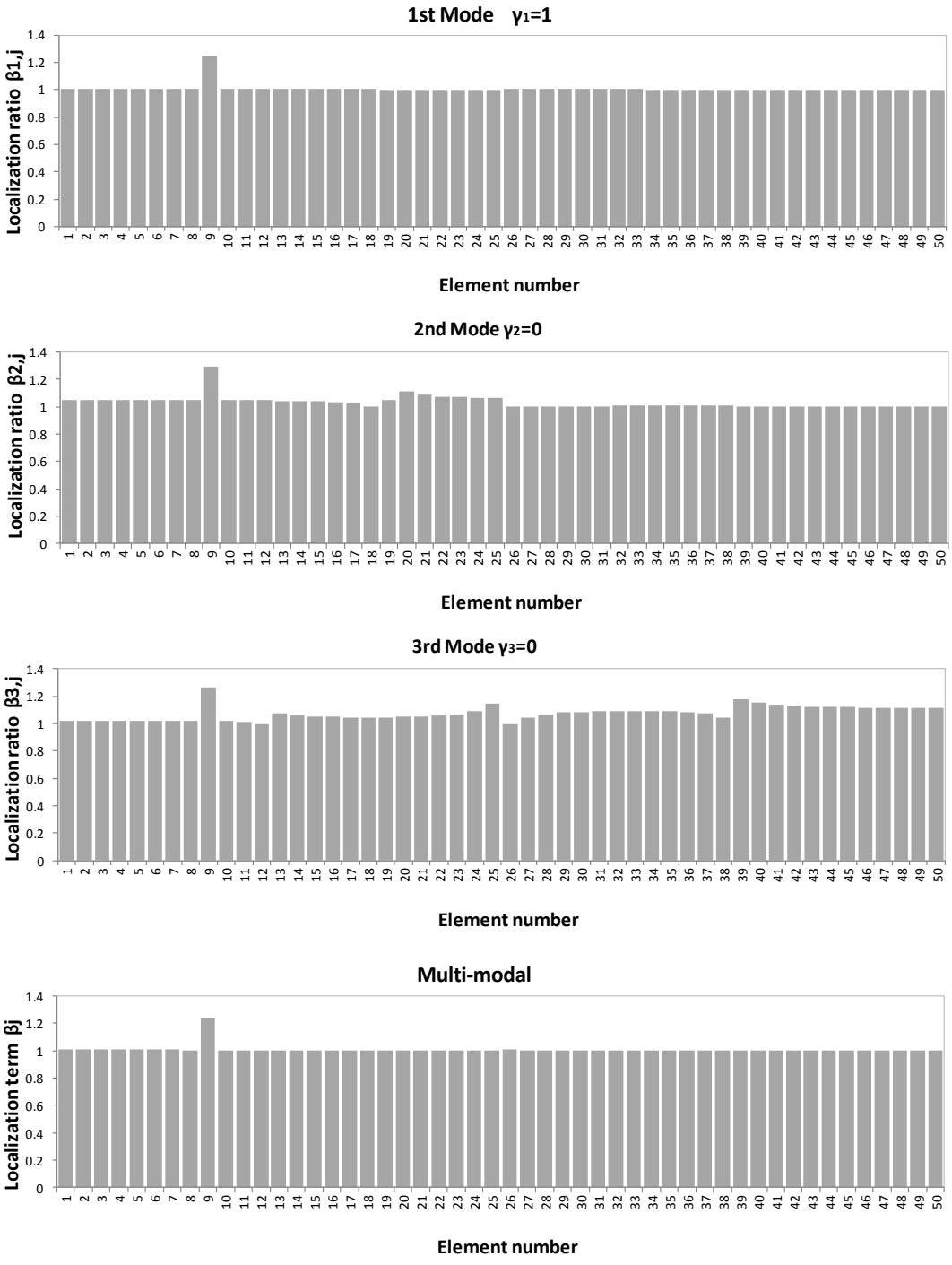

Figure 25. Localization ratios and multi-modal localization term for case no.2.

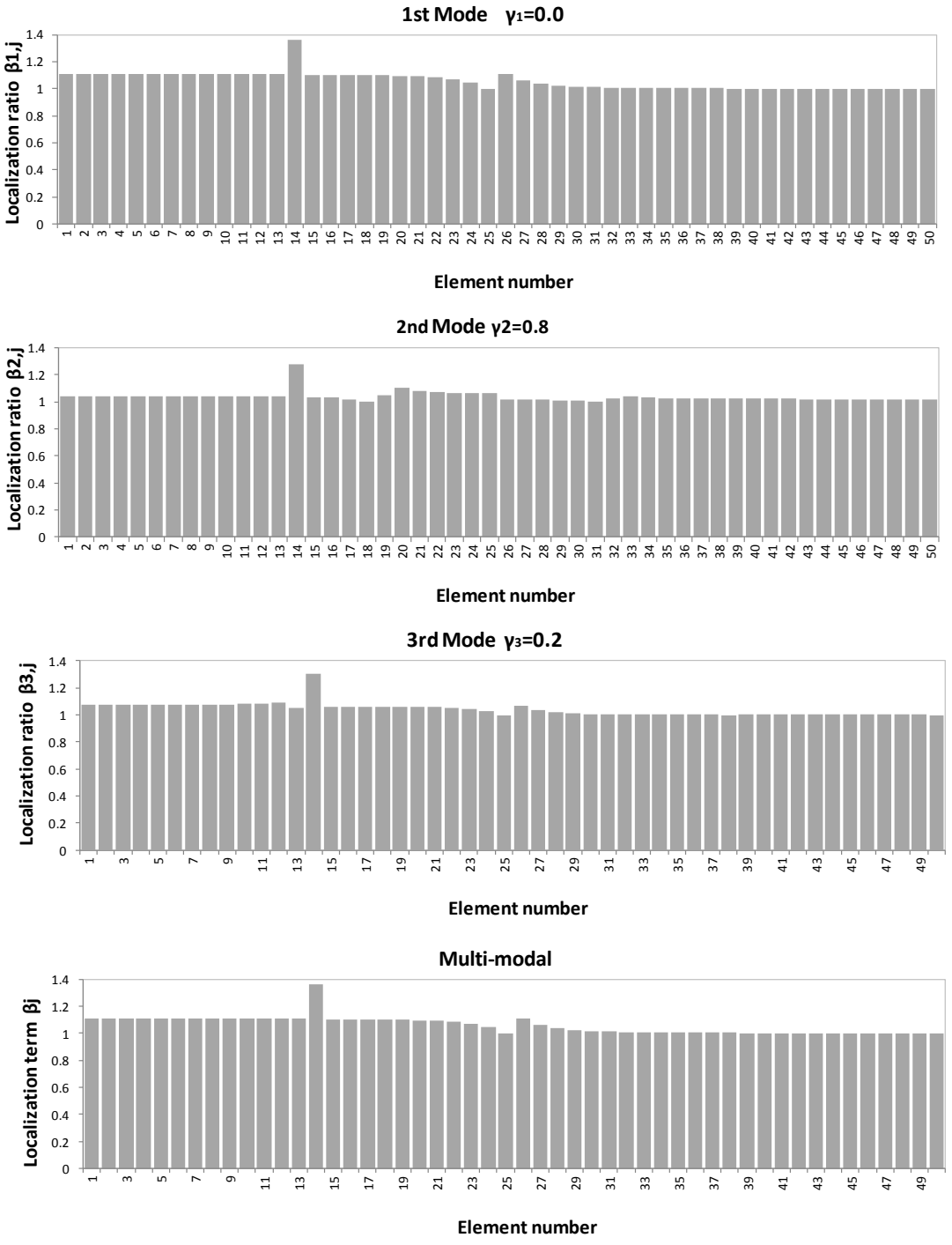

Figure 26. Localization ratios and multi-modal localization term for case no.3.

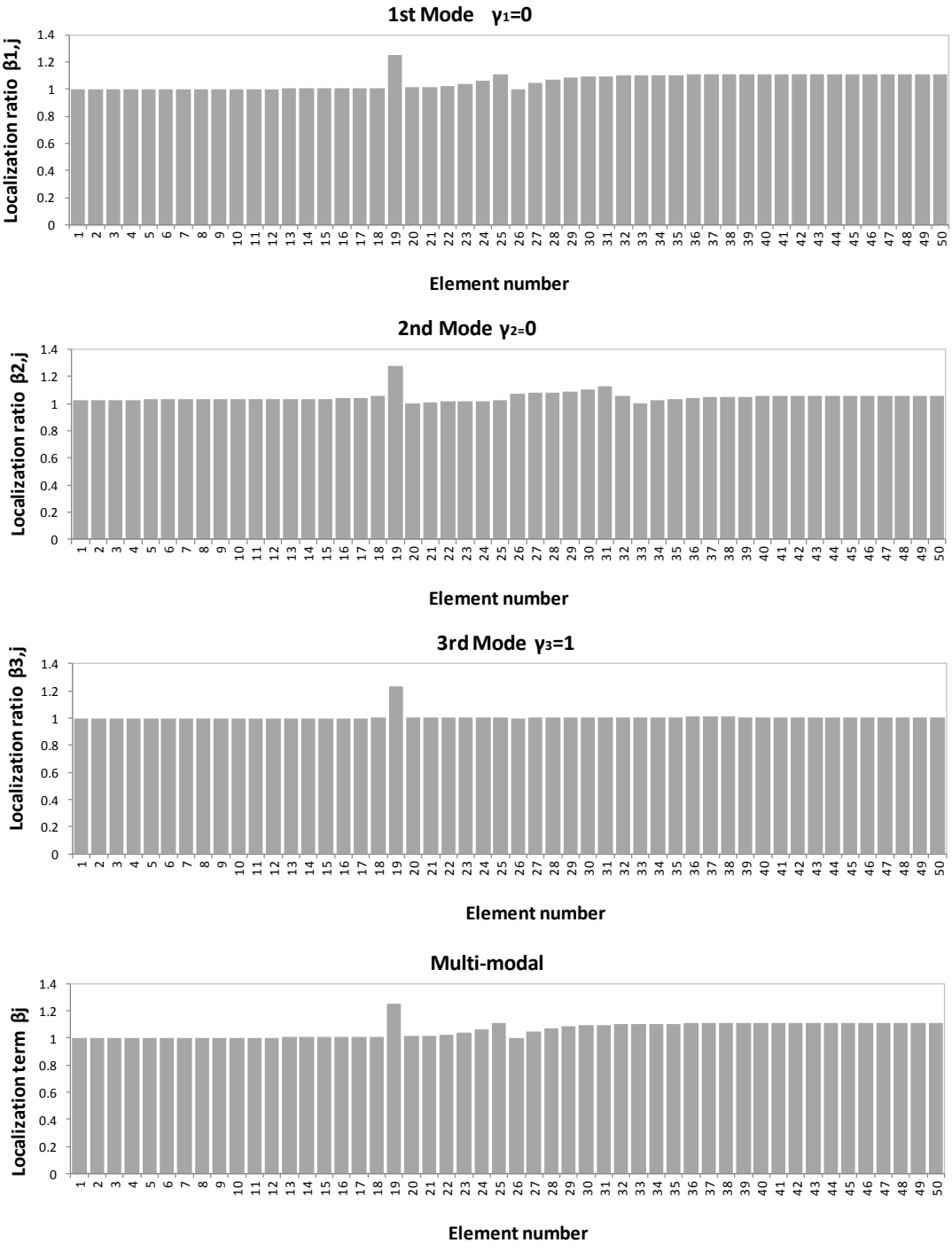

Figure 27. Localization ratios and multi-modal localization term for case no.4.

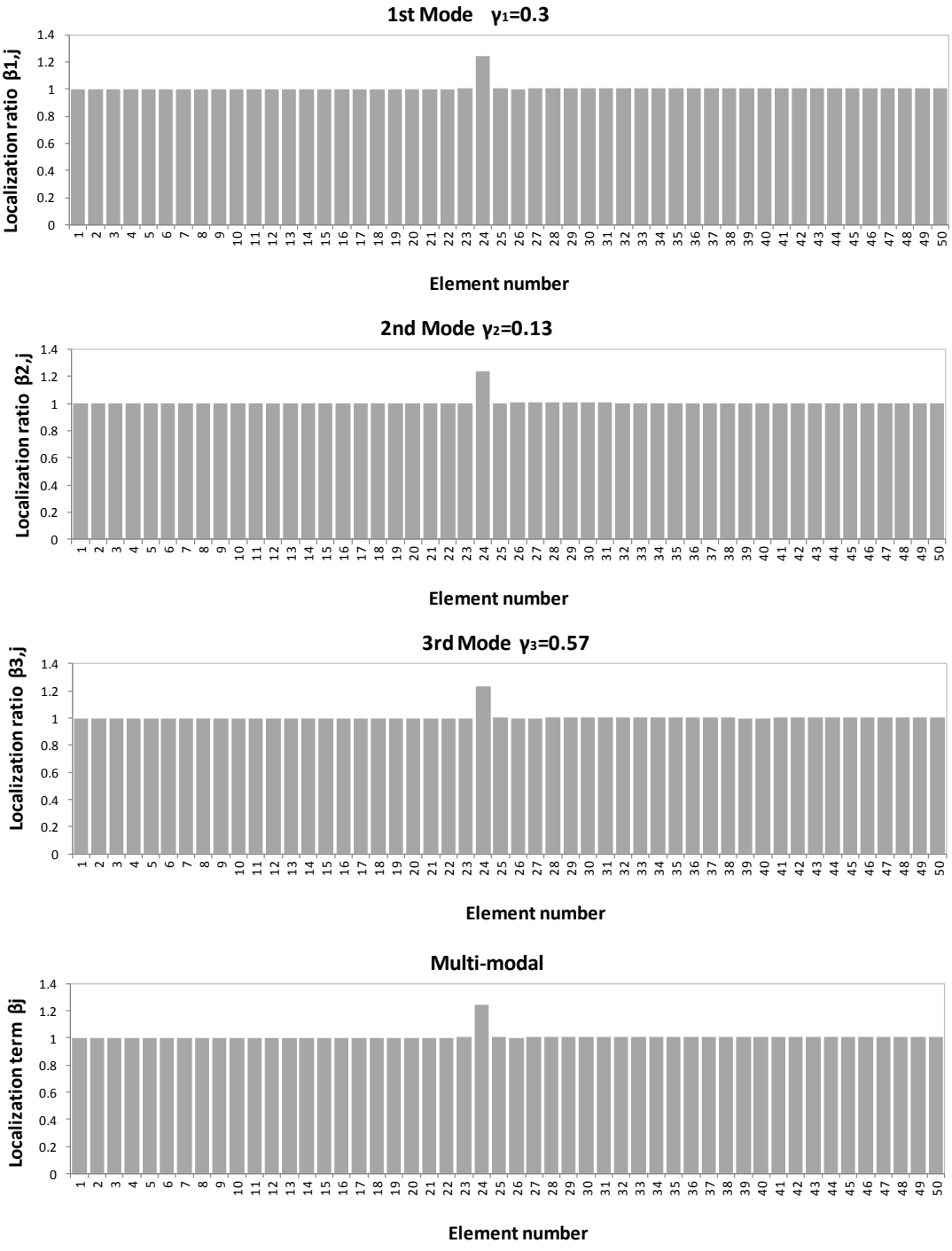

Figure 28. Localization ratios and multi-modal localization term for case no.5.

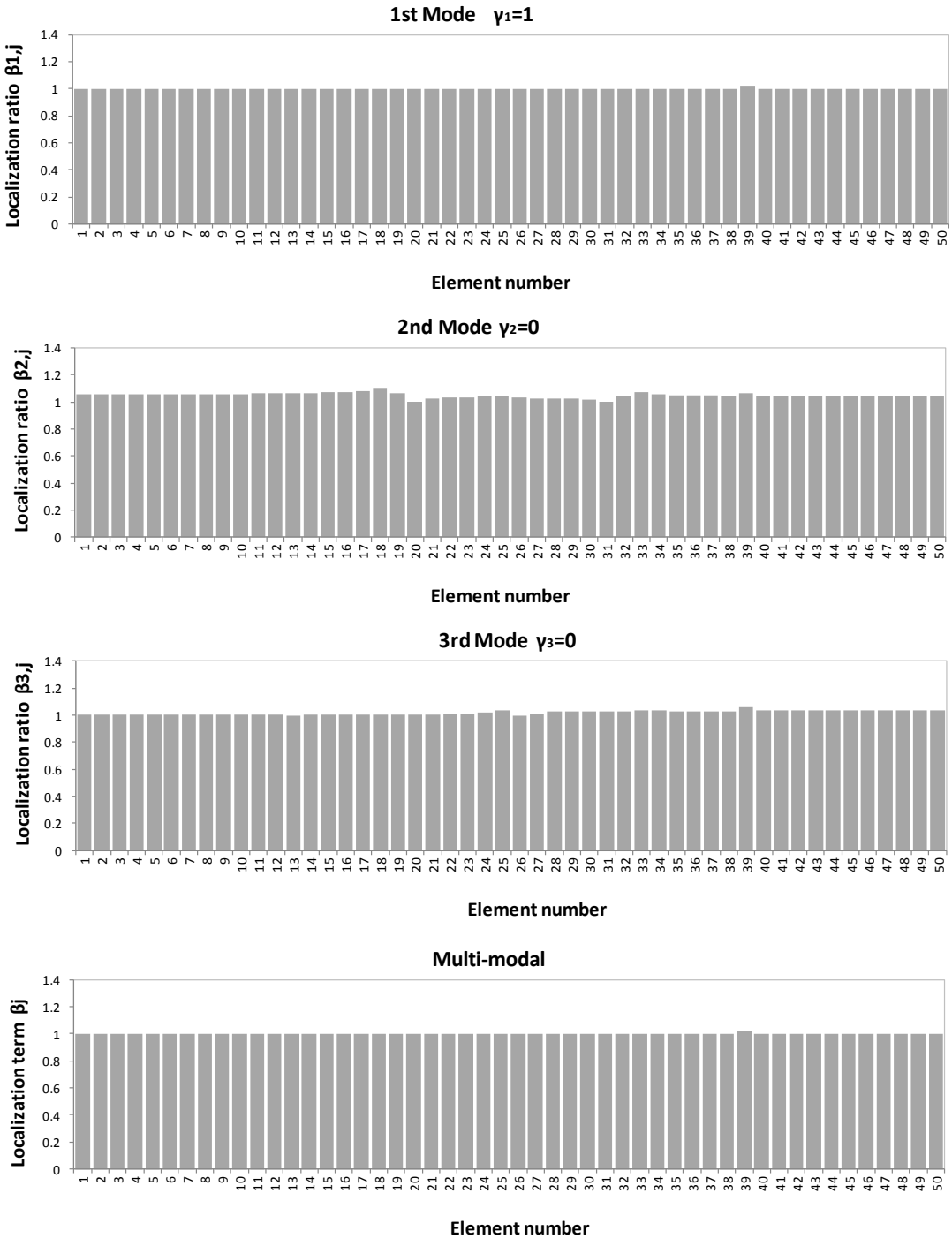

Figure 29. Localization ratios and multi-modal localization term for case no.6.

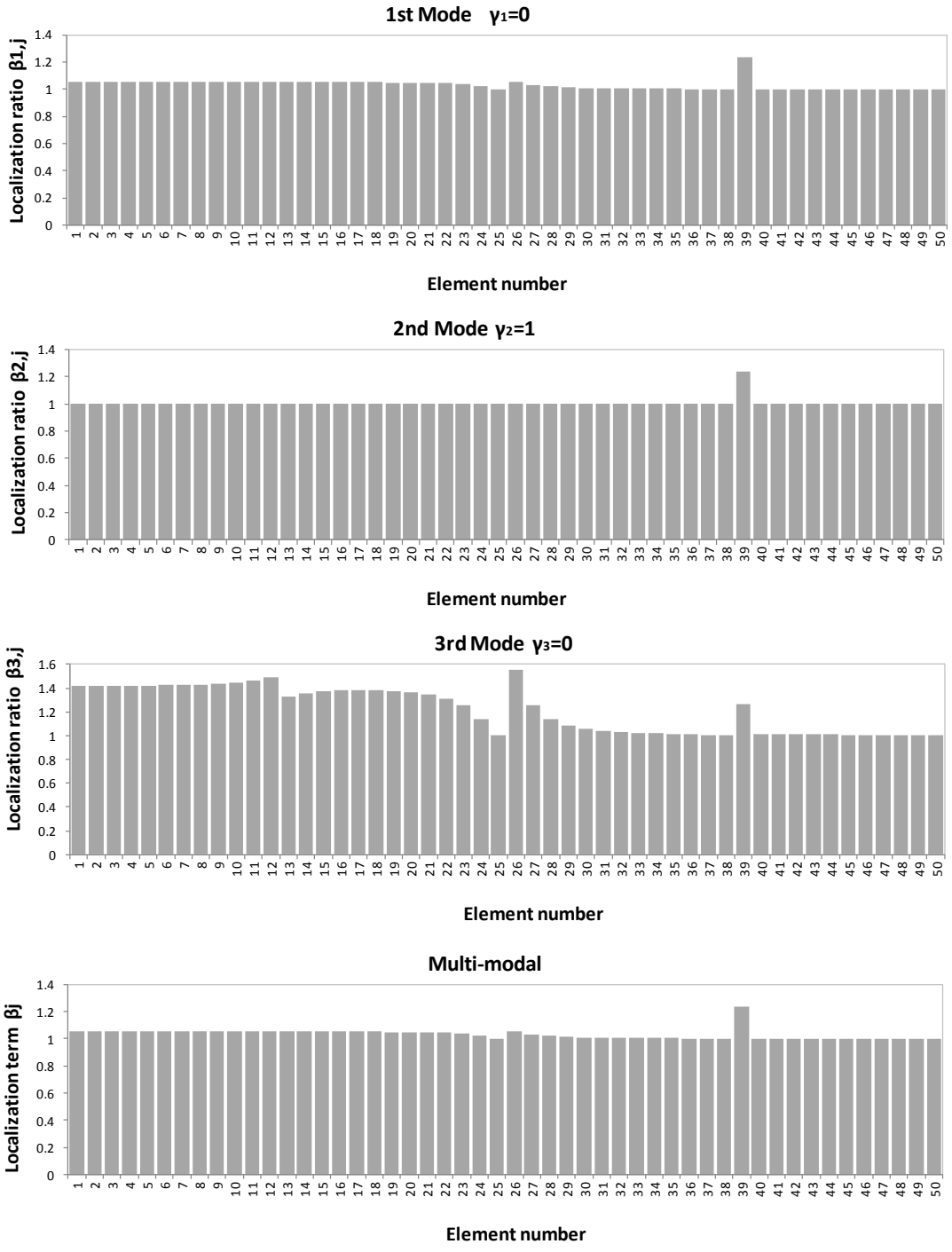

Figure 30. Localization ratios and multi-modal localization term for case no.7.

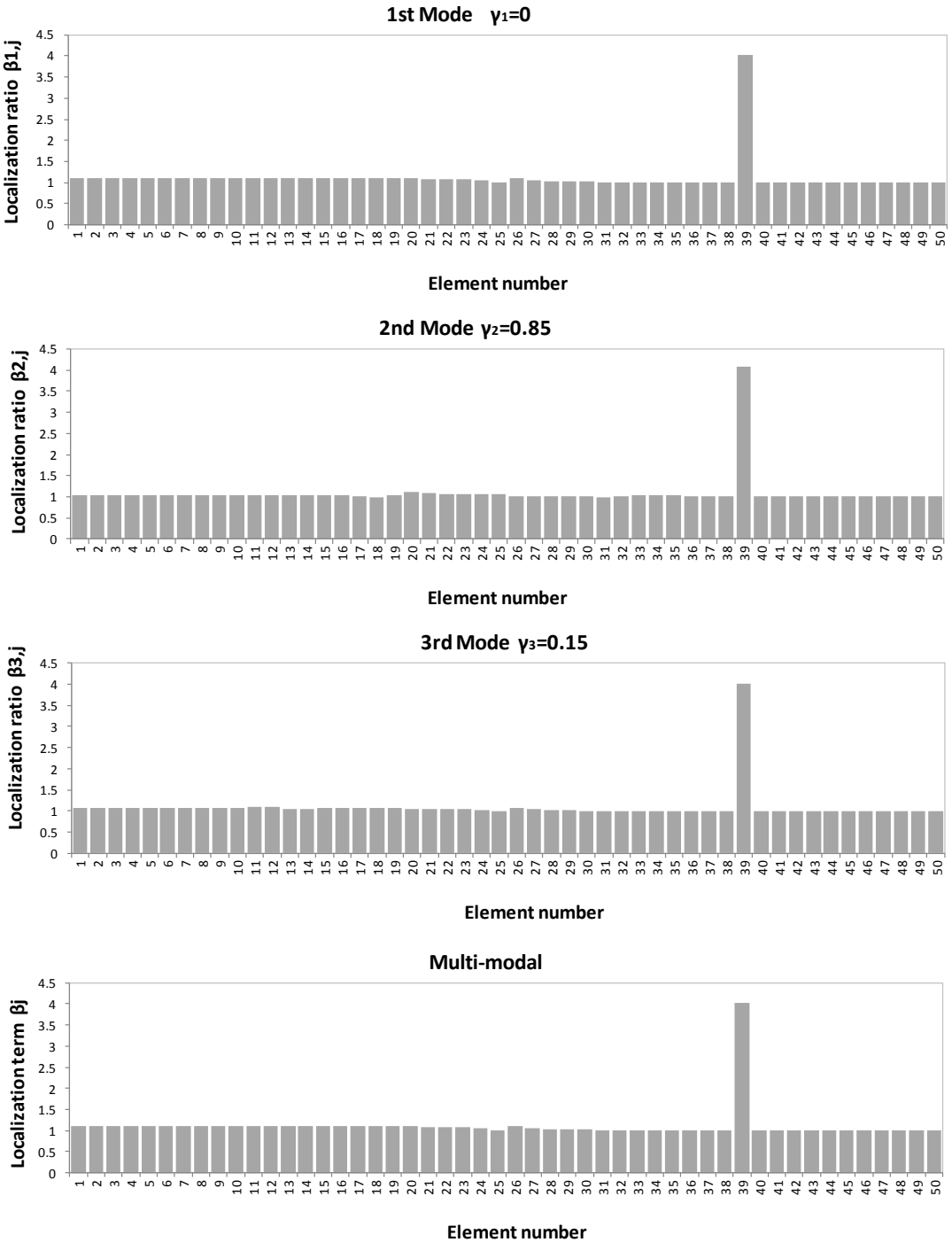

Figure 31. Localization ratios and multi-modal localization term for case no.8.

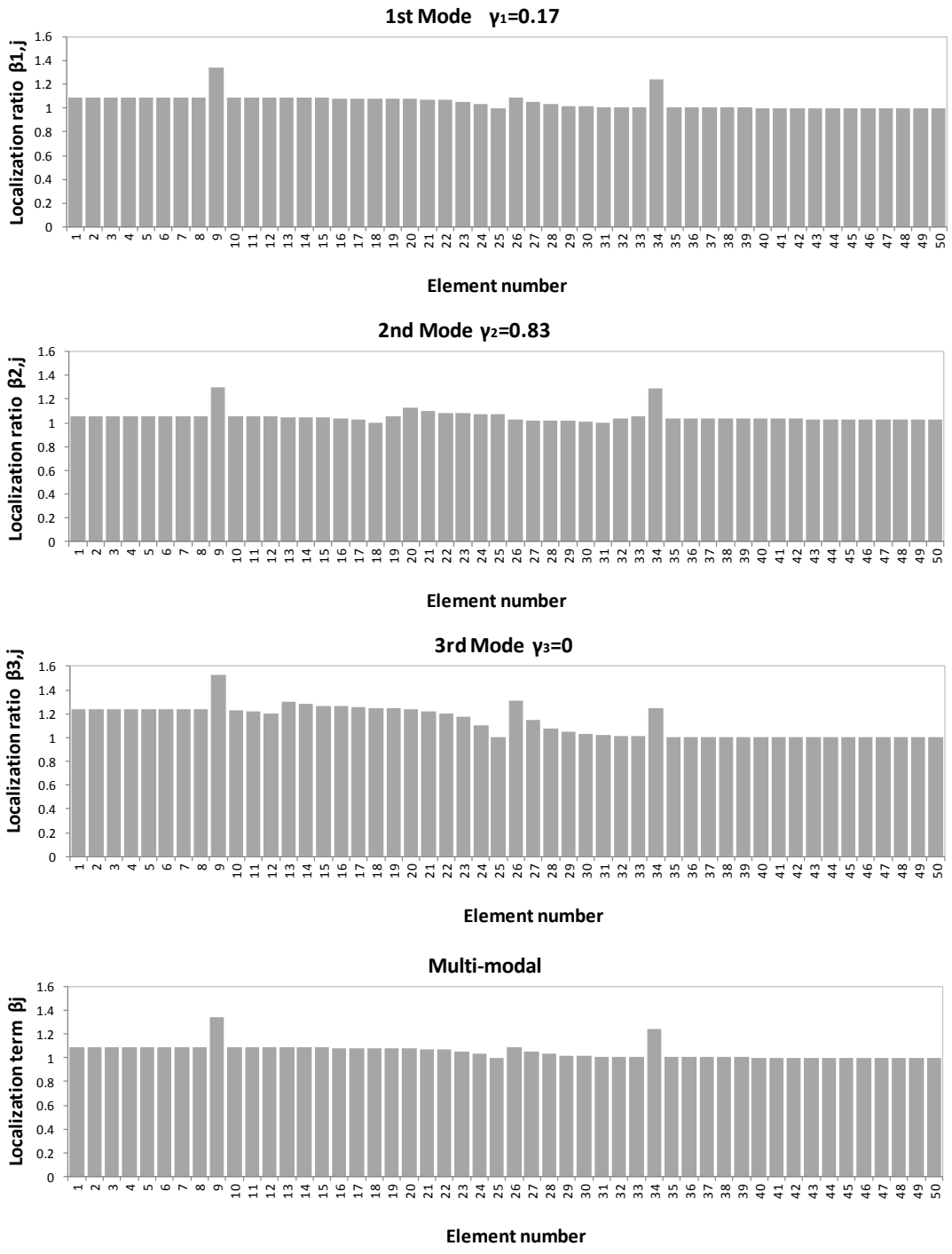

Figure 32. Localization ratios and multi-modal localization term for case no.9.

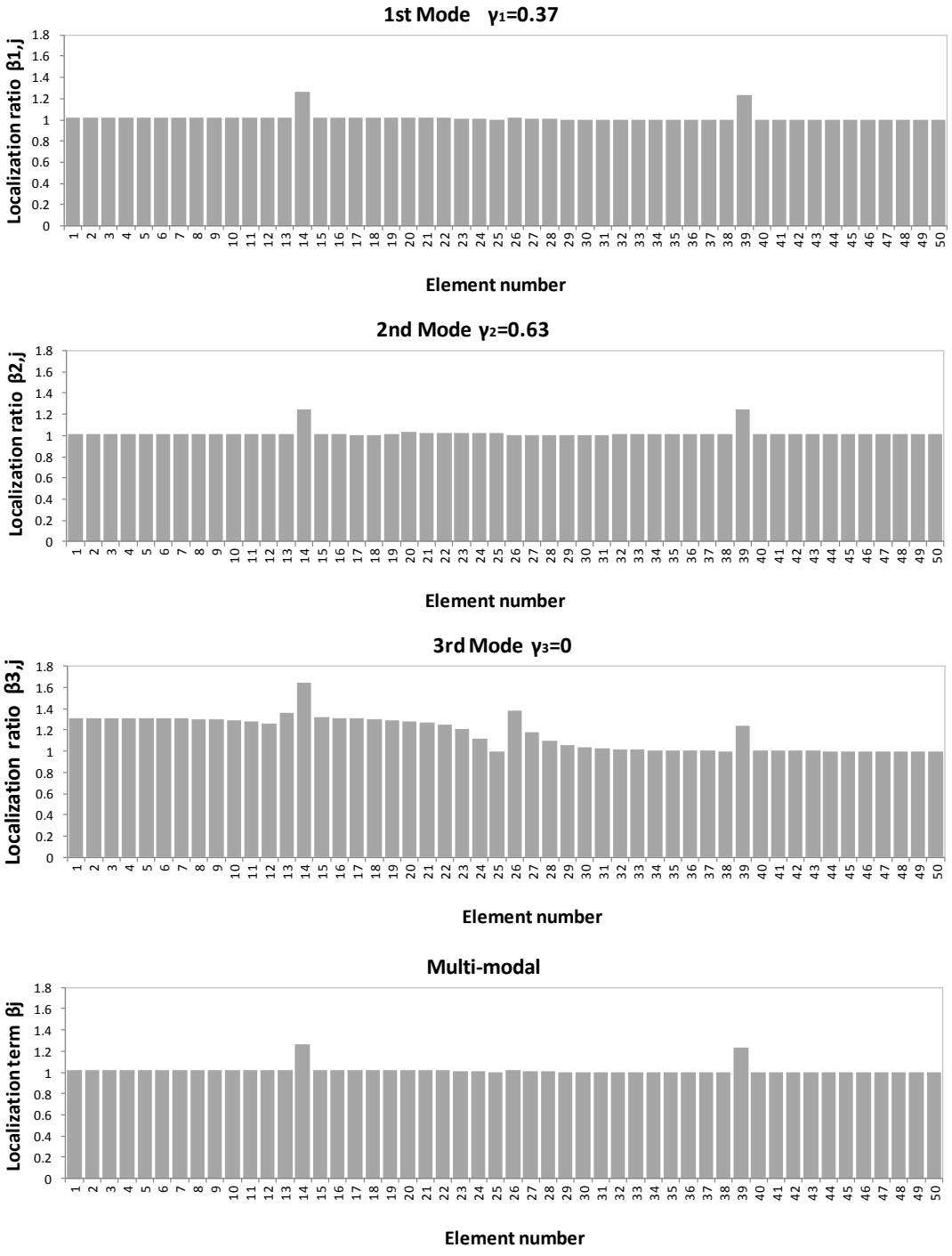

Figure 33. Localization ratios and multi-modal localization term for case no.10.

From the above plots, it is possible to visualize one notable characteristic of the proposed algorithm, which is the weighted combination of the contributions from different modes. Depending on the particular type of damage, one mode is more likely to detect damage than another one. Taking as example the plots of **Figure 33**, referred to case no. 10 in which both element 14 and 39 experienced a stiffness degradation of 10%, it is evident that localization ratios evaluated for the 1st and the 2nd mode are more consistent with the damage scenario than for the 3rd mode. This consistency between the damage scenarios and the localization ratios is well depicted by the modal reliability index γ_i of Eq. 23. For case no. 10, the index γ_i is equal to 0.37, 0.63 and practically 0 for mode 1, 2 and 3 respectively, identifying the first 2 modes as more reliable for the damage detection than the third mode. The higher numerical values of γ_i suggest a good correlation of mode 1 and 2 to the current damage, while mode 3 appears to be poorly involved in the present damaged configuration. The noisy information provided by the 3rd mode should not be considered as important as the information provided by modes 1 and 2 to obtain a clear localization of the damage in element 14 and 39. The procedure described to calculate the multi-modal localization term (Eq. 26), and consequently the normalized damage index Z_j (Eq. 26), combines the modal contributions correctly and results in an unquestionable localization of damage in the degraded elements, as visible in the bottom diagram of **Figure 33**. Even for a simple case such as the beam under analysis, there is a great variability of the modal reliability index γ_i of the modes depending on locations and intensity of the damages. The first mode proved to be the most important one for the damage detection in cases no. 1, 2, and 6. The second mode was most significant in cases no. 3, 7, 8, 9 and 10, while the third mode was predominant for the damage scenarios no. 4 and 5. For case no. 8, in which the damage intensity is very high (50% of the element stiffness) all the considered modes appear sufficiently correlated to the real damage. As expected, for high damage intensity the noisy component that affects the localization ratio distribution becomes less significant. For low damage intensity, the inclusion of more than one mode in the analysis is an important element that allows reduction of false positive and false negative outcomes of the damage detection algorithm.

4.2. Simplified bridge model with isolation devices

The proposed algorithm has been applied to a simplified structural system representing a small bridge structure equipped with seismic isolators. The structure is presented in **Figure 34** and consists of a four span continuous superstructure with maximum distance between piers of 12 m and top elevation under the deck of 5 m. The isolation devices are installed at the top of the piers between deck structure and cap beams. Three devices are installed on each bent and belong to the family of Friction Pendulum Systems (FPS) (Zayas et al., 1987).

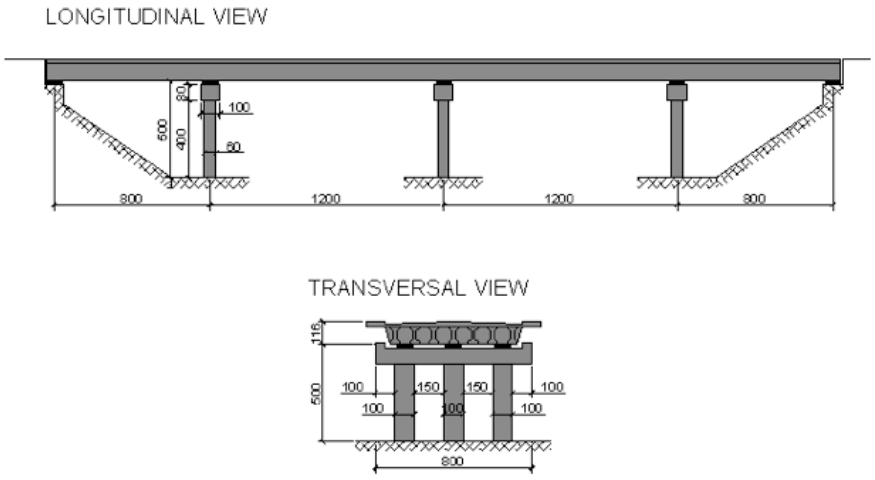

Figure 34. Test bridge equipped with friction isolators (measures in cm).

Even though the algorithm does not require, for its implementation, a Finite Element model of the structure, for the validation of this procedure a 2D non-linear numerical model was implemented in Sap2000® (Computers and Structures, 2000) in order to obtain the response records for an undamaged and damaged configurations.

The numerical model representing the bridge structure was assembled using three columns and a continuous deck as shown in **Figure 35**. Only the elements modeling the isolation devices were treated as non linear elements. The friction devices were modeled using a hysteretic behavior proposed by Wen (1976) and Nagarajaiah et al. (1991). In the model, the friction forces are directly proportional to the vertical load on the devices and the friction coefficients are velocity dependent as proposed by Constantinou et al. (1990).

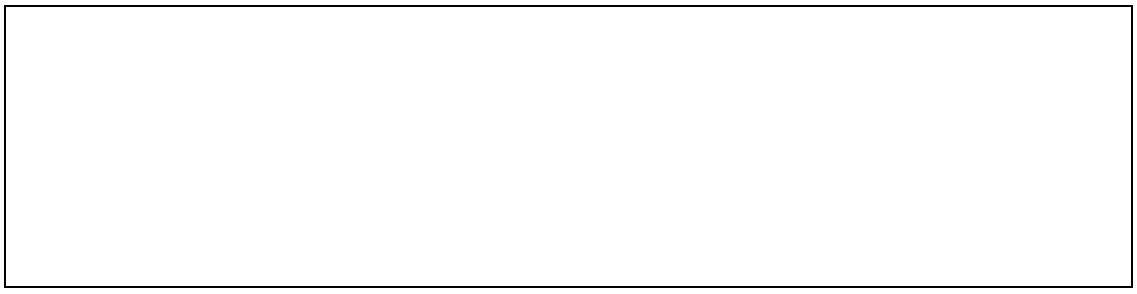

Figure 35. Schematic of the F.E. bridge model.

For this study, it was assumed a Coulomb friction behaviour. The equilibrium of forces on the slider of the isolator (see Eq. 29) results in the typical force-displacement hysteresis loop and force distribution presented in **Figure 36** and **Figure 37**, respectively.

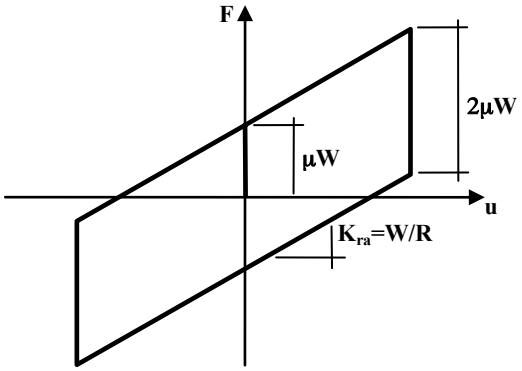

Figure 36. Typical force-displacement hysteresis loop for FPS isolators.

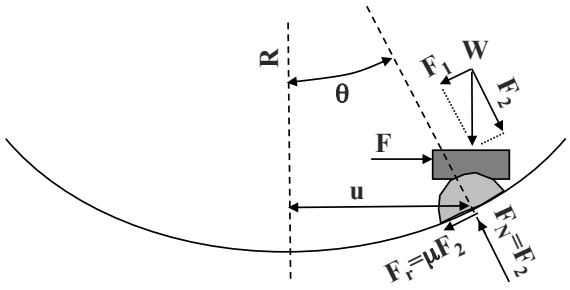

Figure 37. Force diaphragm of FPS for small displacement.

The nominal friction coefficient for the devices was assumed equal to 6% with a radius of curvature of 1m, corresponding to an imposed natural period of 2s obtained from:

$$T = 2\pi\sqrt{\frac{R}{g}} \qquad (30).$$

The structure was subjected to a white noise in the frequency range of 0.05-10Hz, with components both in vertical and horizontal directions. From the response obtained via numerical simulation the mode shapes were assessed through the use of the Covariance Driven Stochastic Subspace Identification Method by Peeters (2000). Twelve damage cases were investigated, with damage location and level of severity indicated in Table 3. Each scenario represents a simulated damage event, localized in the friction devices and/or in one element of the bridge pier or of the superstructure. The damage in the piers and the superstructure was simulated by reducing the elastic modulus of appropriate elements (i.e. reducing the stiffness), while the degradation of the isolator performance was modeled as an increase of the friction coefficient μ. In **Table 3** the maximum variation of the three considered frequencies of the structure, with comparison to the undamaged case, is reported.

Table 3. Damage scenarios and natural frequencies of test-bridge

Case	Simulated damage		Max frequency variation with respect to the undamaged case (%)
	Location	Severity[+]	
Undamaged	-	-	0.00
1	FP1	+50	7.12
2	FP1	+25	3.99
3	FP1	+10	1.53
4	FP2	+25	5.09
5	FP1, FP3	+25, +25	5.68
6	1	-50	-0.08
7	1	-10	0.00
8	1	-1	0.00
9	1, FP1	-10, +25	4.07
10	1, FP3	-10, +25	3.82
11	38	-10	0.00
12	38, FP1	-10, +25	3.98
[+]Severity (%) =	*(E*-E)/E x 100* for column elements *(μ*-μ)/μ x 100* for FP isolators		

A scheme of the longitudinal deformation associated with the first mode of the model, in undamaged configuration, is presented in **Figure 38**. It is visible the relative displacement between the deck and the bridge piers at the locations of the friction devices.

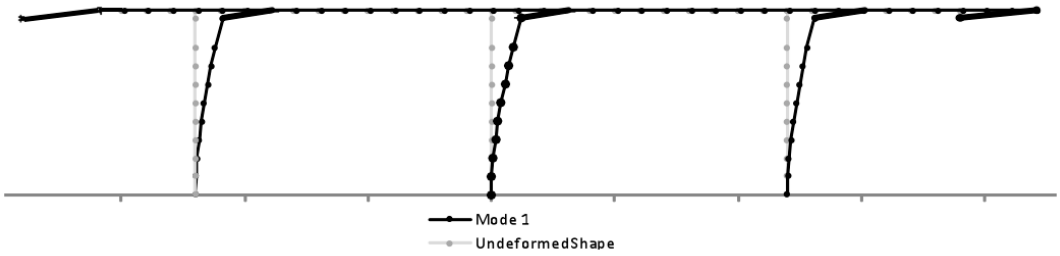

Figure 38. First mode shape of test.

In order to implement the proposed procedure for the considered structure, four structural sub-members were defined: the deck and three bridge piers. The arbitrary subdivision in elements, required for the procedure, is in this case corresponding, for simplicity, to the F.E. discretization. The friction devices are considered as part of the pier members. The mode shapes associated with the first three natural frequencies were calculated for each member. Eq. 15 was used for the deck and the pier members due to prevalent flexural behavior. For the isolators Eq. 14 takes into account the shear deformation. The mode shapes were interpolated with a spline function in order to numerically express the local deformations obtained as double derivatives.

For each mode the index $\beta_{i,j}$ is calculated as indicated in Eq. 17 and the contribution of the three modes is taken into account by the use of Eq. 25 in the definition of the multi modal localization index β_j. In Table 5 are reported the locations of the damages identified through the Z_j index together with the severity index values calculated as in Eq. 27. It must be noted that the predicted stiffness variation, measured by α, can be directly compared with the severity of the simulated damage only for the elements of the deck and the bridge piers. In this case, in fact, the definition of the severity index allows a direct interpretation of this parameter as variation in terms of stiffness. For the friction isolator instead, the severity index α, still obtain through Eq. 27, needs to be converted to a variation of friction coefficient used as the parameter simulating the degradation of the devices. This necessary step is motivated by the validity of providing a physical interpretation of the damage severity indicator as well as to resolve the apparent degradation indicated by the terms in parentheses of **Table 4**.

As mentioned above, due to the non-linear behavior of the friction isolators, increments of their stiffness can be detected when induced by increments of the friction coefficient but also when a reduction of the relative displacement across the isolator is experienced. A damaged condition affecting one isolator, for instance, involves a reduction of the relative displacement across all the isolators. This reduction corresponds to an increment of the stiffness and a consequent higher value of α in all the isolators, also in the undamaged ones. For this reason non zero α values are detected also for undamaged devices indicated by the terms in parentheses of **Table 4**. The phenomenon is also detected by the localization term β_j and the localization indicator Z_j. The localization

terms β_j, localization indicators Z_j, severity indices α_j and friction coefficient variations are shown in **Figure 39** to **Figure 65** for the 12 damage cases of **Table 4**. All the plots of **Figure 39** to **Figure 50** refer to the columns of the bridge and the isolators. As expected, **Figure 49** and **Figure 50** show no apparent damages in the columns. These plots refer to case no. 11 and 12, in which damages were simulated in a beam element. The results for the beam elements are provided in **Figure 51** and **Figure 52**.

Table 4. Predicted stiffness variation results of test-bridge

Damage case	Simulated damage		Predicted Stiffness Variation	
	Location	Severity[+]	Location	Severity[+] α
1	FP1	+50	FP1, FP2, FP3	+67, (+11), (+12)
2	FP1	+25	FP1, FP2, FP3	+33, (+6), (+6)
3	FP1	+10	FP1, FP2, FP3	+12, (+2), (+2)
4	FP2	+25	FP1, FP2, FP3	(+10), +38, (+10)
5	FP1, FP3	+25,+25	FP1, FP2, FP3	+32, (+5), +32
6	1	-50	1, FP1, FP2, FP3	-50, (+7), (+2), (+3)
7	1	-10	1, FP1, FP2, FP3	-10, (+5), (+3), (+3)
8	1	-1	1, FP1, FP2, FP3	-1, (+0.1), (+0.1), (+0.1)
9	1, FP1	-10, +25	1, FP1, FP2, FP3	-10, (+35), (+6), (+7)
10	1, FP3	-10, +25	1, FP1, FP2, FP3	-10, (+7), (+6), +33
11	38	-10	38	-10.3
12	38, FP1	-10, +25	38, FP1, FP2, FP3	-10.3, +33, (+6), (+6)

[+]Severity (%) = *(E*-E)/E x 100* for column elements
(μ-μ)/μ x 100* for FP isolators

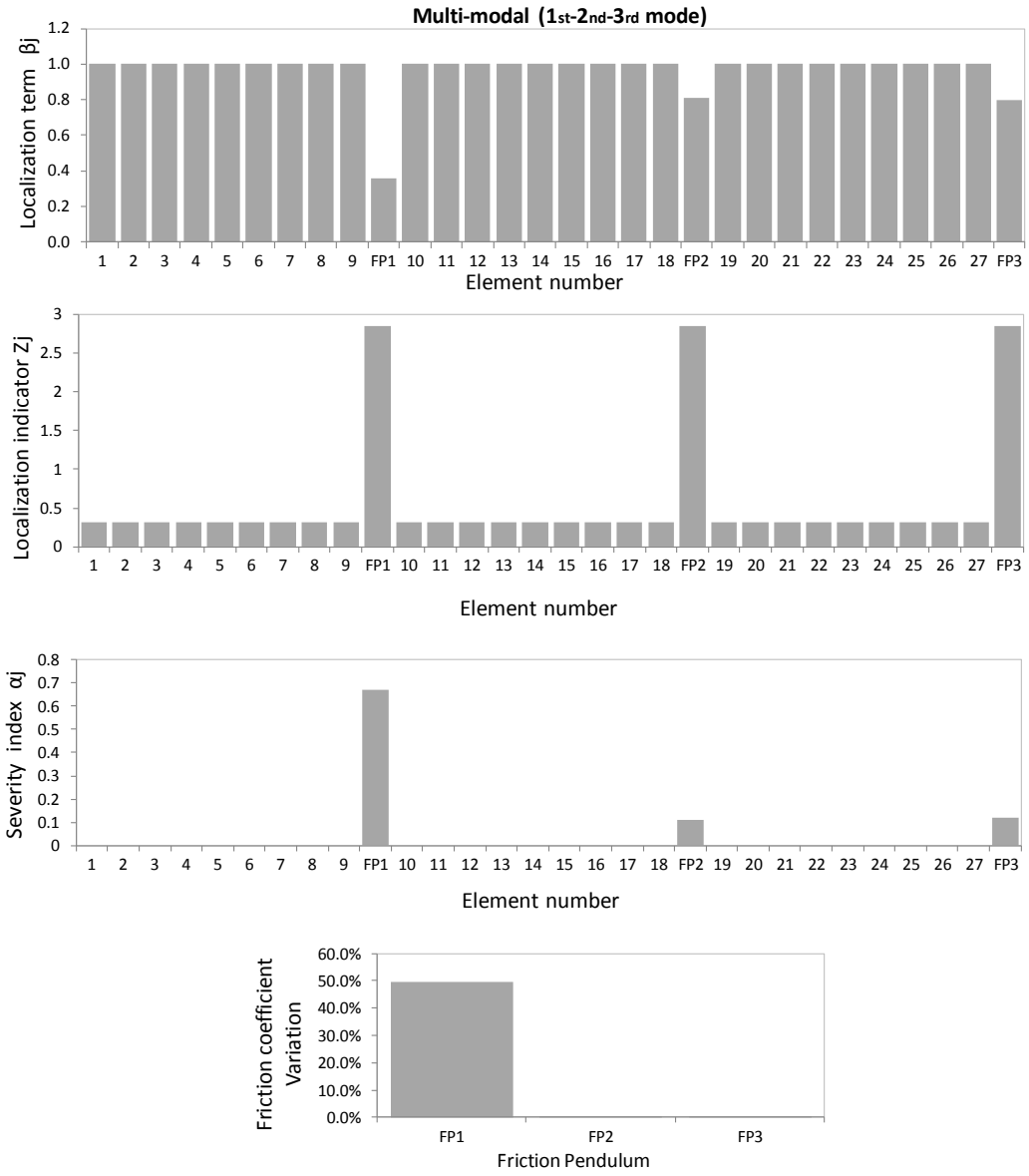

Figure 39. Localization term, localization indicator, severity index for columns' elements and FPs and friction coefficient variation in damage case 1

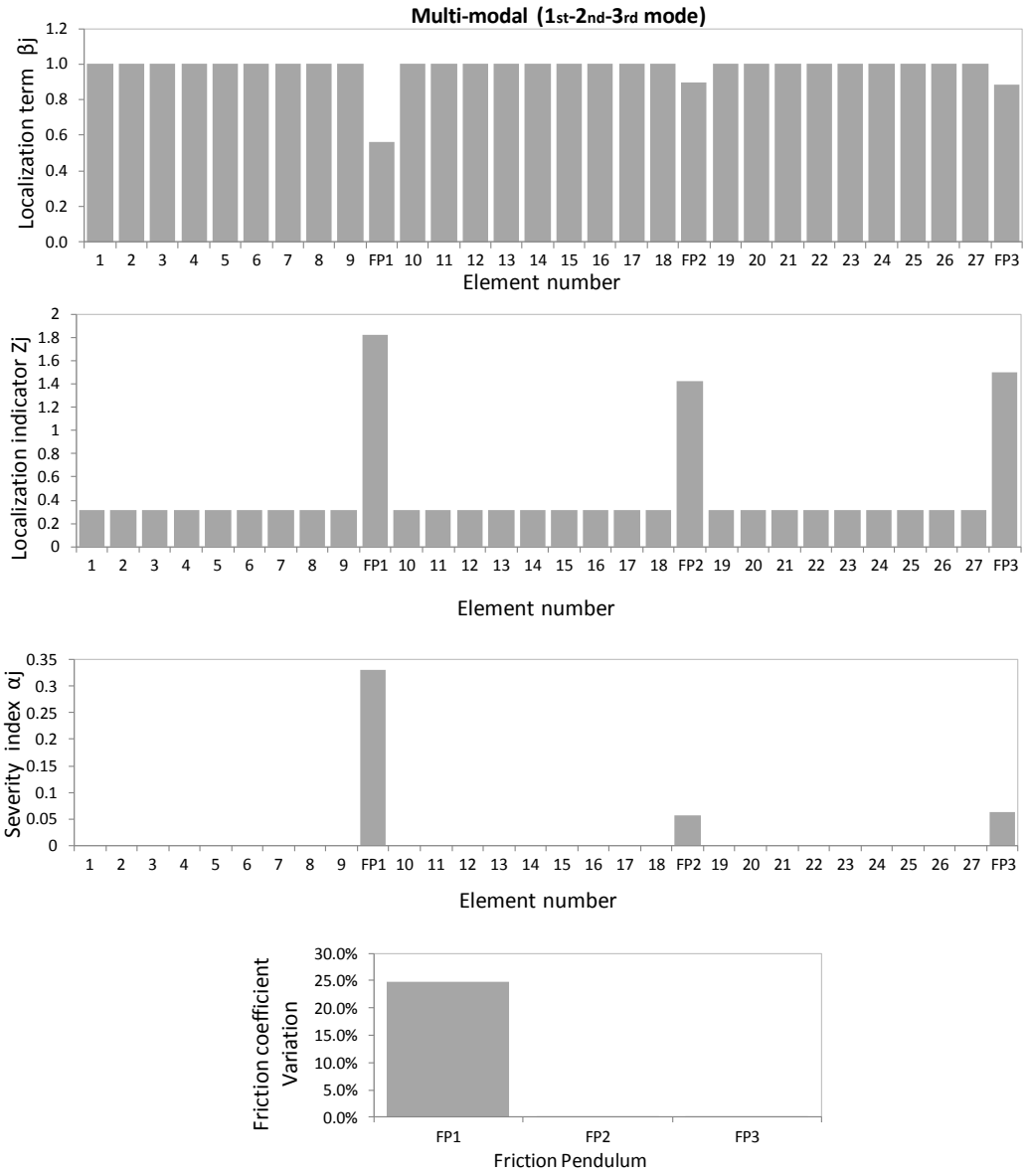

Figure 40. Localization term, localization indicator, severity index for columns' elements and FPs and friction coefficient variation in damage case 2

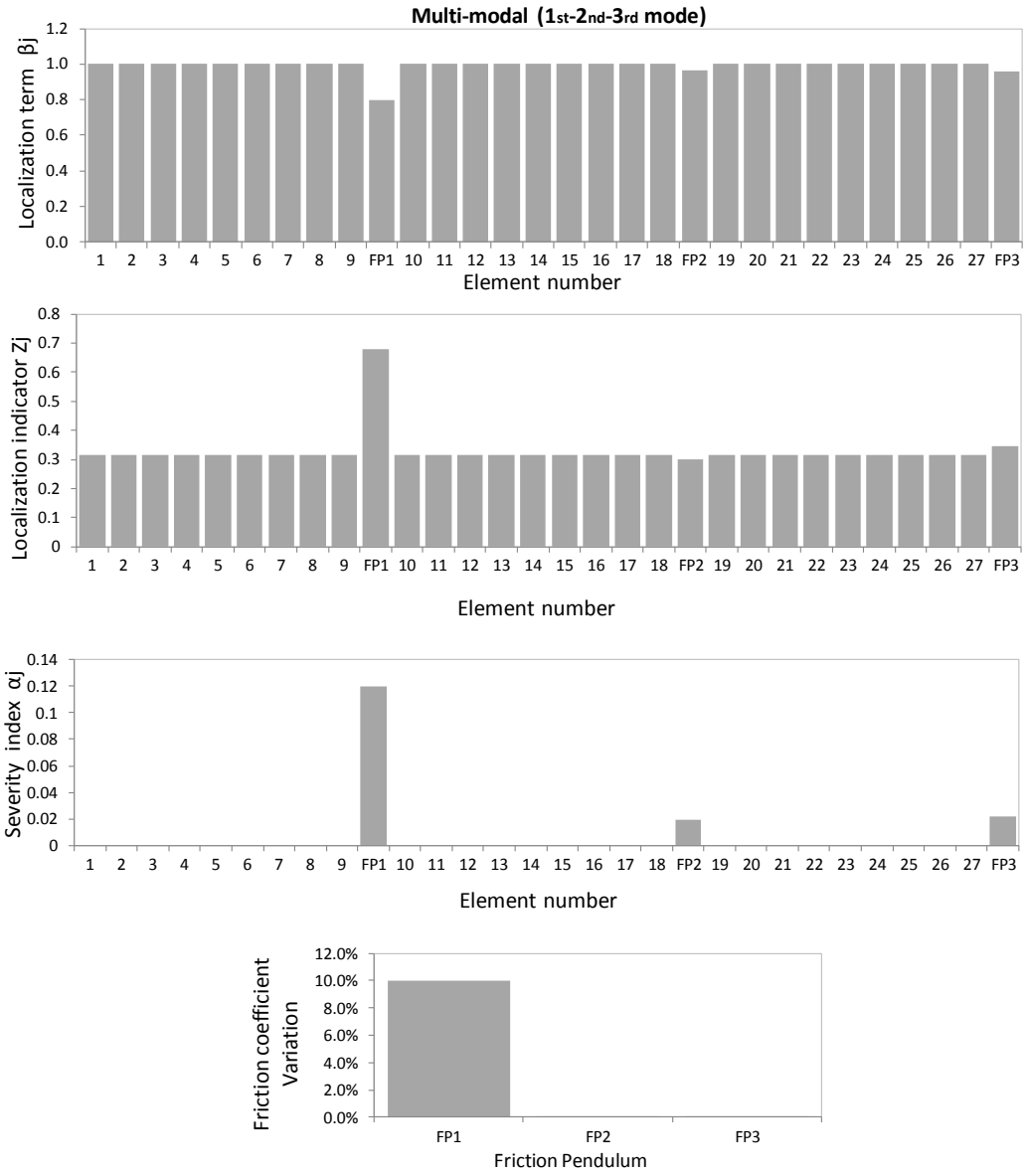

Figure 41. Localization term, localization indicator, severity index for columns' elements and FPs and friction coefficient variation in damage case 3

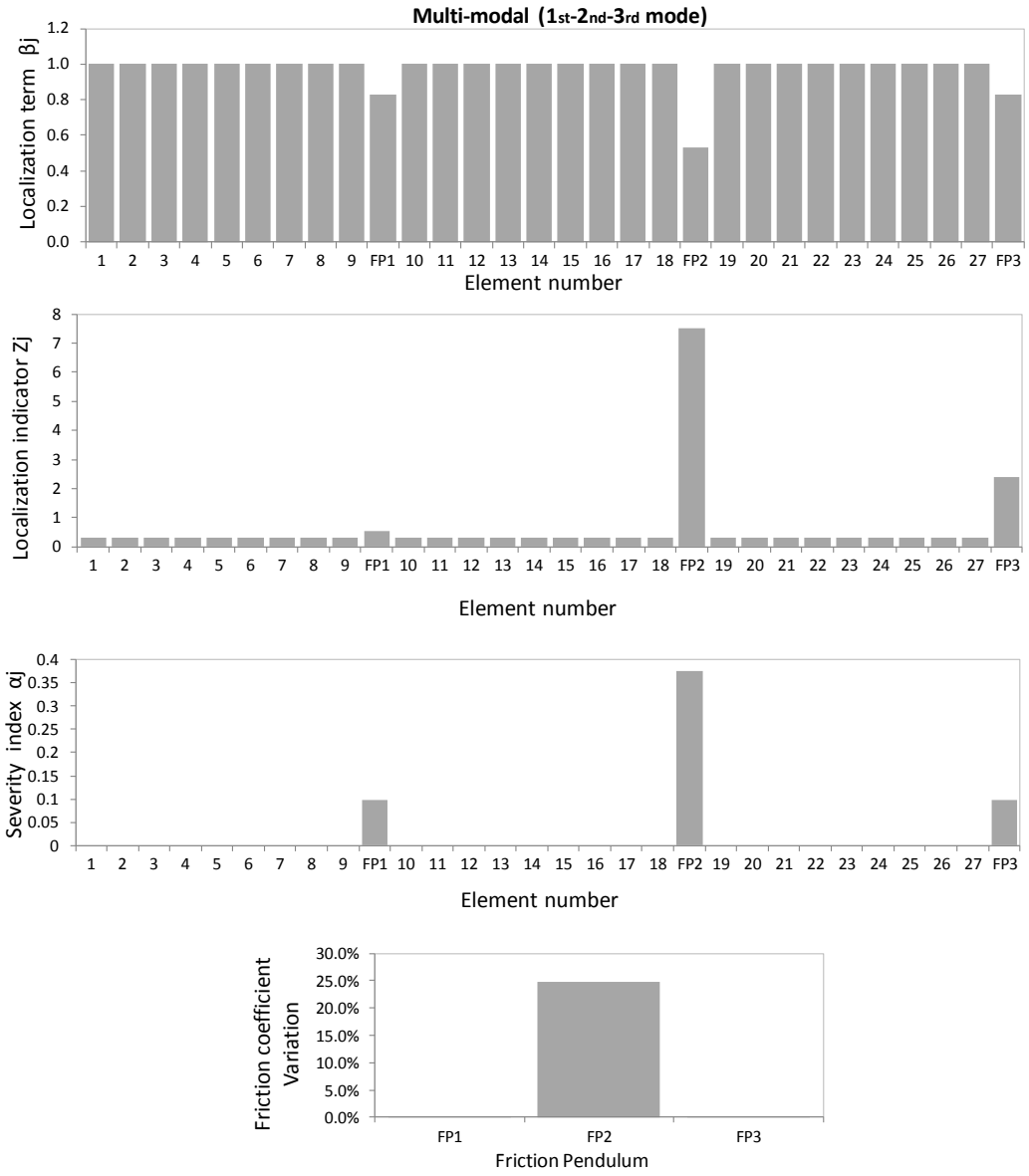

Figure 42. Localization term, localization indicator, severity index for columns' elements and FPs and friction coefficient variation in damage case 4

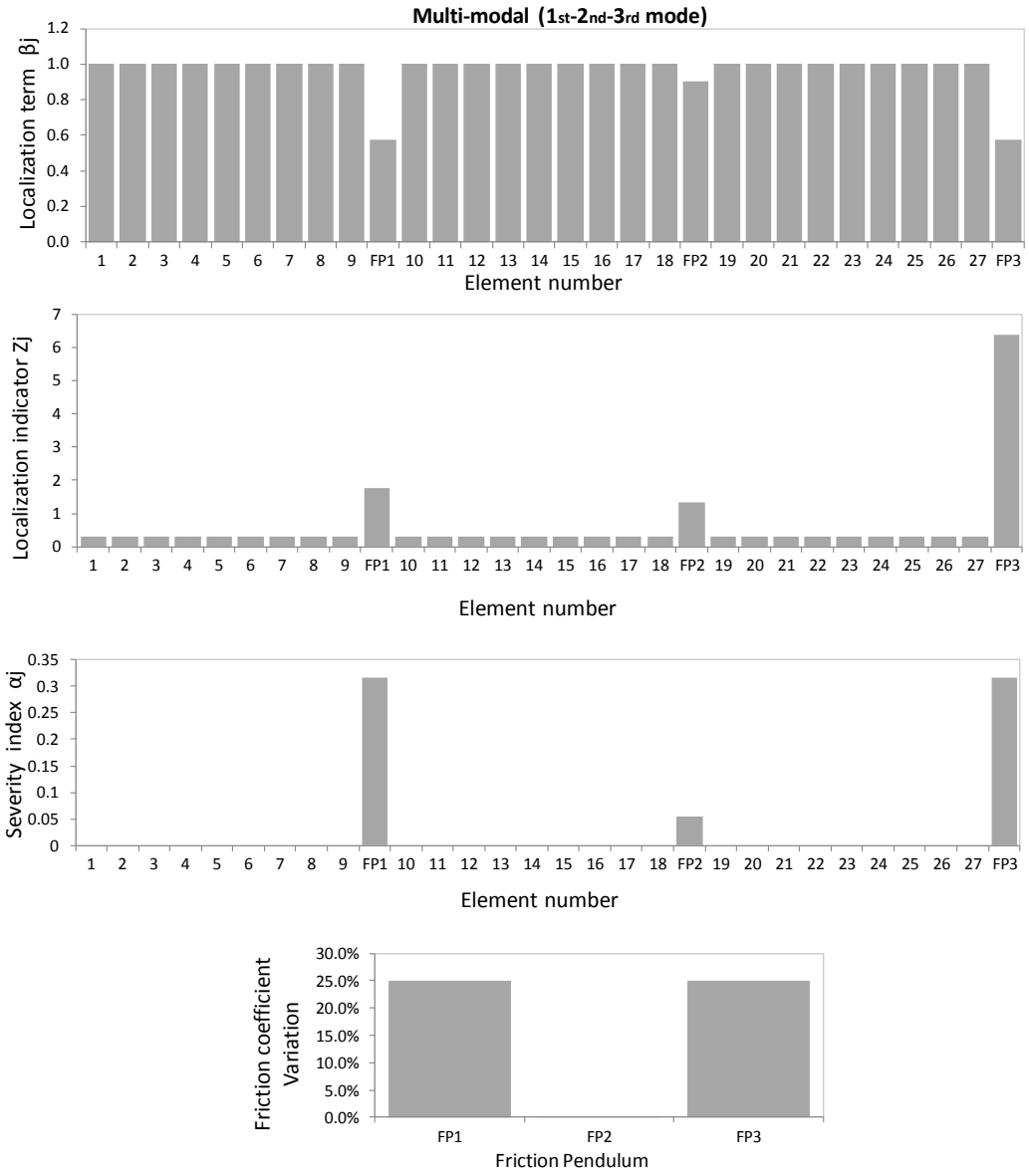

Figure 43. Localization term, localization indicator, severity index for columns' elements and FPs and friction coefficient variation in damage case 5

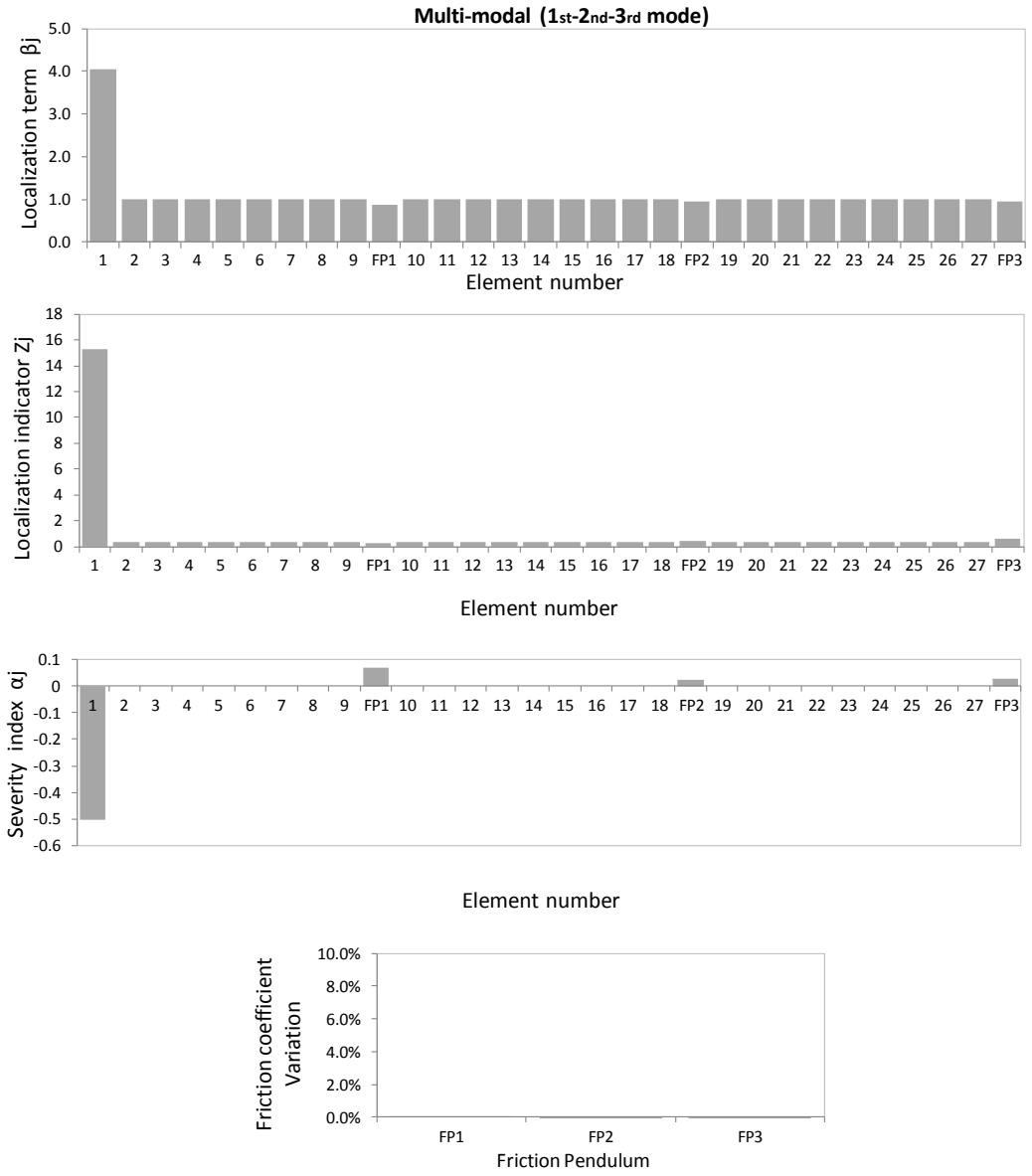

Figure 44. Localization term, localization indicator, severity index for columns' elements and FPs and friction coefficient variation in damage case 6

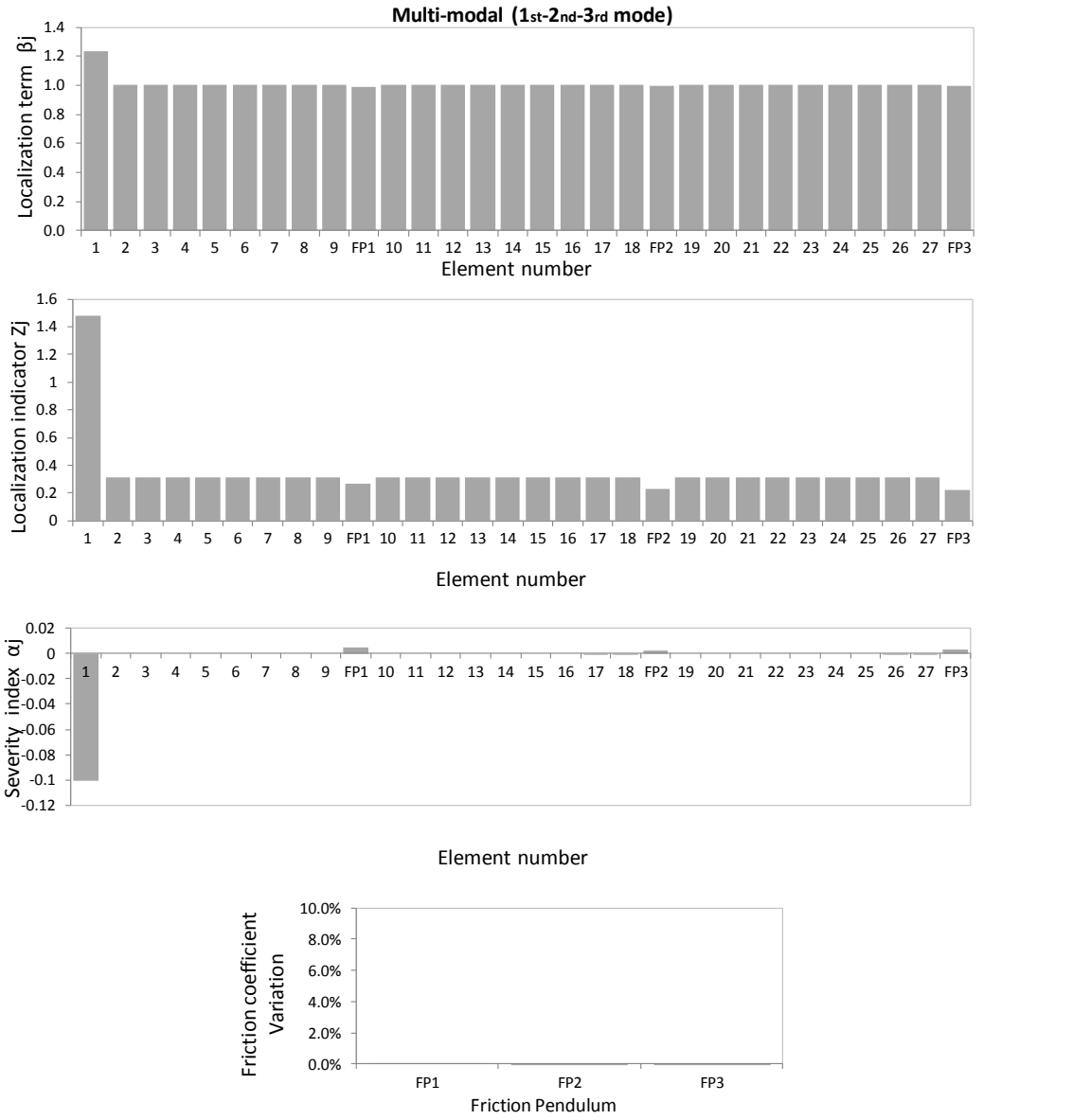

Figure 45. Localization term, localization indicator, severity index for columns' elements and FPs and friction coefficient variation in damage case 7

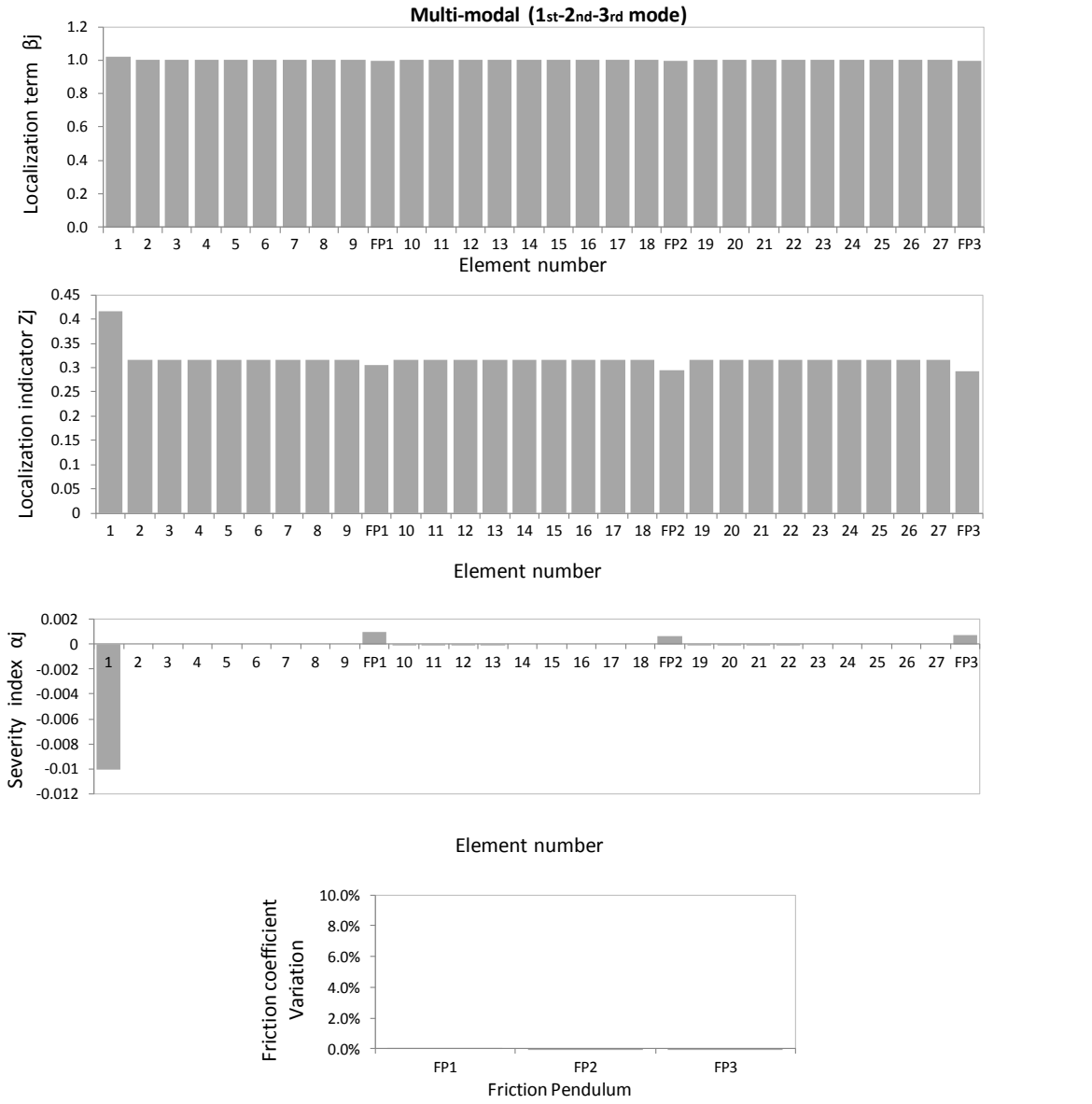

Figure 46. Localization term, localization indicator, severity index for columns' elements and FPs and friction coefficient variation in damage case 8

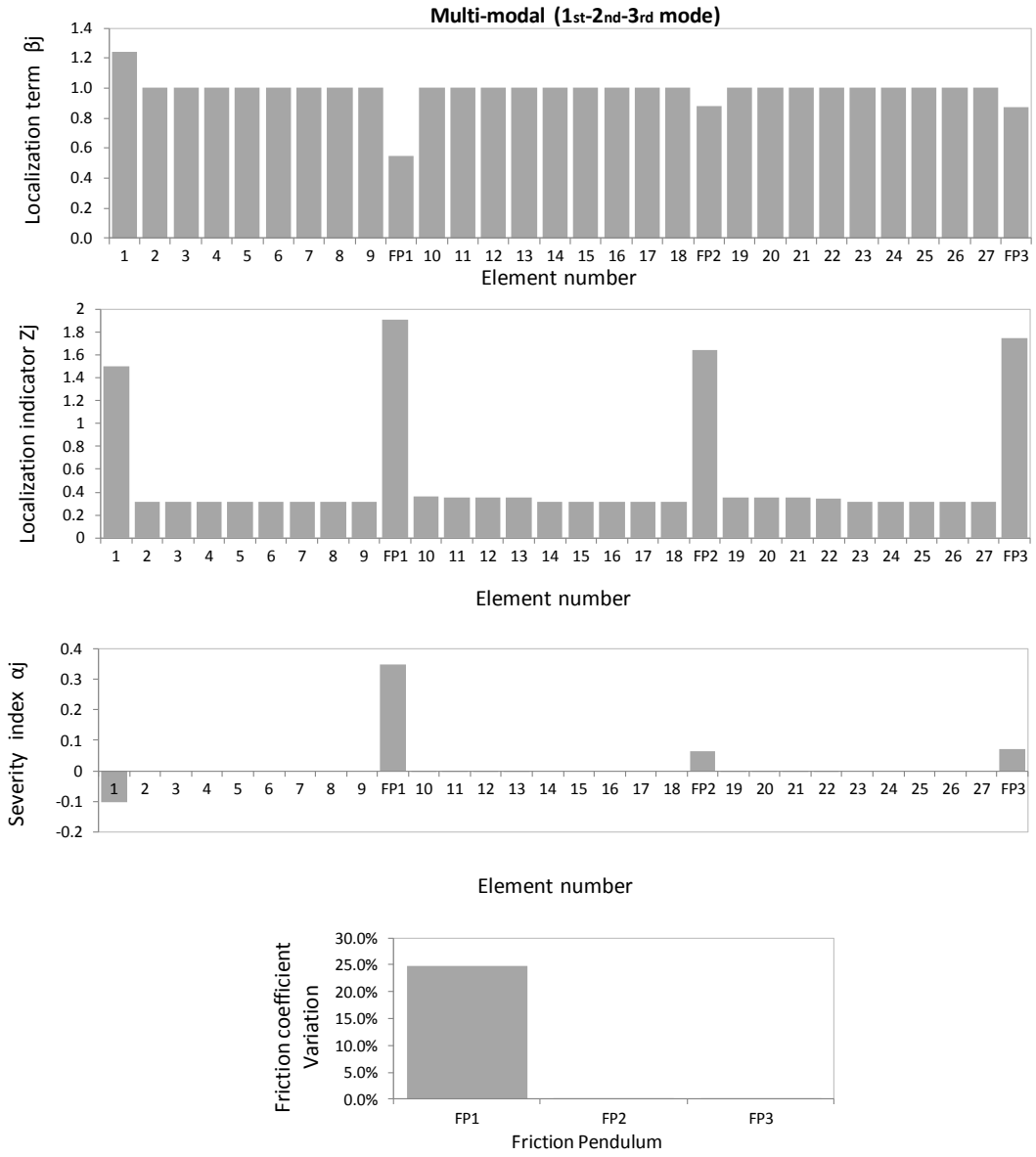

Figure 47. Localization term, localization indicator, severity index for columns' elements and FPs and friction coefficient variation in damage case 9

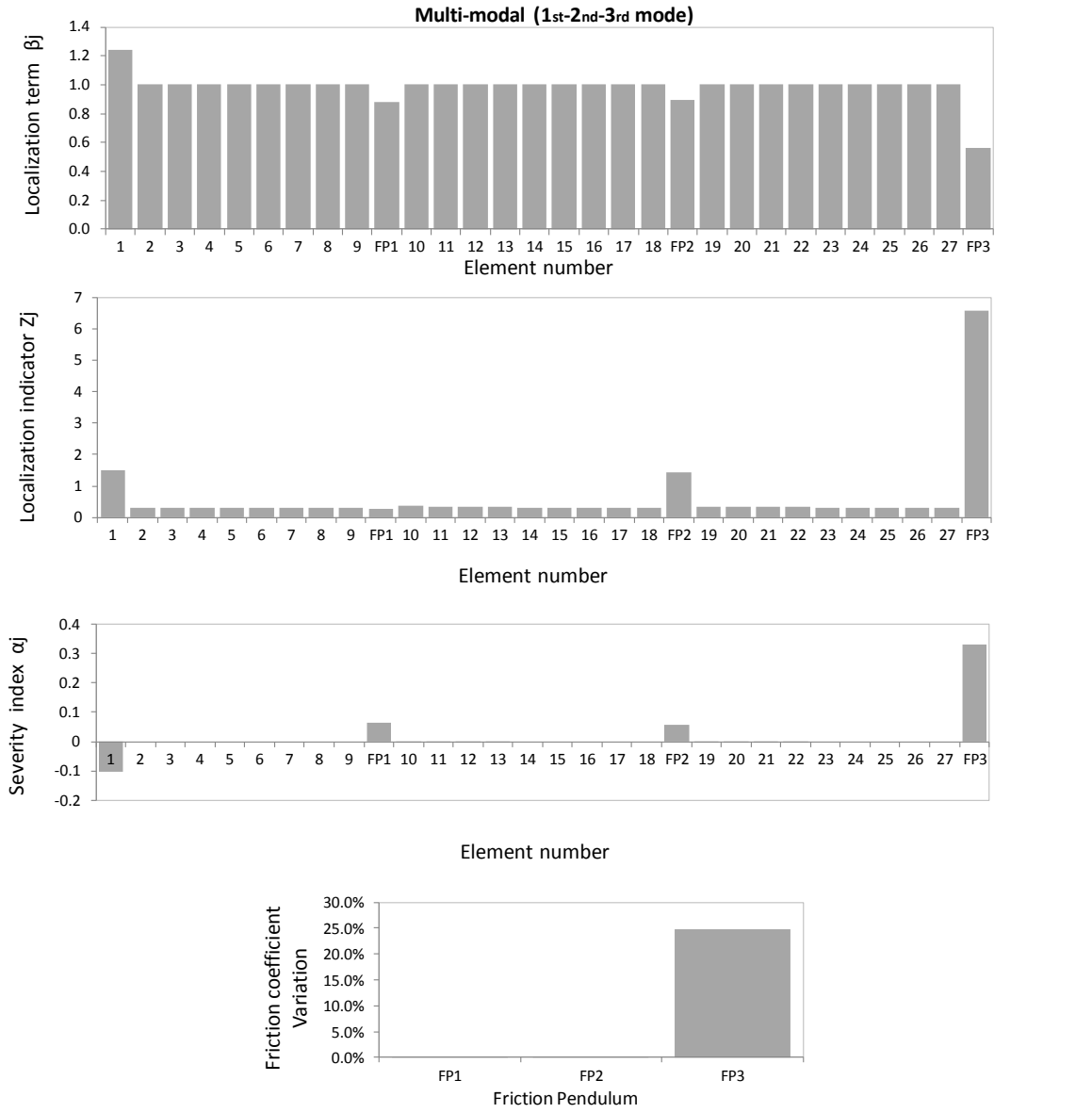

Figure 48. Localization term, localization indicator, severity index for columns' elements and FPs and friction coefficient variation in damage case 10

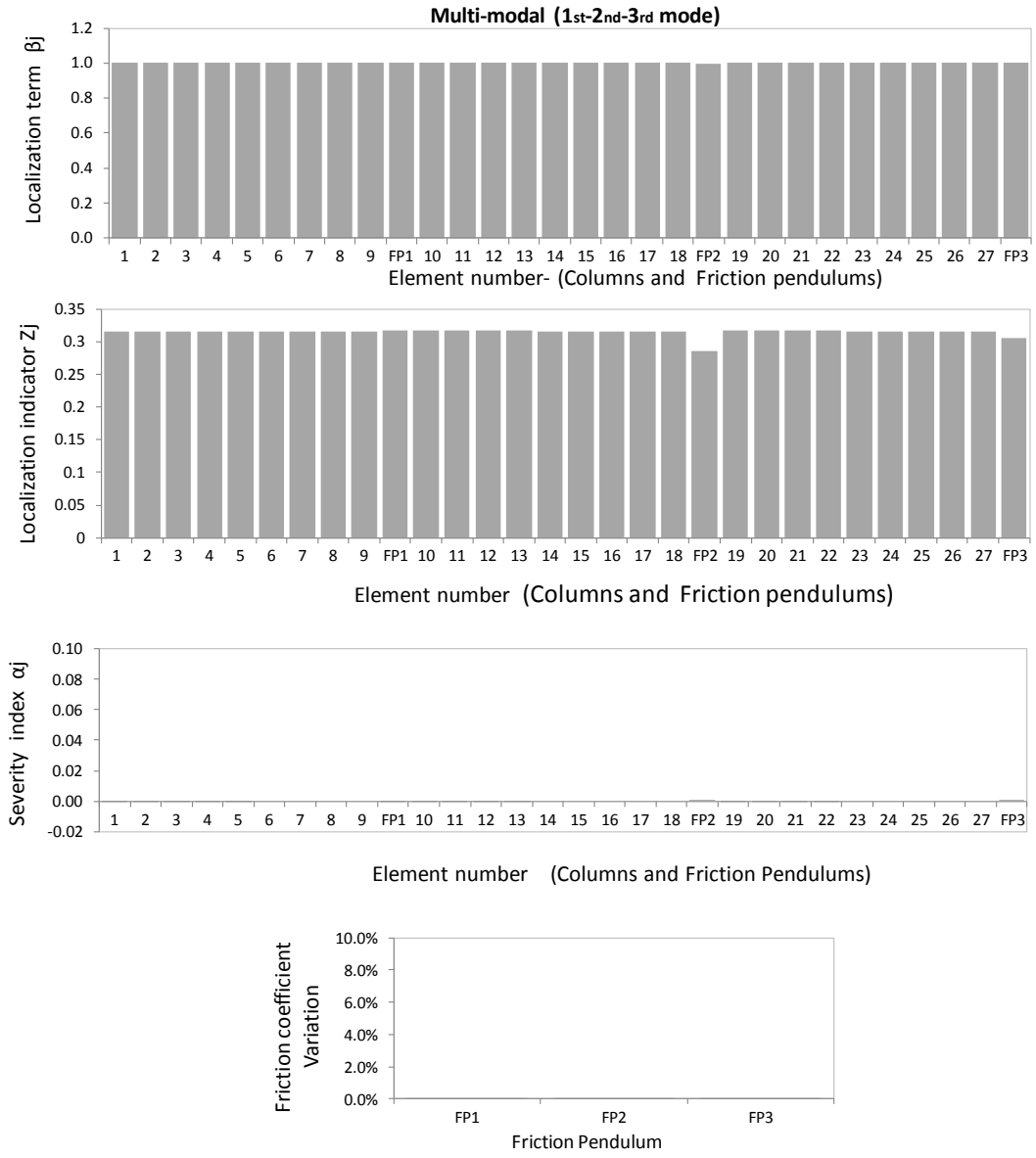

Figure 49. Localization term, localization indicator, severity index for columns' elements and FPs and friction coefficient variation in damage case 11

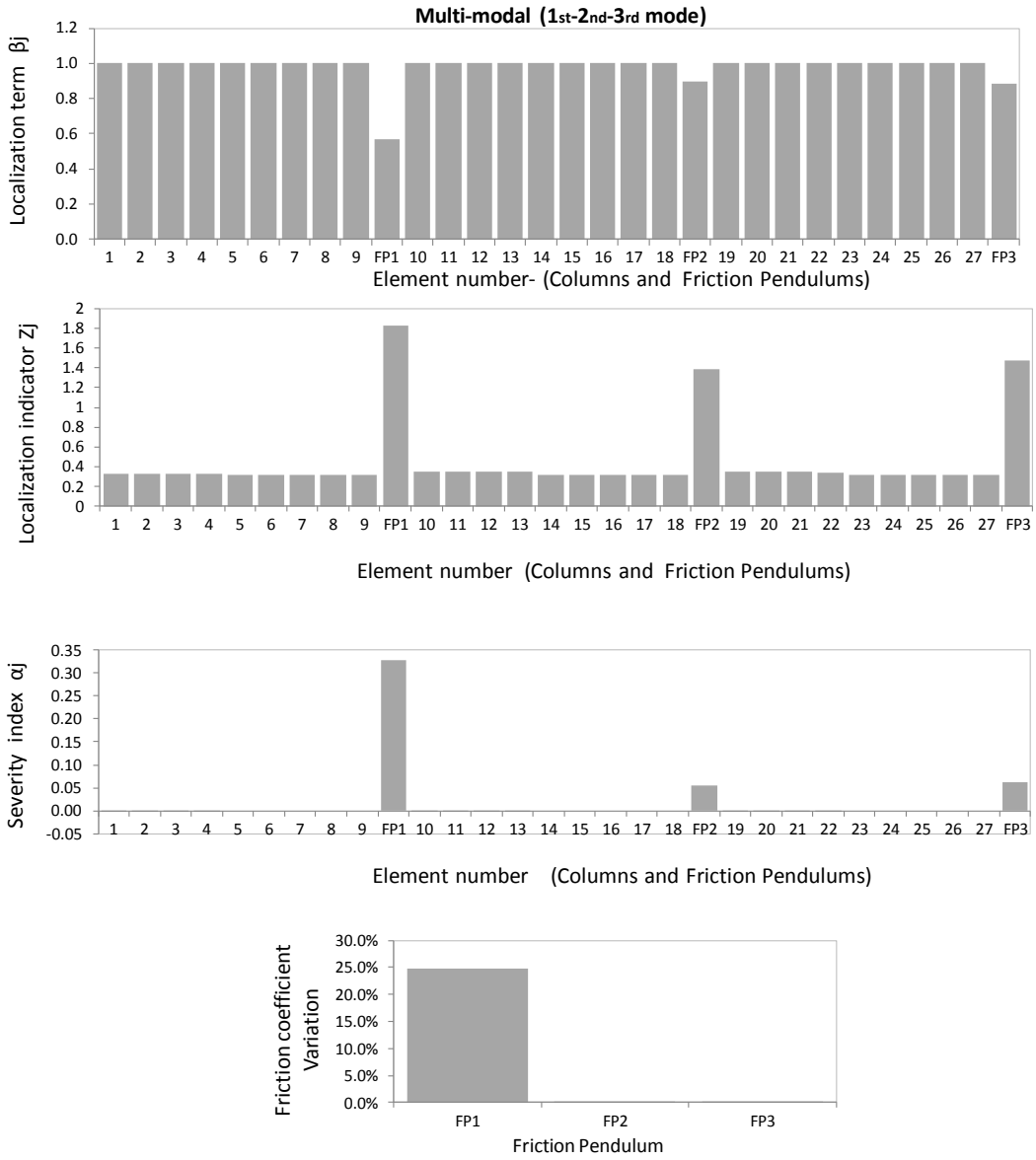

Figure 50. Localization term, localization indicator, severity index for columns' elements and FPs and friction coefficient variation in damage case 12

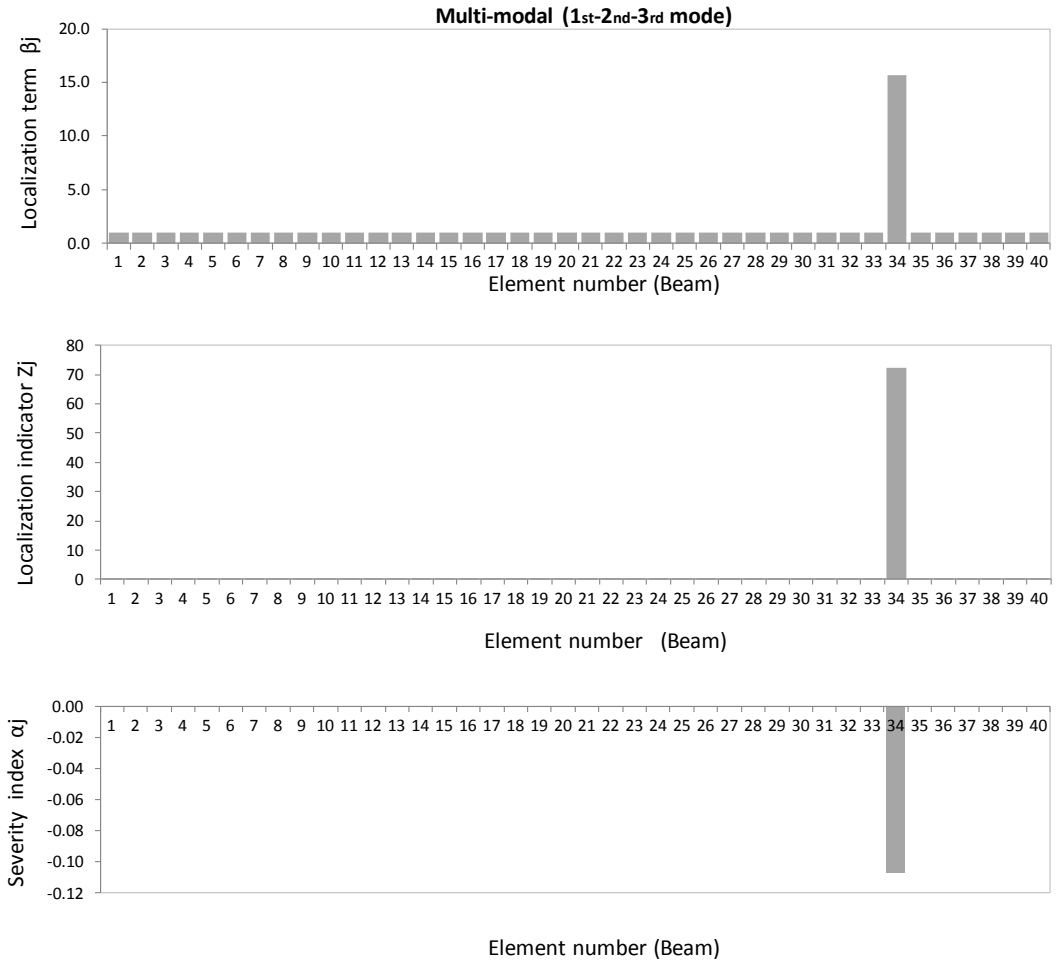

Figure 51. Localization term, localization indicator, severity index for beams' elements in damage case 11

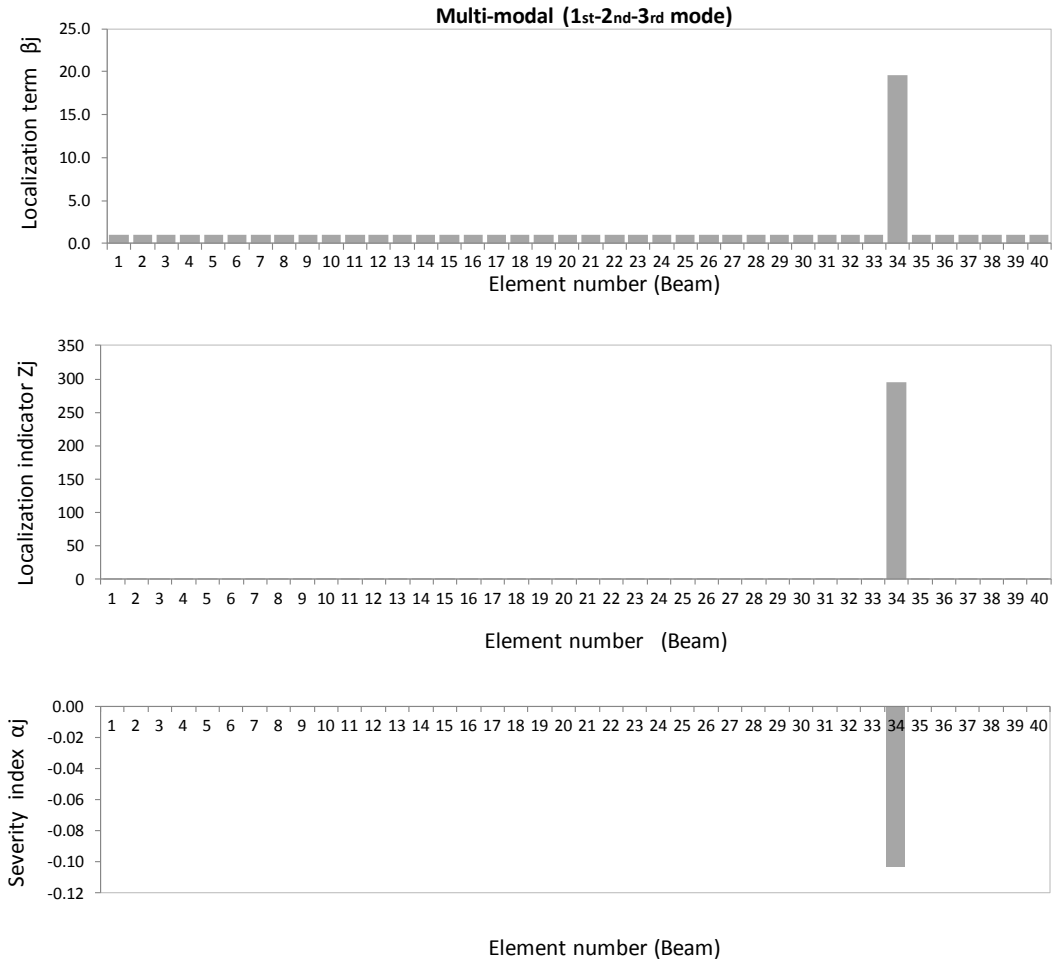

Figure 52. Localization term, localization indicator, severity index for beams' elements in damage case 12

A graphical indication of stiffness variation is visible for isolation devices even when they are not damaged. In order to provide a physical interpretation of the α values for the isolators and to isolate the real occurrence of damage, an additional level of information is required and provided by the measured relative displacements between the top and the bottom of the friction devices. Given the characteristic response of the friction devices the fractional variation $\Delta\mu_j/\mu_j$ of the friction coefficient is obtained from Eq. 32. The current value of the friction coefficient of the *j-th* isolator μ_j^* was then evaluated from Eq. 33.

The predicted friction coefficients are reported in **Table 5**. It can be noted that the additional information provided by the relative displacements across the isolators allows translating the previously indicated values of α (**Table 4**) in terms of effective variation of friction coefficient.

Table 5. Damage prediction results of test-bridge

Damage case:	Devices:	Simulated damage		Stiffness and Deformation Fractional Variation		Predicted damage	
		Variation of Friction Coeff. : $\frac{\mu_j^*-\mu_j}{\mu_j}(\%)$	Friction Coeff.: $\mu_j^*(\%)$	Severity$^+$ $\alpha(\%)$	Variation of Deformations: $\frac{\Delta\sigma_j}{\sigma_j}(\%)$	Variation of Friction Coeff. : $\frac{\mu_j^*-\mu_j}{\mu_j}(\%)$	Friction Coeff.: $\mu_j^*(\%)$
1	FP1	+50	9	+67	-14	+49.7	8.98
	FP2	0	6	+11	-11	+0.2	6.01
	FP3	0	6	+12	-11	+0.3	6.02
2	FP1	+25	7.5	+33	-9	+24.9	7.49
	FP2	0	6	+6	-6	+0.1	6.01
	FP3	0	6	+6	-6	+0.1	6.01
3	FP1	+10	6.6	+12	-3	+9.96	6.60
	FP2	0	6	+2	-2	+0.06	6.00
	FP3	0	6	+2	-2	+0.05	6.00
4	FP1	0	6	+10	-10	+0.16	6.01
	FP2	+25	7.5	+38	-12	+24.85	7.49
	FP3	0	6	+10	-10	+0.16	6.01
5	FP1	+25	7.5	+32	-8	+25.0	7.50
	FP2	0	6	+5	-5	+0.23	6.01
	FP3	+25	7.5	+32	-8	+25.0	7.50
6	FP1	0	6	+7	-7	-0.02	6.00
	FP2	0	6	+2	-3	+0.03	6.00
	FP3	0	6	+7	-3	+0.03	6.00
7	FP1	0	6	+5	-1	0.0	6.00
	FP2	0	6	+3	0	0.0	6.00
	FP3	0	6	+3	0	+0.01	6.00
8	FP1	0	6	+0.1	0	0.0	6.00
	FP2	0	6	+0.1	0	0.0	6.00
	FP3	0	6	+0.1	0	0.0	6.00
9	FP1	+25	7.5	+35	-10	+24.73	7.48
	FP2	0	6	+6	-7	0	6.00
	FP3	0	6	+7	-7	0	6.00
10	FP1	0	6	+7	-7	0.03	6.00
	FP2	0	6	+6	-6	0.02	6.00
	FP3	+25	7.5	+33	-9	+24.74	7.48
11	FP1	0	6	0	0	0	6.00
	FP2	0	6	0	0	0	6.00
	FP3	0	6	0	0	0	6.00
12	FP1	+25	7.5	+33	-9	+24.74	7.48
	FP2	0	6	+6	-6	0	6.00
	FP3	0	6	+6	-6	0	6.00

$^+$Severity (%) = *(E*-E)/E x 100* for column elements
(μ-μ)/μ x 100* for FP isolators

For case 1, for instance, the device FP1 shows a predicted friction coefficient μ_j^*=8.98% almost identical to the imposed friction coefficient (50% increase with respect to the nominal value), while for devices FP2 and FP3 the predicted values of μ_j^*=6.01% and 6.02% indicate the undamaged condition of these devices (original μ_j=6%). In general the approach appears capable of providing a very accurate localization and quantification of the damage for both conventional structural elements and isolation devices as well. The extension of the procedure to alternative type of seismic response modification devices with potential degradation directly related to their stiffness variation, (e.q. viscous dampers) appears straightforward.

4.3. Bridge with Friction Isolators

An additional structure, equipped with friction-based isolators is presented in **Figure 53** and consists of a four span continuous superstructure with maximum distance between piers of 12 m and top elevation under the deck of 5 m. The model represents a portion of the Benicia Martinez Bridge, a 1.2 mile (1.9 km) deck truss bridge opened in 1962 that consists of seven 528-foot (161 m) spans which provide 138 feet (42 m) of vertical clearance. The bridge crosses the Carquinez Strait just west of Suisun Bay. The spans link Benicia, California to the north with Martinez, California. A seismic retrofit project was completed in June 2000 including the installation of isolation bearings in place of the existing steel bearings, a new tapered exterior concrete jacket to most of the piers and adding additional caissons with tie down anchors. The friction pendulum isolation devices are installed at the top of the piers between deck structure and cap beams.

The numerical model representing the bridge structure was assembled using three columns and a continuous deck as shown in **Figure 53**. Only the elements modeling the isolation devices were treated as non linear elements. The friction devices were modeled using a hysteretic behavior proposed by Wen (1976) and Nagarajaiah et al. (1991). In the model, the friction forces are directly proportional to the vertical load on the devices and the friction coefficients are velocity dependant as proposed by Constantinou et al. (1990). The structures have been subjected to a white noise in the frequency range of 0.05-10Hz, with components both in vertical and horizontal directions. From the response obtained via numerical simulation the mode shapes were assessed through the use of the Covariance Driven Stochastic Subspace Identification Method by Peeters (2000).

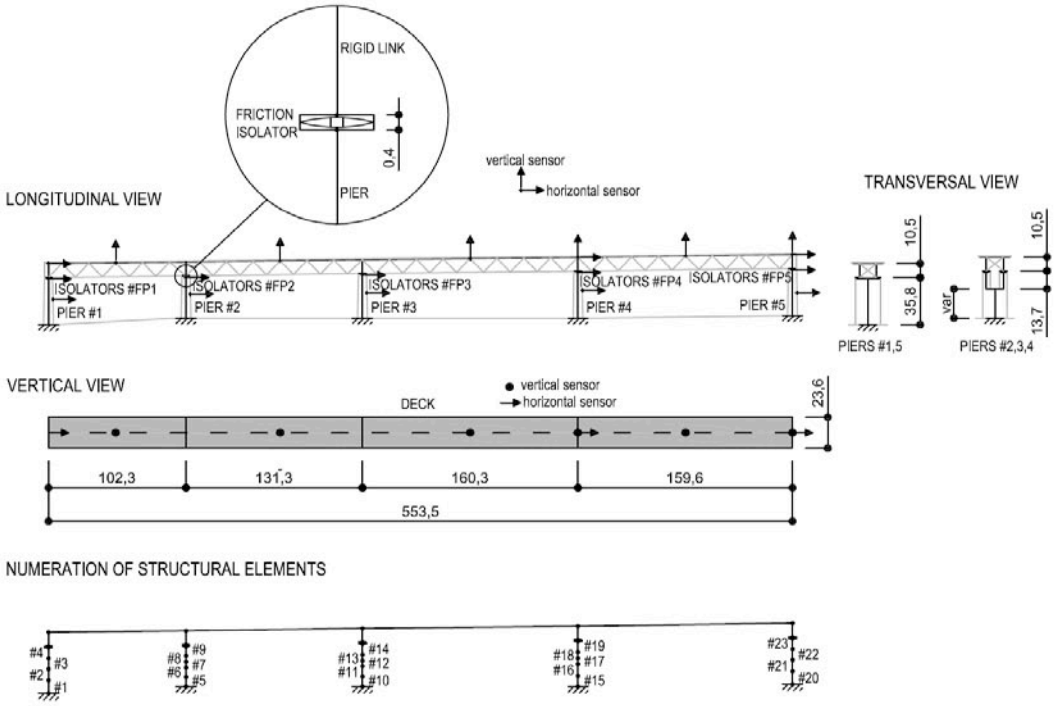

Figure 53. Layout of the bridge with friction isolators.

A total of eight damage scenarios were investigated, with damage location and level of severity indicated in **Table 6**. Each scenario represents a simulated damage event, localized in the friction devices and/or in one element of the bridge pier or of the superstructure. The damage in the piers and the superstructure was simulated by reducing the elastic modulus of appropriate elements (i.e. reducing the stiffness), while the degradation of isolator performance was modeled as a change of the friction coefficient μ.

Table 6. Simulated damages and predicted stiffness variations on the bridge with friction isolators.

Damage case	Simulated damage		Predicted Stiffness Variation	
	Location	Severity[+]	Location	Severity[+] α (%)
1	FP2	+50	FP1, FP2, FP3, FP4, FP5	(+6.9), +30.4, (+7.1), (+7.1), (+6.9)
2	FP2	+25	FP1, FP2, FP3, FP4, FP5	(+6.1), +17.7, (+6.2), (+6.2), (+6.1)
3	FP2	+10	FP1, FP2, FP3, FP4, FP5	(+5.6), +11.0, (+5.7), (+5.8), (+5.6)
4	FP2, FP5	+25,+25	FP1, FP2, FP3, FP4, FP5	(+6.4), +18.2, (+6.6), (+6.6), +17.9
5	FP1,FP2,FP3, FP4,FP5	+25,+25,+25, +25,+25	FP1, FP2, FP3, FP4, FP5	+21.0, +21.5, +21.6, +21.7, +21.0
6	9	-50	5, FP1, FP2, FP3, FP4, FP5	-49.97, (+5.5), (+5.6), (+5.6), (+5.6), (+5.5)
7	9	-10	5, FP1, FP2, FP3, FP4, FP5	-9.95, (+5.5), (+5.6), (+5.6), (+5.6), (+5.5)
8	9, FP2	-10, +25	5, FP1, FP2, FP3, FP4, FP5	-9.94, (+5.9), +17.5, (+6.0), (+6.1), (+5.9)

[+]Severity (%) = (E*-E)/E x 100 for column elements
(μ*-μ)/μ x 100 for FP isolators

In **Figure 54** to **Figure 61** the multi-modal localization term β_j, the localization indicator Z_j, and the severity index α_j, evaluated from Eq. 25, Eq. 26 and Eq. 27 respectively on the first 3 vibration modes of the structure, are graphically reported for each case study. Values are plotted for each element of the model (23 structural elements and 5 friction pendulum isolators). It should be noted that a variation of stiffness is generally identified (Z_j>2) also in undamaged isolators. For example in case no. 8 of **Figure 61**, the numerical values of Z_j show the localization of stiffness variations in the devices FP1, FP2, FP3, FP4 and FP5, as well in the structural element #9. Stiffness variations of the isolators have been translated into friction variations with the use of Eq. 32. The stiffness variation of the isolators FP2 represents an estimated friction coefficient increase of 26.8%; which is very close to the actual simulated variation of +25%. The stiffness variation of isolators FP1, FP3, FP4 and FP5, instead corresponds to practically null variation of friction coefficient (+0.9%, +1.2%, +1.2% and +0.9%). Damage scenarios #6 and #7, characterized by a simulated damage localized in the structural element #9 (top of the second column), shows localization values Z_j>2 in the structural element #9 and in all the devices. The severity index for the damaged element appeared well correlated with the simulated reduction of stiffness for this element while the values of the severity index for the devices translate in a negligible friction coefficient variation.

As before mentioned, the stiffness variation in sliding isolators is not necessarily representative of degradation of the friction coefficient. Any increase of the coefficient of friction in one isolator causes a reduction of the relative displacement between the deck over the isolation plane and the top of the columns. Due to the non linear behavior of these isolators, an apparent variation of stiffness is experienced any time the relative displacement across the isolator varies. This phenomenon appears as an apparent redistribution of the damage from one isolator to the closest undamaged isolators. For this reason, the severity index α_j can not be interpreted as a direct indicator of damage but should be converted into a friction variation through Eq. 32.

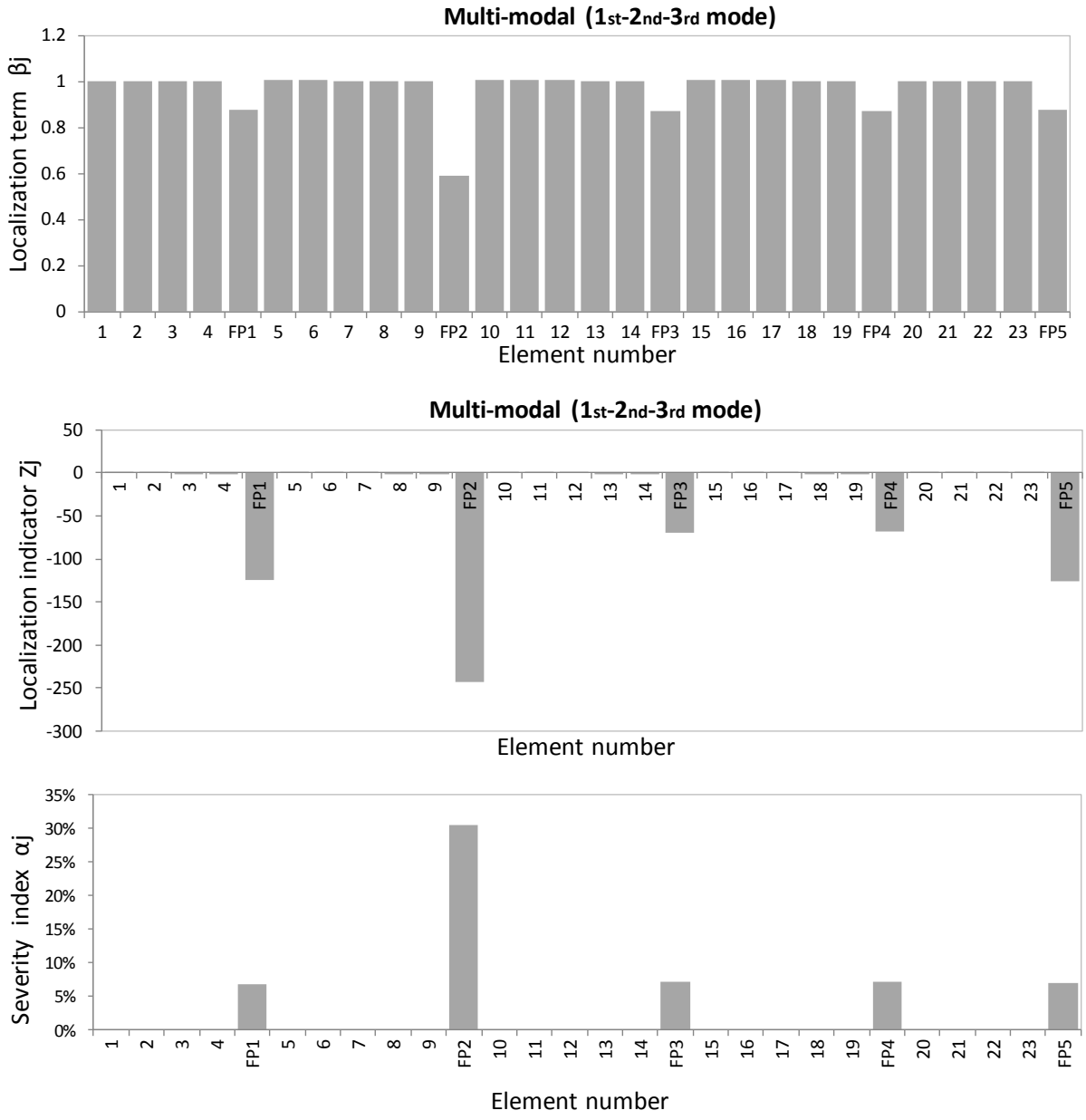

Figure 54. Localization terms β_j, localization index Z_j and severity index α_j for damage case 1.

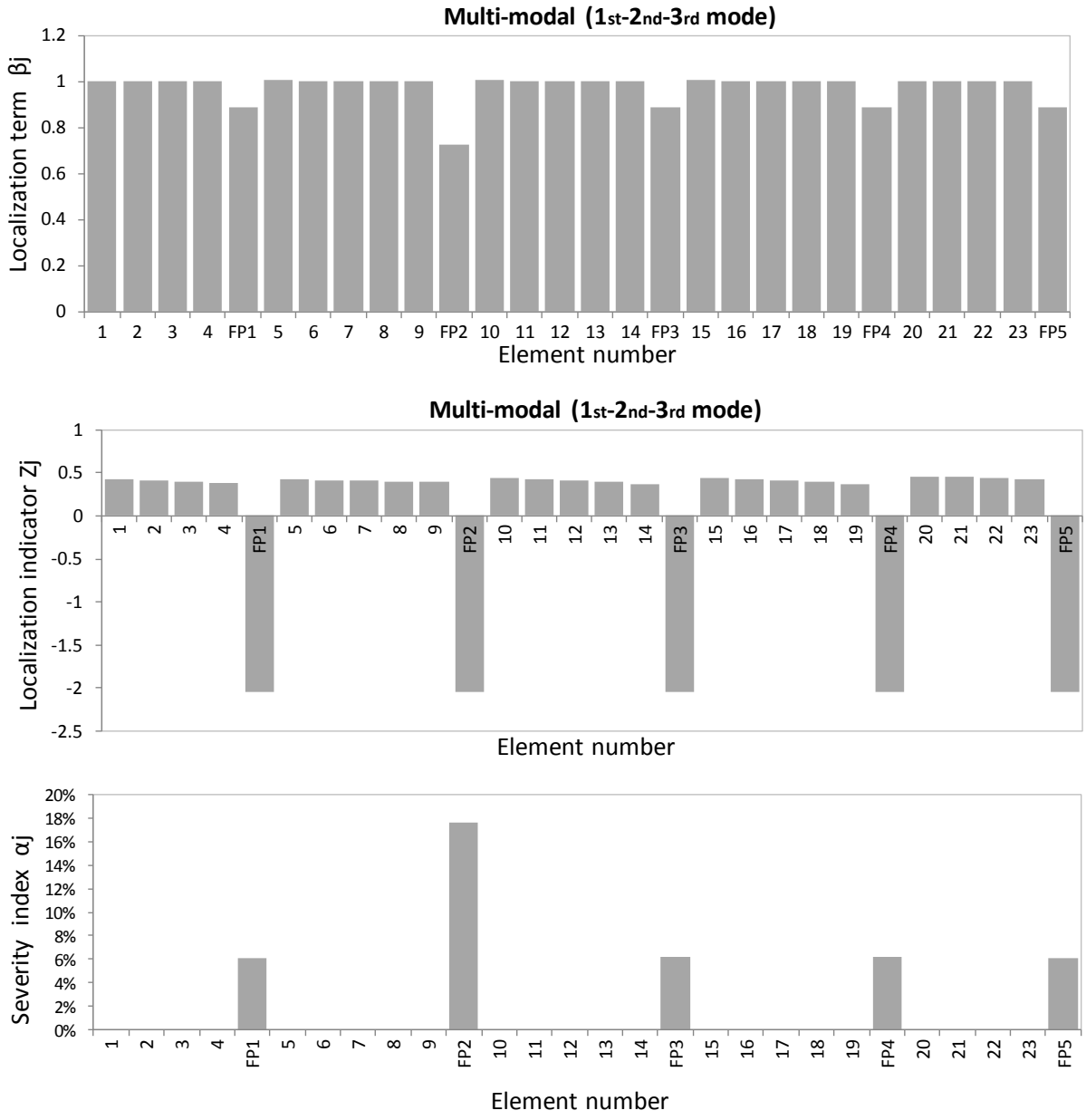

Figure 55. Localization terms β_j, localization index Z_j and severity index α_j for damage case 2.

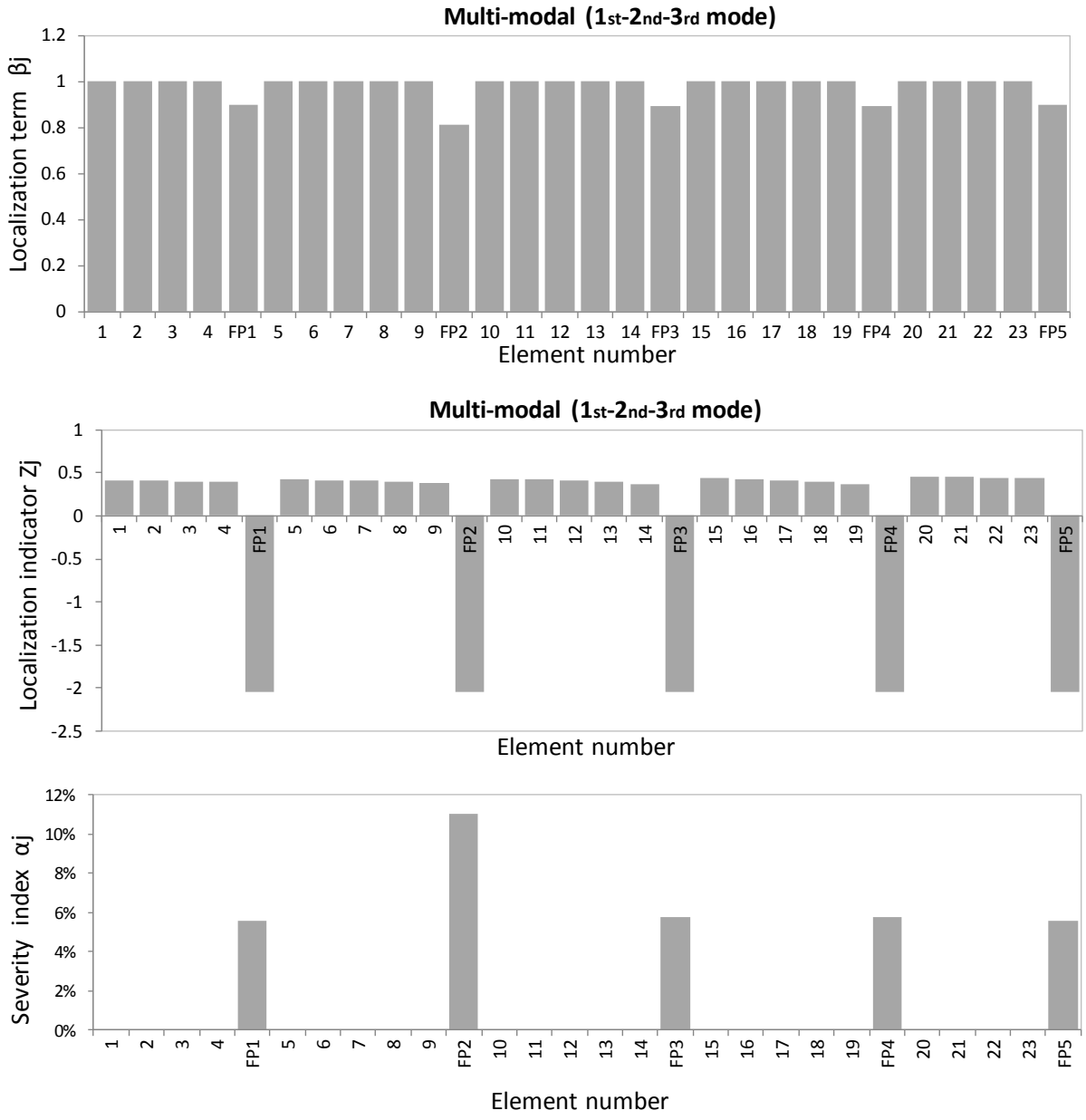

Figure 56. Localization terms β_j, localization index Z_j and severity index α_j for damage case 3.

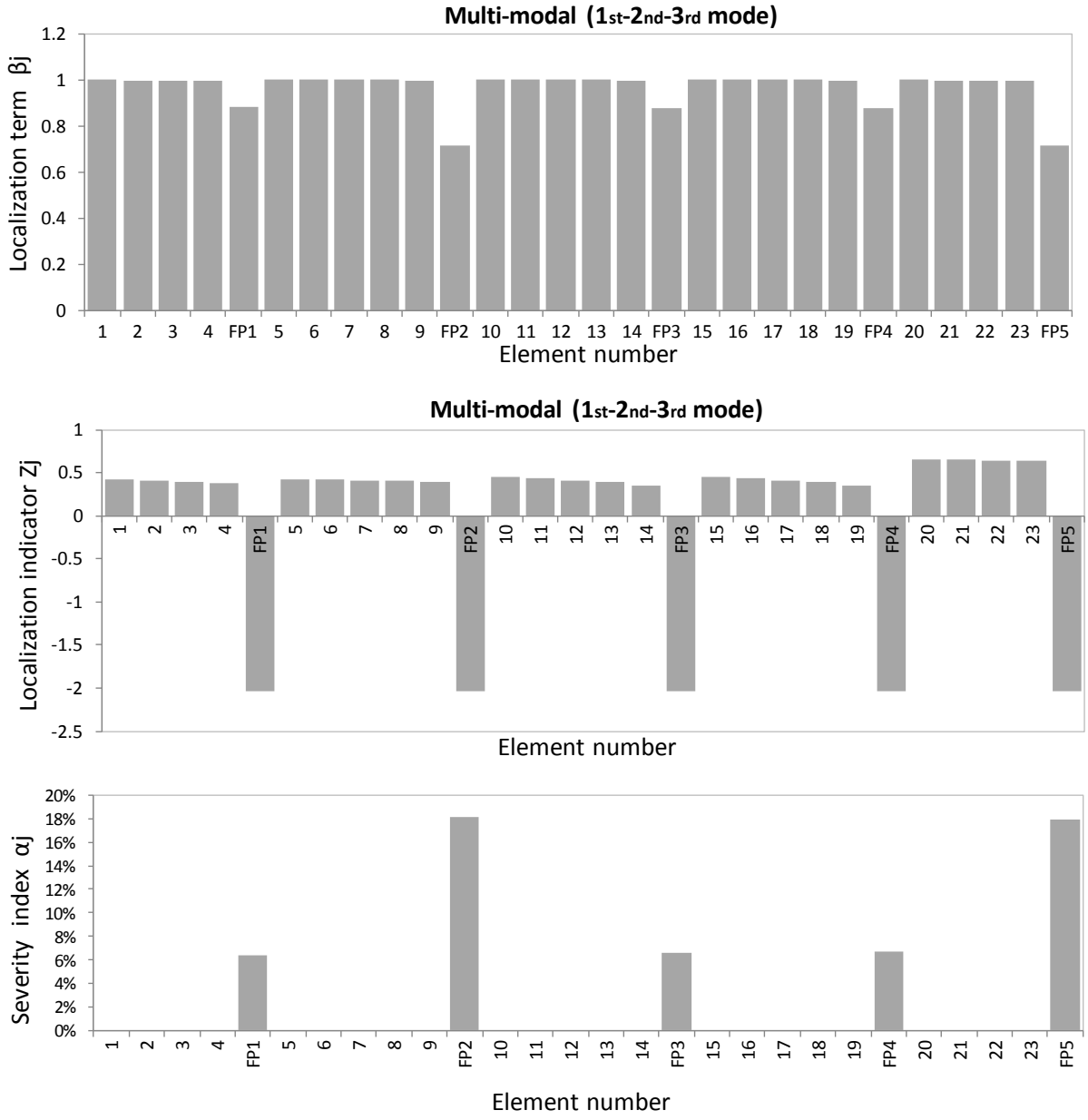

Figure 57. Localization terms β_j, localization index Z_j and severity index α_j for damage case 4.

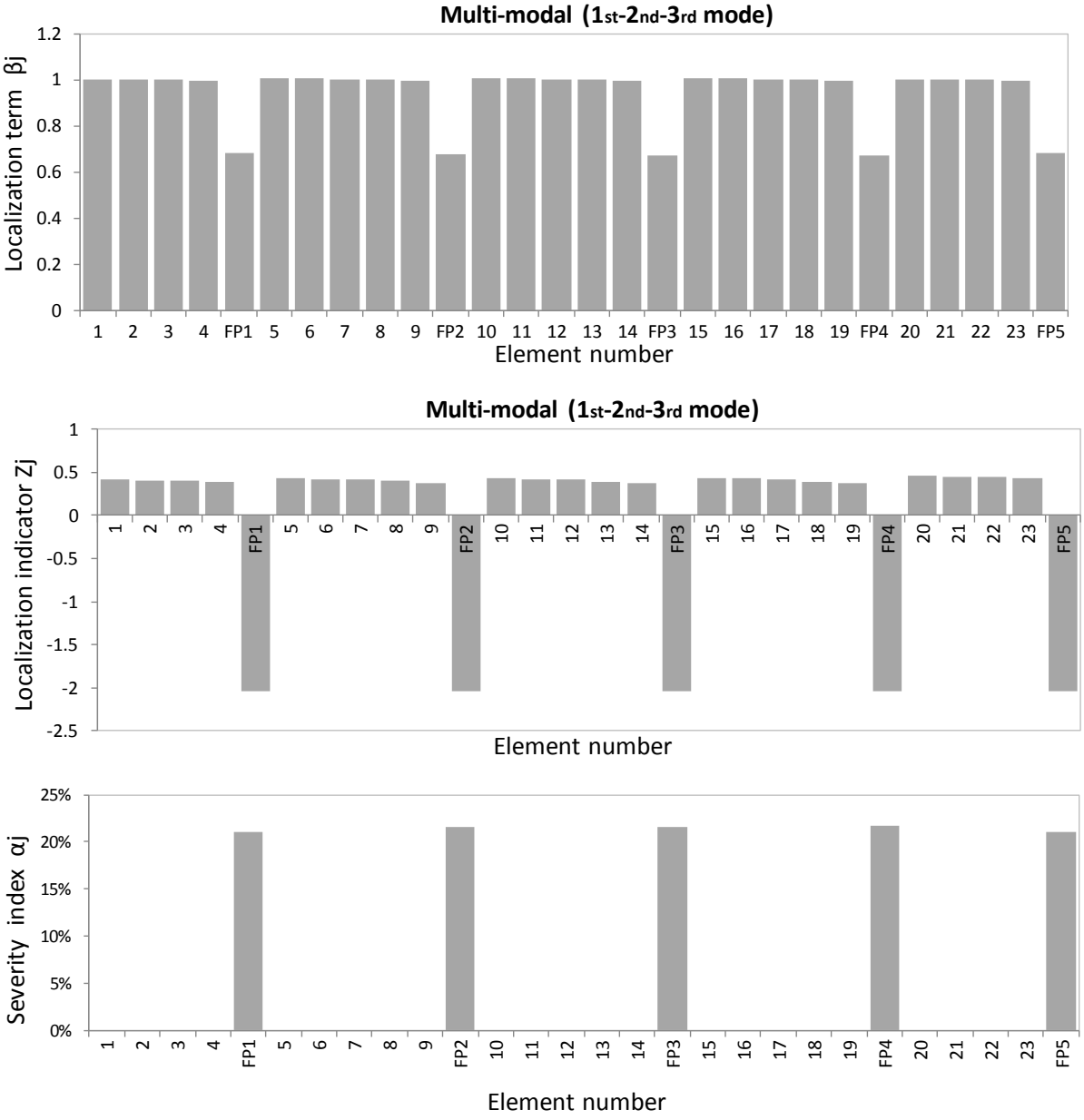

Figure 58. Localization terms β_j, localization index Z_j and severity index α_j for damage case 5.

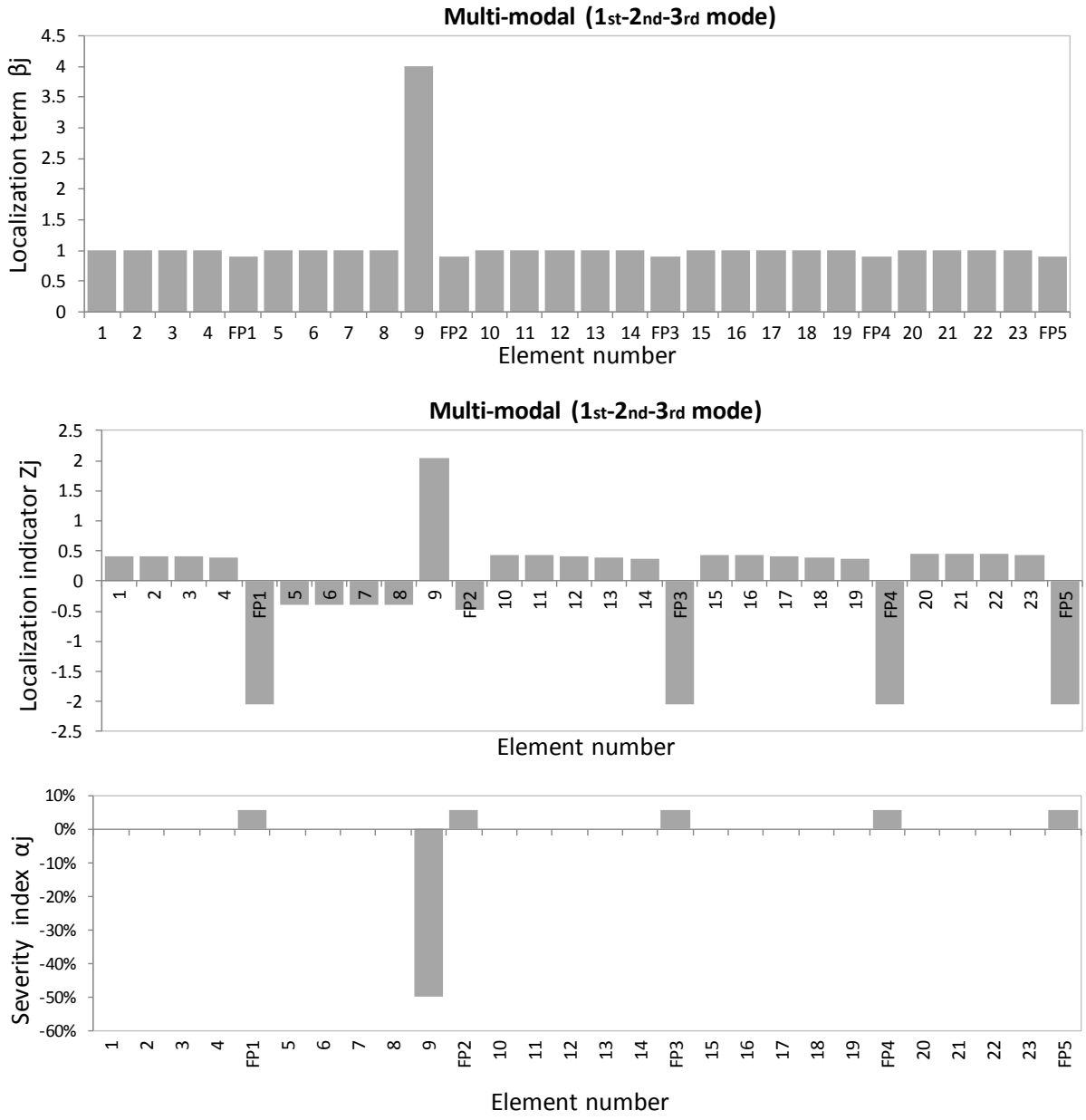

Figure 59. Localization terms β_j, localization index Z_j and severity index α_j for damage case 6.

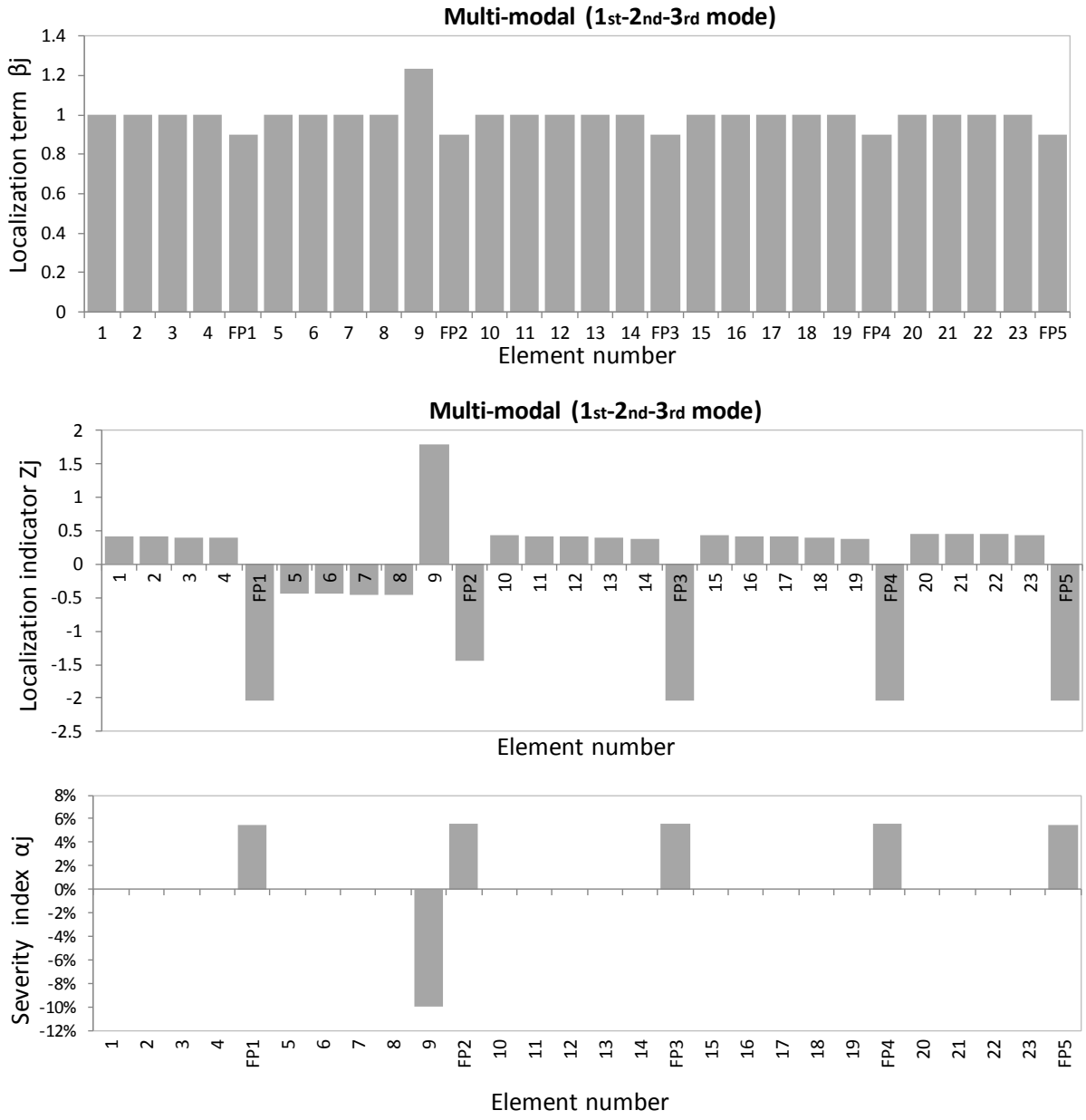

Figure 60. Localization terms β_j, localization index Z_j and severity index α_j for damage case 7.

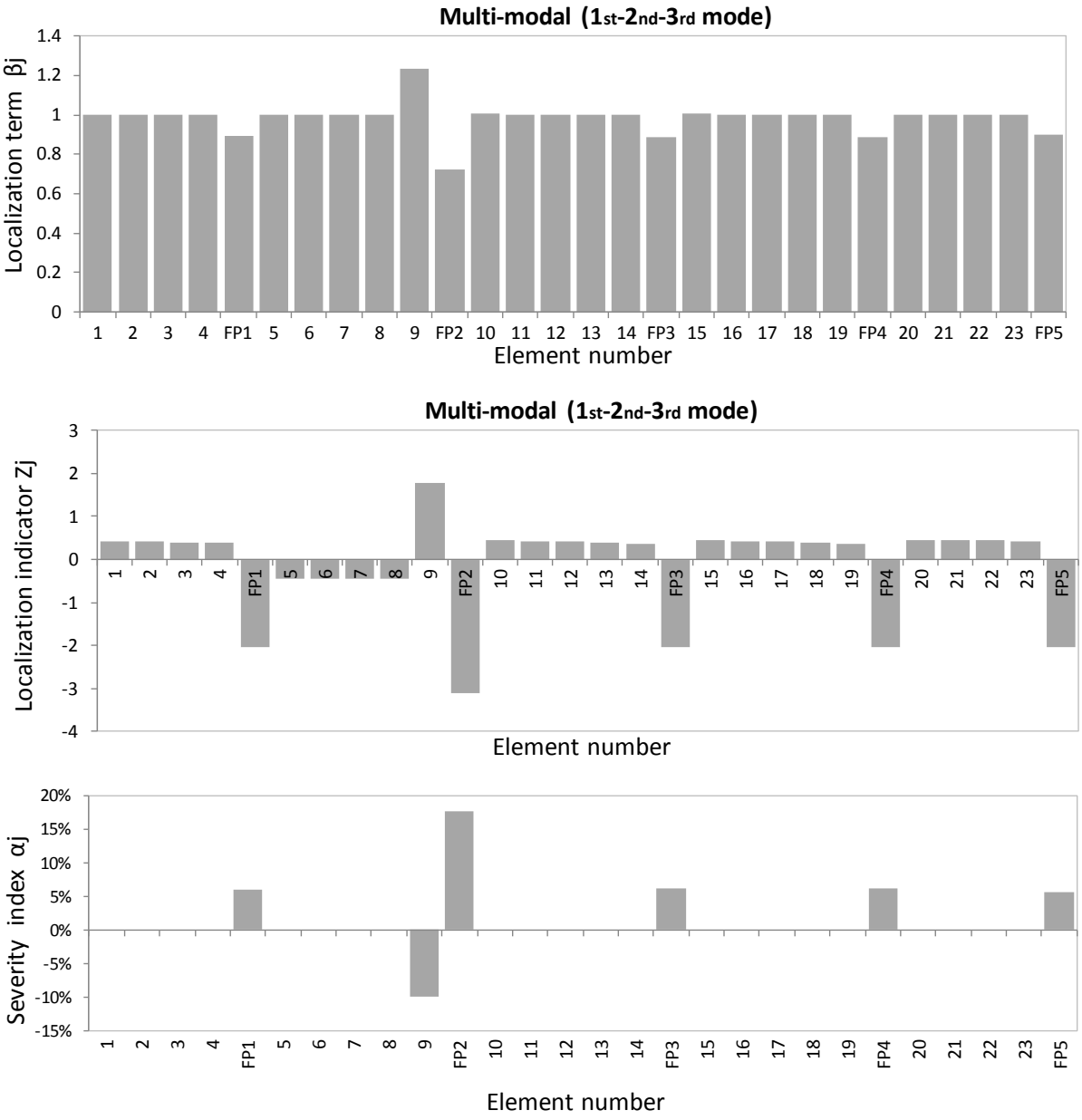

Figure 61. Localization terms β_j, localization index Z_j and severity index α_j for damage case 8.

In **Table 7** the variation of friction coefficient simulated and predicted through Equation 32 are reported for each damage case and for each device. The procedure applied to this case study demonstrates an high level of accuracy in the prediction of friction coefficient variation with a maximum error lower than 3%. The highest level of error of 2.1% corresponds to the damage case #3 characterized by a low level damage (friction coefficient variation of 10%) simulated in the device FP1.

Table 7. Simulated damages and predicted variations on the coefficient of friction of the isolators.

Damage case	Simulated damage Severity[+]					Predicted damage : Variation of friction coefficient (Eq. 32)				
	FP1	FP2	FP3	FP4	FP5	FP1	FP2	FP3	FP4	FP5
1	+0	+50	+0	+0	+0	+0.0	+50.6	+0.5	+0.5	+0.0
2	+0	+25	+0	+0	+0	+0.0	+25.4,	+0.4	+0.4	+0.0
3	+0	+10	+0	+0	+0	+0.0	+12.1	+0.5	+0.4	+0.0
4	+0	+25	+0	+0	+25	+0.0	+25.5	+0.5	+0.5	+25.0
5	+25	+25	+25	+25	+25	+25.1	+26.0,	+26.1,	+26.0,	+25.1
6	+0	+0	+0	+0	+0	+0.0	+0.4	+0.3	+0.2	+0.0
7	+0	+0	+0	+0	+0	+0.0	+0.3	+0.3	+0.2	+0.0
8	+0	+25	+0	+0	+0	+0.9	+26.8,	+1.2	+1.2	+0.9

[+]Severity (%) = $(\mu^*-\mu)/\mu$ x 100 for FP isolators

4.4. Bridge with Viscous dampers

A numerical model of a suspension bridge that represents a simplification of the Vincent Thomas Bridge was used to test the procedure on structures equipped with viscous dampers. The structure is presented in **Figure 62** and consists of a cable-suspension bridge 766 m long, with a main suspended span of approximately 457.2 m, two suspended side spans of 154.4 m each, a roadway width of approximately 15.8 m. The bridge is equipped with four sets of dampers located between towers and spans.

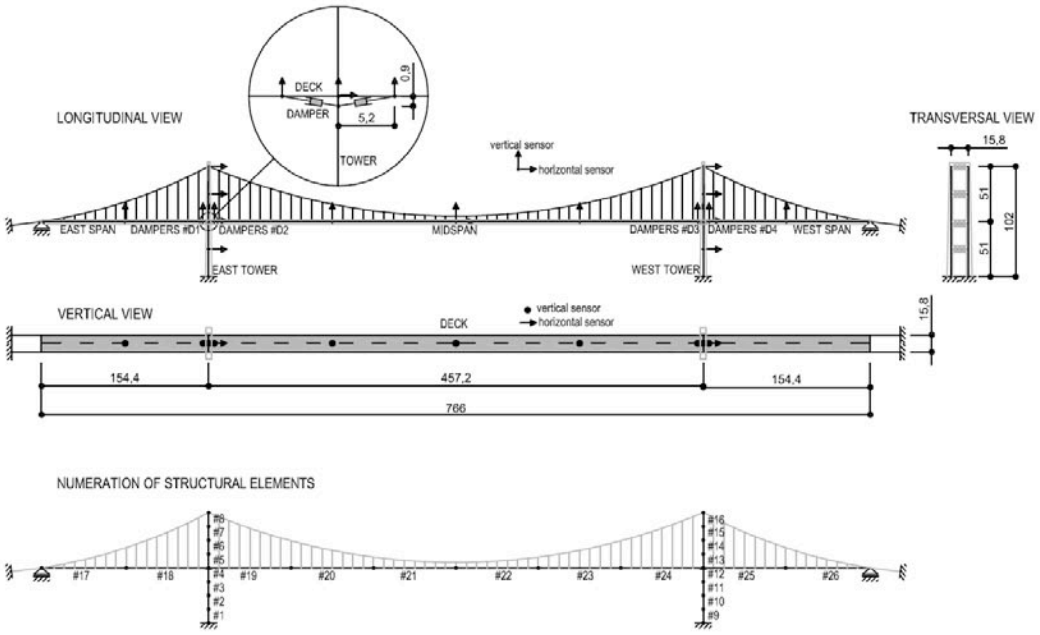

Figure 62. Layout of the bridge with viscous dampers.

Eight damage cases were investigated, with damage location and level of severity indicated in **Table 8**. Each scenario represents a simulated damage event, localized in the viscous dampers and/or in one element of the bridge pier or of the superstructure. The damage in the piers and the superstructure was simulated by reducing the elastic modulus of appropriate elements (i.e. reducing the stiffness), while the degradation of the damper performance was modeled as a reduction of its damping coefficient In case 1, 2 and 3 the damage has been introduced in the damper D1 with different levels of intensity (high, medium and low). The predicted stiffness variations, expressed as severity index values, were calculated by Eq. 27 and reported in **Table 8**. Stiffness variations have been translated into variations of damping ratio by Eq. 34. The predicted damage in term of variation of damping has been compared with the simulated damage for each damper and results are reported in **Table 9**.

Table 8. Simulated damages and predicted variations on the bridge with viscous dampers

Damage	Simulated damage		Predicted Stiffness Variation	
case	Location	Severity[+]	Location	Severity[+] α (%)
1	D1	-50	D1, D2	-25.6, -25.3
2	D1	-25	D1, D2	-11.8, -11.6
3	D1	-10	D1, D2	-5.4, -5.6
4	D1, D2	-25, -25	D1, D2	-25.2, -25.2
5	D1, D2, D3, D4	-25, -25, -25, -25	D1, D2, D3, D4	-24.9, -25.3, -25.3, -24.9
6	D3, D4, 17	-25, -25, -25	D3, D4, 17	-25.01, -25.04, -25.6
7	17	-50	17	-48.4
8	17	-25	17	-25.03

[+]Severity (%) = (E*-E)/E x 100 for column elements

= (μ*-μ)/μ x 100 for FP isolators

Table 9. Simulated damages and predicted variations on the viscous dampers

Damage case	Simulated damage Severity[+]				Predicted damage : Variation of damping ratio. $\Delta\xi_j \big/ \xi_j$ (Eq. 34)			
	D1	D2	D3	D4	D1	D2	D3	D4
1	-50	-0	-0	-0	-25.4	-25.1	-0.0	-0.0
2	-25	-0	-0	-0	-12.2	-12.0	-0.0	-0.0
3	-10	-0	-0	-0	-5.2	-5.3	-0.0	-0.0
4	-25	-25	-0	-0	-25.2	-25.2	-0.0	-0.0
5	-25	-25	-25	-25	-24.9	-25.3	-25.3	-24.9
6	-0	-0	-25	-25	-0.0	-0.0	-25.02	-25.3
7	-0	-0	-0	-0	-0.0	-0.0	-0.0	-0.0
8	-0	-0	-0	-0	-0.0	-0.0	-0.0	-0.0

[+]Severity (%) = (ξ*-ξ)/ξ x 100 for viscous dampers

It must be noted that the predicted damage, even if simulated in only one damper, appears always equally divided between both the dampers converging on the same tower (D1-D2 and D3-D4). This is due to the mechanism of interaction between dampers and bridge structure. The dampers in fact, work as a parallel system in connecting the deck to the

tower. In the damage detection algorithm only in-plane vibrational modes have been used, with the longitudinal swinging mode of the bridge as principal contributing component. To distinguish damages in dampers concurring to the same tower, lateral modes should be included in the analysis and 3D deformations of the structure have to be considered.

In **Figure 63** to **Figure 70** the localization terms β_j, obtained through the multimodal combination of Eq. 25 taking into account the first three structural modes, the localization indicators Z_j and the severity indices α_j are graphically reported for each damage case. The localization indices show a clear localization of the damaged elements for all the scenarios. As expected, the localization is noisy when damages have a low severity, such as in case #3 of **Figure 65** where only 10% of variation of the damping ratio of one damper was simulated.

The localization indicators Z_j for this structure indicate a lower level of accuracy underlined by the reduced (but not zero) values for undamaged elements (see for instance **Figure 65**). This phenomenon is attributed to the peculiar bridge response variation in case of degradation of the damper performance. The structural response appears in fact particularly sensitive to the performance of the energy dissipators. The damper's degradation results in significant variations of the curvature of the mode shapes with consequent high values of the term $\beta_{i,jk}$, in case of very small denominator of Eq. 17. The use of a higher number of mode shapes involved in the proposed algorithm proved to significantly mitigate this effect.

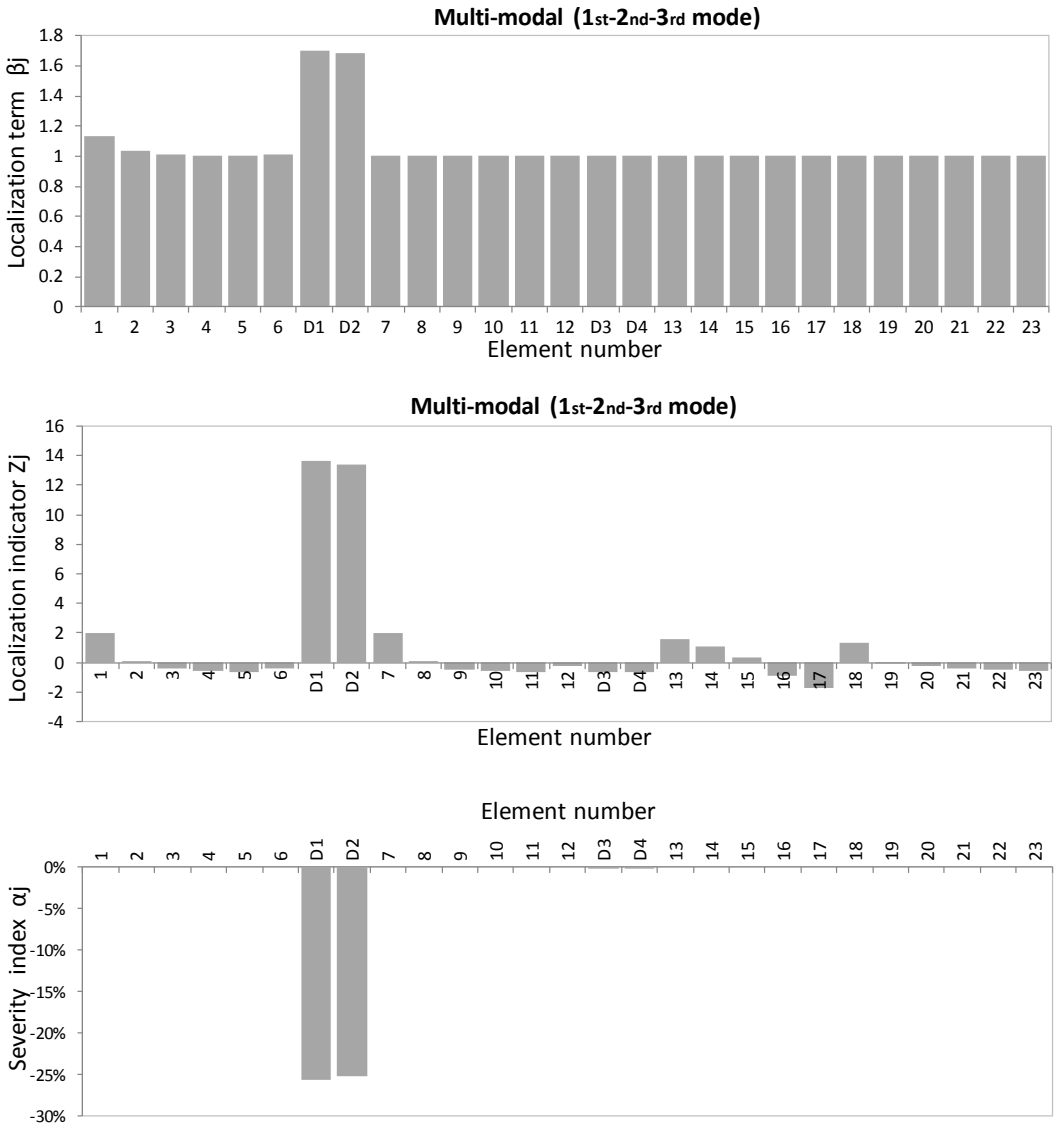

Figure 63. Localization terms β_j, localization index Z_j and severity index α_j for damage case 1.

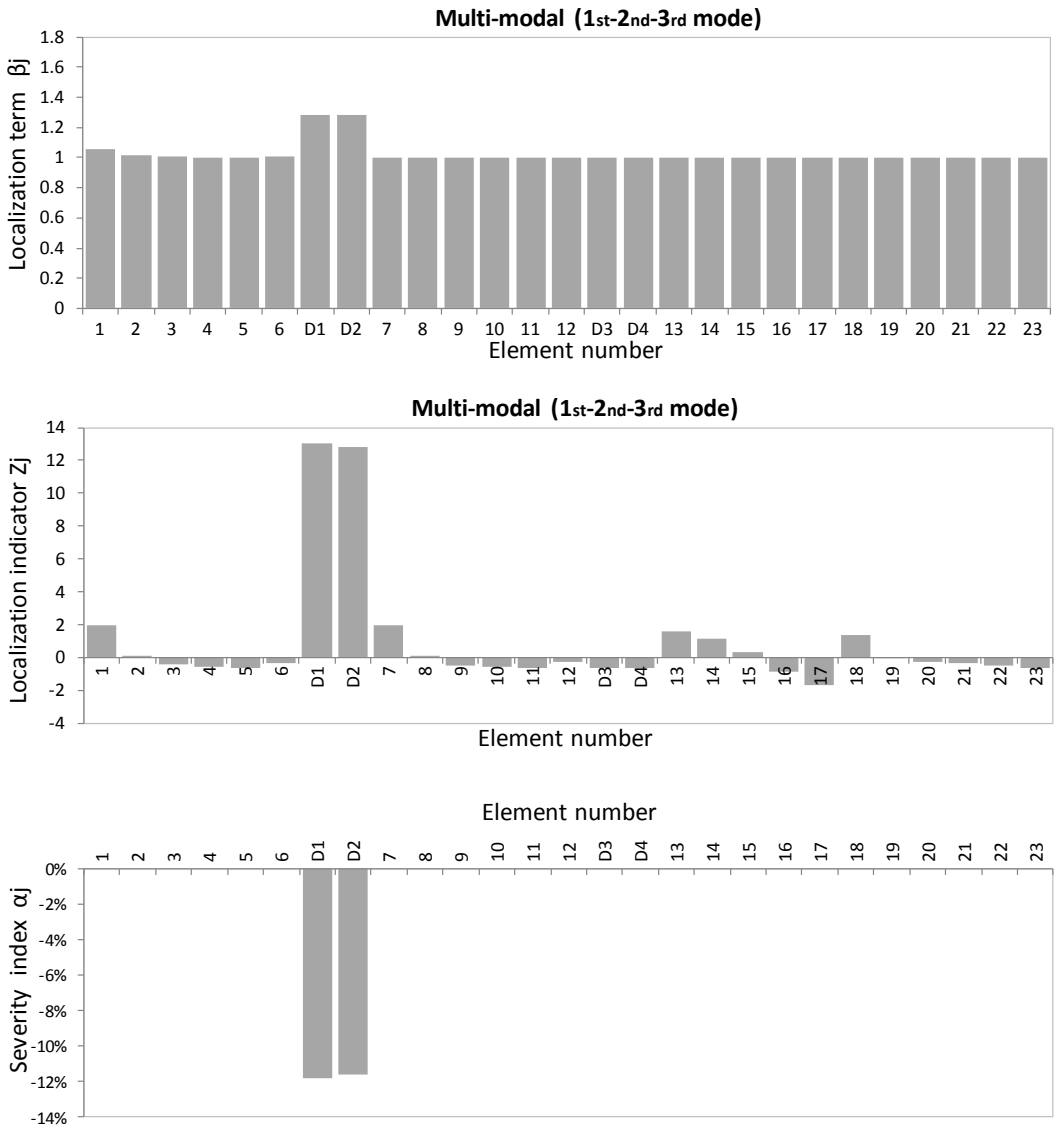

Figure 64. Localization terms β_j, localization index Z_j and severity index α_j for damage case 2.

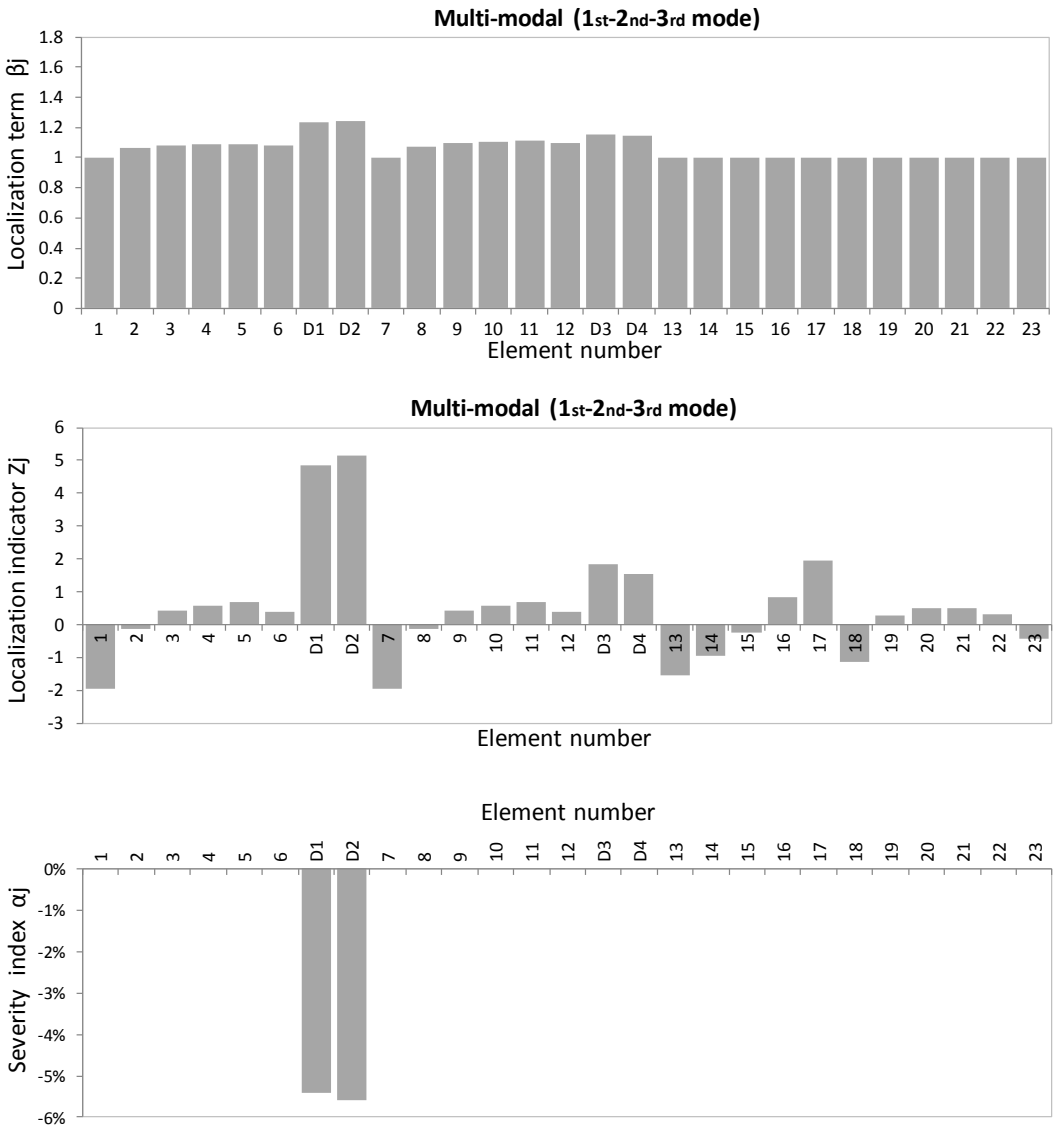

Figure 65. Localization terms β_j, localization index Z_j and severity index α_j for damage case 3.

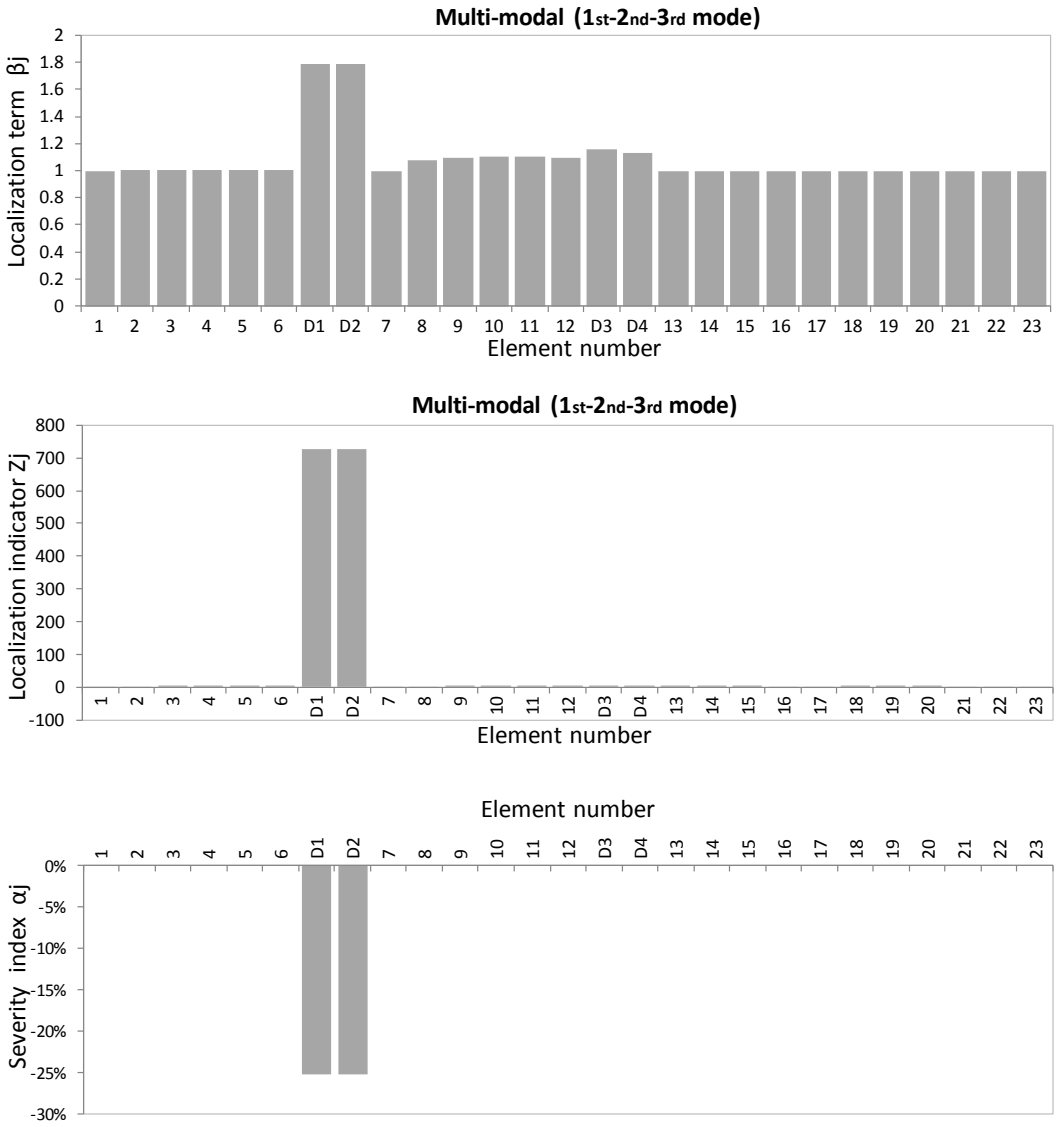

Figure 66. Localization terms β_j, localization index Z_j and severity index α_j for damage case 4.

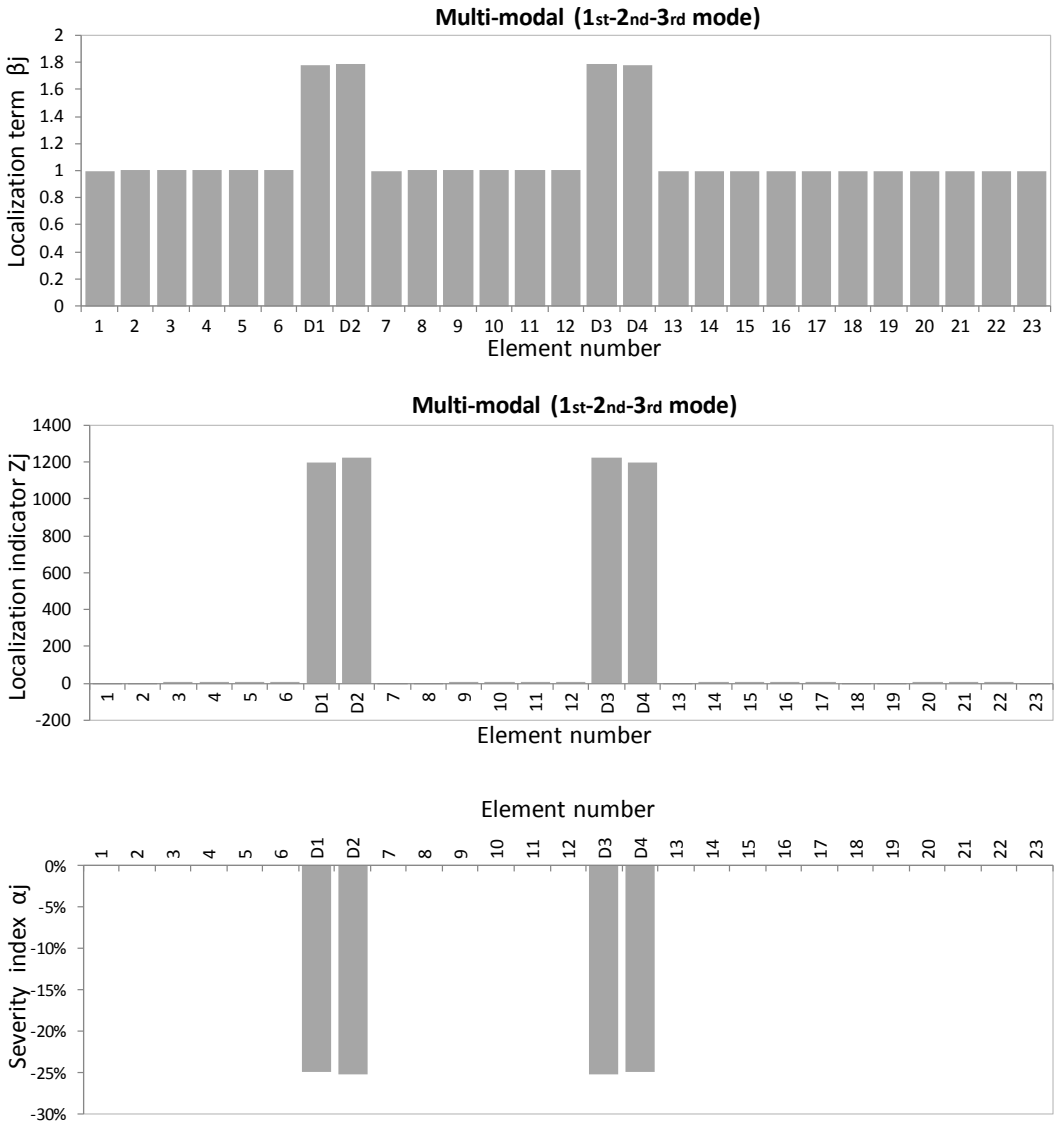

Figure 67. Localization terms β_j, localization index Z_j and severity index α_j for damage case 5.

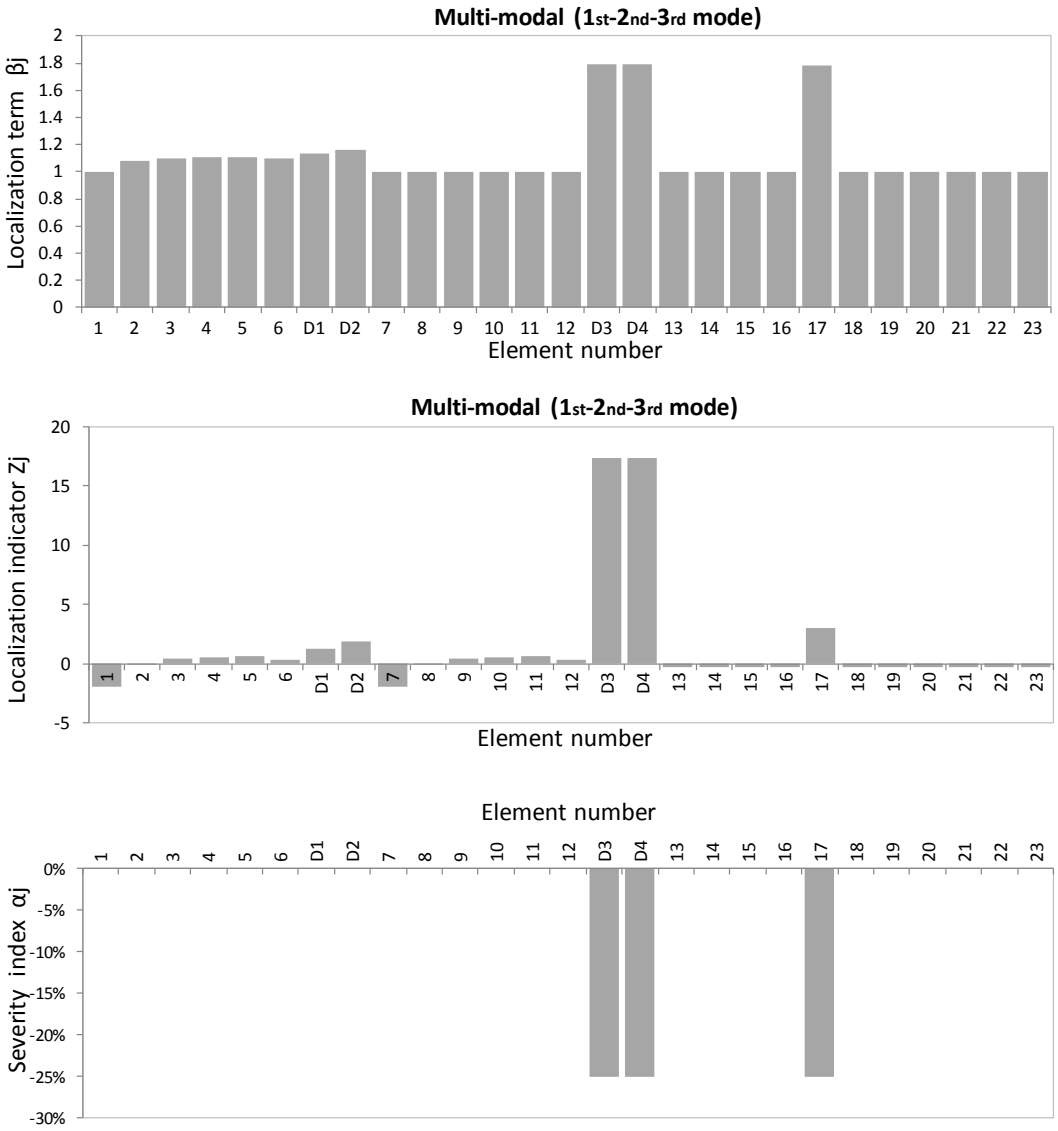

Figure 68. Localization terms β_j, localization index Z_j and severity index α_j for damage case 6.

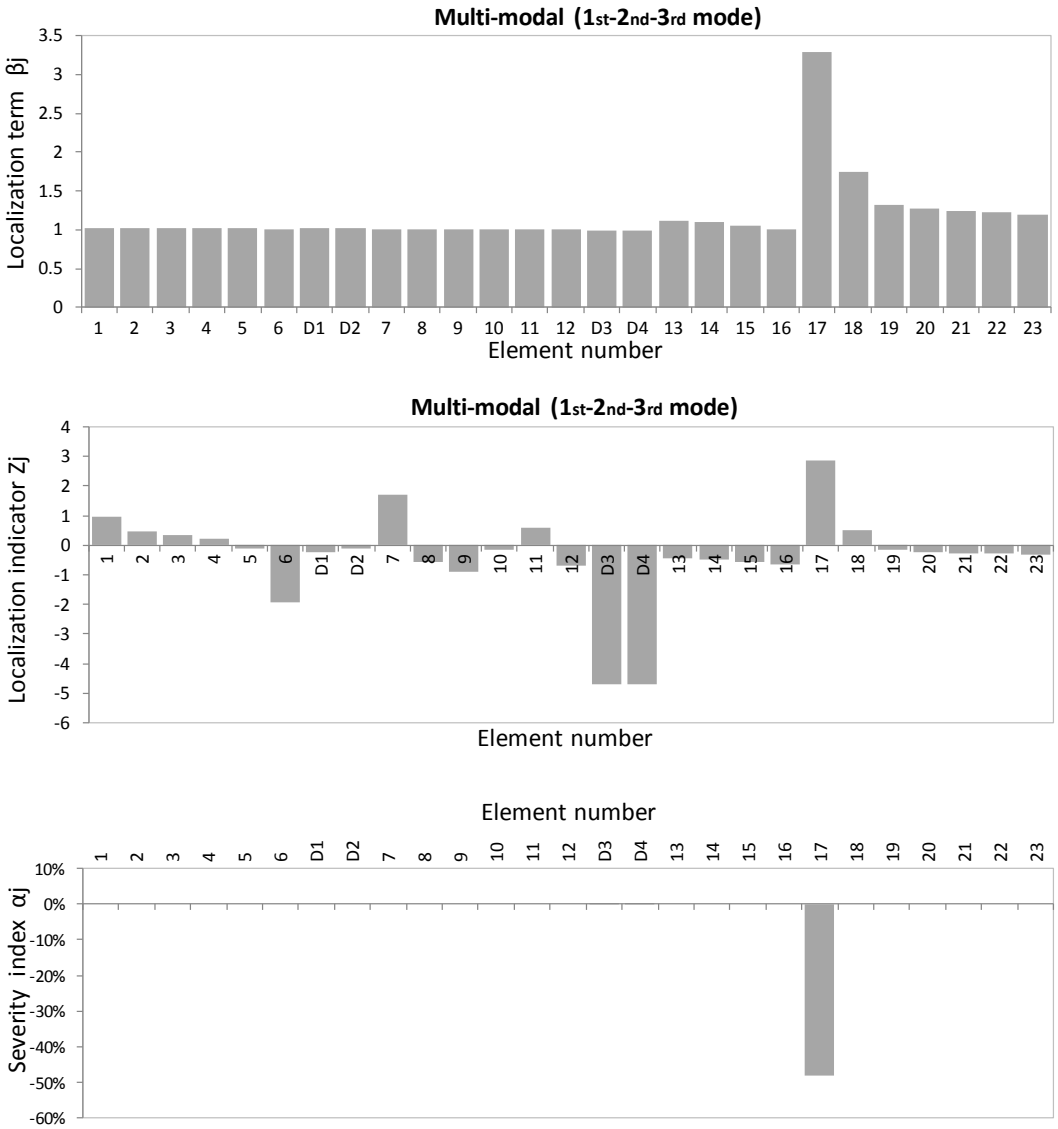

Figure 69. Localization terms β_j, localization index Z_j and severity index α_j for damage case 7.

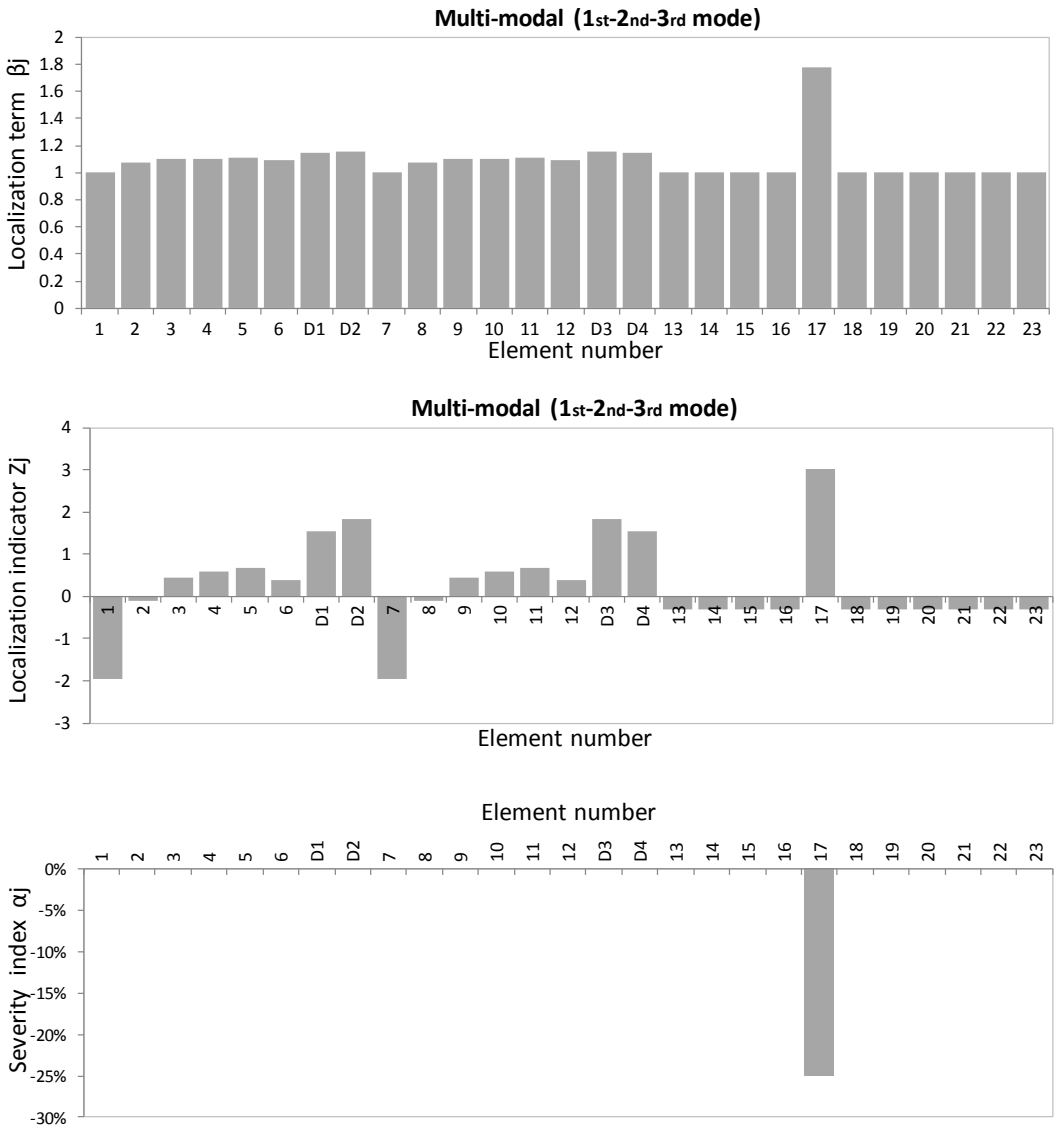

Figure 70. Localization terms β_j, localization index Z_j and severity index α_j for damage case 8.

5. Vincent Thomas Bridge application

The main case study of the overall research project consists of the Vincent Thomas Bridge, a cable-suspension structure retrofitted in different stages, and lately equipped with 48 viscous dampers. The Vincent Thomas Bridge is located in the Los Angeles metropolitan's area (**Figure 71**) on Route 47 (P.M. 0.86). The route is a critical artery for commercial traffic in and out of Los Angeles Harbor, and is a risk in the seismically active Southern California Region, particularly because it straddles the Palos Verdes fault zone. The structure is a cable suspension bridge, 1849 m long, consisting of a main suspended span of approximately 457.5m, two suspended side spans of 154 m each, ten spans in the San Pedro Approach of approximately 560.6 m total length, and ten spans in the Terminal Island Approach of approximately 522 m total length (see **Figure 72**, **Figure 73**, and **Figure 74**). The roadway width between curbs is typically 16 m, and accommodates four lanes of traffic. The clear height of the navigation channel is approximately 56.4 m. The design of the bridge was completed by Caltrans in 1960. The substructure contract was completed in 1962 while the superstructure contract was completed in early 1964. Stage 1 seismic upgrading in the form of cable restrainers, shear keys abutment seat extenders and girder lateral supports was completed in 1980.

Modifications to the vertical cross frames, and the lateral bracings near the bents, and inclusion of a full length cat-walk were also made in 1980 as part of the seismic upgrading contract. New elevators at Bents 9 and 15 were added in 1992. In 1998 a seismic retrofit was completed consisting on the installation of dampers (**Figure 75** and **Figure 76**) between the stiffening trusses and the towers of the bridge, stiffening of the bridge towers, as well as installation of structural fuses in the side spans of the bridge. There are generally two main strategies for seismic retrofit of structures; strengthening, to increase the capacity for resisting the seismic demand, or using isolation or energy dissipation devices to reduce the seismic demand. Both approaches could also be combined to achieve an optimal solution. It is typical in retrofitting old steel suspension bridges to strengthen their towers, stiffening trusses and, more importantly, the

connection of the deck system to the towers. At expansion joints, cable restrainers could be used to reduce the earthquake movements and, in some cases where their use is not enough to resist unseating leading to potential collapse, catcher blocks are used to avoid collapse. Additionally, sacrificial expansion joints, also known as structural fuses, have been used on a limited scale to provide additional movements during earthquakes and may potentially be used for a broader range of bridges if design details and guidelines are developed for their use. Energy dissipation devices (dampers) have also been used on a limited scale as a seismic retrofit measure for long span suspension bridges by absorbing energy from the structural system and then dissipating it, usually as heat. For such long-span bridges, these devices need to be large, able to perform in extreme environments, reliable, and durable with low maintenance. The plan proposed for the seismic upgrade of the Vincent-Thomas Suspension Bridge included both tuning the bridge to reduce the violent actions caused by the ground motion of a strong earthquake, and strengthening the bridge to minimize the damage caused by these actions. Among the major seismic retrofit measures proposed were providing longitudinal viscous dampers in the suspended side spans to dampen the axial forces in the stiffening truss members, in addition to other dampers placed between the bridge stiffening truss and the towers in both the center and side spans, and between the truss and the cable bents in the side spans. Another retrofit measure was to allow the formation of plastic hinges at the base of the tower shafts during severe seismic events in order to limit the longitudinal bending moment at the tower base to its plastic moment capacity. These proposed retrofit schemes have been evaluated in this investigation by performing a rigorous nonlinear seismic-response analysis of the as-built bridge and the retrofitted bridge, using a three-dimensional analytical model of the bridge provided by the California Department of Transportation (Caltrans). Such numerical model, including cables, suspenders, suspended structure, towers, cable bents and anchorages, reflects the state of the structure after the last retrofit phase, when dampers and fuses were installed and towers were stiffened. The static and time-history analyses of the bridge were both geometrically nonlinear (large displacement analyses) to account for the geometric stiffness of the cables and suspenders.

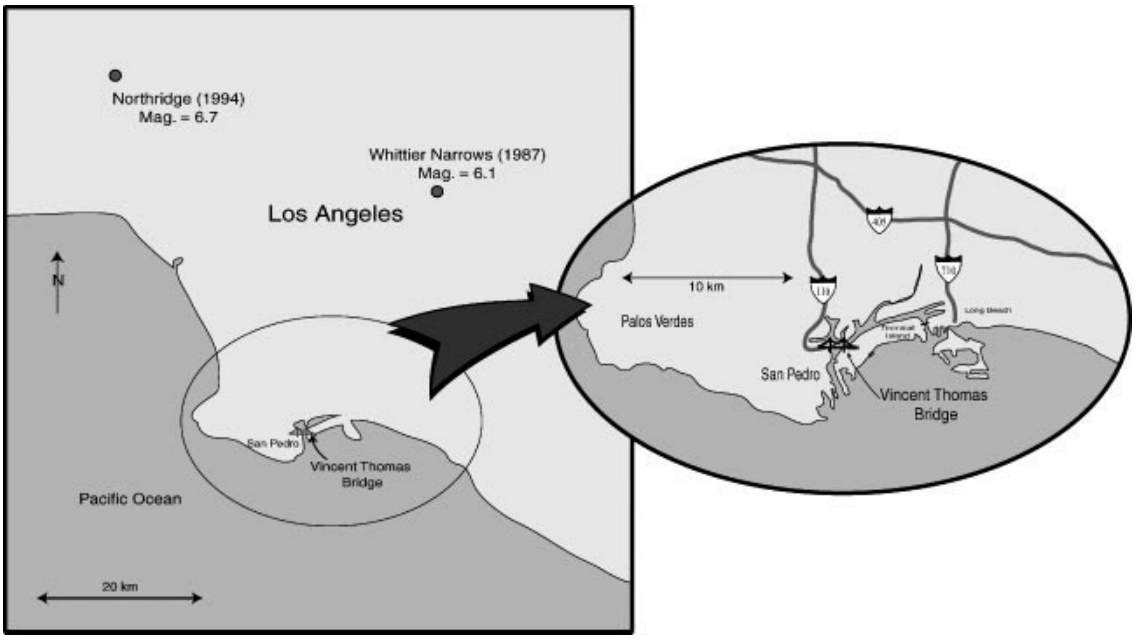

Figure 71. Location of the Vincent Thomas Bridge with respect to the 1987 Whittier Narrows earthquake and the 1994 Northridge earthquake.

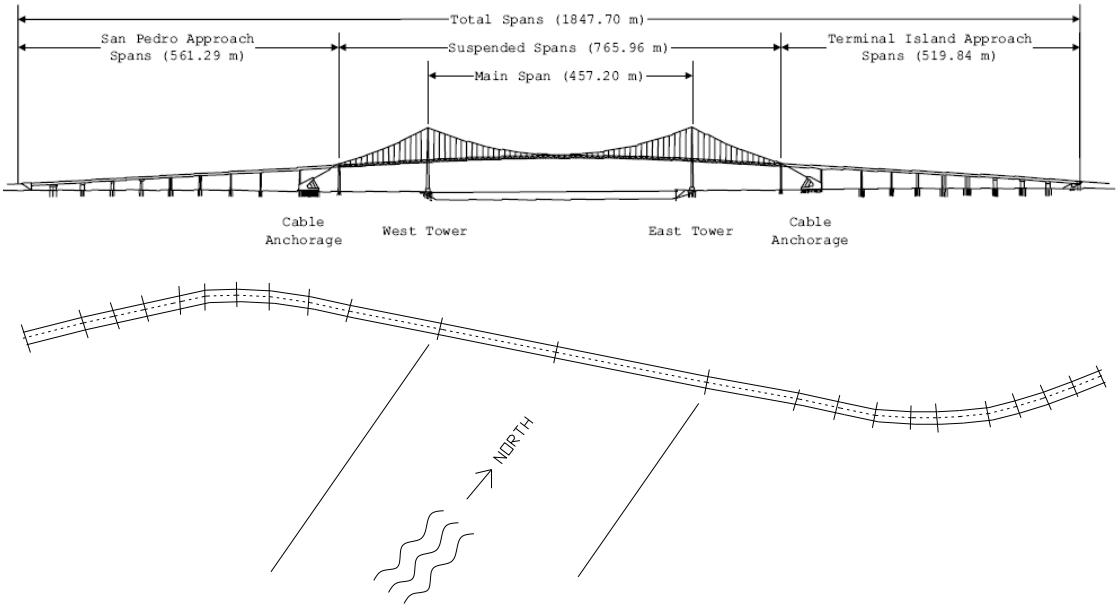

Figure 72. Vincent Thomas Bridge: front and plan views.

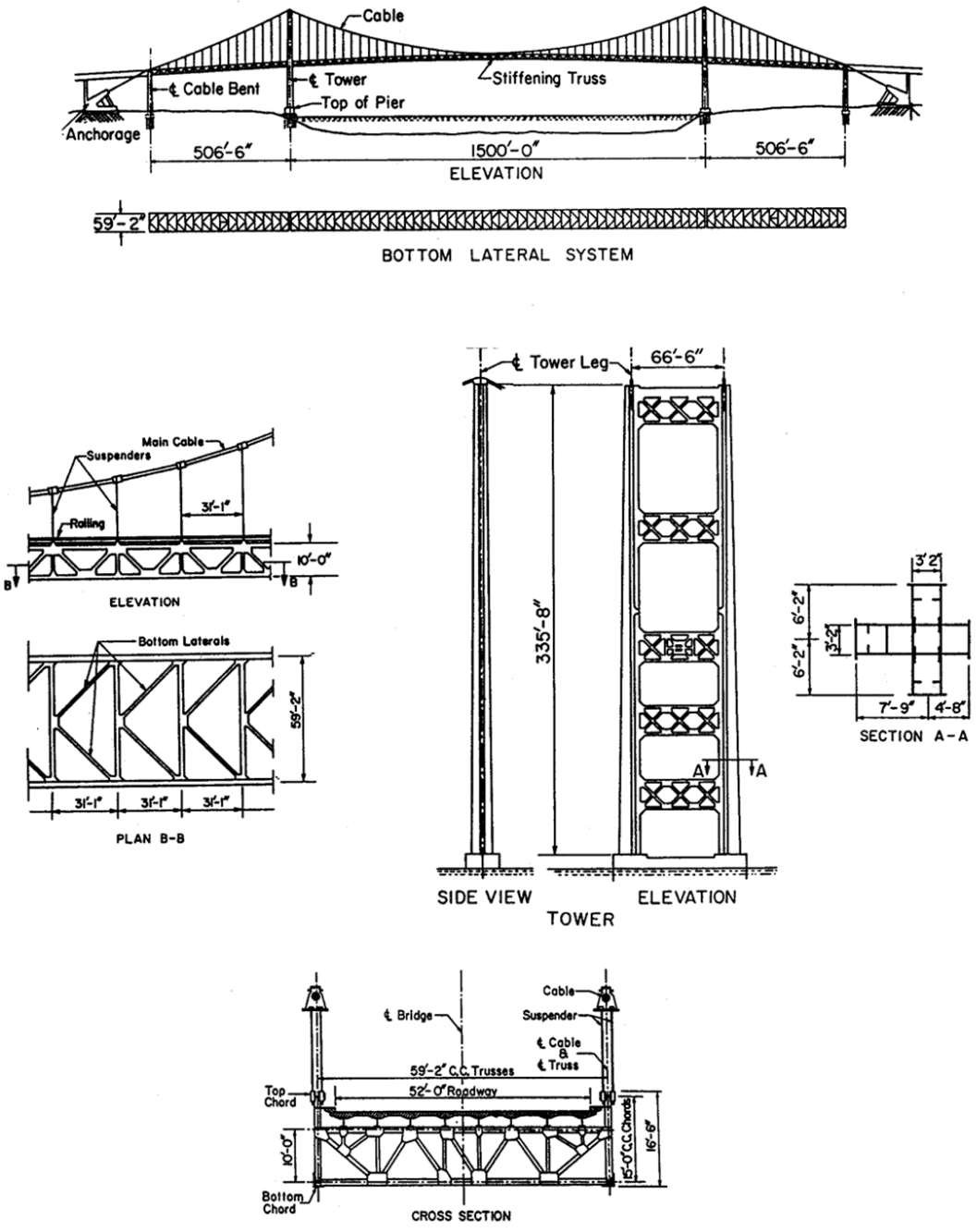

Figure 73. Vincent Thomas Bridge, elevation and details

Figure 74. Vincent Thomas Bridge, overall view.

Figure 75. Vincent Thomas Bridge, dampers localization - sides.

Figure 76. Vincent Thomas Bridge, dampers localization - antennas.

Currently, twenty-six seismic sensors are installed on the bridge to record ambient and seismic behavior. **Figure 77** shows the layout of the location of all 26 sensors mounted on the bridge. A summary of the sensor numbering system and measurement directions is presented in **Table 10.** An enlarged view of sensor locations is presented in **Figure 78**. Six sensors (15, 16, 17, 18, 21 and 22) are used for the deck's mode shape and other four sensors (10, 11, 12, and 13) are used for the pylon's mode shape.

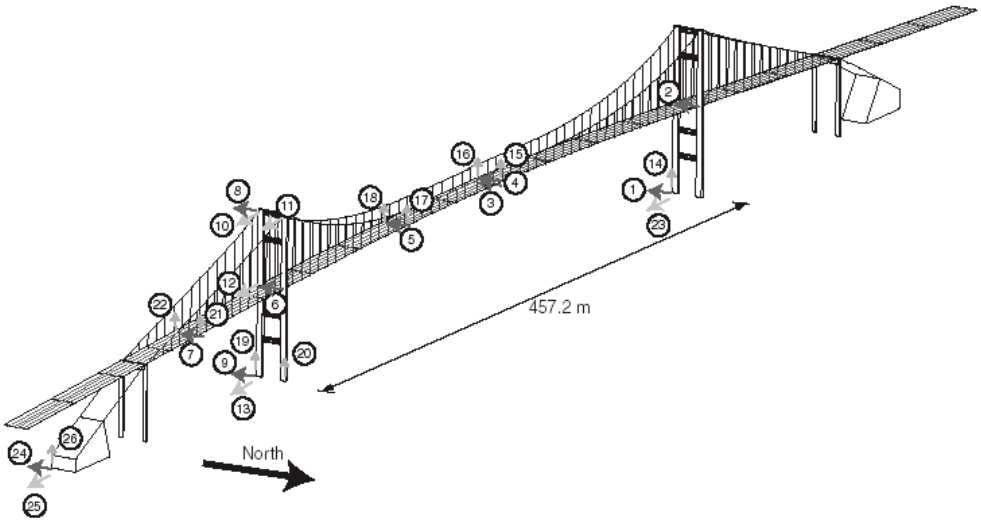

Figure 77. Vincent Thomas Bridge, accelerometer locations and direction (Smyth et al., 2003)

Table 10. Sensor localization (Smyth et al., 2003)

Location	Sensor	Sensor direction
Tower base	14, 19, 20	Vertical
	1, 9	lateral
	13, 23	longitudinal
Anchorage	26	vertical
	24	lateral
	25	longitudinal
Truss top, i.e. deck	15, 16, 17, 18, 21, 22	Vertical
	2, 4, 5, 6, 7	Lateral
	12	Longitudinal
Truss bottom	3	Lateral
Tower	8	Lateral
	10, 11	Longitudinal

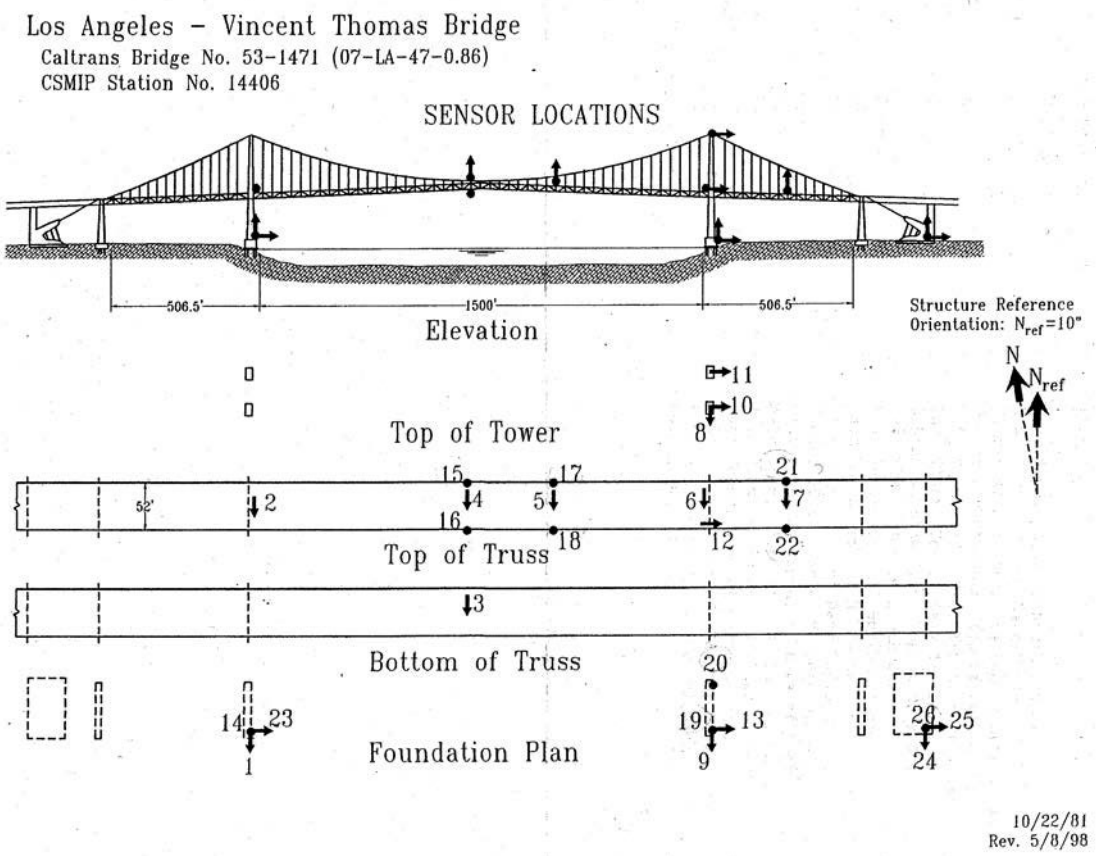

Figure 78. Vincent Thomas Bridge, sensor localization (Smyth et al., 2003)

5.1. Preliminary FE analysis

A detailed three-dimensional finite element model of the bridge developed using the finite element analysis software Adina (2001) was provided by Caltrans.

This finite element model is composed of 3D elastic truss elements to represent the main suspension cables and suspender cables, 2D solid and shell elements to model the bridge deck, and beam elements to model the stiffening trusses and tower shafts.

The goal of this FE analysis was to evaluate the accuracy of the available model in order to guarantee a reasonable dynamic response to be used in the design phase of the damage detection algorithm. A preliminary validation of the numerical model of the bridge was carried out by comparing the numerical response with recorded signals during seismic events like the 1987 Whittier-Narrow earthquake (M=6.1) and the 1994 Northridge

earthquake (M=6.7). The proximity of these earthquake epicenters relative to the Vincent Thomas Bridge is shown in **Figure 79**. Despite the greater distance to Northridge, because of the larger magnitude of that earthquake, the observed peak input and response accelerations ranged anywhere from 1.5 to 3 times of those recorded during the Whittier–Narrows earthquake. The time history records recorded in the proximity of the bridge (see **Figure 79**, station 82) were selected as excitations for the F.E. model.

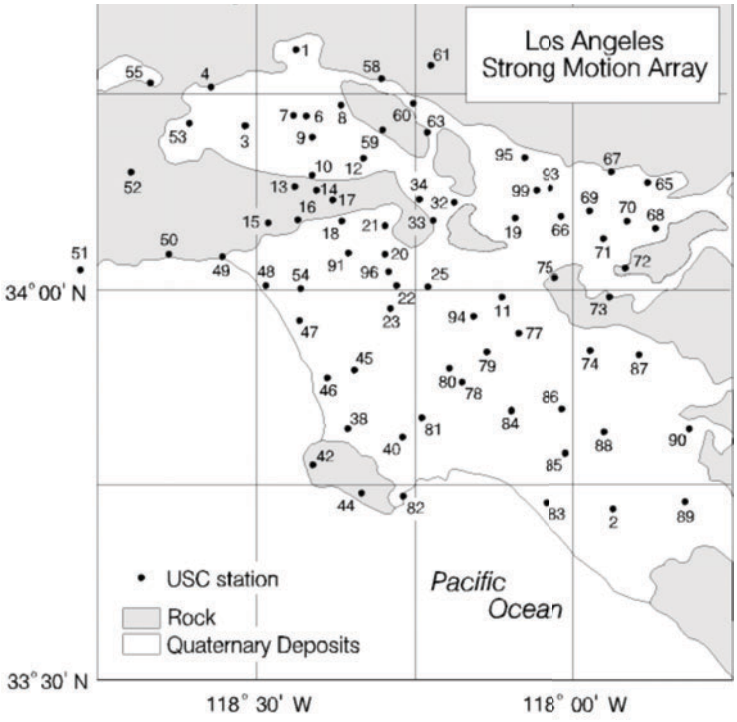

Figure 79. Strong Motion Array (USC): the recording station nearest to the bridge is the number 82 (Terminal Island)
(www.usc.edu/dept/civil_eng/earthquake_eng/LA_array)

It must be noted that either one of the two seismic events was experienced at the bridge location after the completion of the seismic upgrade that included the installation of viscous dampers (1998). The F.E. model is instead designed consistently with the present bridge configuration. This scenario clearly invalidates the use of these recorded responses as direct reference behavior. However, the use of the records was considered appropriate for the definition of basic dynamic characteristics of the F.E. model and for a preliminary

analysis of the possible effects on the structural response of the performance changes of the energy dissipators. As presented in detail in a companion report (Benzoni et. al, 2005) the recorded responses were applied at the tower base, as dynamic excitations for the model results. The numerical response time histories, in terms of displacement, velocity and accelerations are not identical to the recoded ones for the disagreement between model and physical configuration at the seismic event time. To minimize the effects of the structural modifications, the dampers elements in the model were initially de-activated. As indicated in the following figure (**Figure 80**) the model (red line) and recorded (black line) responses are however similar at some location, indicating a reasonable performance of the numerical model.

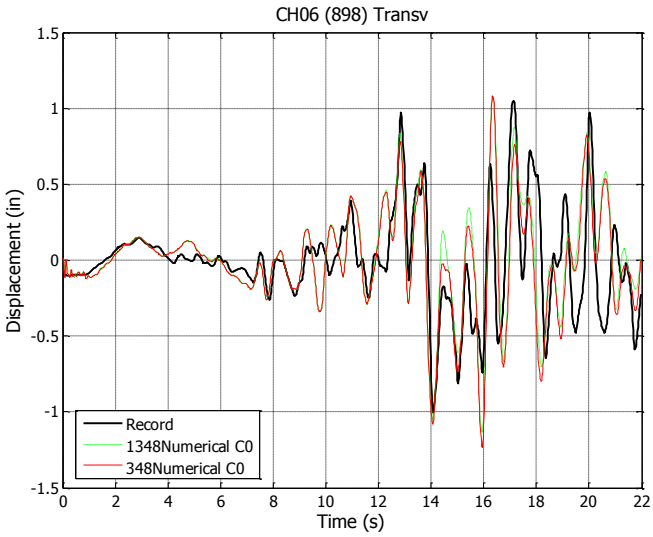

Figure 80. Northridge Earthquake. Model and Recorded transverse displacement at location of Sensor 6

Table 11 shows the main frequencies obtained from the modal analysis of the bridge and recognizable in the transfer functions, both from numerical and recorded signals. Results appear in satisfactory agreement with previous works presented in literature (Conte et al., 2003; Ingham et al., 1997). The frequencies identified in the recorded response are reasonably matched by the ones provided by the present numerical model. However more significant frequencies are indicated by the modal analysis and the transfer functions of the response obtained by the F.E. analysis. This is again attributed to the differences in

the configuration of the FE model and of the actual bridge at the time of the earthquake event. Within the scope of the present project, the obtained agreement with the recorded data still indicates a general reliability of the FE model.

Table 11. Comparison of system identification results (AS=Anti-Symmetric, S=Symmetric, V=Vertical, T=Torsional)

Mode Shapes	**Modal Frequency [Hz]**					
			Conte et al. (2003)		**Ingham et al. (1997)**	
	Numerical signal	Recorded signal	Identified frequency	Computed frequency	Computed frequency	Northridge frequency
1-AS-V	-	-	0.168	0.182	0.135	0.145
1-S-V	0.130	0.210	0.224	0.226	0.229	0.220
2-S-V	-	-	0.356	0.364	0.356	0.370
1-S-T	0.570	0.570	0.483	0.511	0.471	0.551
3-V	0.910	0.902	-	-	-	-

5.2. Application of the damage detection algorithm to simulated data

The procedure for the damage identification was applied to the responses provided by the above mentioned numerical model of the Vincent Thomas Bridge structure. As a first approach to the damage identification procedure, applied to the bridge, responses were obtained from the numerical model of the bridge in three different configurations: bridge un-damaged and bridge with reduction of the performance characteristic of the dampers by 30% and 50%. In particular, the damping coefficient of the dampers was reduced by the above mentioned percentage with respect to the nominal values. In order to relate the applied reduction of dissipation performance to actual conditions of the dampers and to the impact on the bridge performance the reader is referred to two preliminary reports (Benzoni et. al, 2005 and Benzoni et. al, 2007). In the first report (Benzoni et. al, 2005) the bridge performance was numerically evaluated for different levels of degradation applied to the dampers. In the second one (Benzoni et. al, 2007) an experimental

campaign was conducted on a damper specimen with intentional removal of quantities of viscous fluid to correlate the level of damage to the damper dissipation capacity.
For the numerical validation reported hereafter, the input signal selected was a white noise with frequency between 0 and 60Hz (**Figure 81**). The same signal was utilized for the bridge in the un-damaged and damaged configuration.

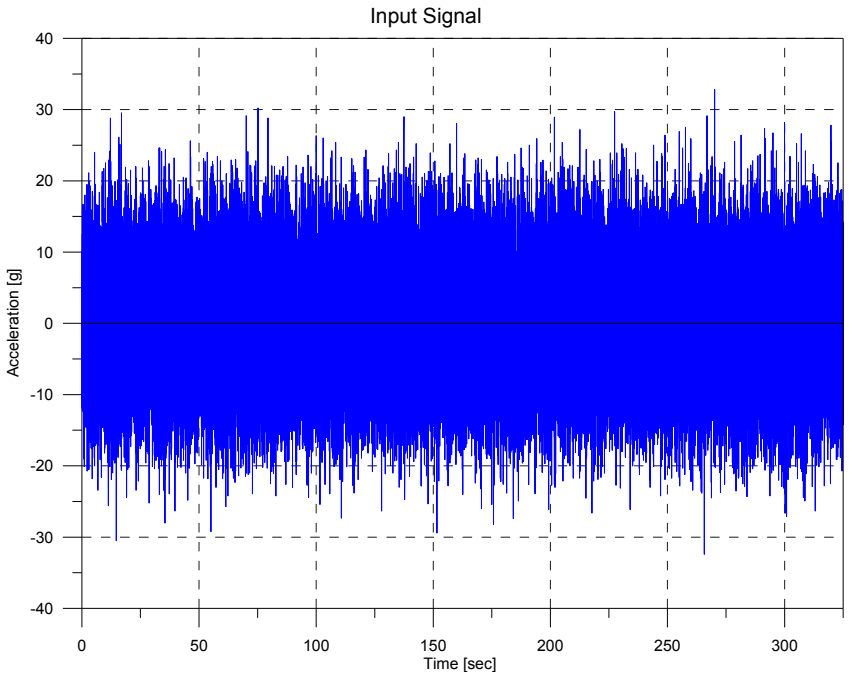

Figure 81. Input signal for the Vincent Thomas Bridge Model

The numerical model is utilized here only to produce responses for the bridge conditions at different levels of degradation. It is important to note that the application of the damage identification procedure does not require the existence of a F.E. model. What is required is instead a simplified interpretative scheme. The scheme is used for the discretization of the real structure in elements and sub-components (e.g. column, deck etc.), in order to be able to assemble the normalized Damage Indicator Z_j (Eq. 26) for all the *jth* elements. The number and length of the elements that constitute the interpretative scheme is arbitrary. The procedure is in fact unaltered by the number and length of the elements. It is of course suggested that a preliminary analysis be conducted with a reduced number of elements and eventually detailed in regions where a structural

deficiency is suspected. A reasonable balance between number of elements and data signals available should also be maintained. For instance, for the F.E. model of the Vincent Thomas Bridge, the response is available in every node. For this reason it is theoretically possible to describe the mode shapes with a very extensive number of points. However, it was experienced that the higher the number of points utilized, the higher will be the noise level in the assessed mode shapes. For the interpretative scheme of the bridge application, configurations with different number of elements (12, 25 and 64) were tested. The application reported here is limited to 12 elements, to show the capacity of the approach to function also in case of high simplification level. It must be noted also that the interpretative scheme does not have to include all portions of the existing structure. The interaction between all the structural components is in fact accounted for in the response signals, but the energy approach can be used to inspect only a limited portion of the real structure. The interpretative scheme assumed for this specific application is reported in **Figure 82**.

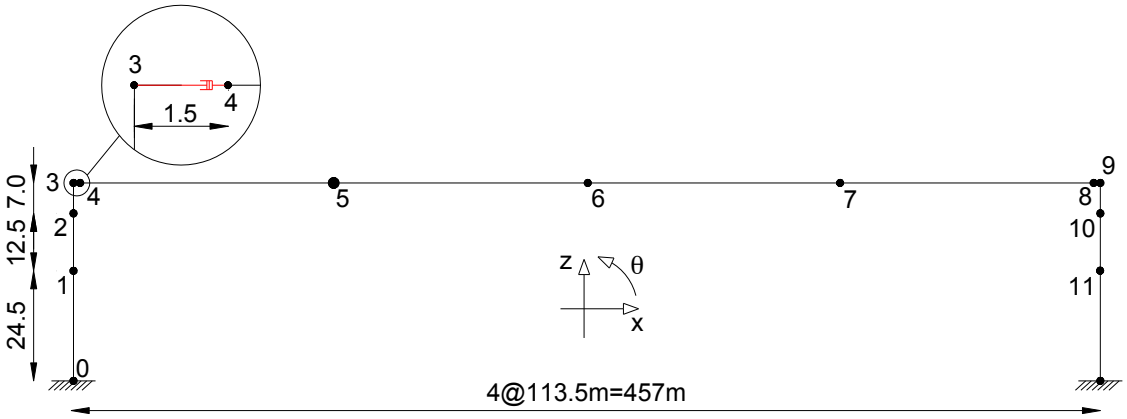

Figure 82. Bridge Interpretative Scheme with 12 elements (units: meters)

For the specific interest of this research, only the portion of the structure directly interested by the dampers (the piles and the deck of the main span), was considered. As indicated above, additional portions can be added, like the complete height of the towers and the structure from the towers to the abutments, but the considered part of the bridge

seemed appropriate for the goal to validate the performance of the procedure. The dampers connecting the bridge towers and the deck are also grouped, in the scheme of **Figure 82**, in two elements (element between node 3 and 4 and element between node 8 and 9). Each element represents a set of 4 dampers in the real structure. This is just a simplification in the interpretative scheme that could be removed introducing additional elements in the calculation of the damage indicators.

Displacement read-outs were extracted from the 3D Finite Element model, at locations corresponding to the nodes indicated in **Figure 82**. Based on these signals the mode shapes needed to be assessed. Two approaches were followed, as described in the following paragraph.

The assessment of the mode shapes from the F.E. model responses was initially attempted by using the output-only response method proposed by Kim (Kim et al., 2005). The accuracy of the mode shapes was found not satisfactory, for the use in the proposed procedure. For this reason a different approach, based on the Covariance-driven Stochastic Subspace Identification method (SSI-Cov) was implemented (Peeters, 2000).

The SSI-Cov method is as well an output-only response approach. This characteristic is considered of paramount importance for the proposed application because the structure is treated as excited by an unknown input and only output measurements (e.g. accelerations) are available. This condition closely represents the reality of a complex structure under a program of monitoring for structural health assessment purposes. For the SSI-Cov method the deterministic knowledge of the input is replaced by the assumption that the input is a realization of a stochastic process (white noise).

Measurements for modal analysis applications typically contain some redundancy. Since the spatial resolution of the experimental mode shapes is determined by the position and the number of the sensors, usually many sensors (mostly accelerometers) are used in a modal analysis experiment. Theoretically, if none of the sensors is placed at a node of a mode, all signals carry the same information on eigen-frequencies and damping ratios. To decrease this redundancy, some signals are *partially* omitted in the identification process, leading to algorithms that are faster and require less computer memory without losing a significant amount of accuracy. In the end, the omitted sensors are again included to yield the "full" mode shapes. With the SSI-Cov method it is possible to separate the uncertain

variables (input and noise) from periodic variable such as vibrations frequencies of structure.

For large, real structures, in order to obtain a good model for modal analysis applications the construction of a stabilization diagram appears very practical. In case of the SSI-Cov method, an efficient construction of the stabilization diagram is achieved by computing the SVD of the covariance Toeplitz matrix only once. This is an iterative procedure where the system order *n* is fixed, step by step, and the modal parameters for the order (frequency of vibration 'ω', damping ratio 'ξ' and modal vector '*v')* are determined.

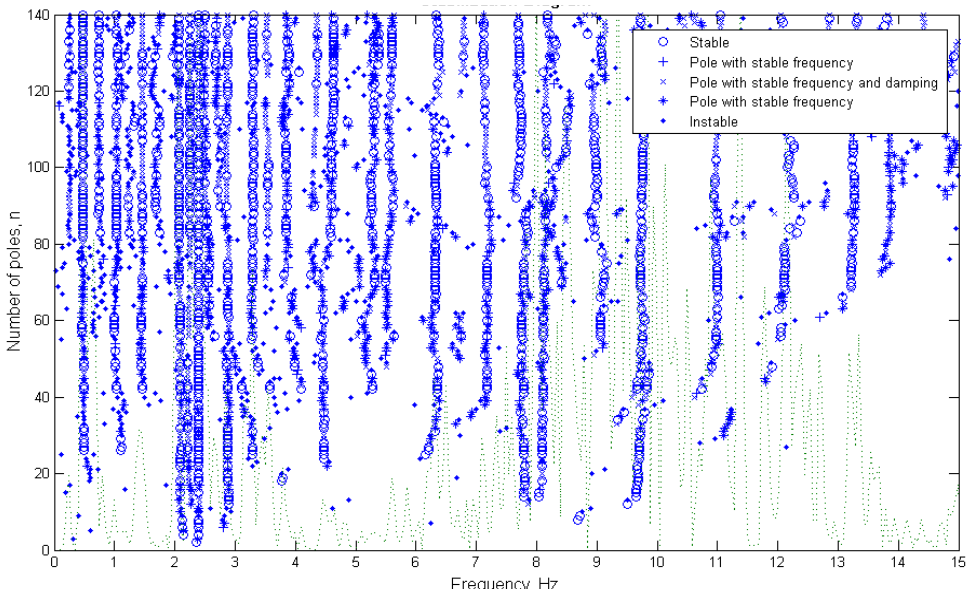

Figure 83. Example of Stabilization diagram obtained with the SSI-COV method for the undamaged case. The criteria are 1% for frequencies, 5% for damping ratios and 1% for the mode shape correlations

The repetition of blue dots (stable poles) corresponding to peaks of the green dashed curve (the PSD of the signal) isolates the natural frequencies. A band-pass filter is then applied in order to separate the single modal components. For the bridge application the natural frequencies for the first three modes and the ranges of frequency used to extract each modal contribution are reported in **Table 12** and **Table 13**, respectively.

Table 12. Modal frequencies

	Frequency [Hz]		
	Undamaged	**Damaged 30%**	**Damaged 50%**
I mode	0.260	0.274	0.276
II mode	0.480	0.477	0.477
III mode	0.739	0.746	0.750

Table 13. Filter ranges

	Filter Ranges		
	Undamaged	**Damaged 30%**	**Damaged 50%**
I mode	0.2 - 0.3 Hz	0.2 - 0.3 Hz	0.2 - 0.4 Hz
II mode	0.4 - 0.5 Hz	0.4 - 0.5 Hz	0.4 - 0.6 Hz
III mode	0.7 - 0.8 Hz	0.7 - 0.8 Hz	0.6 - 0.8 Hz

In **Figure 84** to **Figure 92** the modes shapes identified by the Kim approach and by the SSI-Cov method are compared with the mode shapes identified by the F.E. Model (FEM). It is visible the improvement of the SSI-Cov method in terms of symmetry of the mode shapes.

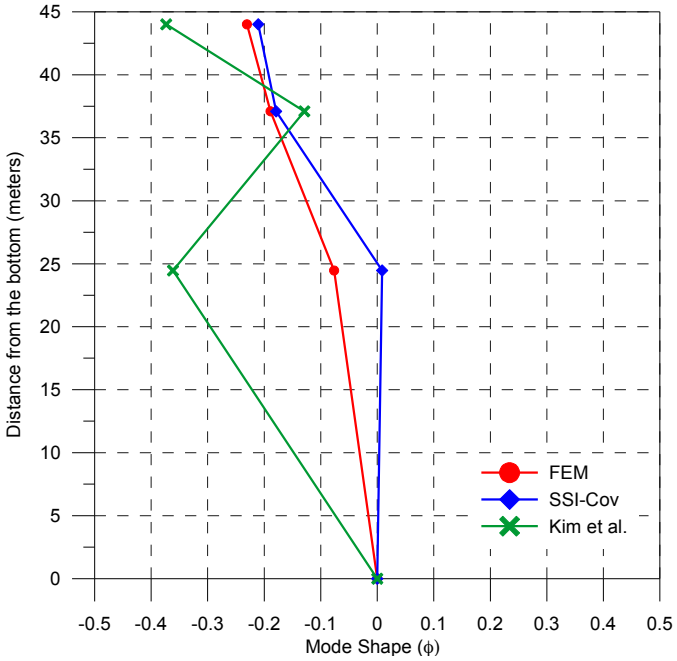

Figure 84. Undamaged Structure: first mode for the East Pylon

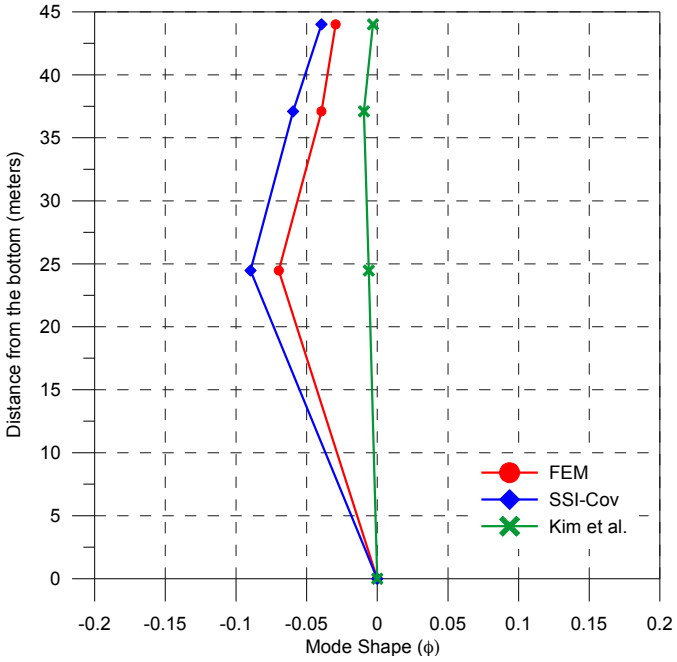

Figure 85. Undamaged Structure: second mode for the East Pylon

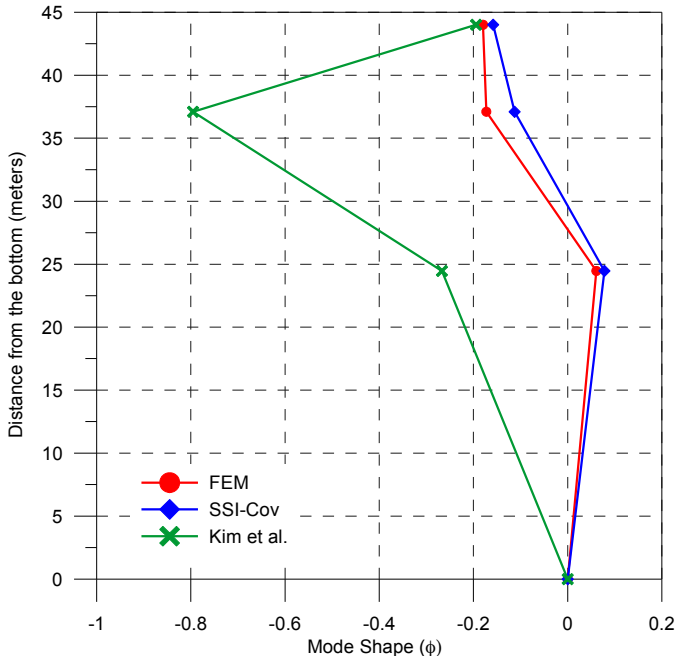

Figure 86. Undamaged Structure: third mode for the East Pylon

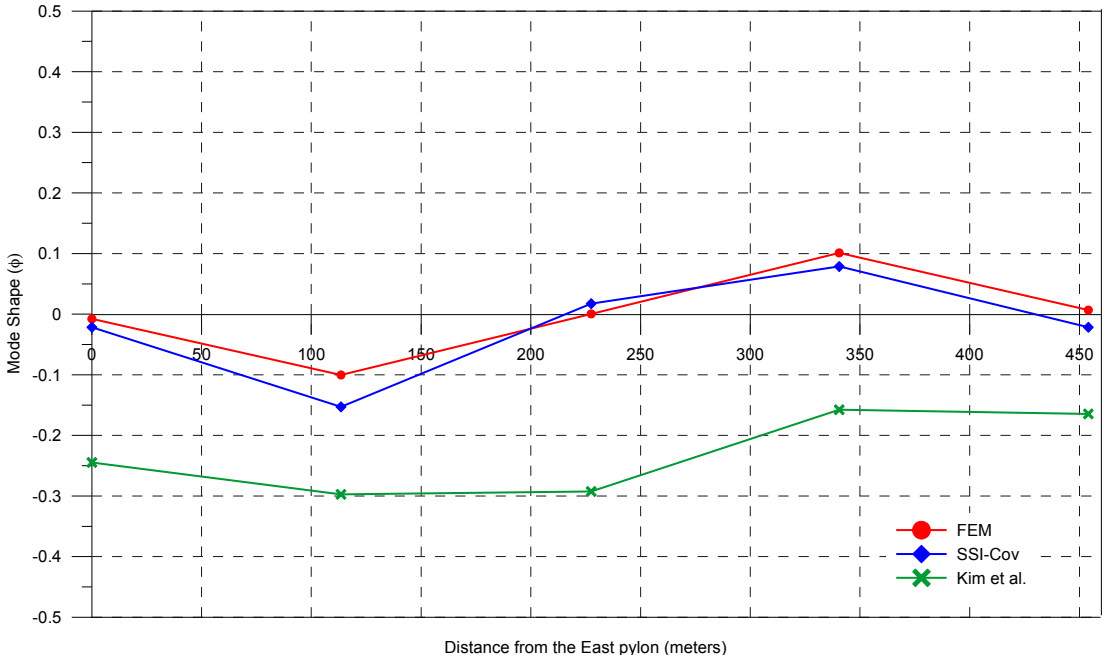

Figure 87. Undamaged Structure: first mode for the deck

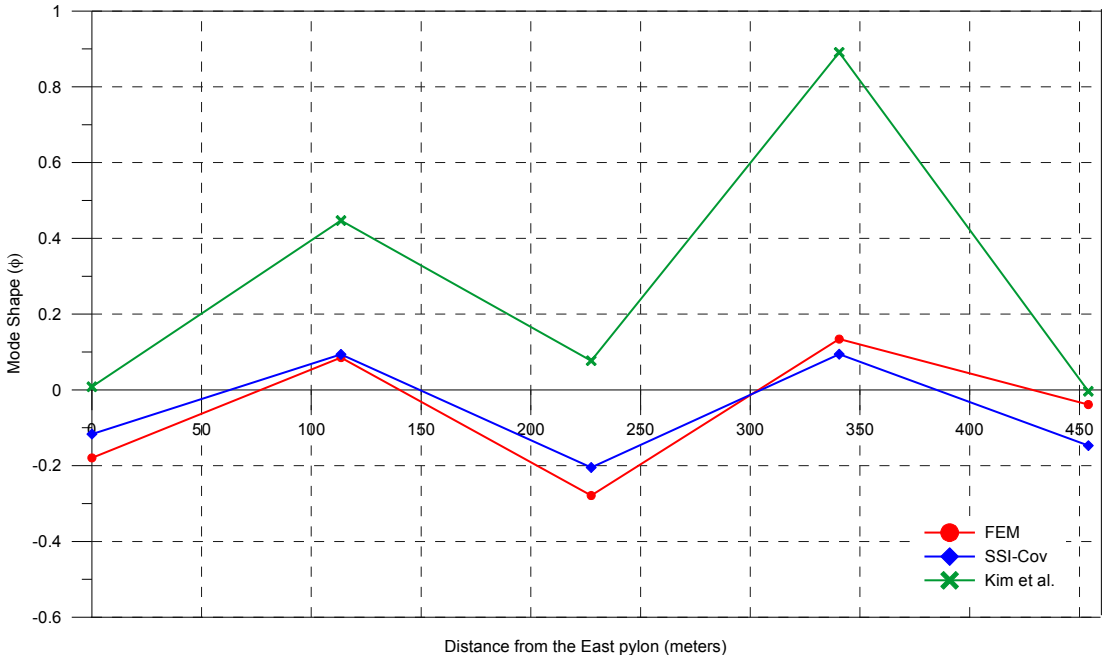

Figure 88. Undamaged Structure: second mode for the deck

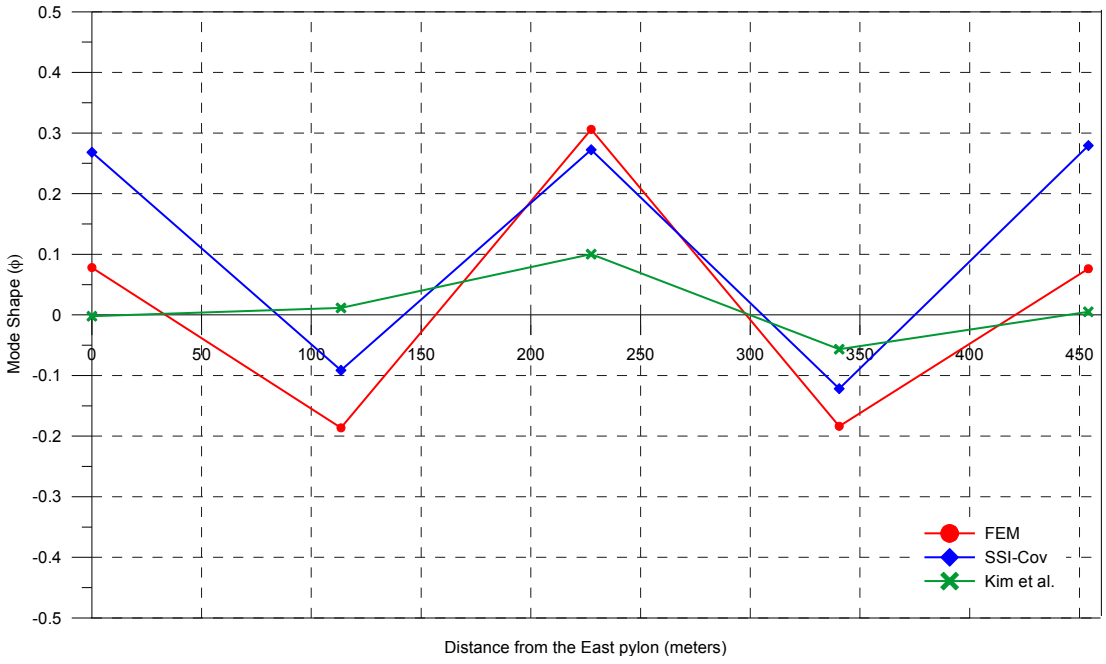

Figure 89. Undamaged Structure: third mode for the deck

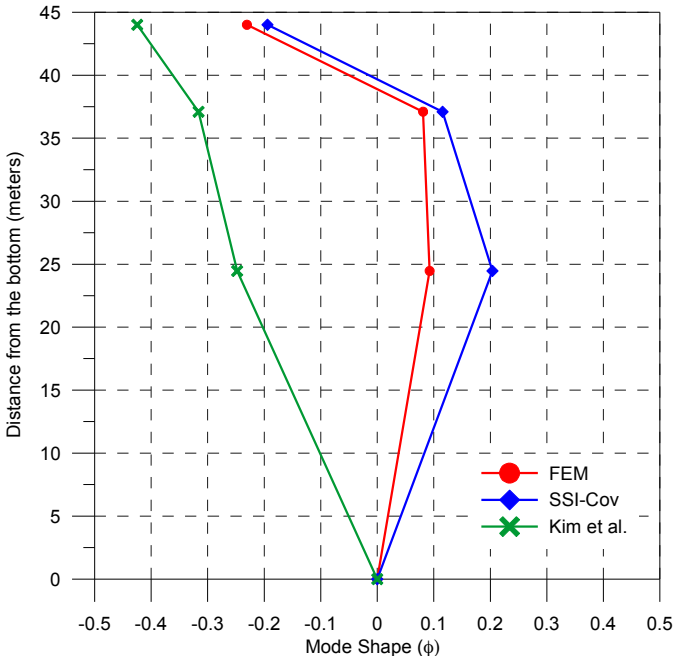

Figure 90. Undamaged Structure: first mode for the West Pylon

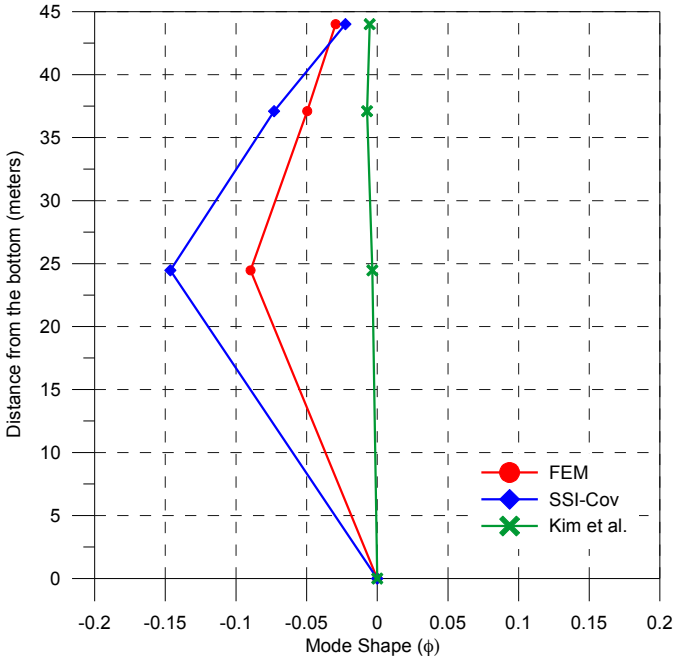

Figure 91. Undamaged Structure: second mode for the West Pylon

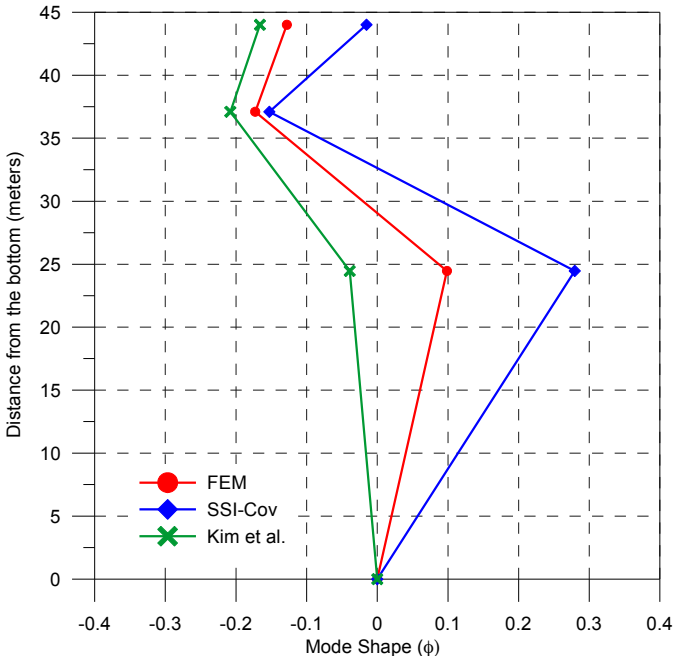

Figure 92. Undamaged Structure: third mode for the West Pylon

Case 1: 30% simulated damage in dampers

The mode shapes for the bridge pylons and deck are shown in **Figure 93** to **Figure 101**. Three modes shapes were considered. The dashed lines indicate the shapes obtained from the displacement records, while the solid lines correspond to the polynomial interpolation. The first three dominant mode shapes of the damaged structure occur at 0.274, 0.477 and 0.746Hz compared to 0.260, 0.480 and 0.739 Hz for the un-damaged structure.

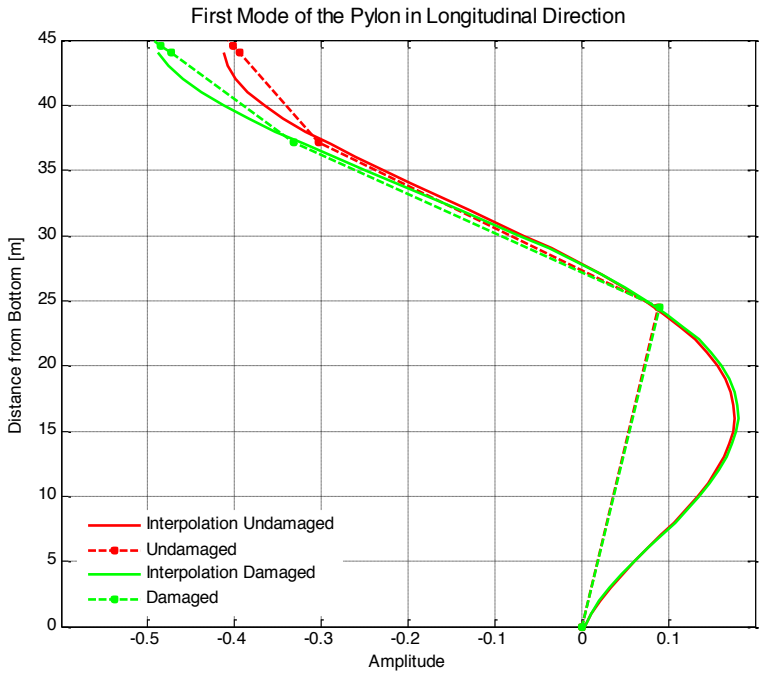

Figure 93. Damage 30%:First mode of the East pylon

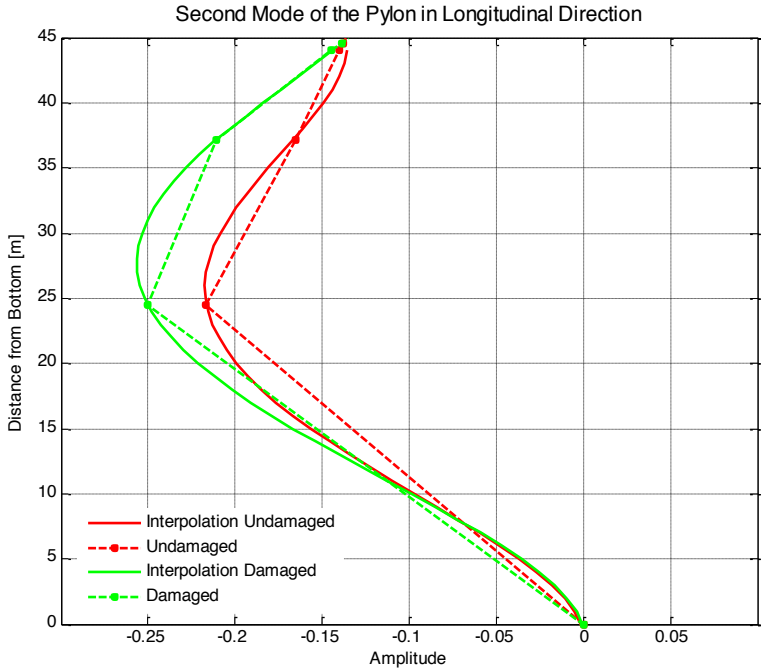

Figure 94. Damage 30%: Second mode of the east pylon

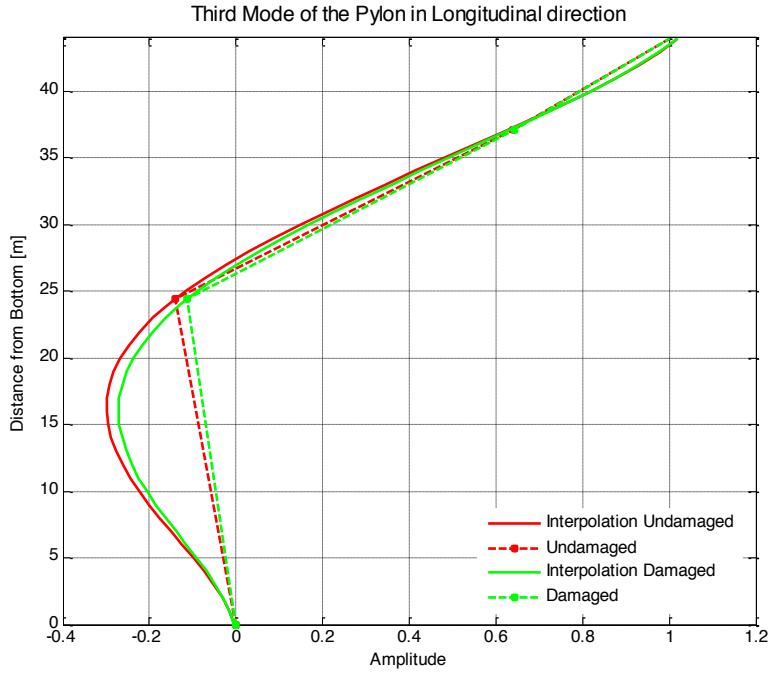

Figure 95. Damage 30%: Third mode of the East pylon

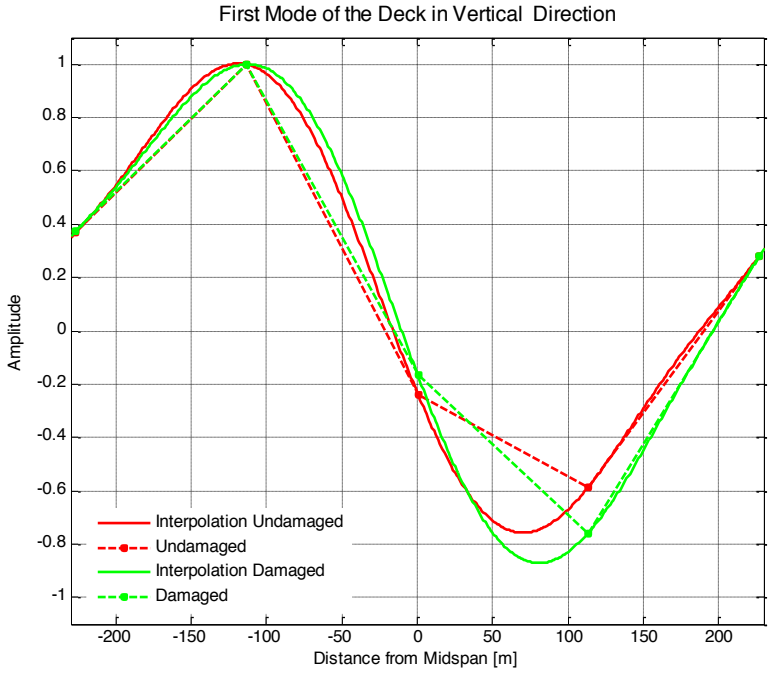

Figure 96. Damage 30%: First mode of the deck

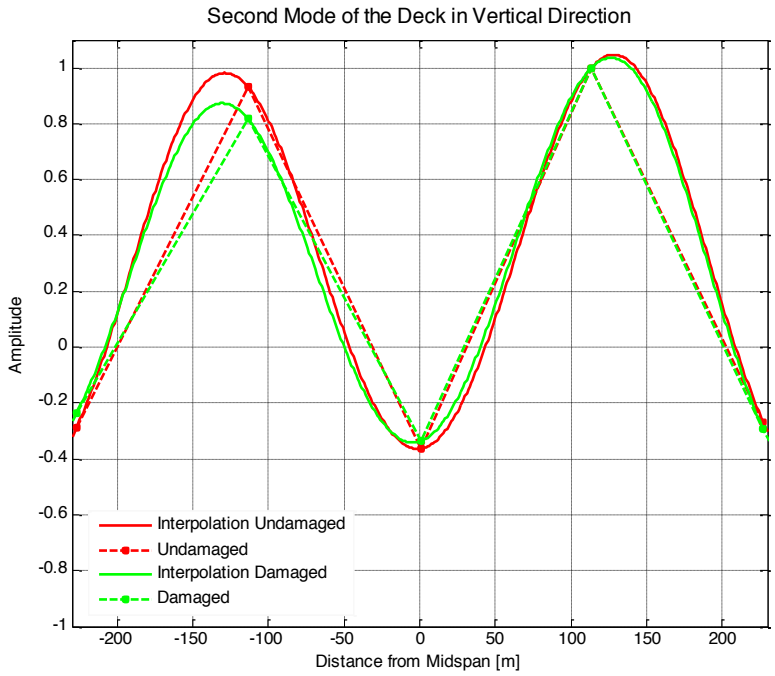

Figure 97. Damage 30%: Second mode of the deck

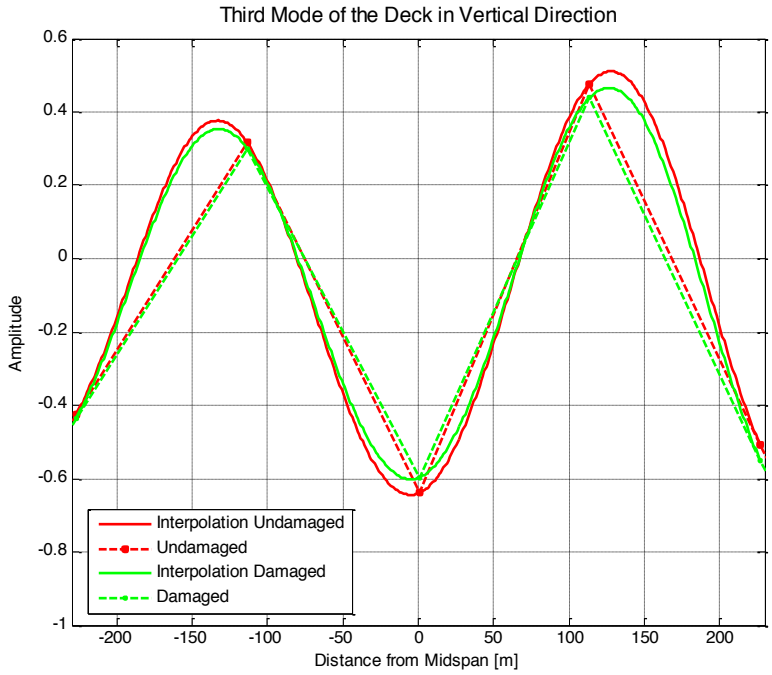

Figure 98. Damage 30%: Third mode of the deck

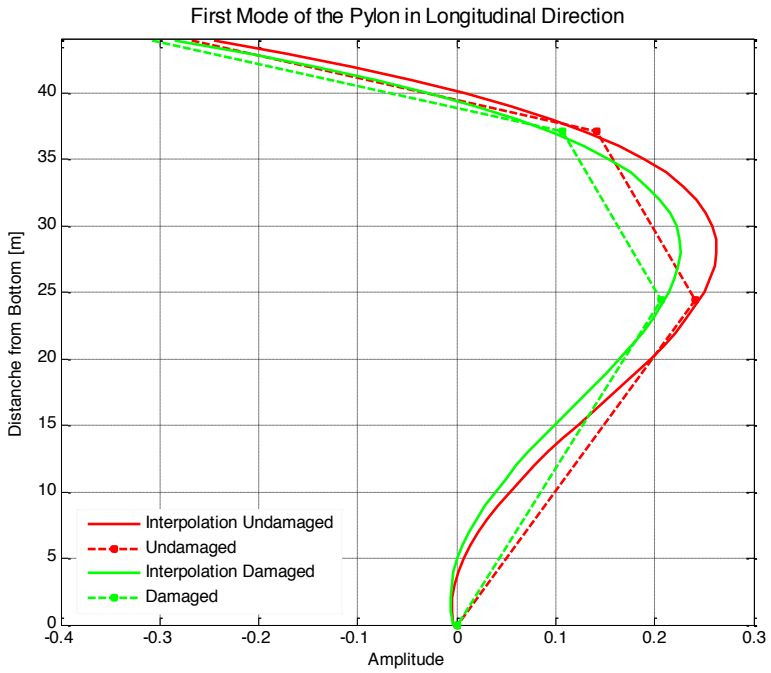

Figure 99. Damage 30%: First mode of the West pylon

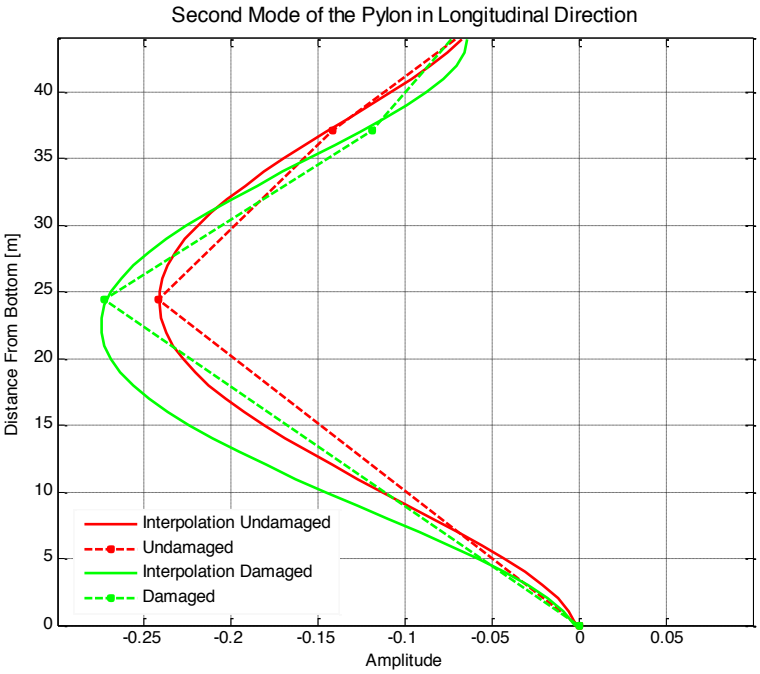

Figure 100. Damage 30%: Second mode of the West pylon

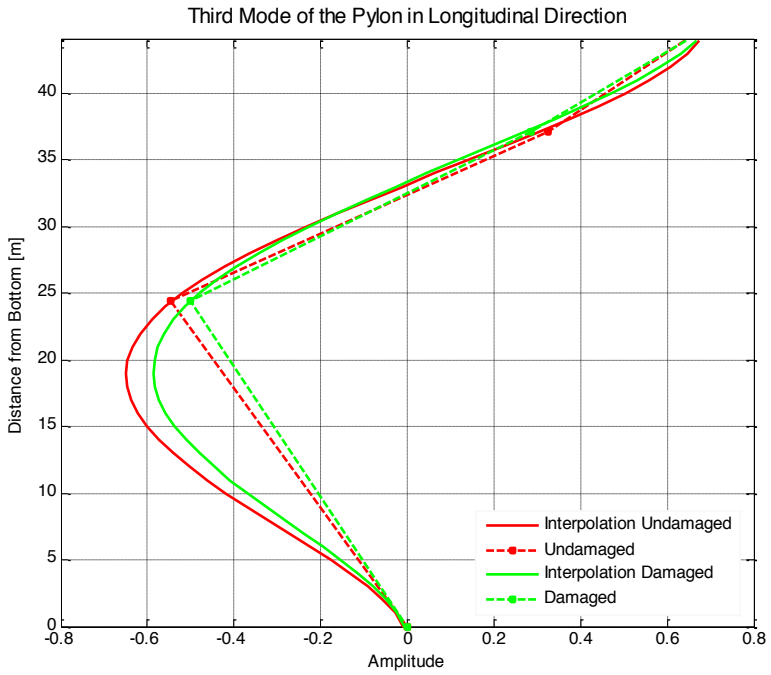

Figure 101. Damage 30%: Third mode of the West pylon

After the assessment of the best polynomial functions reproducing the mode shapes, the interpretative scheme of the structure was sub-divided in 1 m long elements. The availability of a continuous polynomial functions allows to estimate the curvature of each single element and so the damage indicators.

The damage indices are presented in **Figure 102** to **Figure 104** for the 30% damage case. The East pylon, the deck and the West pylon are projected on the same x axis. The last two elements correspond to the energy dissipators. The figures indicate that the damage exists in the dampers. Peaks of the parameter Z_{ij} are visible also for elements at the top of the West pylon. However due to the definition of the coefficient of severity these locations are not considered as associated to damage.

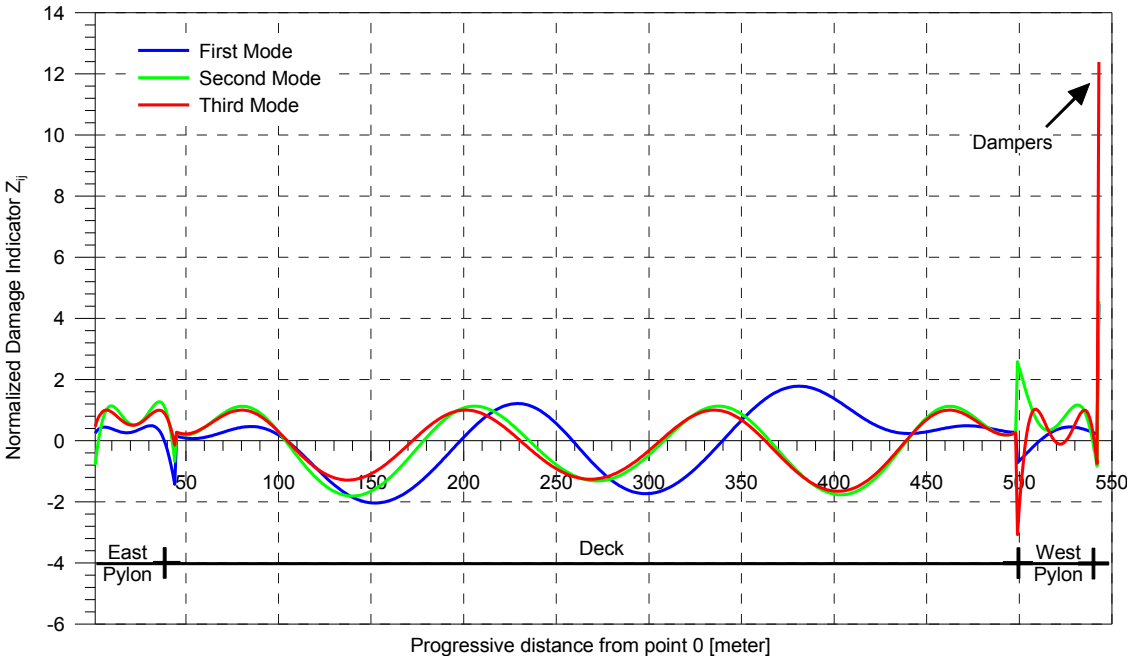

Figure 102. Damage 30%: Normalized Damage Indicator Z_{ij} for each mode

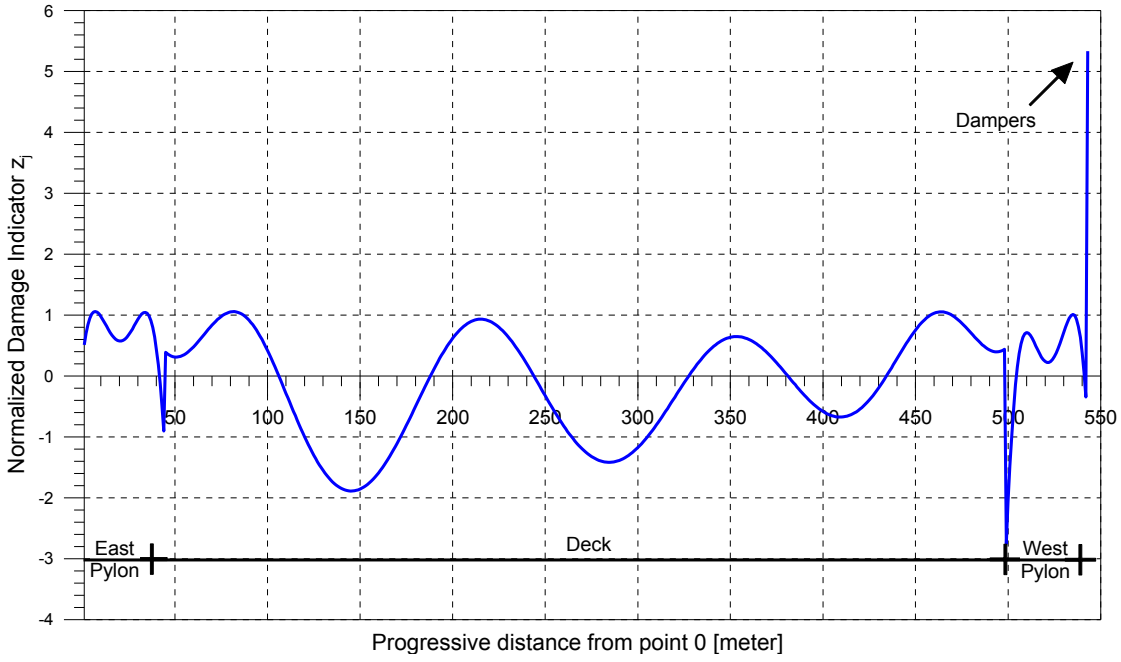

Figure 103. Damage 30%: Multimodal Normalized Damage Indicator Z_j

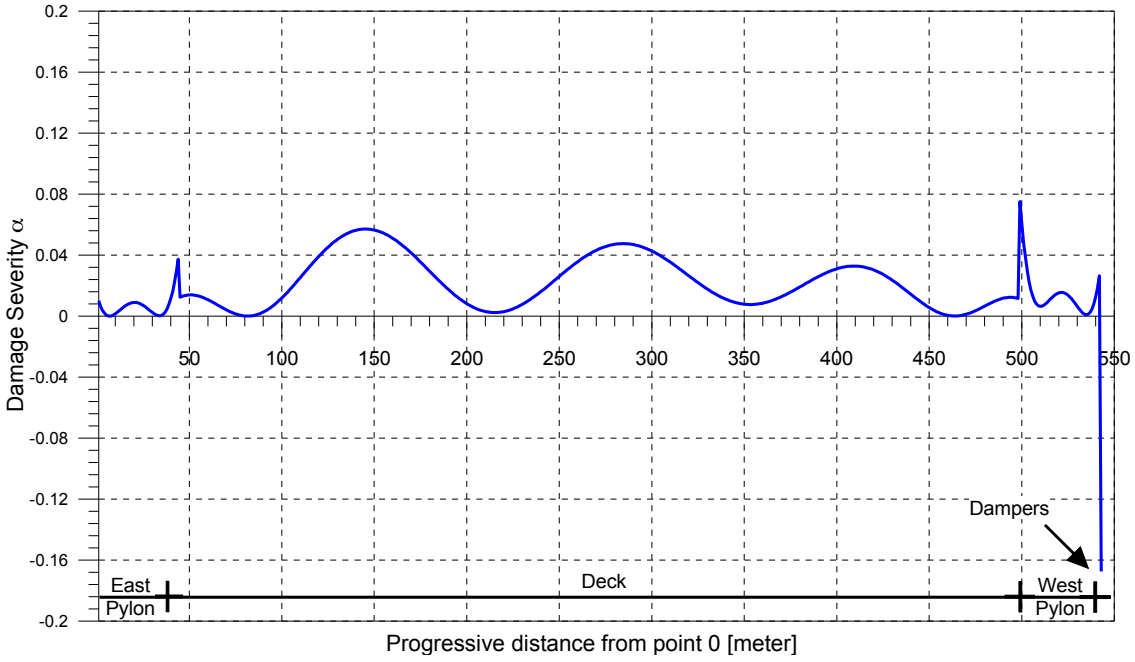

Figure 104. Damage 30%: Damage Severity Indicator α_j

Case 2: 50% simulated damage in dampers

As presented before, the following figures report mode shapes and damage indices for the configuration of damaged dampers, in the amount of 50% reduction of their original damping coefficient. The first three dominant mode shapes of the damaged structure occur at 0.274, 0.477 and 0.750Hz compared to 0.260, 0.480 and 0.739Hz for the un-damaged structure. From the severity indicator α_j it is detected a degradation of ~55% for the dampers on the East side of the main span and of ~65% for the dampers on the West side.

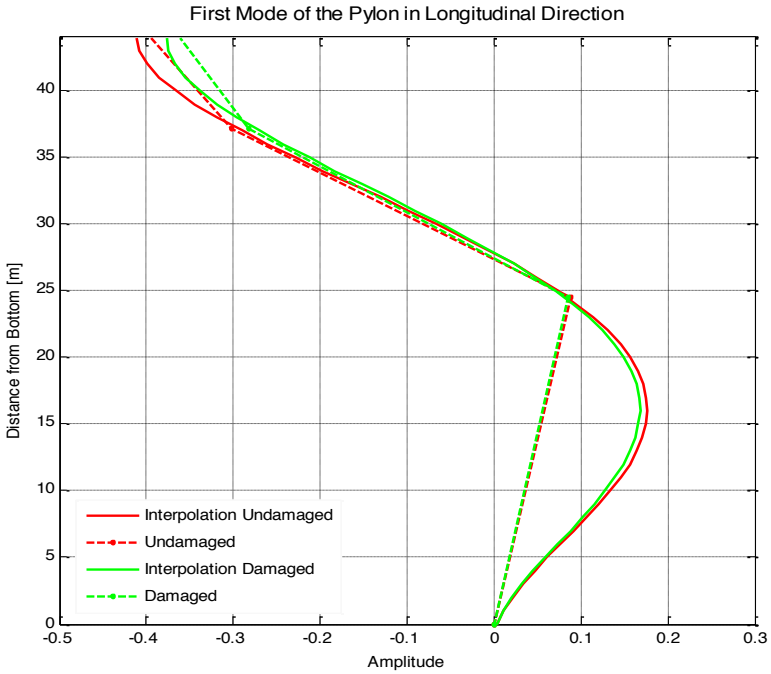

Figure 105. Damage 50%: First mode of the East pylon

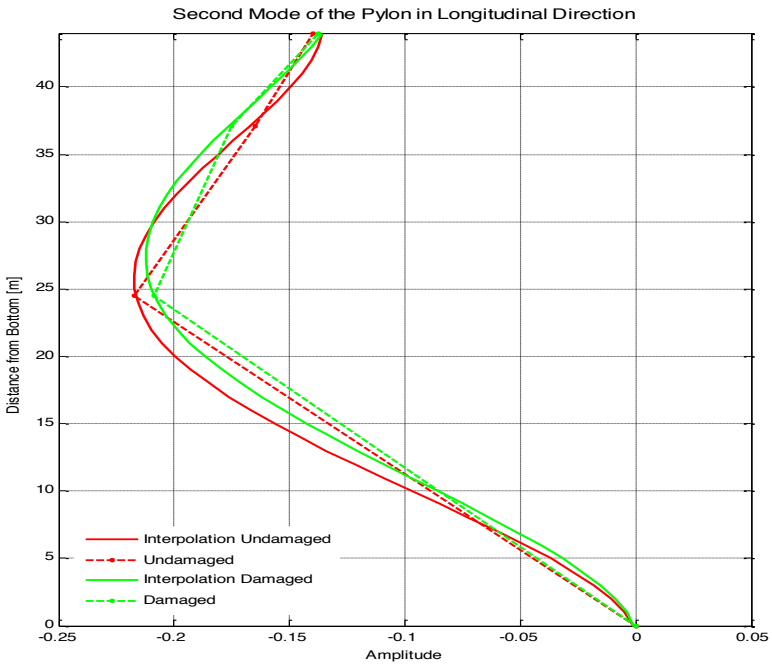

Figure 106. Damage 50%: Second mode of the East pylon

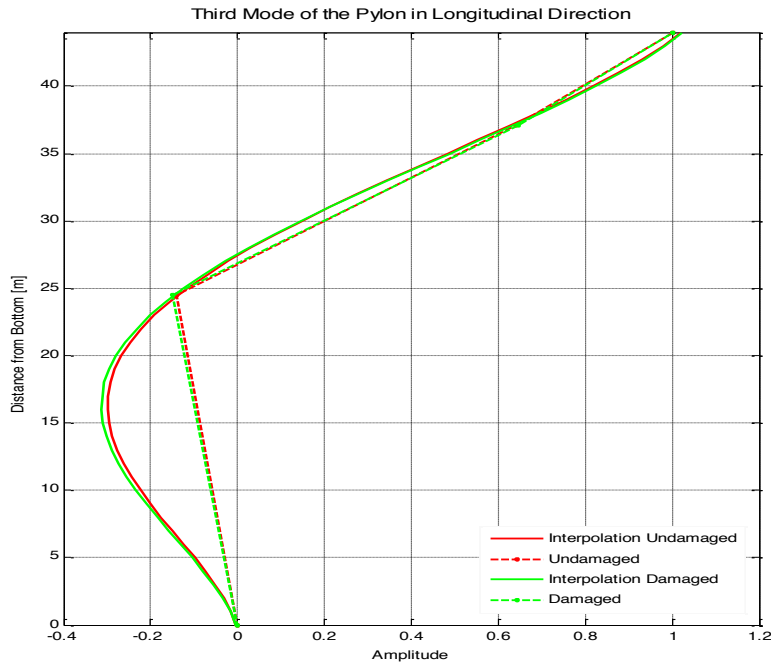

Figure 107. Damage 50%: Third mode of the East pylon

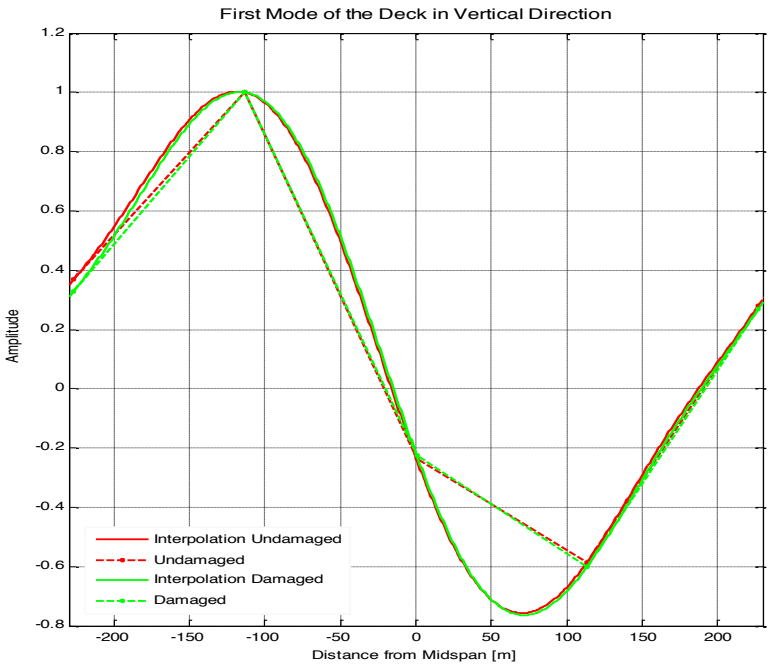

Figure 108. Damage 50%: First mode of the deck

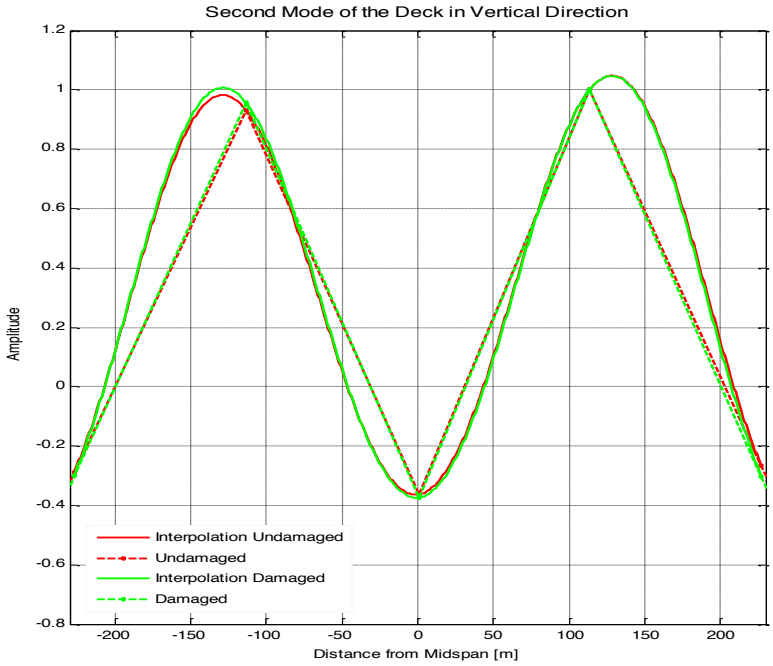

Figure 109. Damage 50%: Second mode of the deck

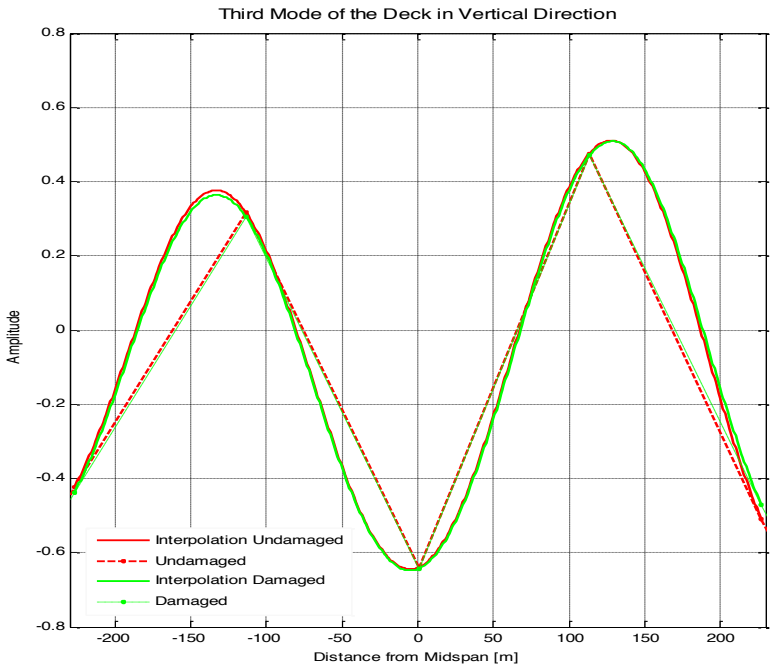

Figure 110. Damage 50%: Third mode of the deck

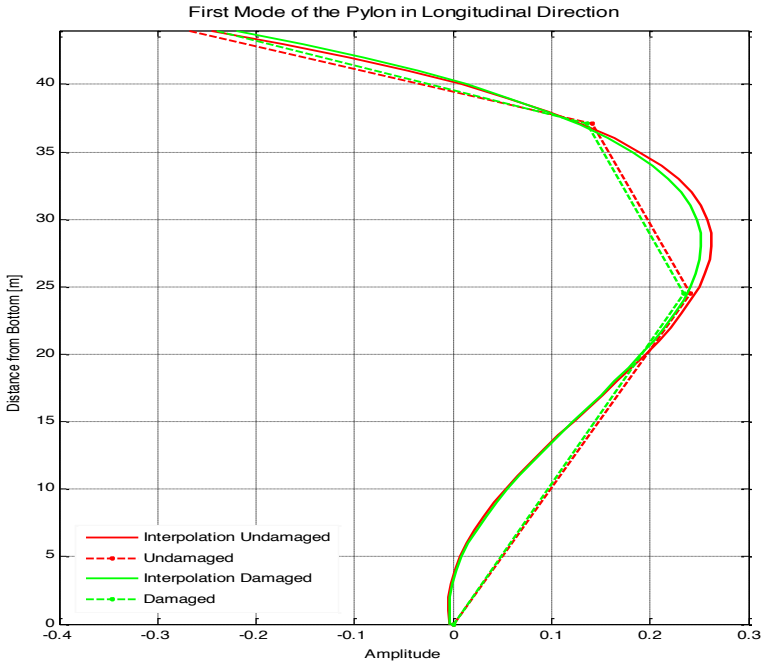

Figure 111. Damage 50%: First mode of the West pylon

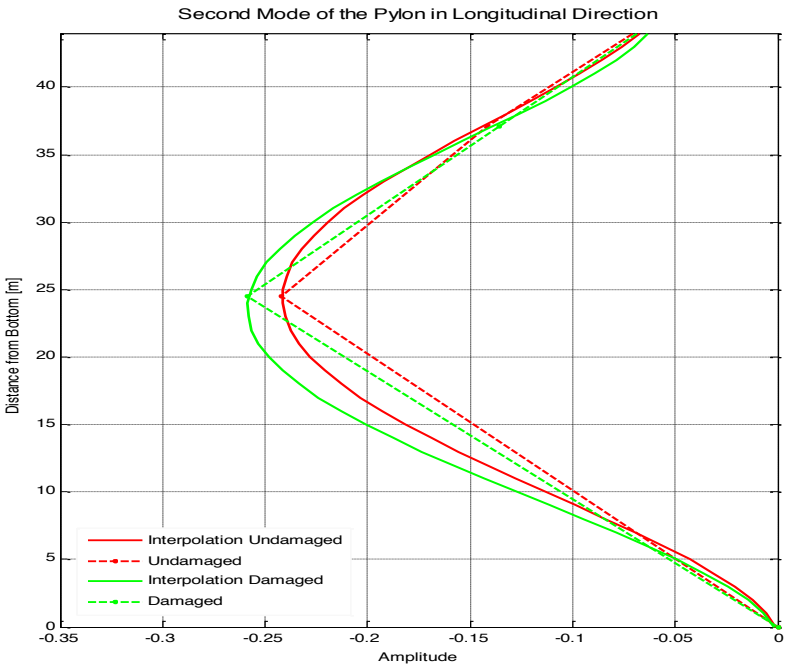

Figure 112. Damage 50%: Second mode of the West pylon

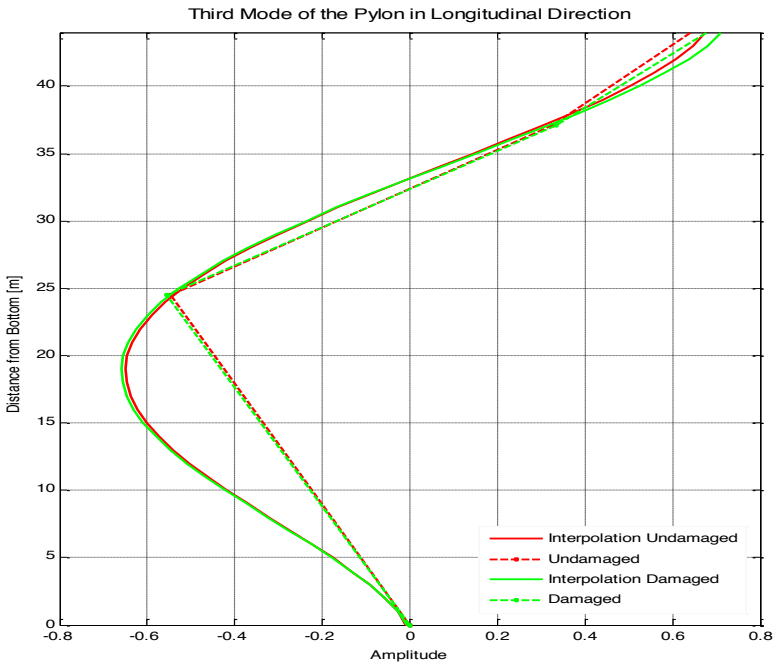

Figure 113. Damage 50%: Third mode of the West pylon

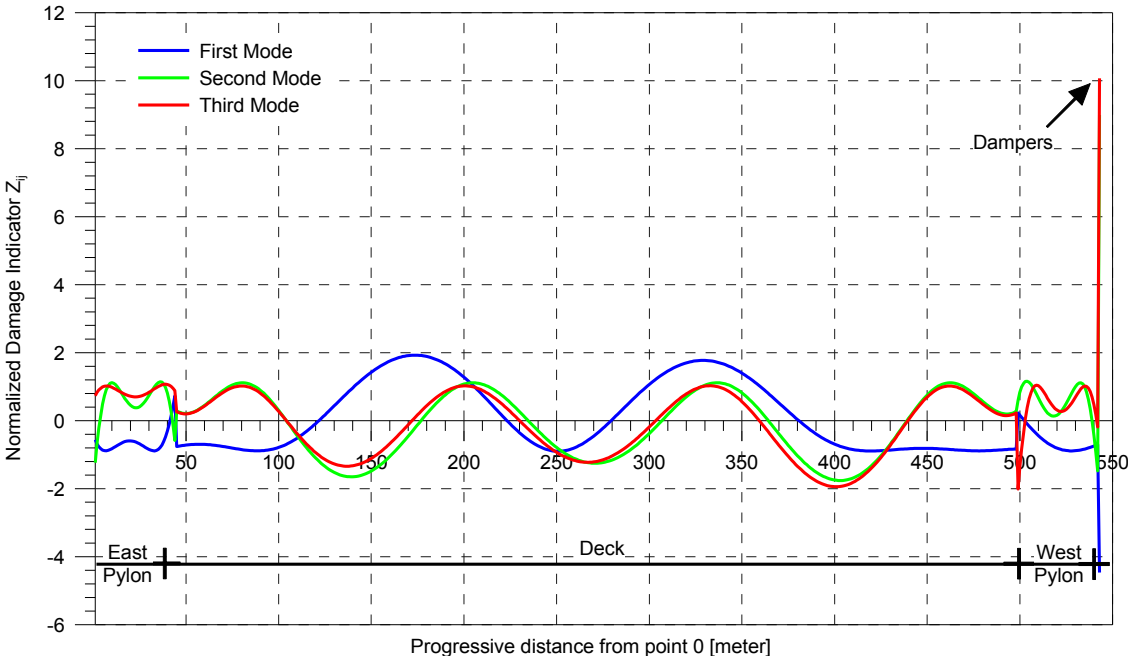

Figure 114. Damage 50%: Normalized Damage Indicator Z_{ij} for each mode

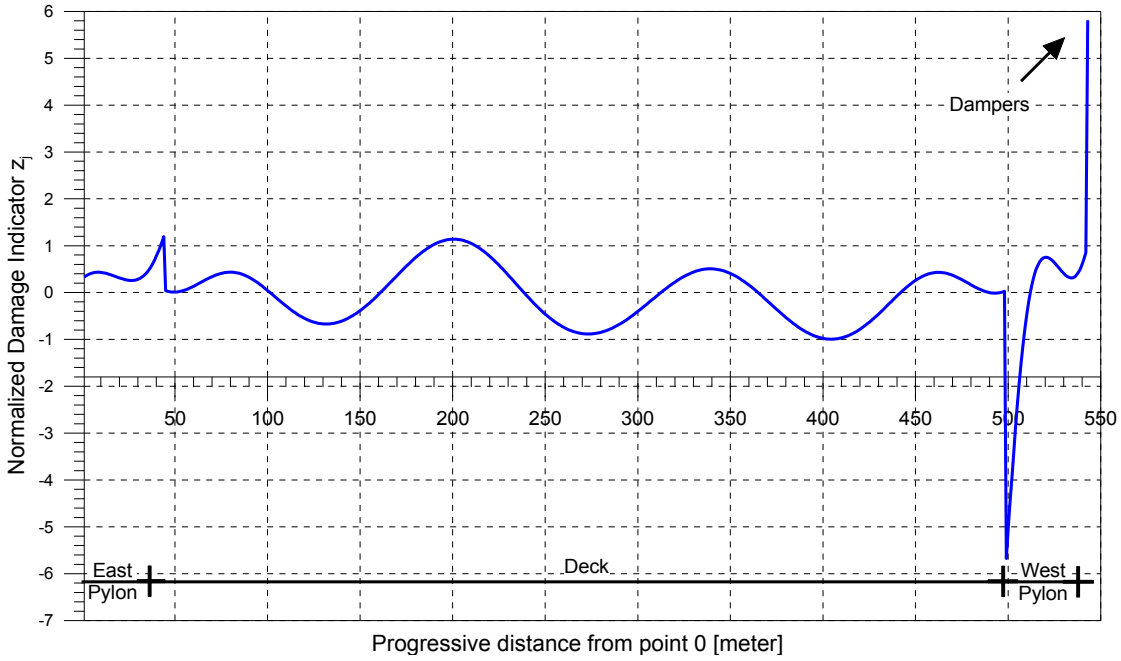

Figure 115. Damage 50%: Multimodal Normalized Damage Indicator

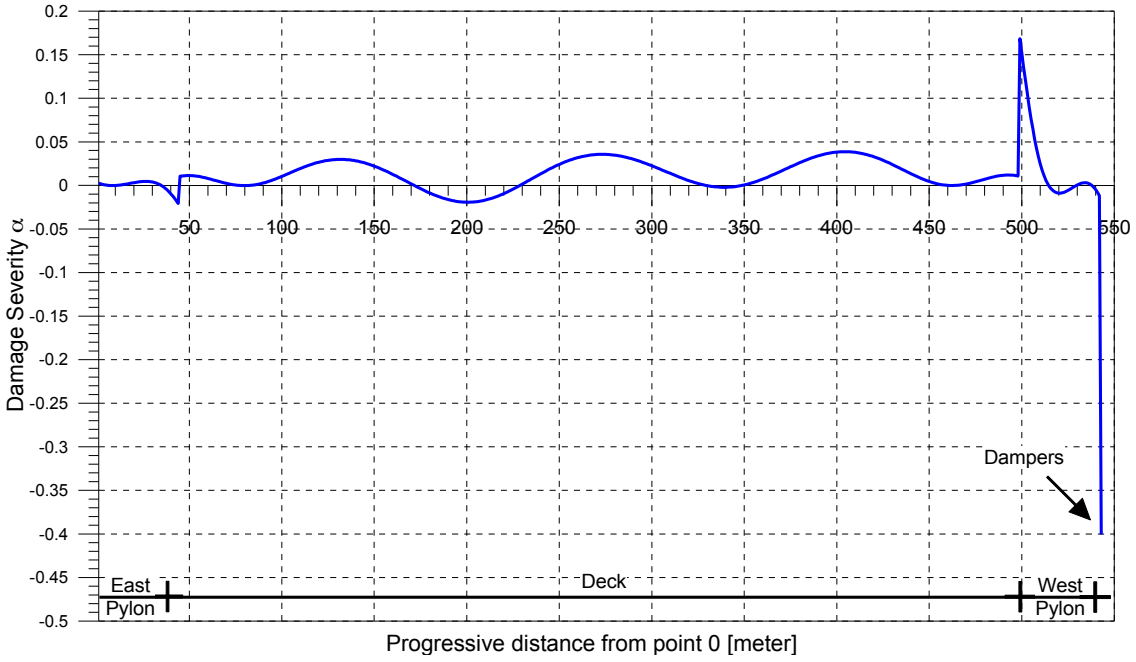

Figure 116. Damage 50%: Damage Severity Index α_j

5.3. Application of the damage detection algorithm to recorded data

Because of the location of the sensors it was impossible to consider the entire bridge structure but only the East side from mid-span to the abutment. The modal system identification and the damage evaluation of the bridge were completed by using acceleration data recorded from April 2003 to June 2011. A total of 13 sets of ambient-vibration acceleration records have been used in this study (**Table 14**). Data recorded in December 2006 are used as baseline undamaged scenario for the investigation of the degradation evolution in dampers. This is because the structure, at the time of this event, was equipped with a new series of dampers.

Table 14. Acceleration data sets

No	Year	Date	Hour	Record Length (sec)
1	2003	Apr	-	380.0
2	2006	June	-	129.0
3	2006	7 Dec	14:57:40.0	67.0
4	2007	11 July	08:58:27.0	58.0
5	2007	7 August	09:31:37.0	61.0
6	2011	7 June	09:59:38.0	54.0
7	2011	7 June	21:59:39.0	55.0
8	2011	14 June	09:59:38.0	54.0
9	2011	14 June	21:59:39.0	54.0
10	2011	21 June	09:59:38.0	54.0
11	2011	21 June	21:59:39.0	54.0
12	2011	28 June	09:59:38.0	54.0
13	2011	28 June	21:59:39.0	54.0

The Stochastic Subspace Identification method (SSI-Cov) (Peeters, 2000) was utilized to extract the modal parameters of the bridge from the recorded data. To locate and estimate the severity of the damage in the structure the proposed damage identification algorithm, with the appropriate modifications to take into account the existence of dampers, was applied.

The vertical component of motion of the deck was used for the damage detection procedure applied to the deck structure between mid-span and the east pylon. The motion in the bridge longitudinal direction was considered to detect possible degradation in the elements of the East Pylon. The vertical motion of the deck and the motion in longitudinal direction were used to estimate possible degradation in the dampers between main span and east tower and between east side span and east tower.

The nodes indicated in **Figure 117** and **Figure 118** represent positions where actual data are available on the deck and on the pylon (#1, 2, 5 for the deck, and #7, 8, 10 for the pylon). Additional nodes were used for the placement of the dampers and for restraining

conditions. The interpretative scheme needed for the damage assessment procedure is reported in **Figure 119**. As described above, this interpretative scheme is used for the assessment of the mode shapes. After the mode shapes are obtained a further discretization in a large number of elements is completed for the computation of the damage indicators.

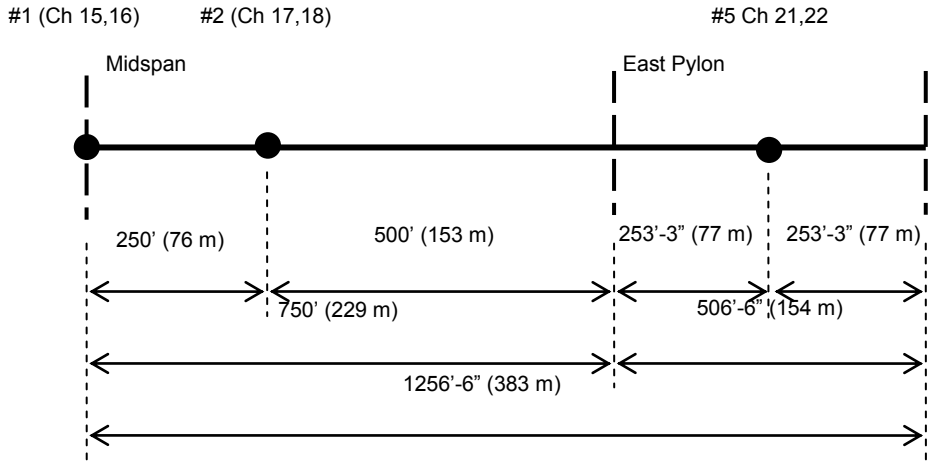

Figure 117. Location of the vertical channel on the deck.

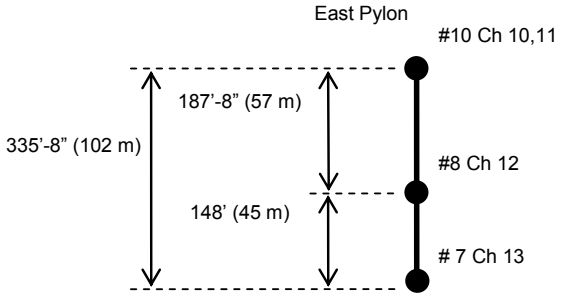

Figure 118. Location of the channel on the East Pier.

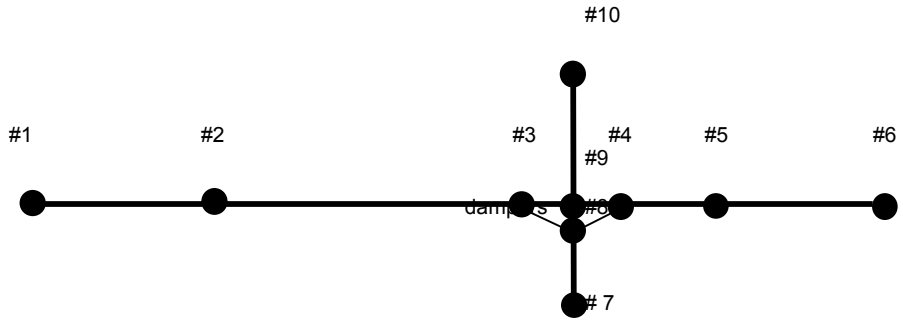

Figure 119. Location of the channel on the East Pier.

The mode shape obtained with the SSI-Cov method from the set of data recorded on December 2006, were used as a reference condition to estimate the location and the severity of the possible degradation that occurred in structural elements and/or energy dissipators. Mode characteristics of the first four vertical modes have been identified from each of the 13 acceleration data sets of **Table 14**. The structural identification process is affected by a number of factors, including non-linearities of the bridge behavior, environmental conditions, and limited information due to the reduced number of sensors. These factors can induce significant effects in both mode shapes and vibration frequencies. Based on a study on the Tamar Suspension Bridge, a 643m long suspension bridge which stands across the Tamar River connecting Saltash in Cornwall with the city of Plymouth in Devon, Cross et al. (2011) evidenced the importance of the variations of the deck's first five natural frequencies, along with the temperature and wind speed. These effects were found to account up to 20% of the variance in the frequency data, with non-linear behavior and limited information accounting for about 80% of the variance. The variations in frequency that the authors found for the Tamar Bridge were up to 0.04 Hz over a time period of a single day. For the Vincent Thomas Bridge, the frequency variation due to the mentioned effects is likely to be higher than the frequency variation due to damages in the dampers, which only slightly affect the natural frequencies of the bridge. In **Table 15** the identified mode frequencies are summarized.

Table 15. Modal frequencies

Event #	1st mode	2nd mode	3rd mode	4th mode
1	0.225	0.399	0.432	0.580
2	0.225	0.361	0.440	0.580
3	0.234	0.360	0.457	0.567
4	0.235	0.346	0.440	0.553
5	0.227	0.366	0.440	0.580
6	0.240	0.350	0.440	0.547
7	0.240	0.350	0.466	0.547
8	0.240	0.346	0.432	0.553
9	0.240	0.350	0.432	0.580
10	0.240	0.372	0.433	0.553
11	0.220	0.350	0.432	0.553
12	0.220	0.346	0.432	0.580
13	0.224	0.346	0.440	0.580

The vibration frequency of the modes is plotted for each event in **Figure 120**. In agreement with results of Cross et al. (2011), higher modes frequencies were found more subject to changes than the 1st mode. A maximum variation (0.05Hz) was found for the 2nd (asymmetric mode) vibration frequency, while the 1st (symmetric mode) frequency is more stable, with a variation of about 0.02 Hz through the whole range of events.

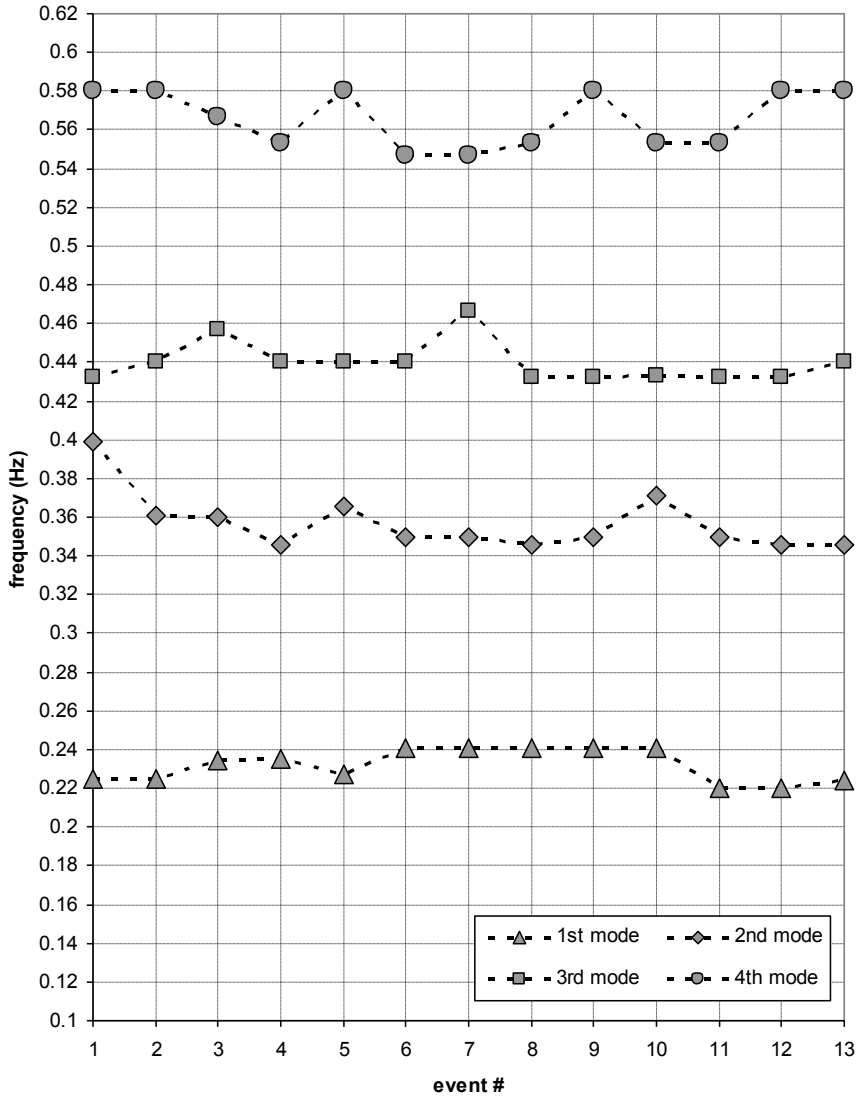

Figure 120. Identified vibration frequencies.

Mode shapes of the four principal vertical modes are reported graphically in **Figure 121** to **Figure 133**.

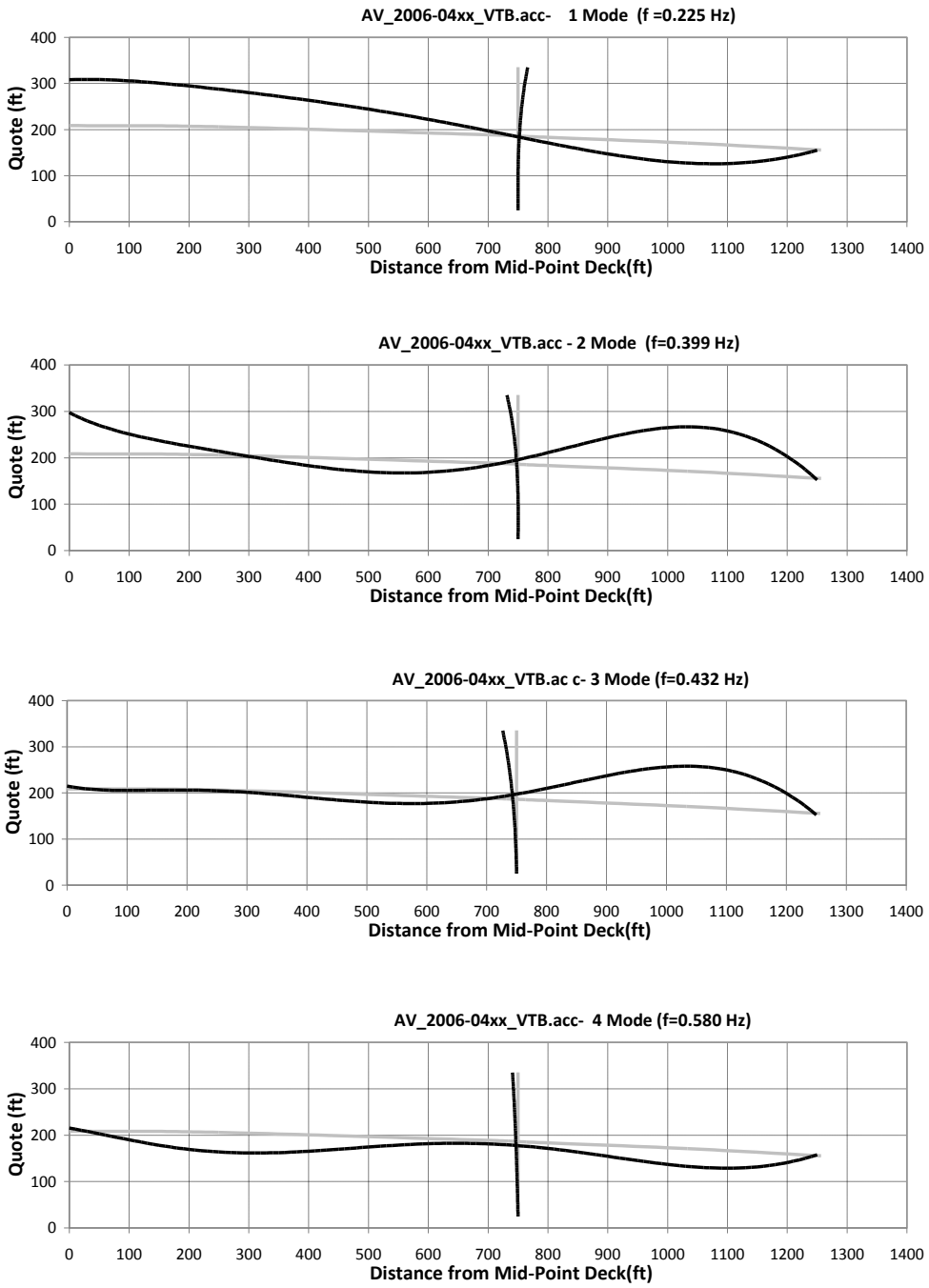

Figure 121. Identified mode shapes – data set 2006, April.

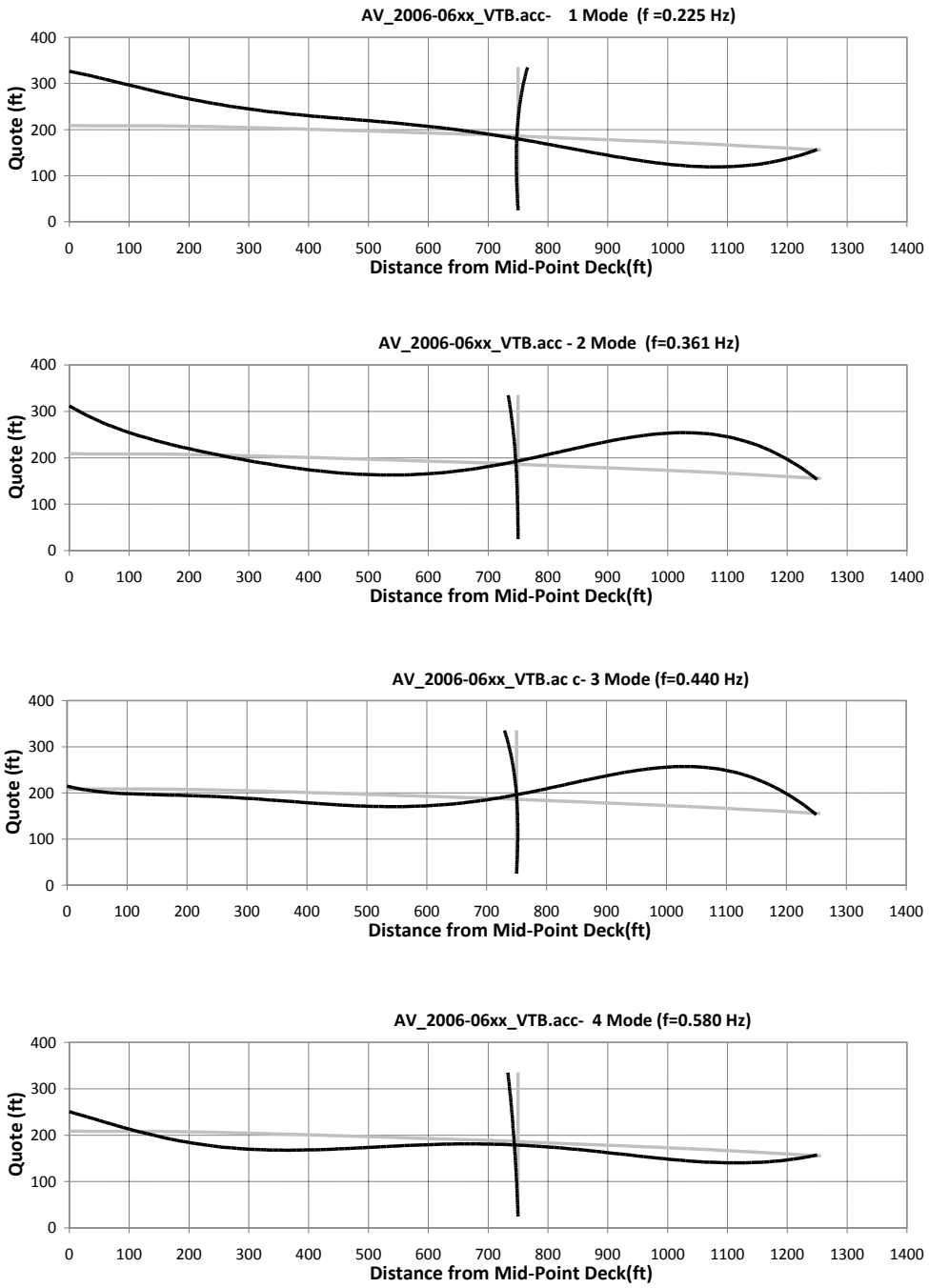

Figure 122. Identified mode shapes – data set 2006, June.

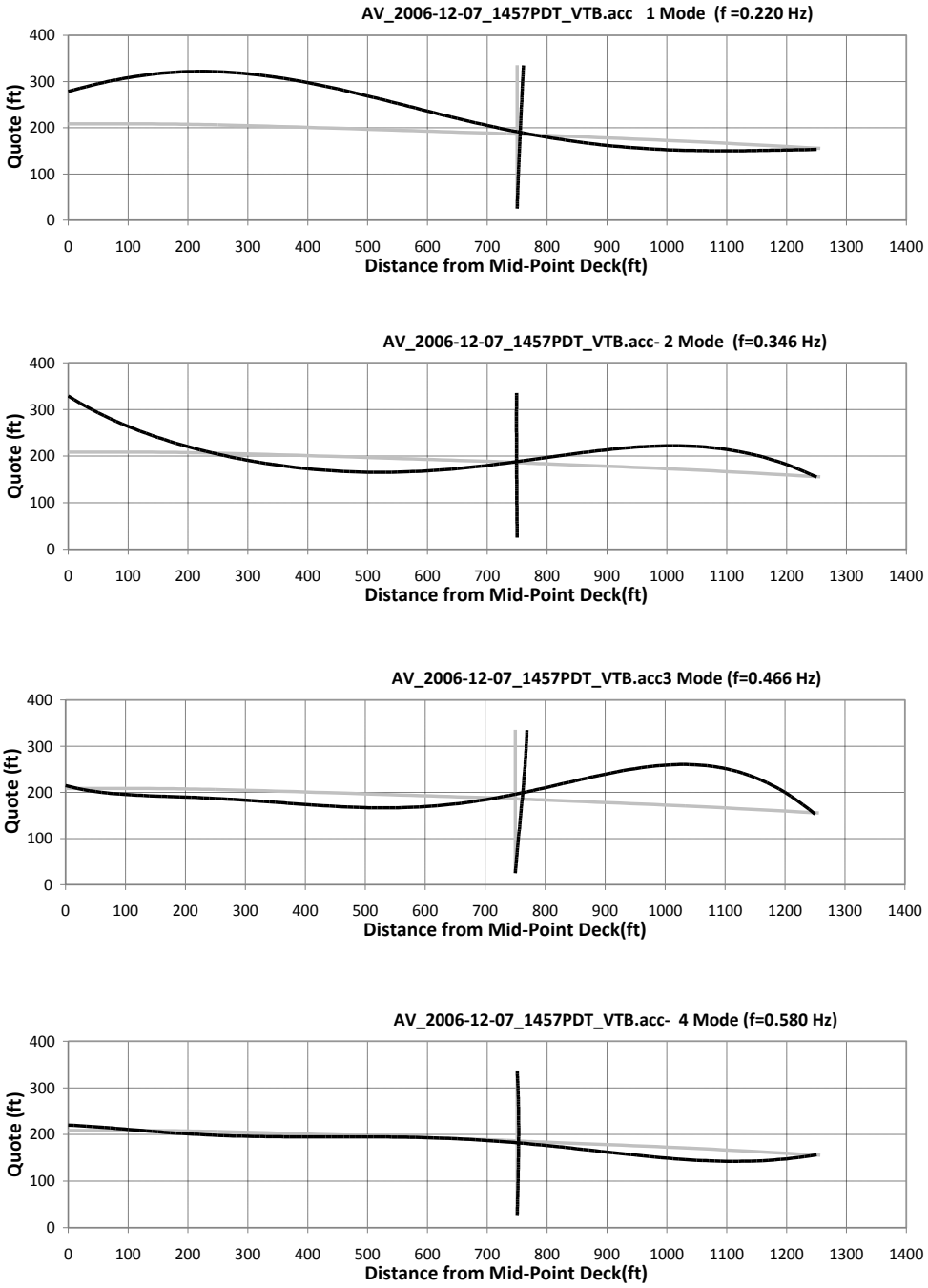

Figure 123. Identified mode shapes – data set 2006, Dec 07.

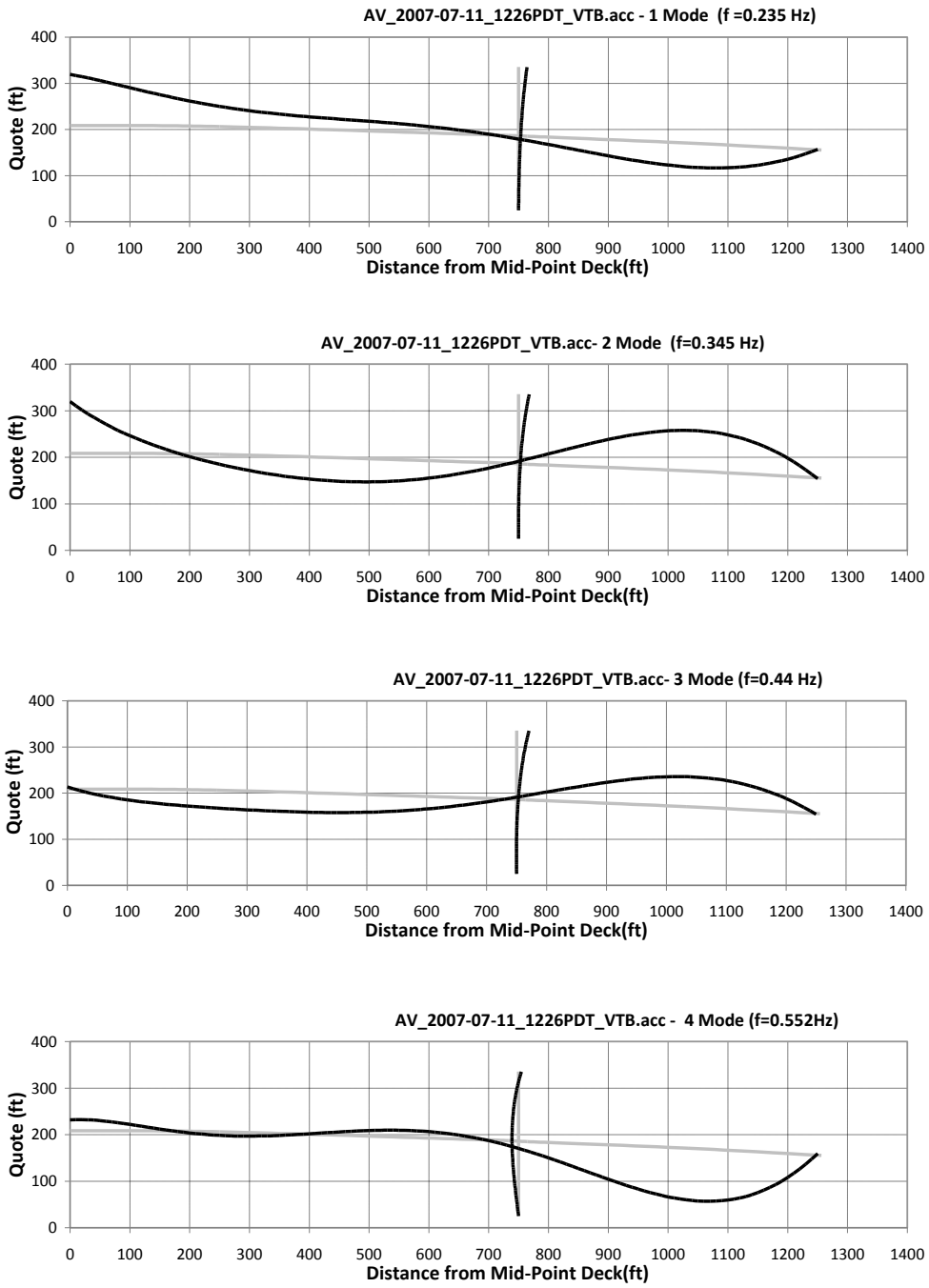

Figure 124. Identified mode shapes – data set 2007, Jul 11.

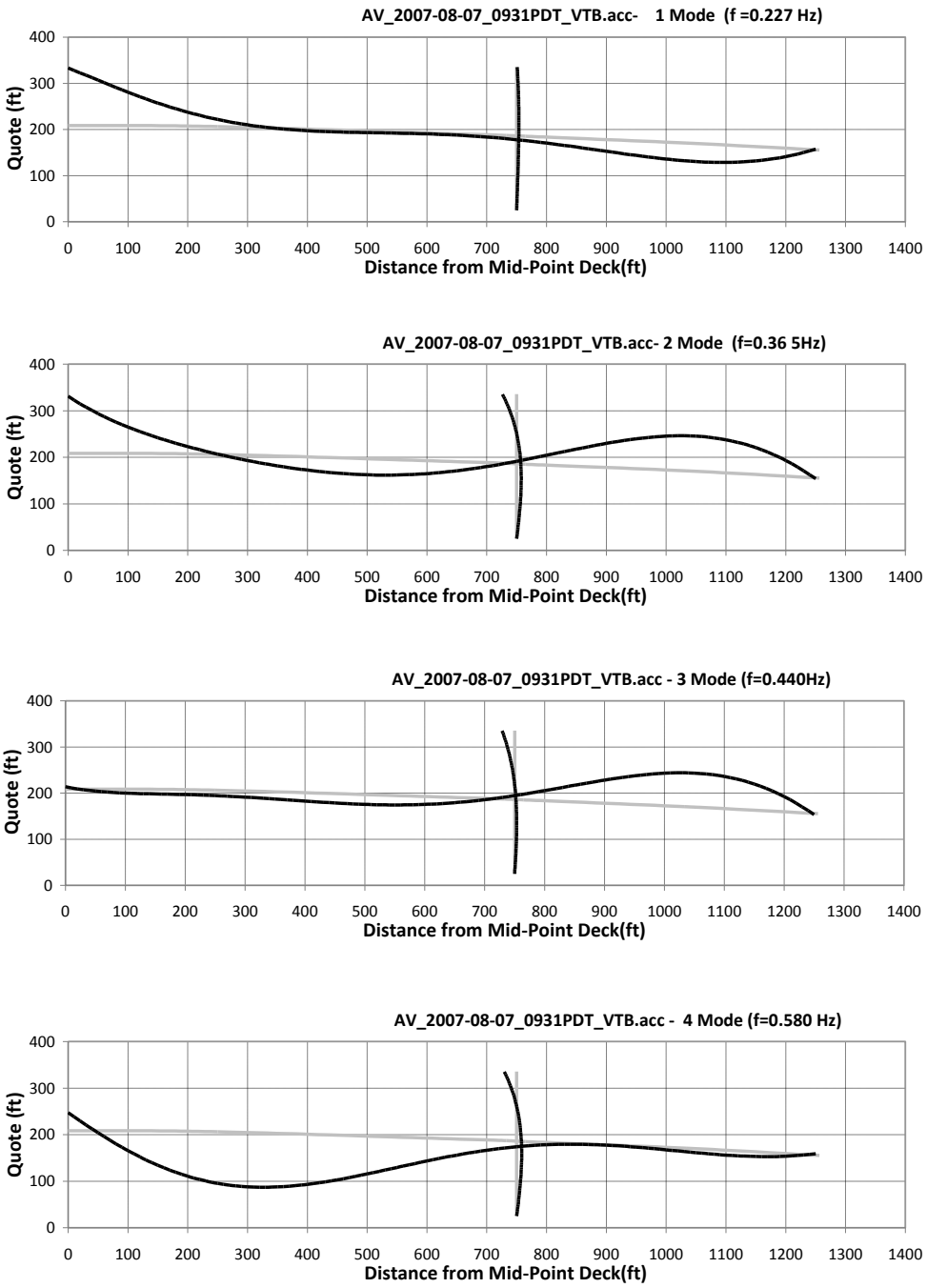

Figure 125. Identified mode shapes – data set 2011, Aug 07.

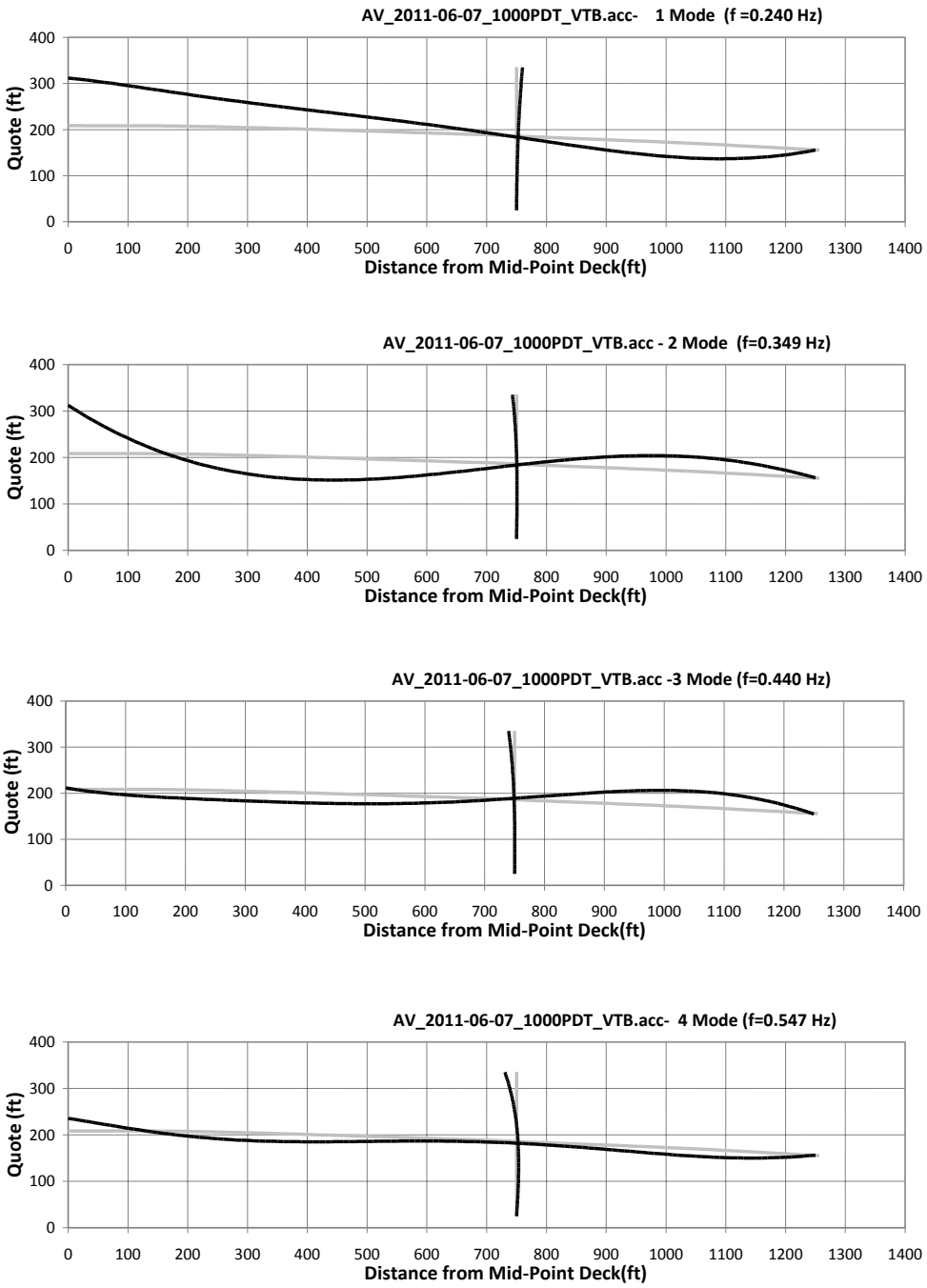

Figure 126. Identified mode shapes – data set 2011, Jun 07 – 10AM.

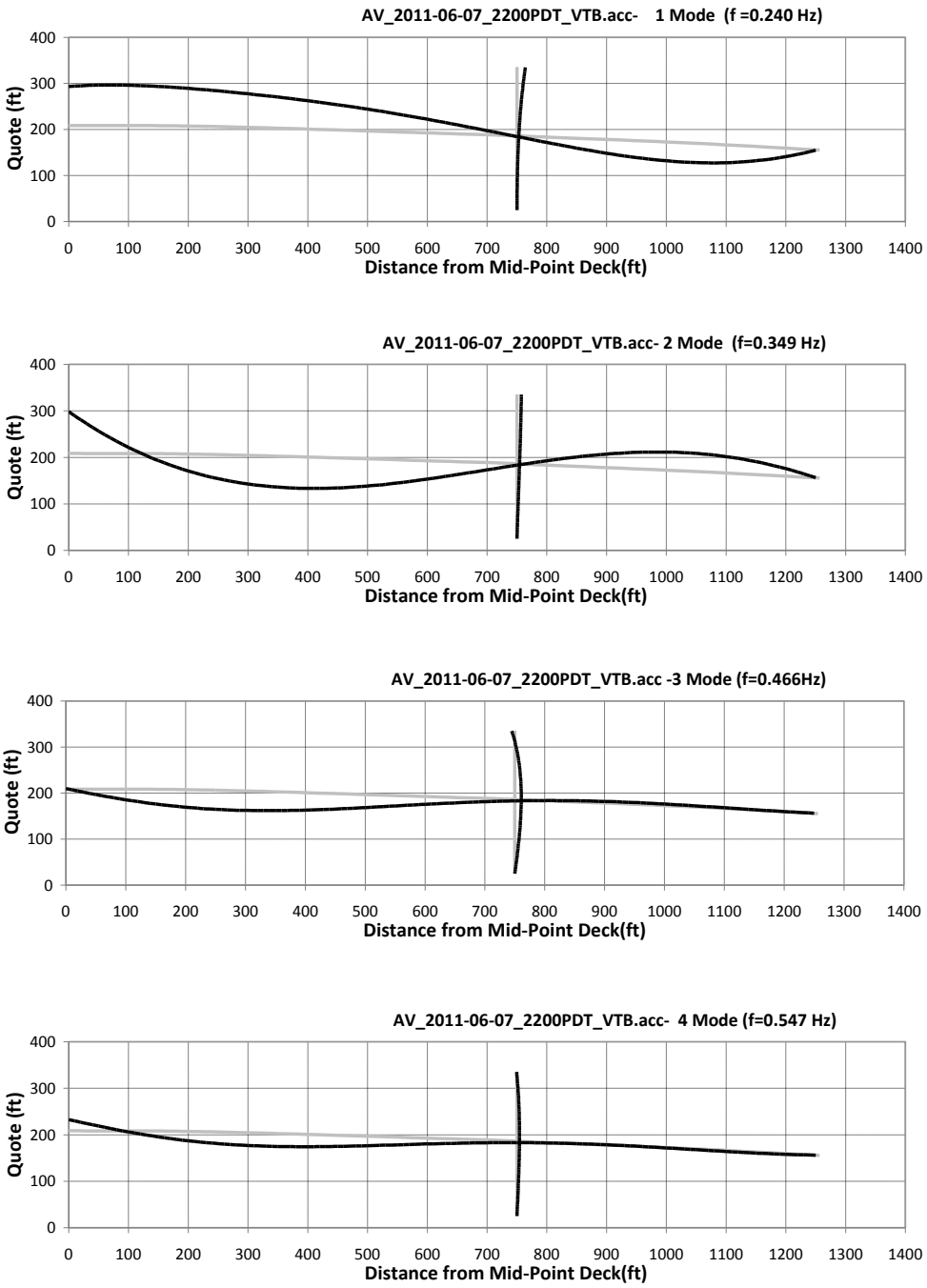

Figure 127. Identified mode shapes – data set 2011, Jun 07 – 10PM.

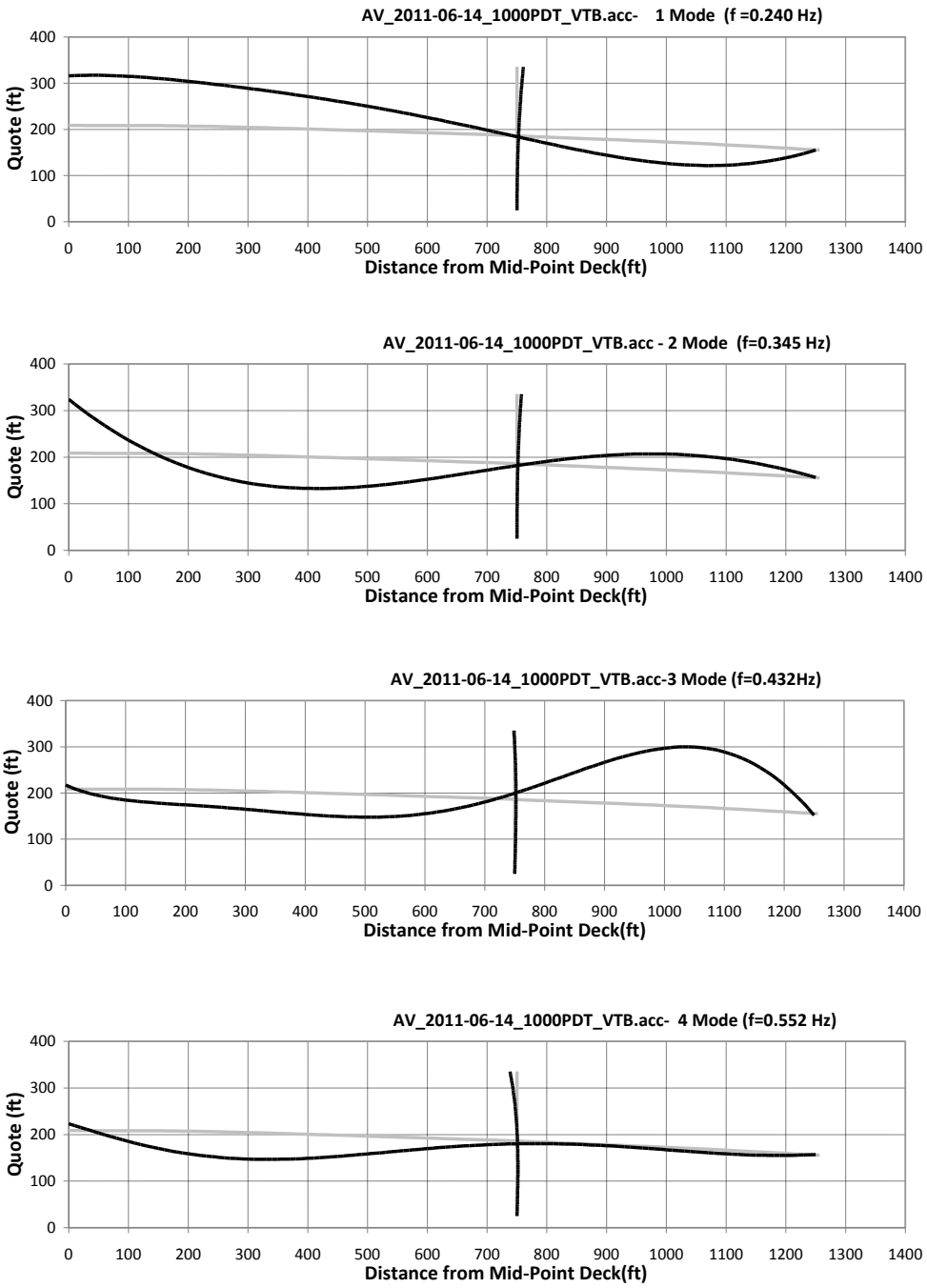

Figure 128. Identified mode shapes – data set 2011, Jun 14 – 10AM.

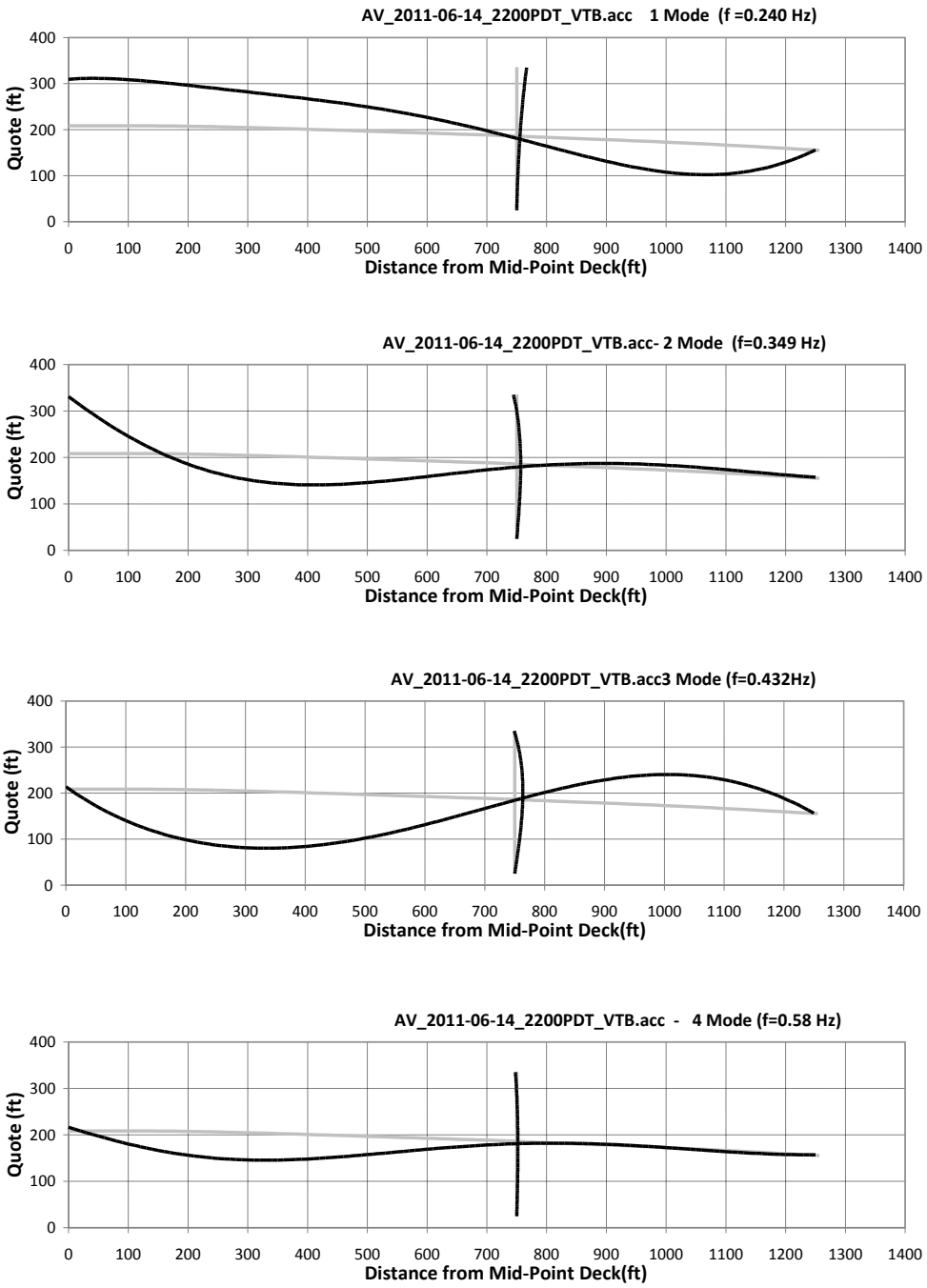

Figure 129. Identified mode shapes – data set 2011, Jun 14 – 10PM.

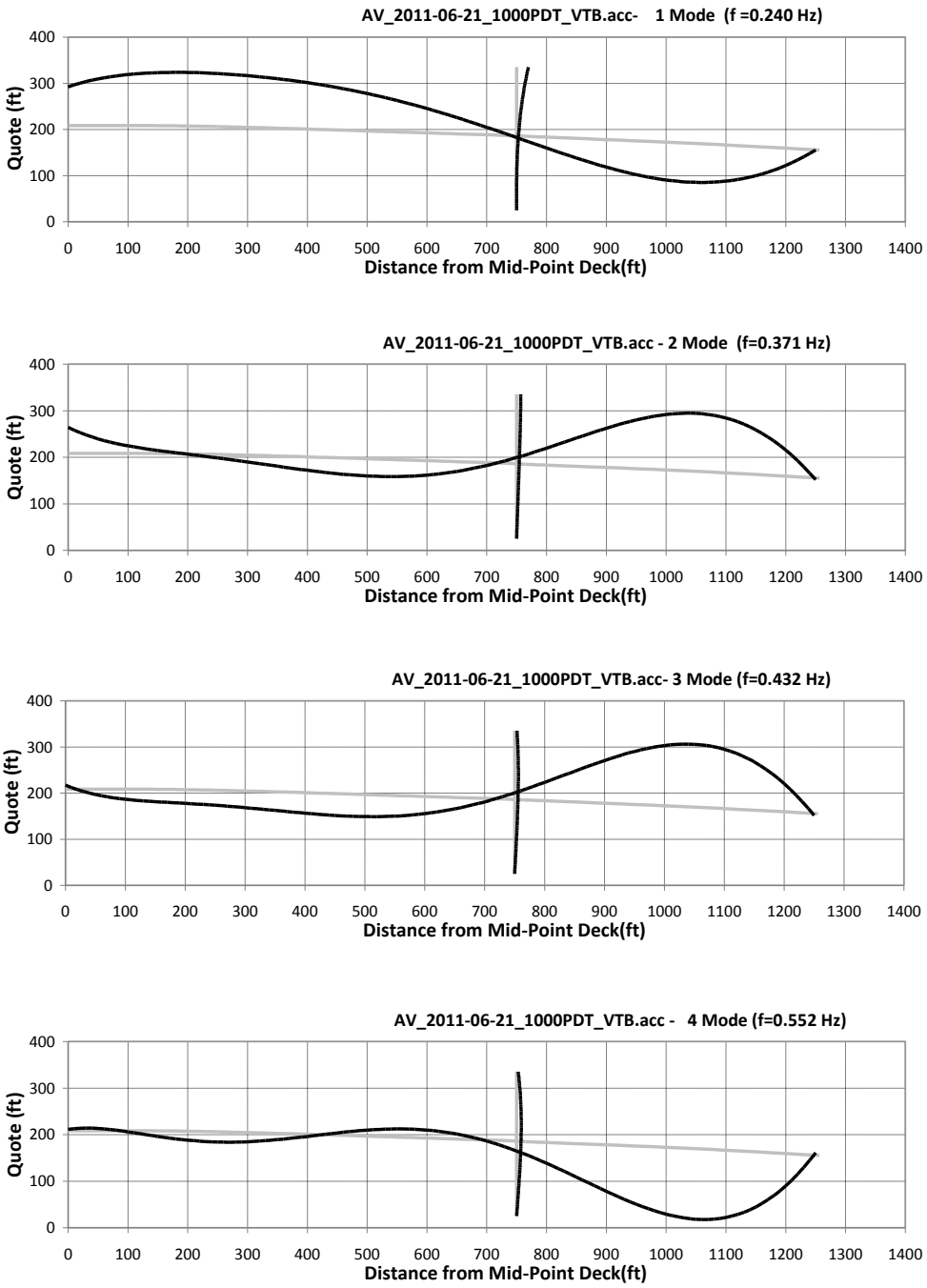

Figure 130. Identified mode shapes – data set 2011, Jun 21 – 10AM.

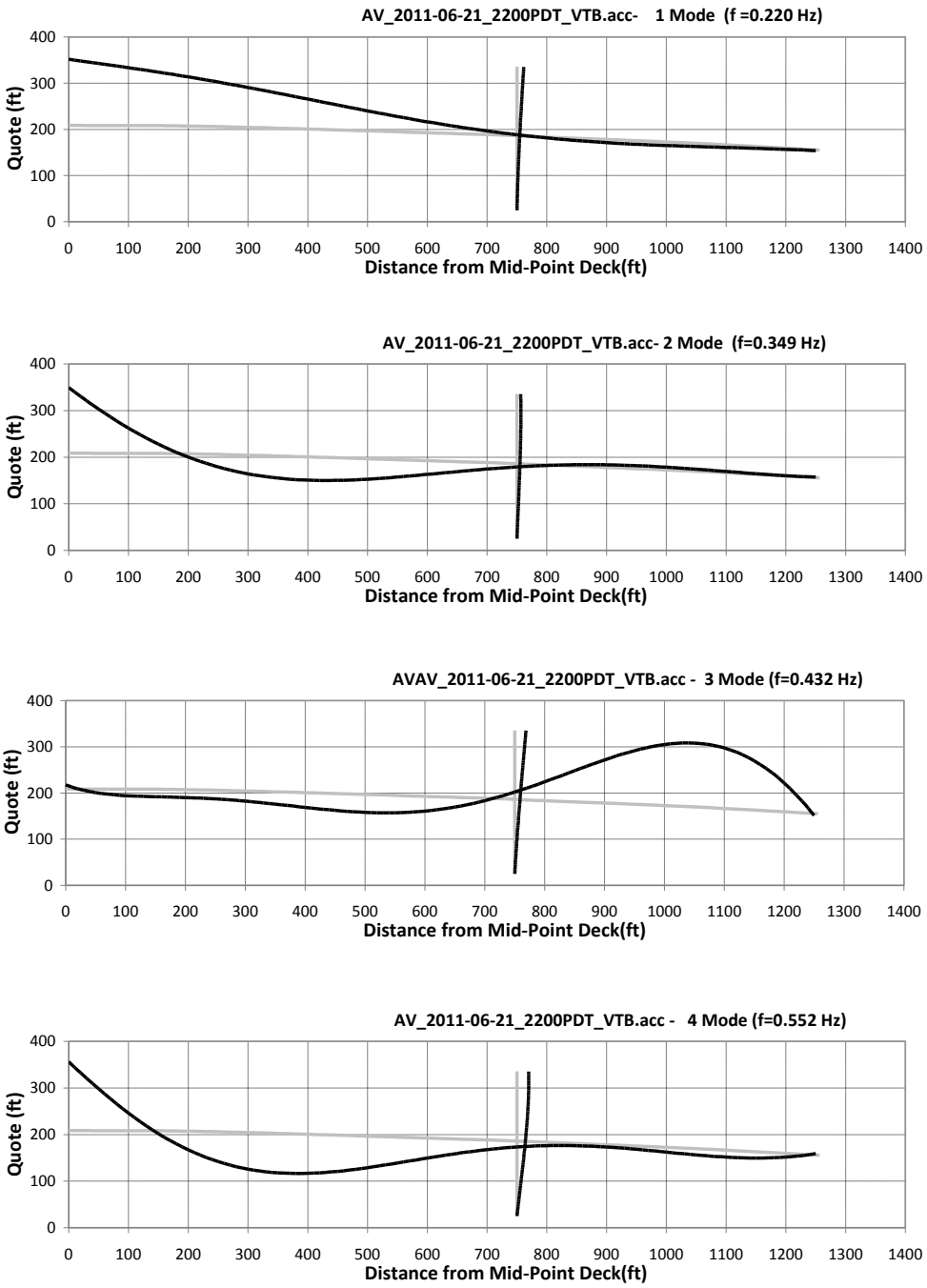

Figure 131. Identified mode shapes – data set 2011, Jun 21 – 10PM.

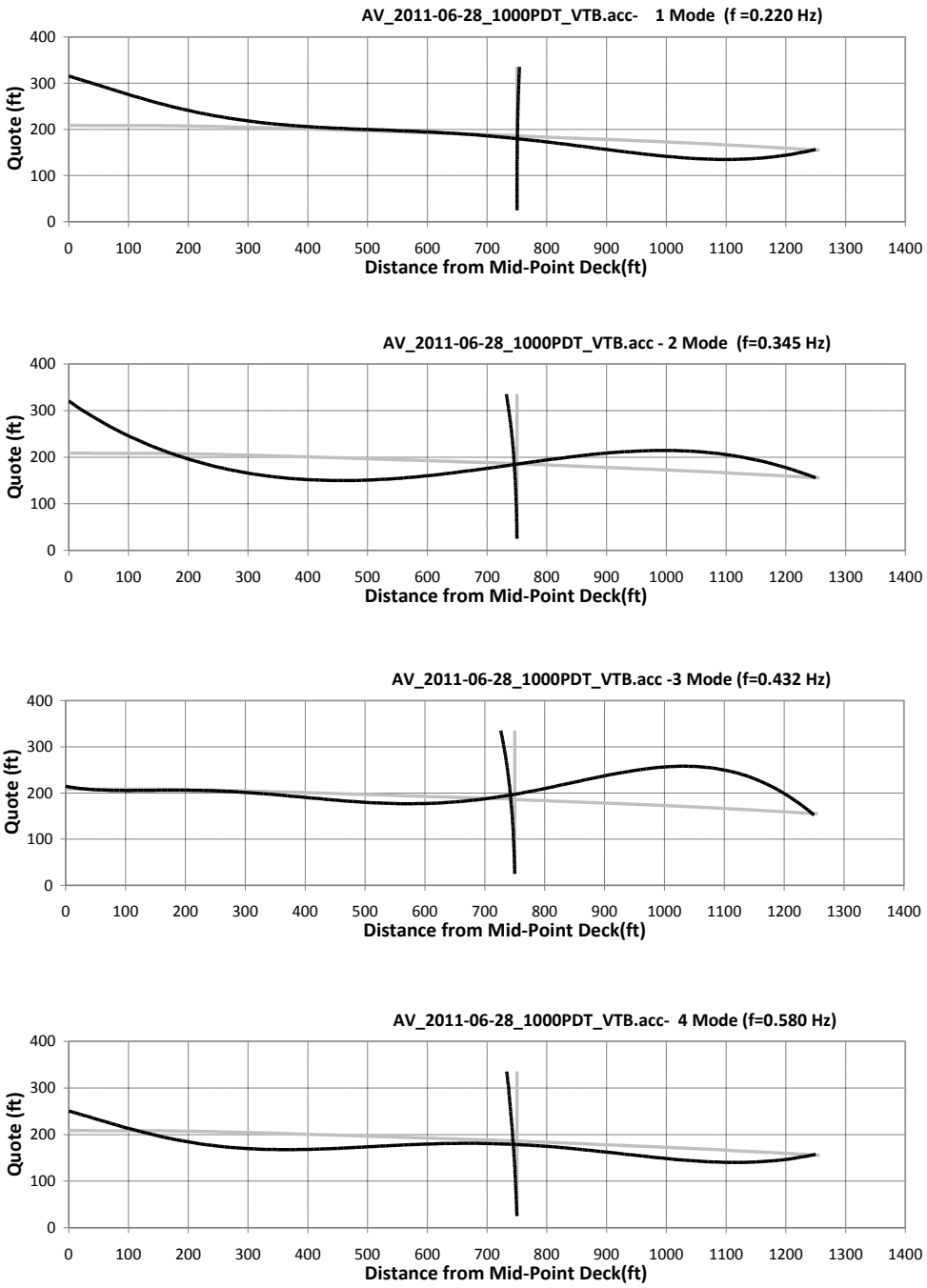

Figure 132. Identified mode shapes – data set 2011, Jun 28 – 10AM.

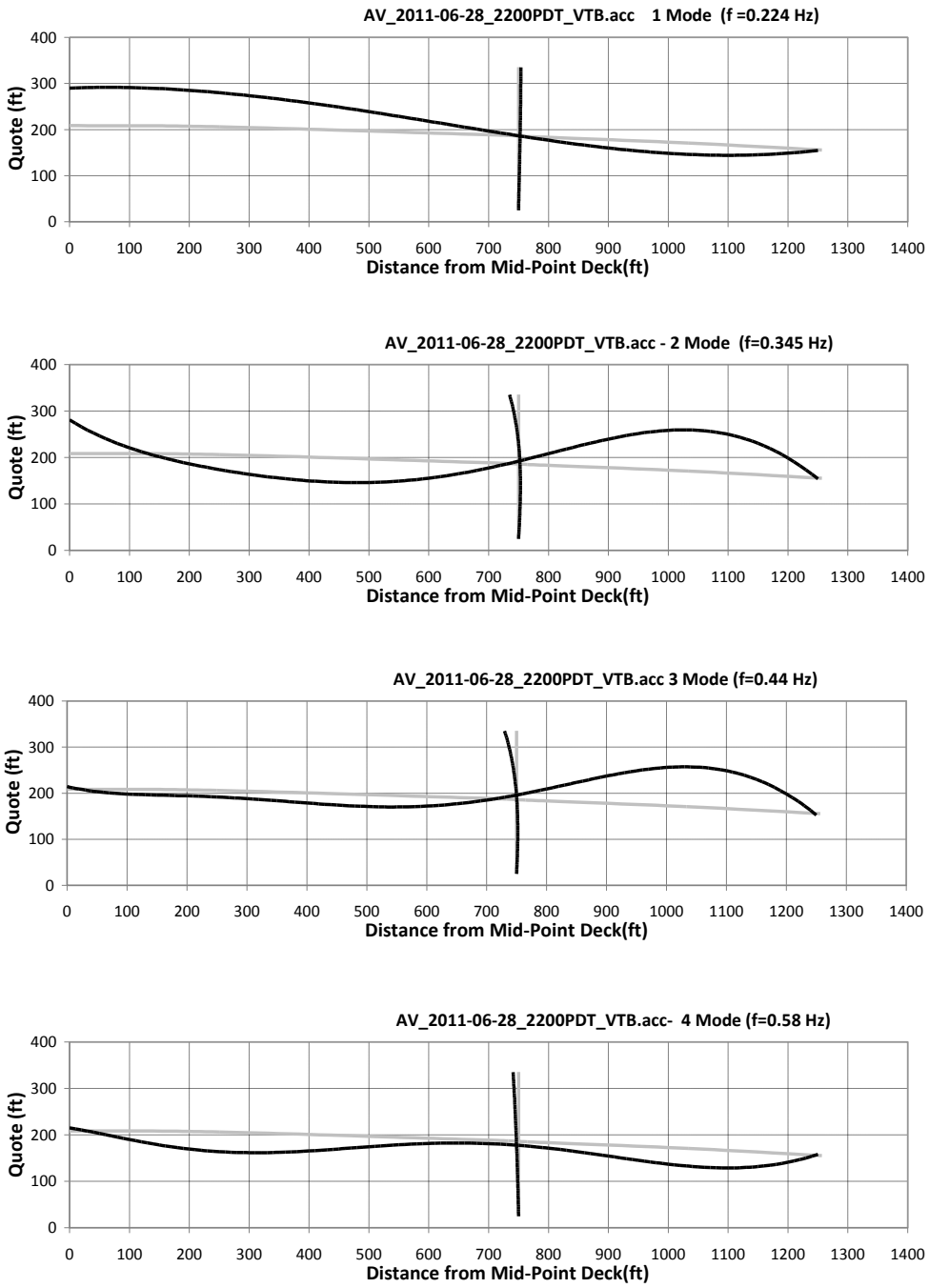

Figure 133. Identified mode shapes – data set 2011, Jun 28 – 10PM.

The uncertainty associated with the modes shapes identification affects also the results of the damage detection algorithm. Any changes in the single mode shape can be interpreted

as due to a local change in the stiffness of a portion of the structure and hence produce false positive in the damage identification. For this reason, a reasonable number of vibration modes can be used to reduce the occurrence of such errors. It must be noted that for this case study higher changes were found for the 3rd and 4th mode. The damage identification procedure combines results from the four modes through Eq. 25. The multimodal localization indicator Z_j (Eq. 26) and severity index α_j (Eq. 27) are plotted in **Figure 134** to **Figure 145**, where the event #3 (December 2006) has been used as a reference condition. The indices are plotted for the deck, the east tower, and the dampers separately. Information is limited to the east portion of the bridge, due to lack of sensors on the other side of the structure. The first two modes were found to have higher contributes to the multimodal damage indices, respect to higher modes.

For events #1, 2, occurred before December 2006, i.e. before the damaged dampers were replaced, no damage was identified in the deck and in the tower. For the dampers connecting the tower to the main span, instead, a consistent reduction of stiffness was detected. The amount of the effective stiffness reduction was higher than 80% and is indicative of a severe reduction of their dissipative performance.

For the events after Decembers 2006, i.e. events #4 to 13, no significant stiffness reduction was identified for the tower. From the acceleration data sets #6, 8, 9, and 12, low severity index values were found for the deck. In events #6, 8, and 12, these stiffness reductions were localized in the portion of the deck close to the tower, where the dampers are connected. For event #9 of **Figure 141**, severity index values up to -0.35 were found in proximity of the bridge mid-span. The stiffness reductions however appear only for few events and are likely to be related to shift of null curvature points along the deck, which can produce false positive in the damage detection algorithm.

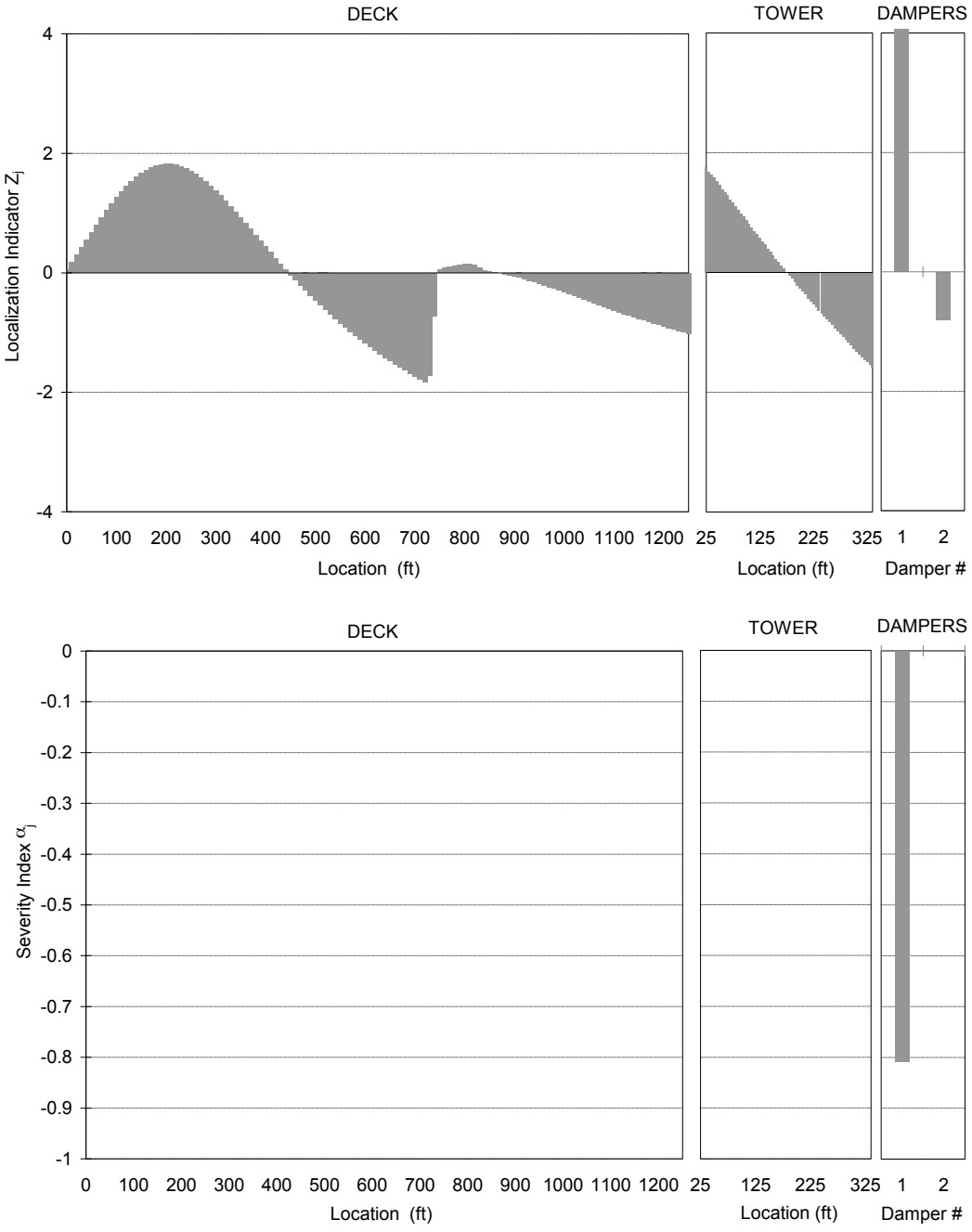

Figure 134. Damage localization indicator and damage severity index – 2006, Apr.

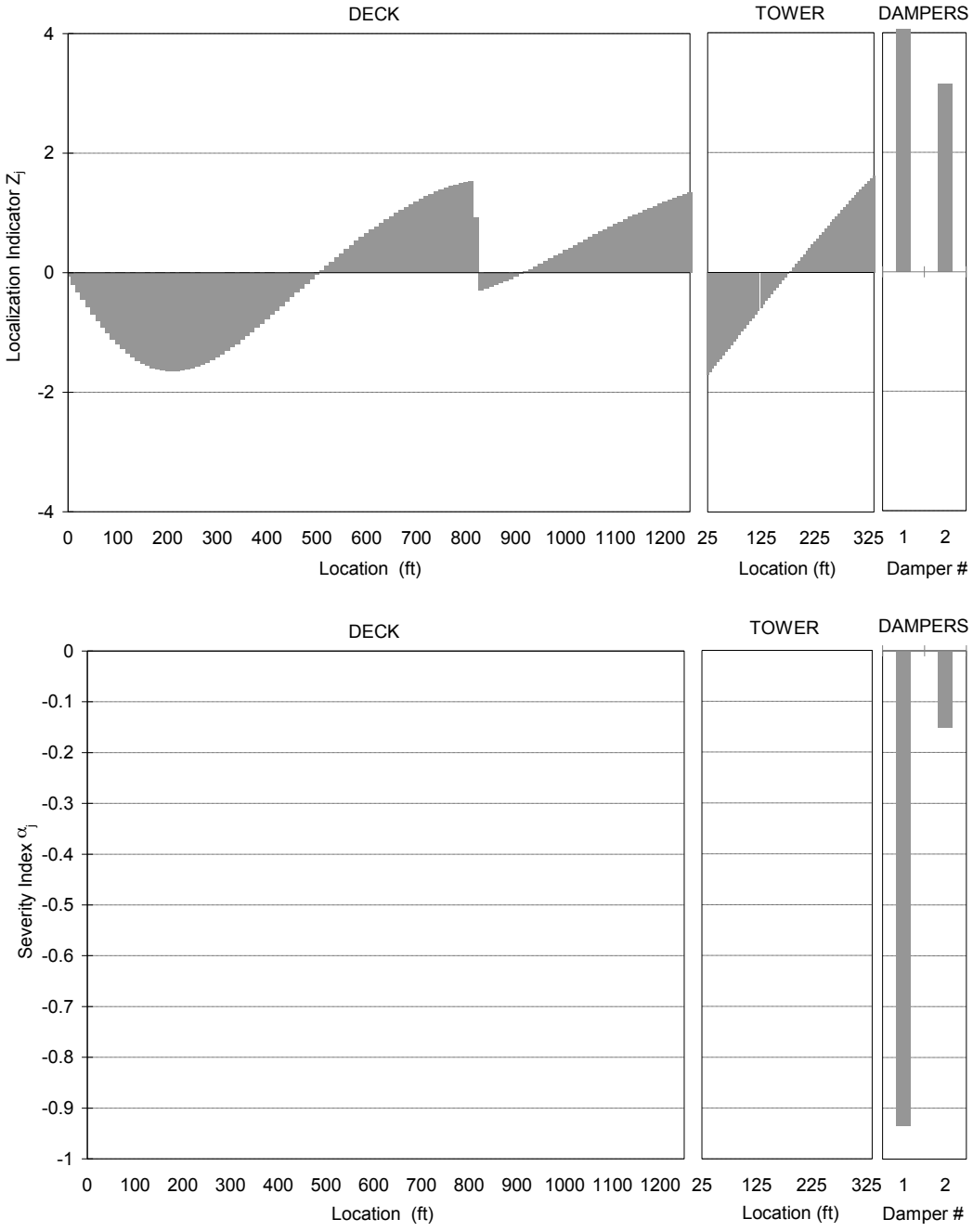

Figure 135. Damage localization indicator and damage severity index – 2006, June.

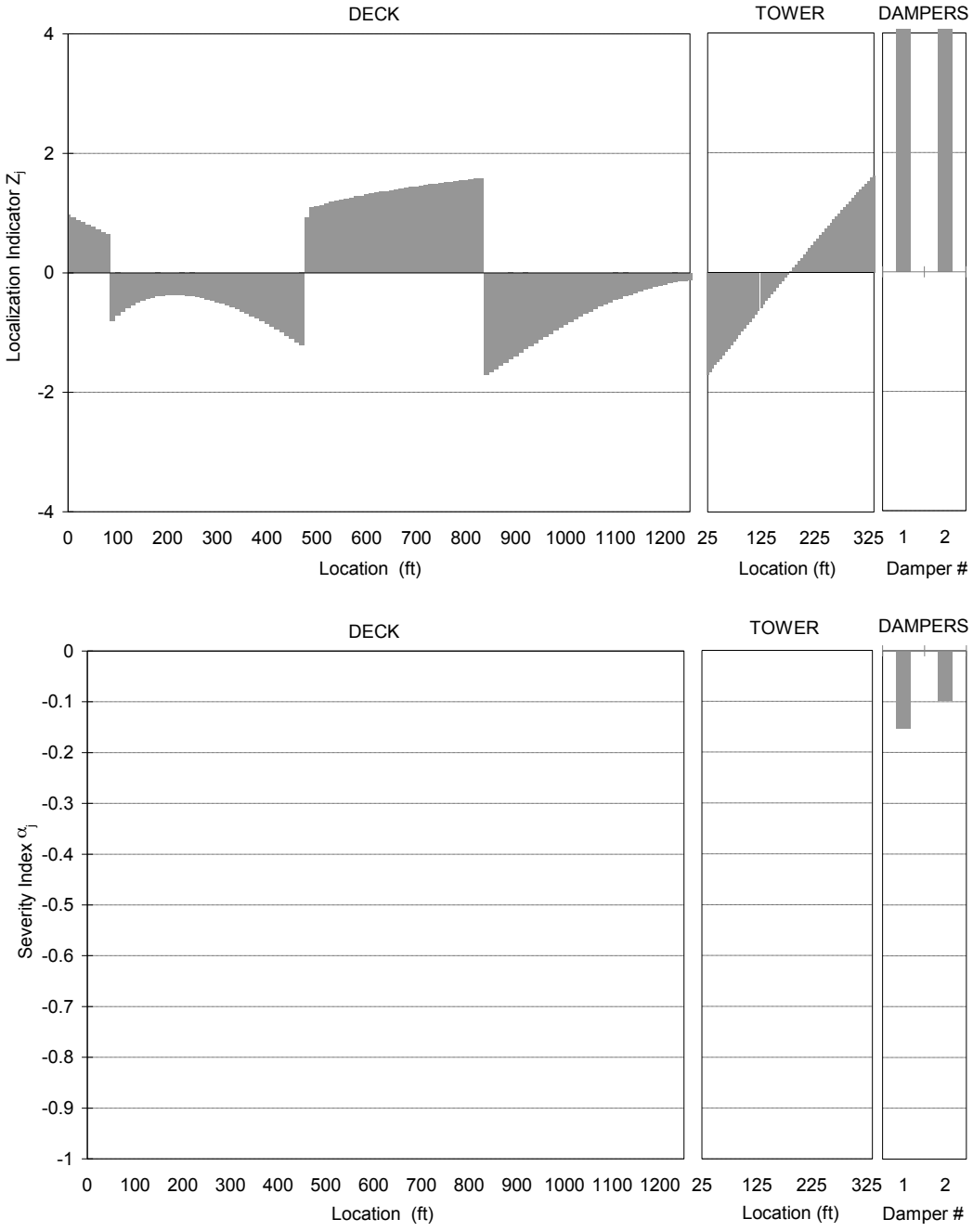

Figure 136. Damage localization indicator and damage severity index – 2007, Jul 11.

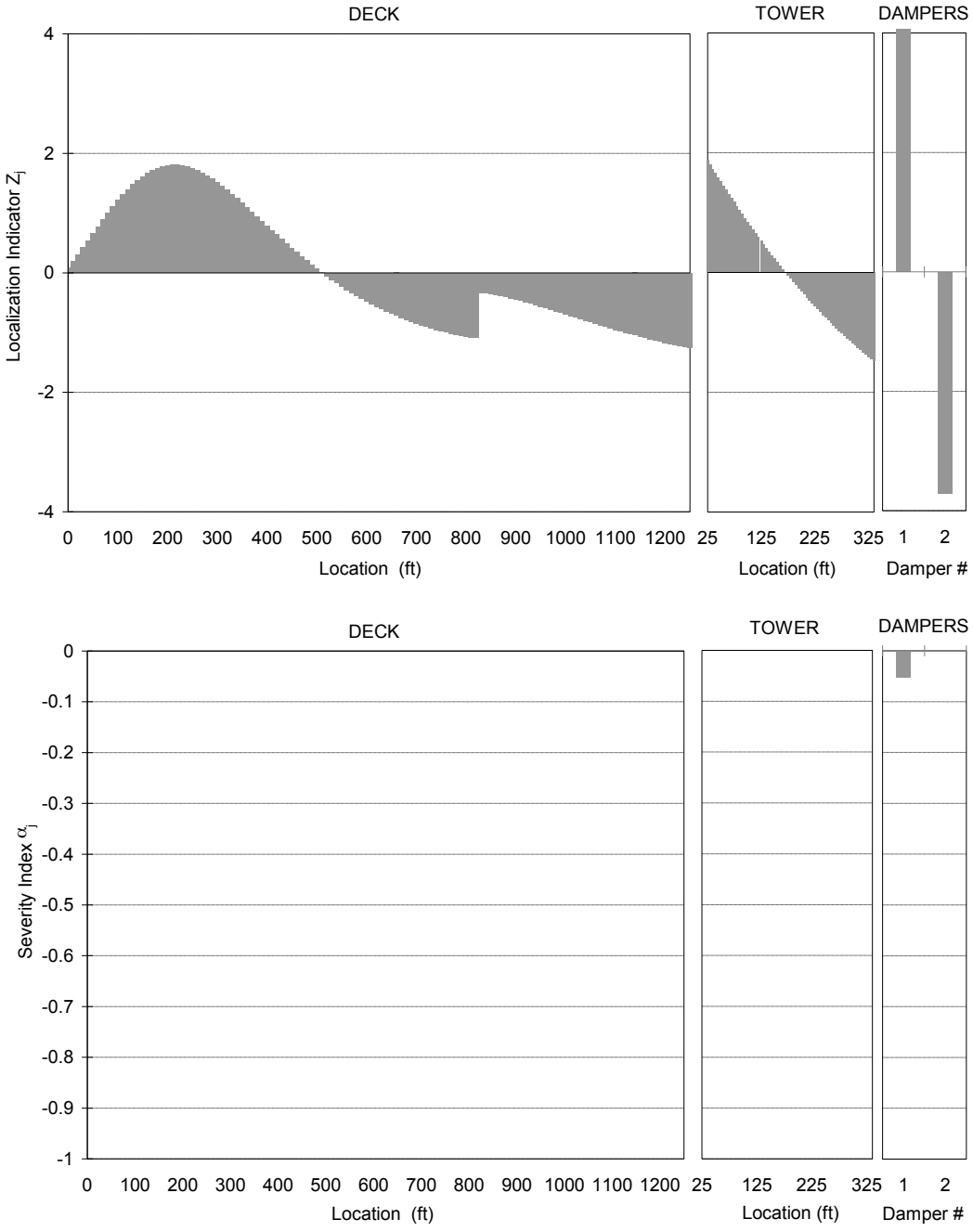

Figure 137. Damage localization indicator and damage severity index – 2007, Aug 07.

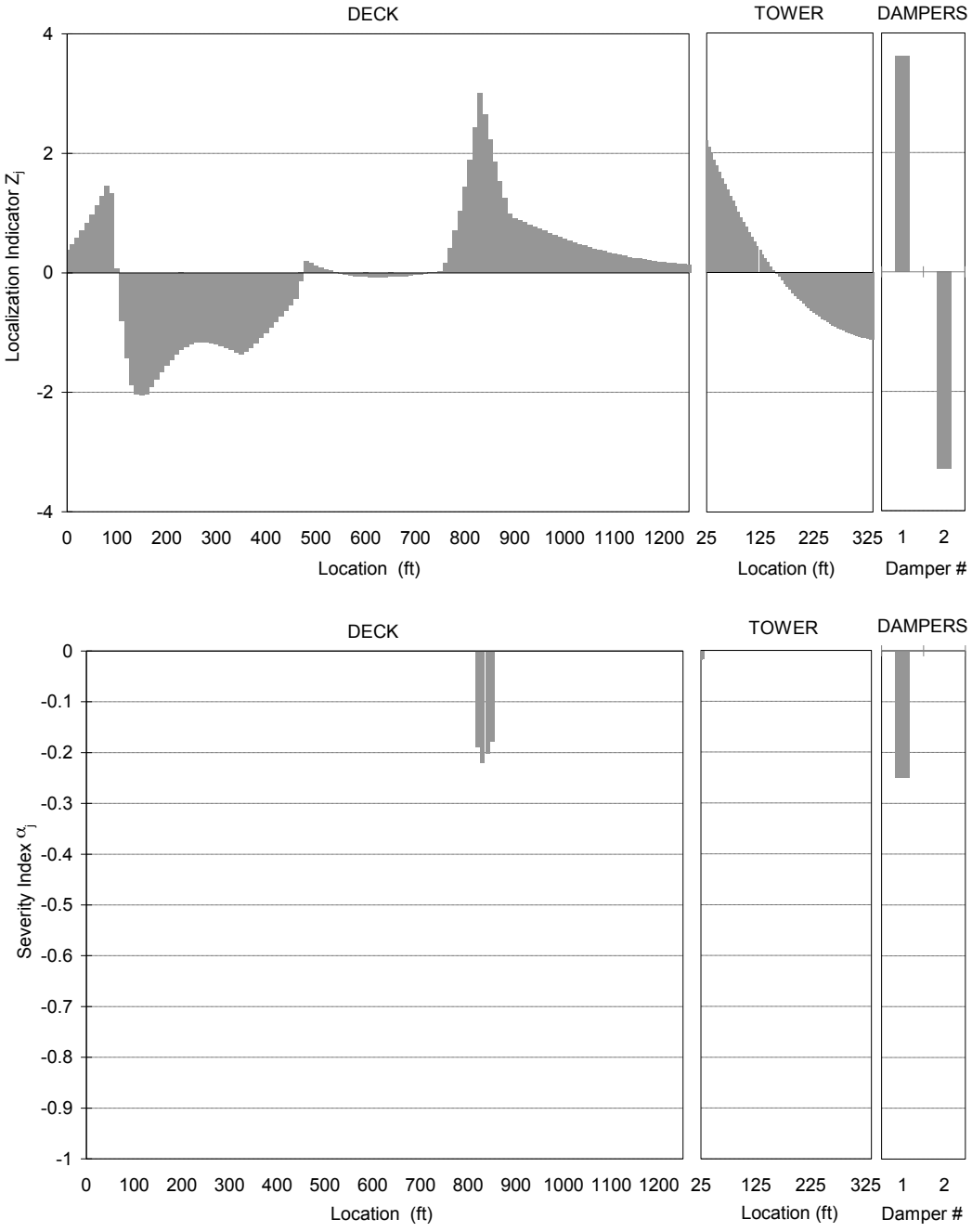

Figure 138. Damage localization indicator and damage severity index – 2011, Jun 07 - 10AM.

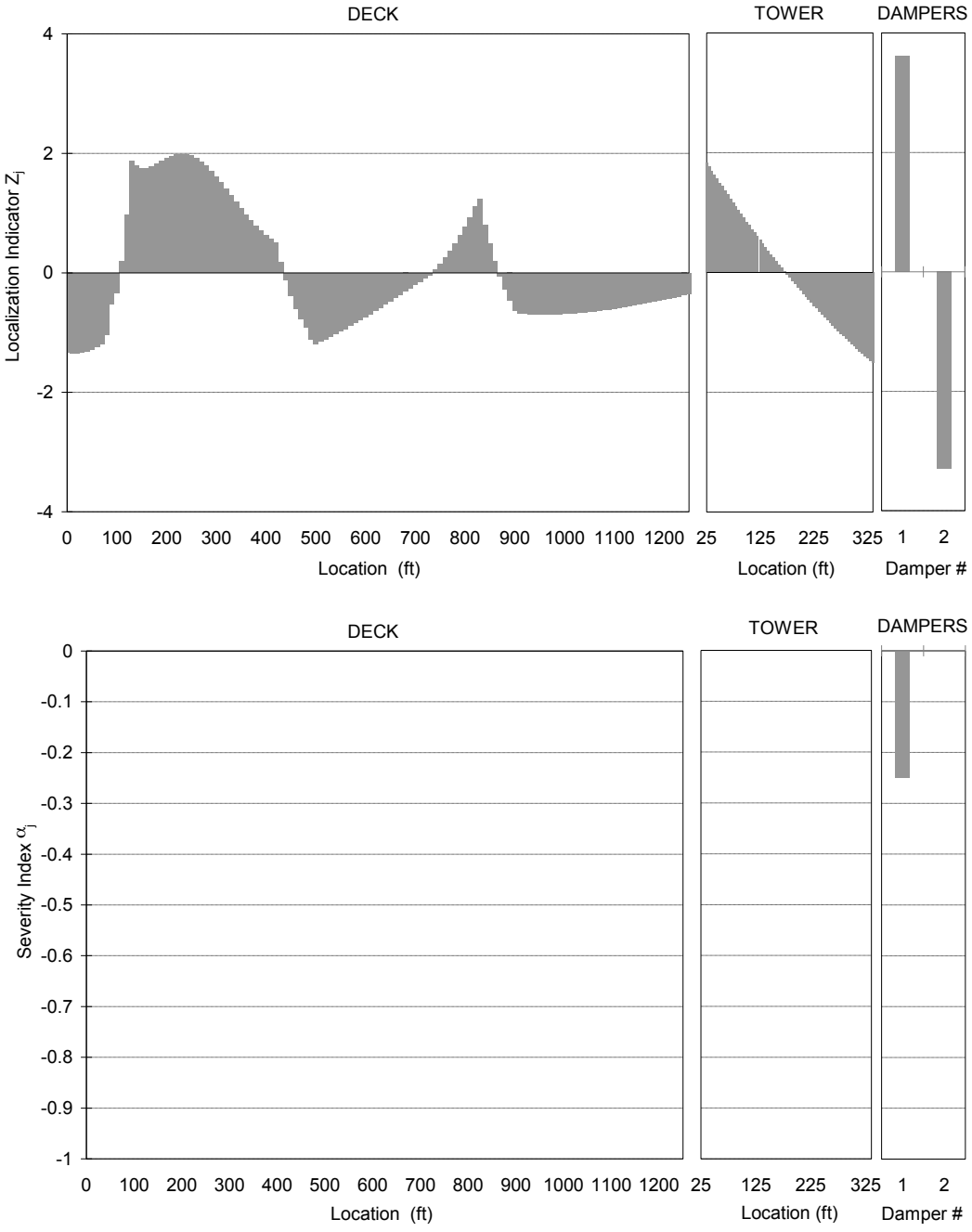

Figure 139. Damage localization indicator and damage severity index – 2011, Jun 07 - 10PM.

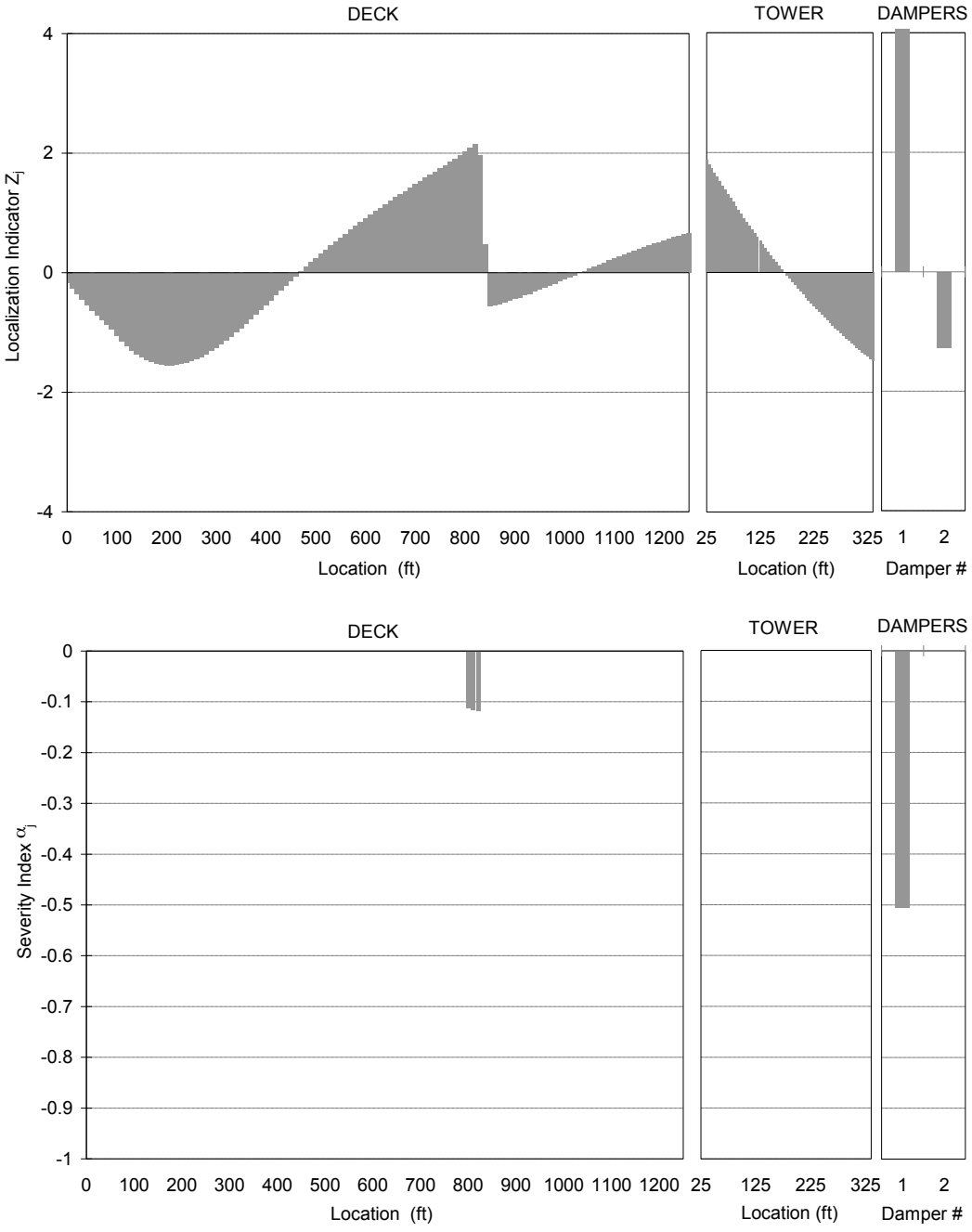

Figure 140. Damage localization indicator and damage severity index – 2011, Jun 14 - 10AM.

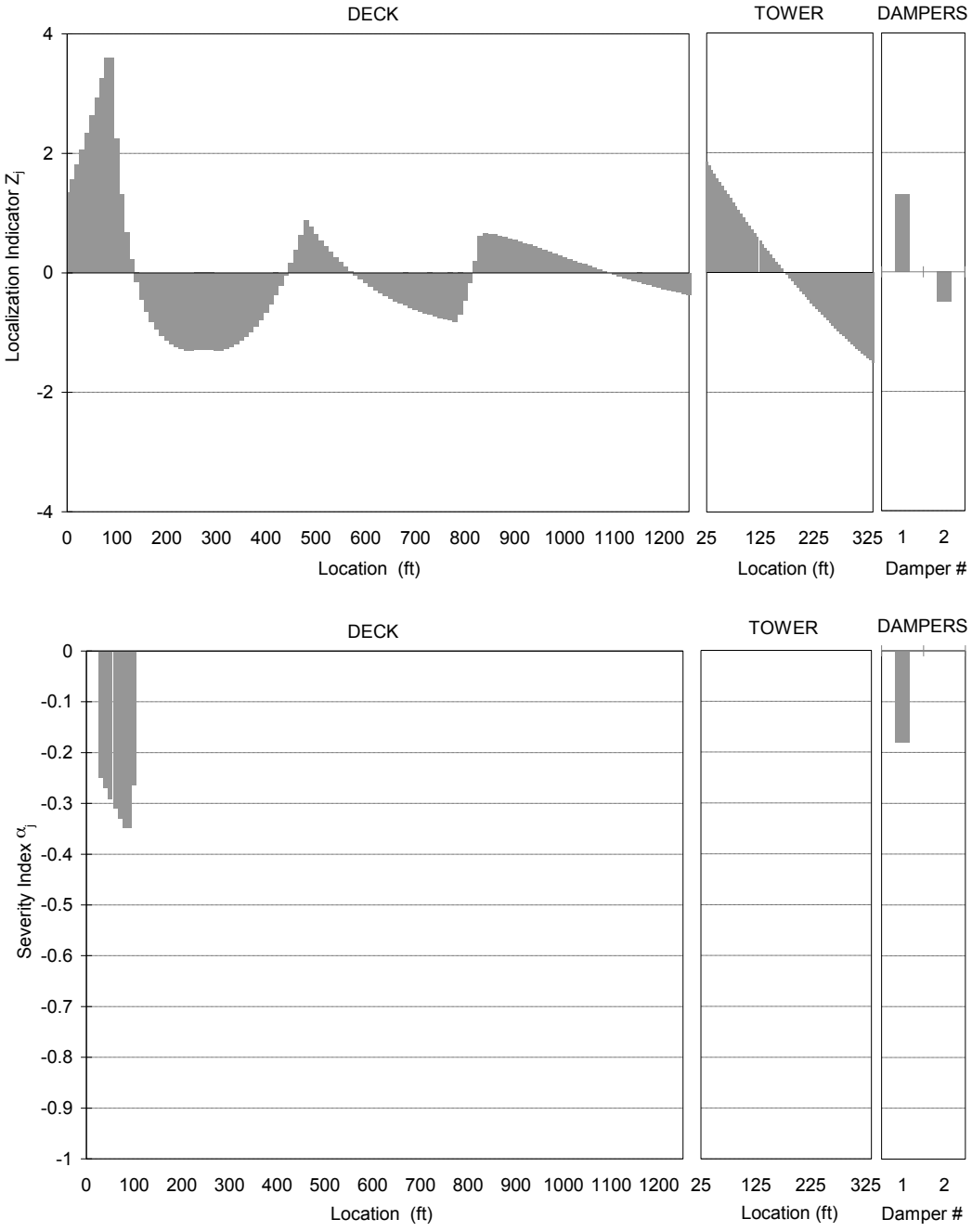

Figure 141. Damage localization indicator and damage severity index – 2011, Jun 14 - 10PM.

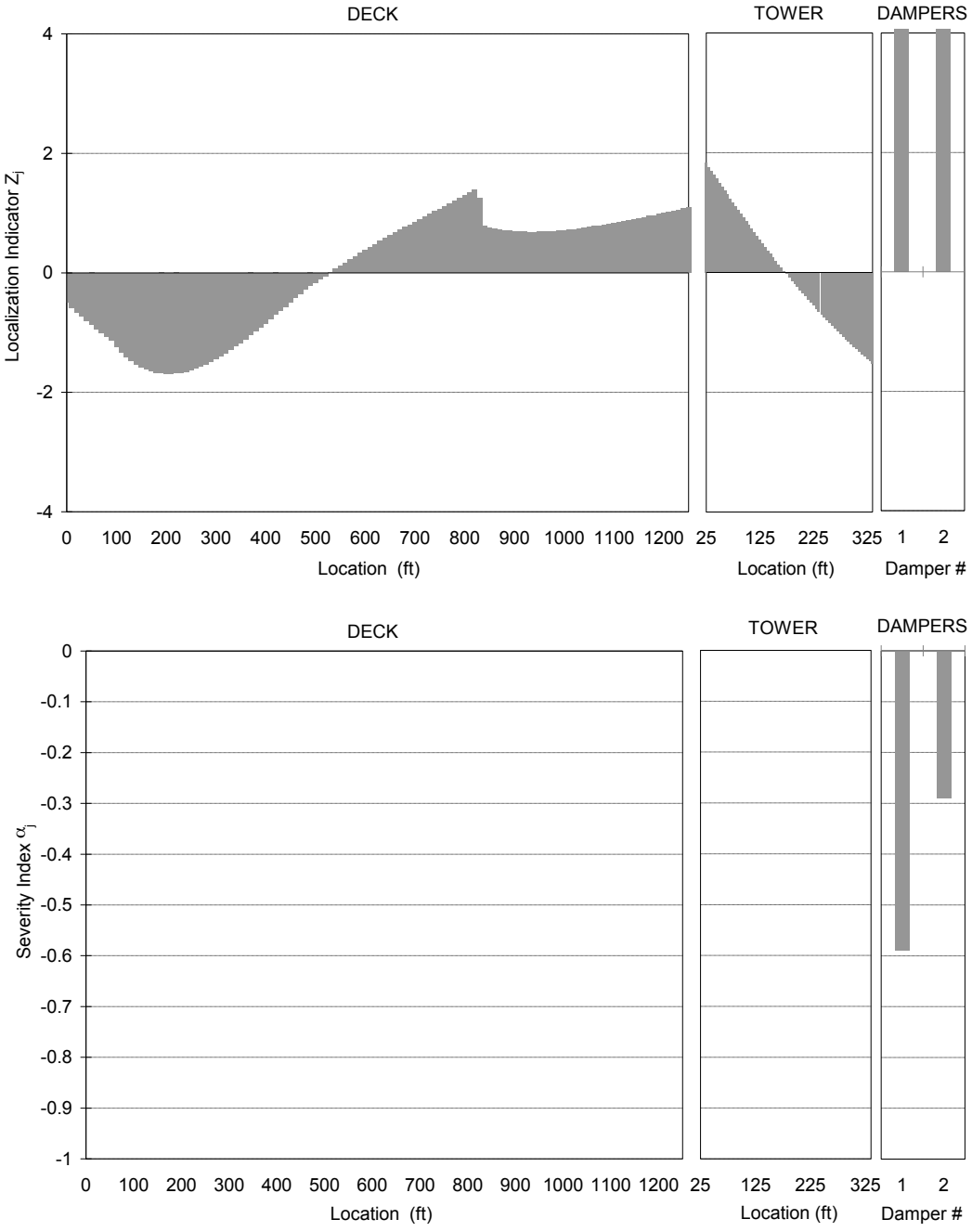

Figure 142. Damage localization indicator and damage severity index – 2011, Jun 21 - 10AM.

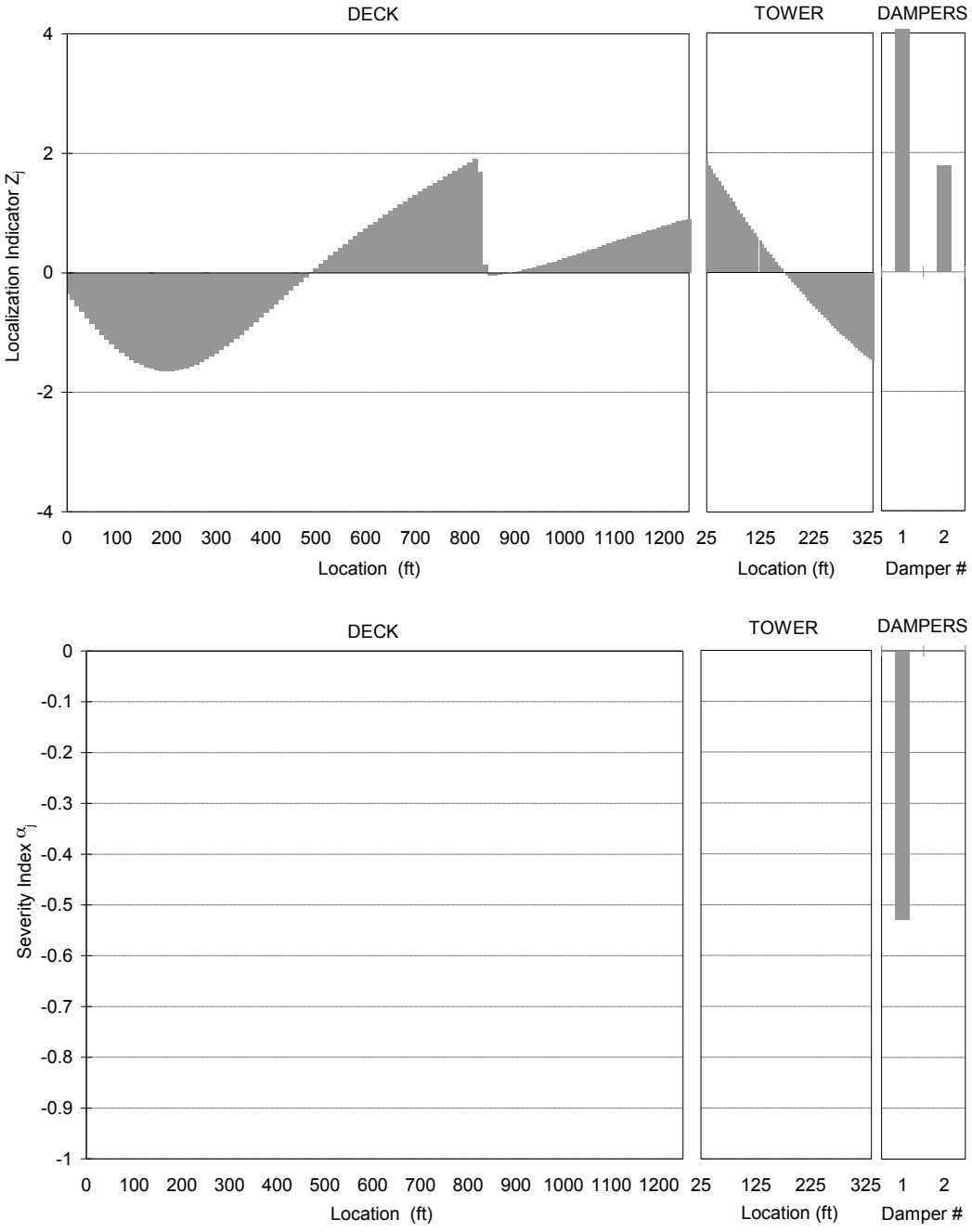

Figure 143. Damage localization indicator and damage severity index – 2011, Jun 21 - 10PM.

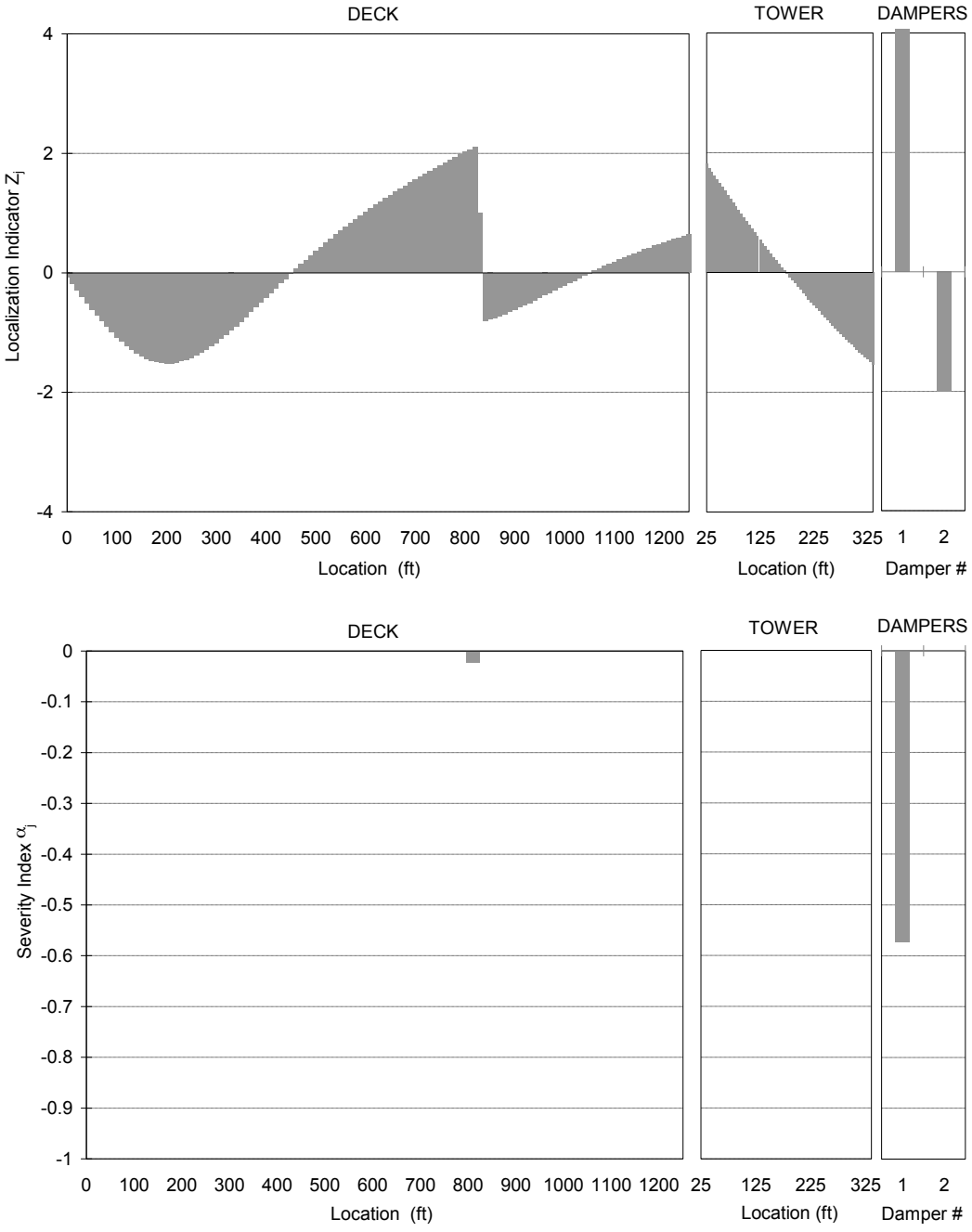

Figure 144. Damage localization indicator and damage severity index – 2011, Jun 28 - 10AM.

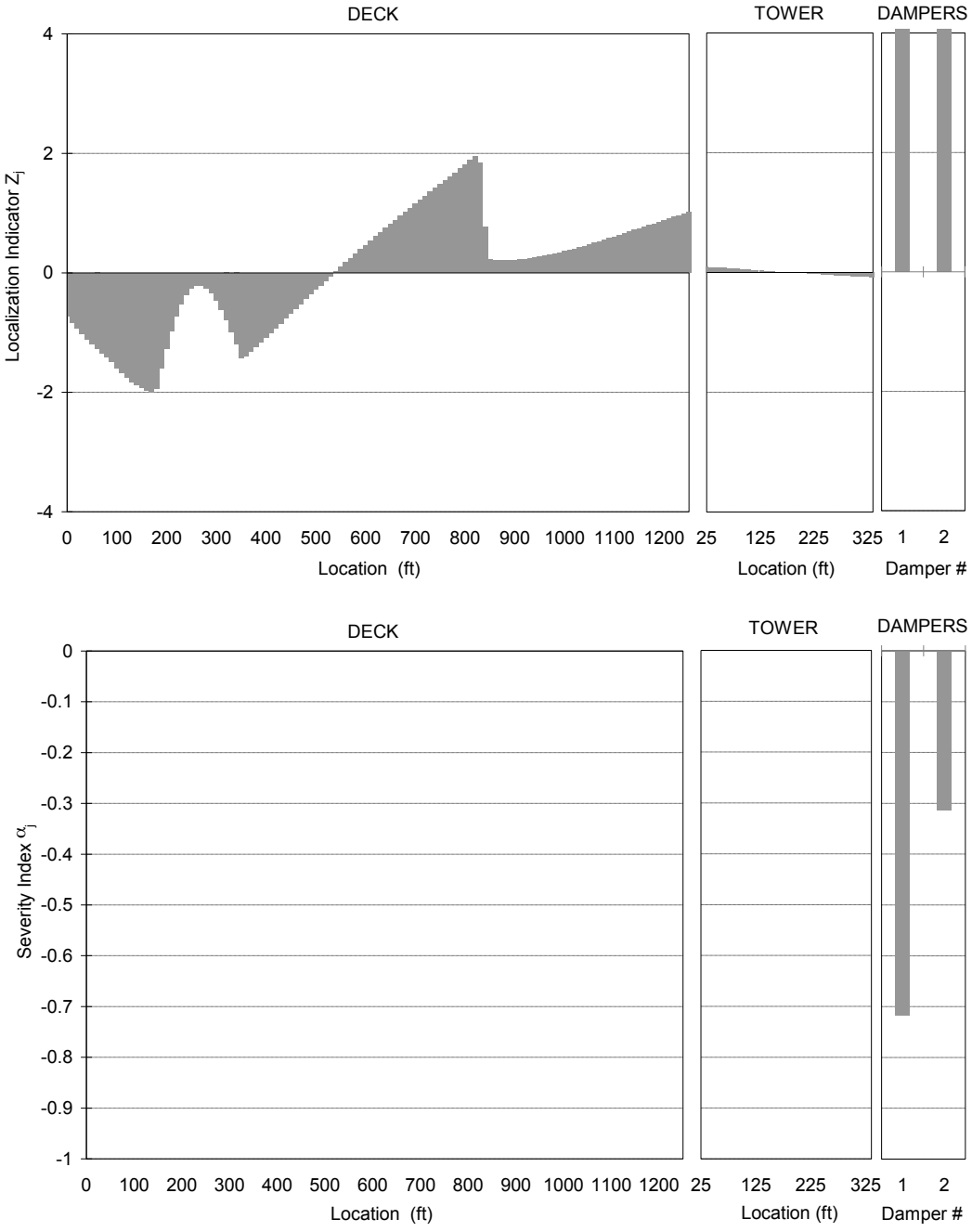

Figure 145. Damage localization indicator and damage severity index – 2011, Jun 28 - 10PM.

In **Figure 146**, the evolution of the damage severity index α of Eq. (7) has been reported for the damper set located between the main span and the west column.

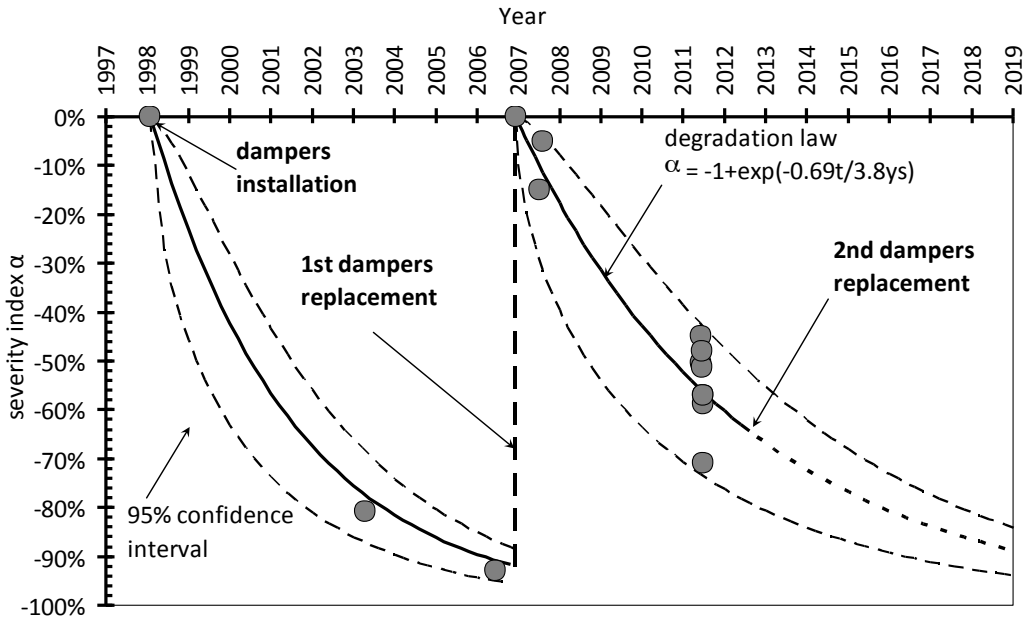

Figure 146. Severity damage index α vs time.

The trend curve of the damage severity index shows a clear deterioration of the dissipative capacity of the damper over the years. A 95% log-normal confidence interval has been added to account for the dispersion of the data. Average severity index values of -13% and -58% were found in 2007 and in 2011, respectively. The dispersion of the severity index values is mainly due to the uncertainty in the structural identification of vibration mode shapes. The damage detection procedure could significantly benefit from improvement in the sensors' distribution. A more systematic data acquisition, to be correlated with environmental effects, would also improve results and reduce the confidence interval associate with the degradation curve presented in **Figure 146**. Based on the available data, an exponential trend was identified for the degradation of the damper performance with time:

$$\alpha(t) = 1 + e^{-\frac{0.69t}{T_{50}}} = 1 + e^{-\frac{0.69t}{3.8ys}} \quad (35)$$

where T_{50} is the period of time that corresponds with a 50% reduction of the damper performance. For the dampers' set under analysis, T_{50} = 3.8 years. It should be noted that the degradation trend appears continuous over time. However, further analyses including more data appear necessary to confirm this result.

6. Practical deployment

The damage detection procedure was implemented in an executable program, which has been named DIIB (Damage Identification on Isolated Bridges). The software allows checking the health status of the bridges with seismic devices based on accelerometric records from sensor networks. A set of records for a given event (ambient vibration or seismic excitation) representative of the current status of the bridge (PRESENT STATE) are compared with a reference scenario (REFERENCE STATE). The reference state could be assumed as a set of data collected from the sensor network in a time frame where the structural components and anti-seismic devices could be considered in optimum conditions, as well as a generic event recorded before the present state. This second approach allows the assessment of possible "relative" performance degradations from previous events.

The conceptual framework behind the software is represented in **Figure 147**. A set of records for a given event

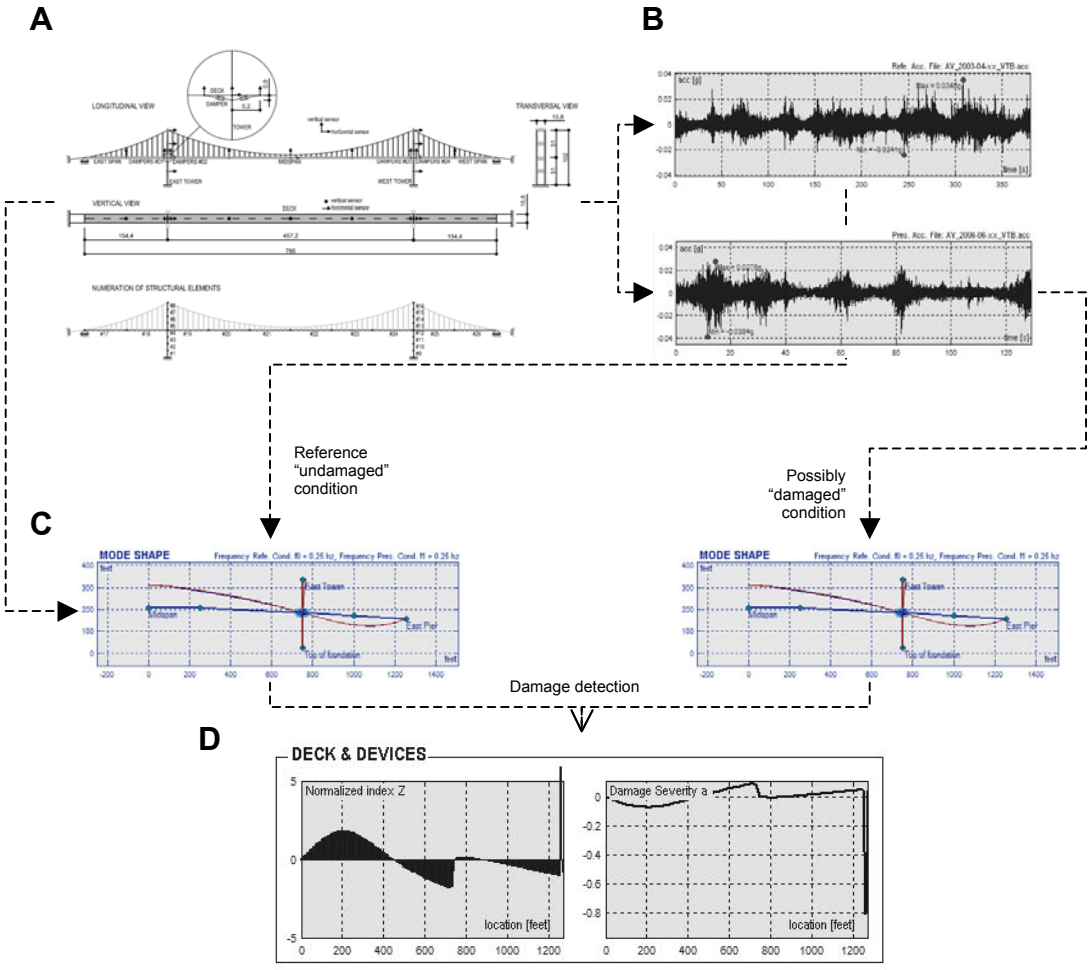

Figure 147. Conceptual framework of the DIIB program: **A** Instrumented bridge; **B** Accelerometric records from the sensor network; **C** Identified modal shapes; **D** Damage localization indicator Z and damage quantification index α.

The software code features a MATHWORKS-MATLAB® graphic user interface (GUI) and a MICROSOFT VISUAL C++ engine. The DIIB software works with two types of input data files: the Bridge Geometry files (containing information on the geometry of the bridge) and the Sensor Data files (containing information on the sensor system and acceleration histories recorded by each sensor). In what follows, a brief description of the data file is given:

The Bridge Geometry files collect nodes, elements, and seismic devices. Locations are specified for each of these items in terms of global coordinates XYZ referred to a conventional reference origin of the coordinate system. A different numbering is used for each of these items. The file includes also tags, associated with relevant nodes of the structure, which can be displayed on the graphical representation of the bridge (e.g. midspan, east tower etc.). Bridge Geometry files have been defined for two Caltrans bridge structures:

1. the Vincent Thomas Bridge (GEOM_VTB file)
2. the Benicia Martinez Bridge (GEOM_BMB file)

The geometry files are accessible on the "Front page" graphical interface in the top-right control panel, through a drop-down list indicated as "bridge structure" (**Figure 148**).

In the same control panel, drop-down lists are also used to upload the –ASCII Sensor Data files. These files contain information about the type of records (Ambient Vibration Acceleration Records or Earthquake Acceleration records), the bridge name, date, measure units (length, time), sensor numbers, sensor directions, nodes of the geometry that corresponds to sensor locations, time and acceleration data (in columns separated by tabs). Two sensor data files need to be uploaded to start the damage analysis of the bridge: one used as a baseline (i.e. reference condition, in which the bridge is supposed undamaged) and one for the condition under investigation (i.e. present condition, in which the bridge is supposed damaged), as shown in the screenshot of **Figure 148**.

A new geometry input file can be created to upload any new bridge geometry in the DIIB program. Any further modification to existing sensor networks (addition of new sensors, modification of existing ones etc.) can be easily implemented in the program through the sensor data files.

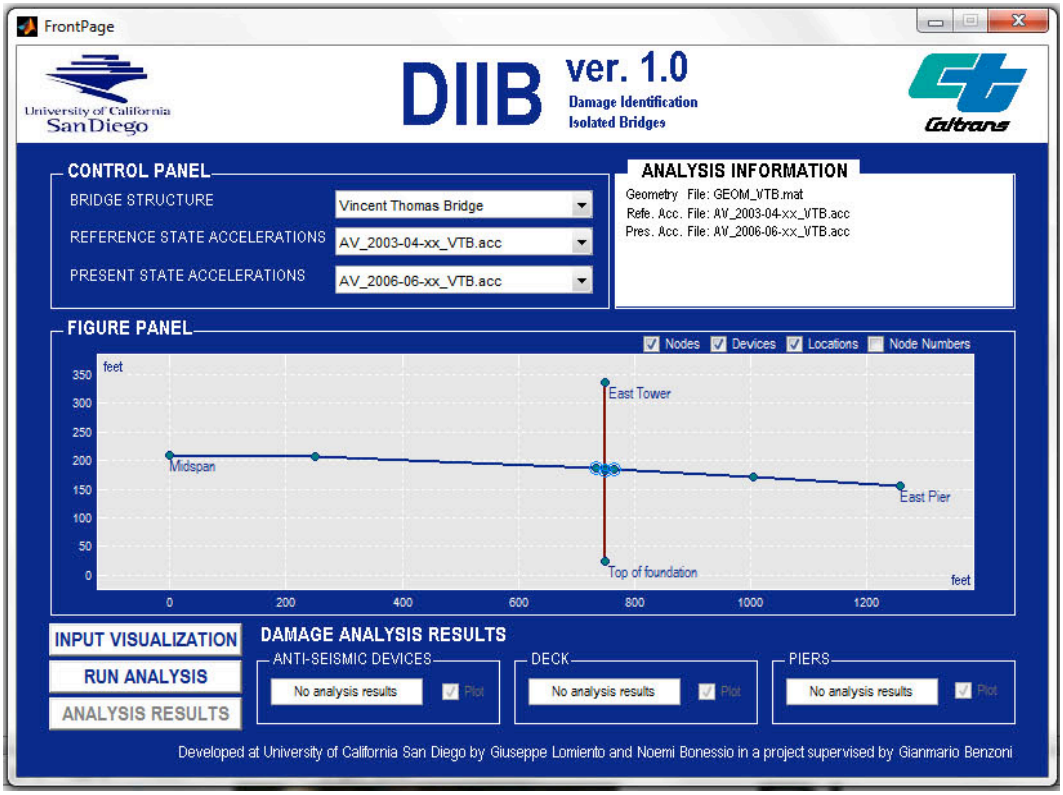

Figure 148. "Front Page" display screen.

The uploaded geometry and data files are shown in the "Analysis information" screen on the top-left side of the graphical interface. The bridge geometry is displayed in the "Figure panel", where check boxes are used to select items to be displayed (i.e. nodes, elements, devices, and tags). Once the geometry and the data files have been uploaded, the "Input visualization" and "Run analysis" buttons are unlocked.

Through the "Input visualization" button, the "input visualization" graphical interface of **Figure 149** is accessible.

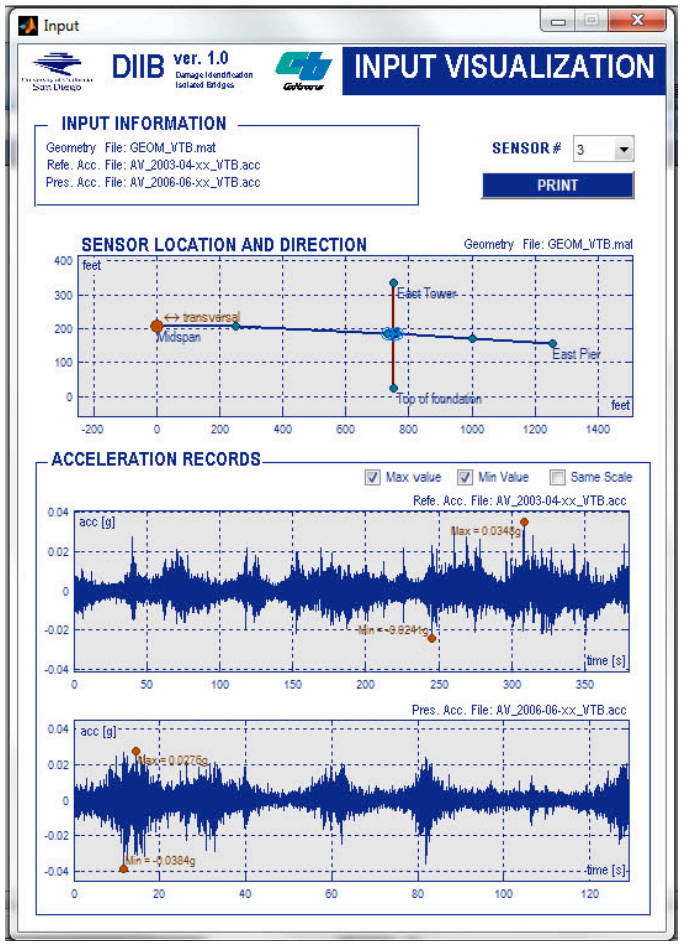

Figure 149. "Input Visualization" display screen.

The Input visualization allows checking the uploaded acceleration data for each sensor. In the "Input Visualization" display screen, accelerometric records are shown for the desired sensor in the reference and present state, together with the localization and the direction of the sensor.

By using the loaded accelerations, the software assesses the modal information of the bridge and compares the modal shapes in order to evaluate the damage indicators Z_j and α_j.

A first visual screening of the results in shown in the "Front Page" display screen, where the number of warning situations are displayed and localized on the bridge, as shown in **Figure 150**. Implementing a request from Caltrans Engineers the front page warning visualization allows an immediate visualization of the occurrence of change in

performance characteristics on structural elements and/or in SRMD devices. A red button is activated in case of detected degradation and the localization of the damage is visualized on the bridge schematic. In Figure 150, for instance, a degradation for a damper at the connection between central span and East tower is detected.

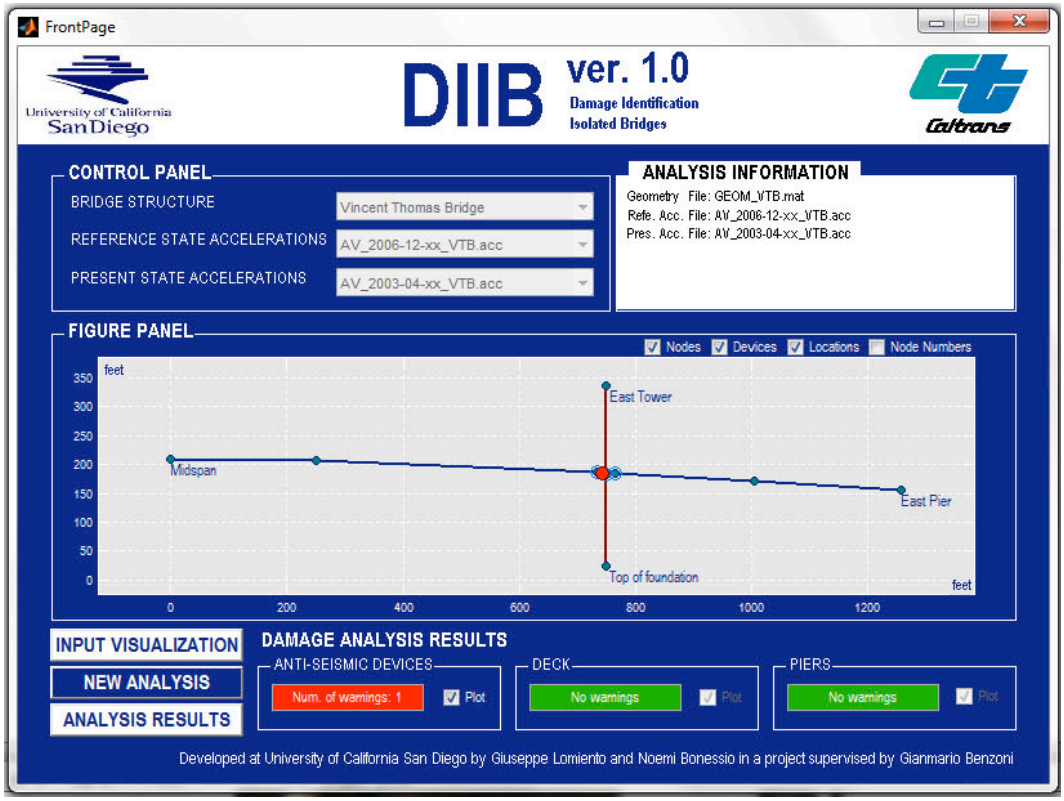

Figure 150. "Front Page" display screen with results.

In case of positive event (red button) more detailed information can be found in the "Analysis Results" display screen of **Figure 151,** where localization index Z_j values along the deck elements, the pier elements and in the devices are plotted together with the quantification index α_j. Mode shapes identified by software and used in the damage assessment can be checked in the "Mode Shapes" display screen (**Figure 152**), together with their frequencies in the reference and present state.

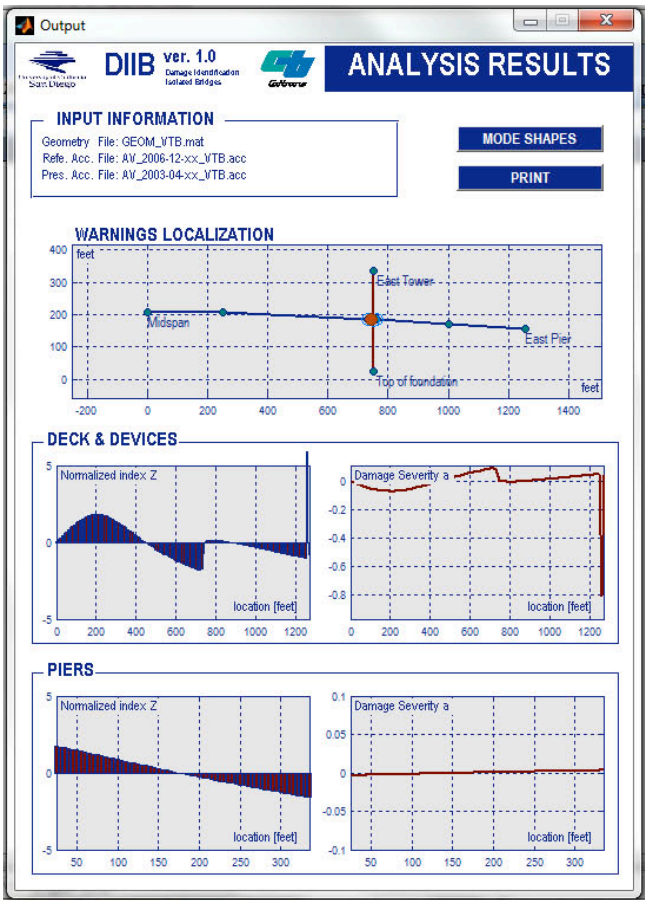

Figure 151. "Analysis Results" display screen.

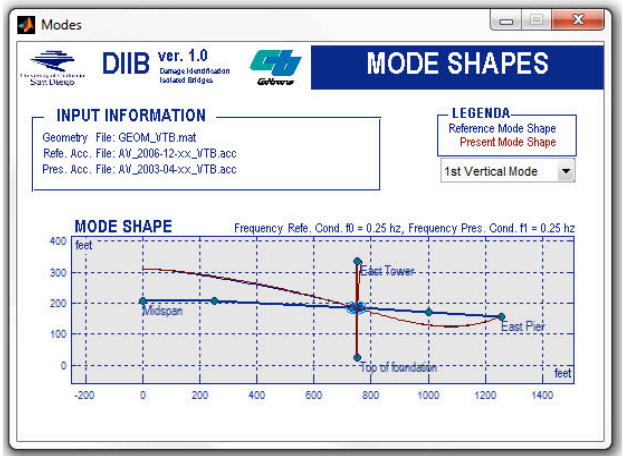

Figure 152. "Mode Shapes" display screen.

Due to the minimum manual intervention needed to execute the damage identification algorithm, the procedure is ready to be implemented in an automatic way. Assuming a set of data recording is available at a given time (reference configuration), the streaming of further data can be temporary stored and can activate a trigger of the algorithm execution. The new set of data can be compared, through a defined interpretative scheme, with the reference signals. The analysis is performed in Matlab in few seconds and could be linked to a mechanism that activates the option to save the new data or discharge them in case no significant response variations are detected. In this sense the procedure allows the continuous monitoring of seismic isolated bridges where the continuous condition does not require a constant streaming of data but a systematic and period activation of the procedure.

6.1. Suggested improvement of existing sensor networks

The DIIB software has been deployed to include the Vincent Thomas Bridge and the Benicia Martinez Bridge, equipped with viscous dampers and Friction Pendulum isolators, respectively. However, in order to take full advantage of the software capabilities improvements to the existing sensor networks on the two bridge structures are needed. Few recommendation are proposed hereafter.

Vincent Thomas bridge: Only a portion of the bridge is monitored by 26 sensors. A couple of sensors appear not functioning as demonstrated by many recordings (#4 for sure, other are randomly performing). The exact location and orientation of the sensors is unknown. Despite these limitations the procedure can be applied to the bridge for both the monitoring of the devices and the structural integrity. The un-symmetric distribution of the sensors however does not allow guaranteeing the absolute location of the "damage" in the devices. The procedure is quite sensitive and precise in the localization phase but a "transfer" of a problem originated in the un-sensored portion of the bridge to another location cannot, at this stage, be excluded. In the proposed extension of the sensor network (see **Figure 153**) the focus was dedicated to the minimum number of accelerometers needed to resolve the above mentioned uncertainty. The proposed sensor network improvements include the installation of 24 additional sensors, and the replacement of malfunctioning accelerometers.

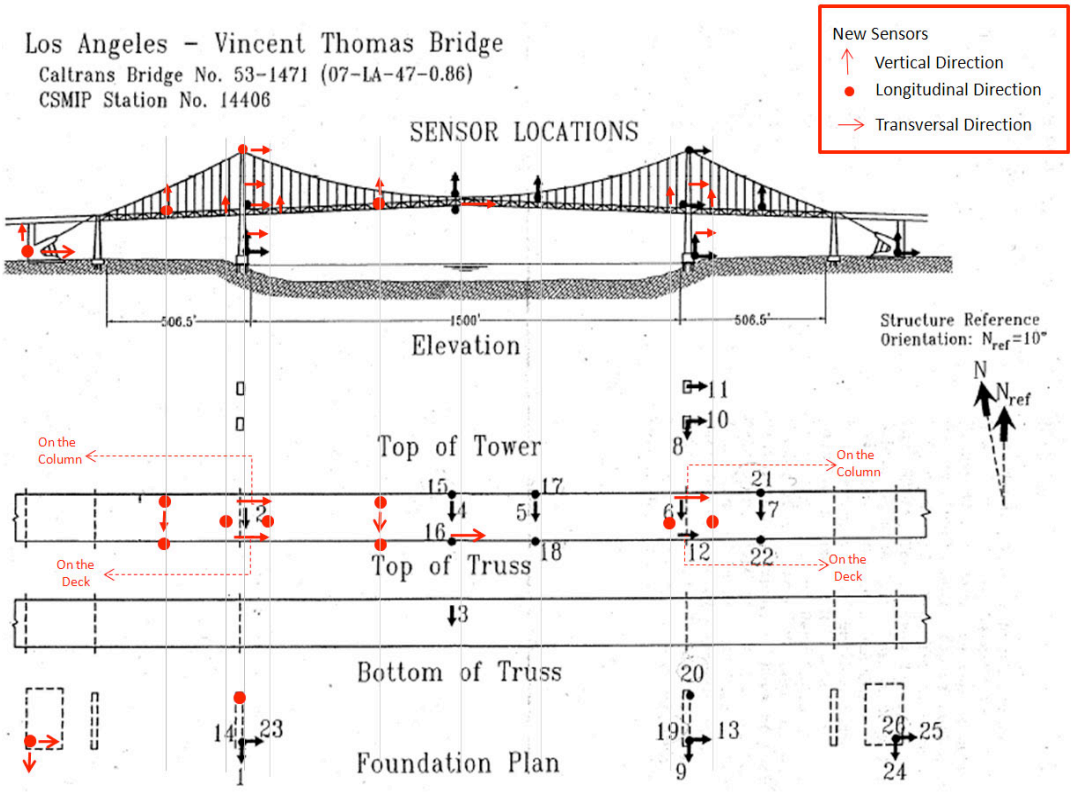

Figure 153. Suggested sensor layout Vincent Thomas Bridge

Benicia-Martinez Bridge. In order to perform a damage detection analysis on the Benicia Martinez Bridge, significant improvements to the sensor network are required. The existing network includes a limited number of accelerometers, which allows detecting critical performance variations of only two sets of seismic isolators (devices on Pier 6 and 12). Three major limitations of this installation are listed below:

1) The piers are not monitored sufficiently to allow the assessment of mode shapes and, as a consequence, the monitoring of their possible degradation.

2) For piers 3,4,5,7,8,9,10 and 11 the lack of sensors across the devices (top of pier and bottom of deck) does not allow to monitor the device performance.

3) The sensors monitoring the vertical motion of the deck are limited.

In **Figure 154** and **Figure 155** three sets of additional sensors are suggested with different colors. Two level of priority are also identified. Sensors included in a black circle are intended for a "high performance configuration" but not of immediate need.

Red dots instead are used to identify the sensors needed to provide monitoring of the devices performance. Blue dots sensors are needed to solve limitation No. 1 (monitoring of piers). Green dots identify sensors that can solve the limitation No. 3 (monitoring of deck). The blue arrows indicates sensors that allow monitoring of the transverse mode of the pier (expected to be less critical that the longitudinal mode). The transverse sensors (red arrows) on piers 4,5, 7, 8, 9 and 10 complete the information across the bearings provided by existing longitudinal accelerometers such as #20, #22, #55 and #57.

The proposed number of additional sensors is here summarized:

1. For SHM of devices: 15 (Red dots)
2. For minimum SHM of bridge and devices: 37 (Red dots+Blue dots+green arrows)
3. For “high performance” SHM (including transverse direction): 73 (all the sensors)

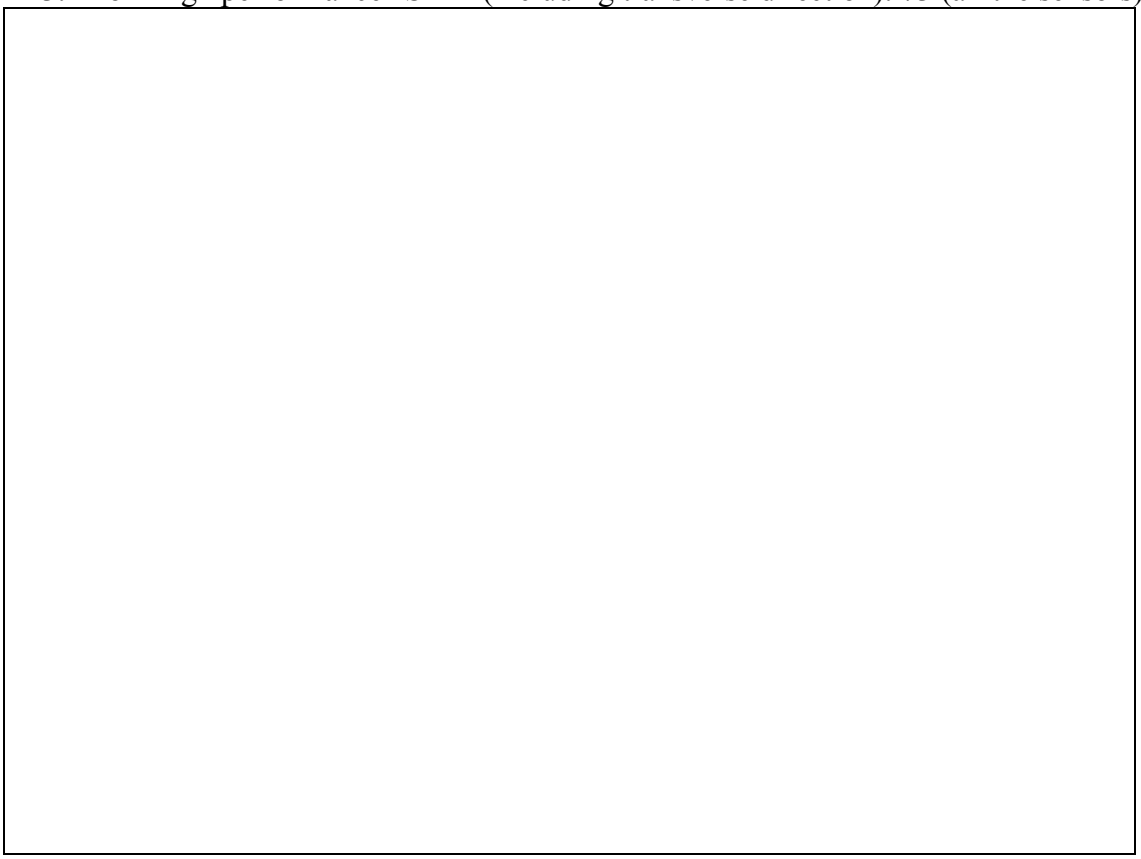

Figure 154. Suggested additional sensors Benicia-Martinez Bridge

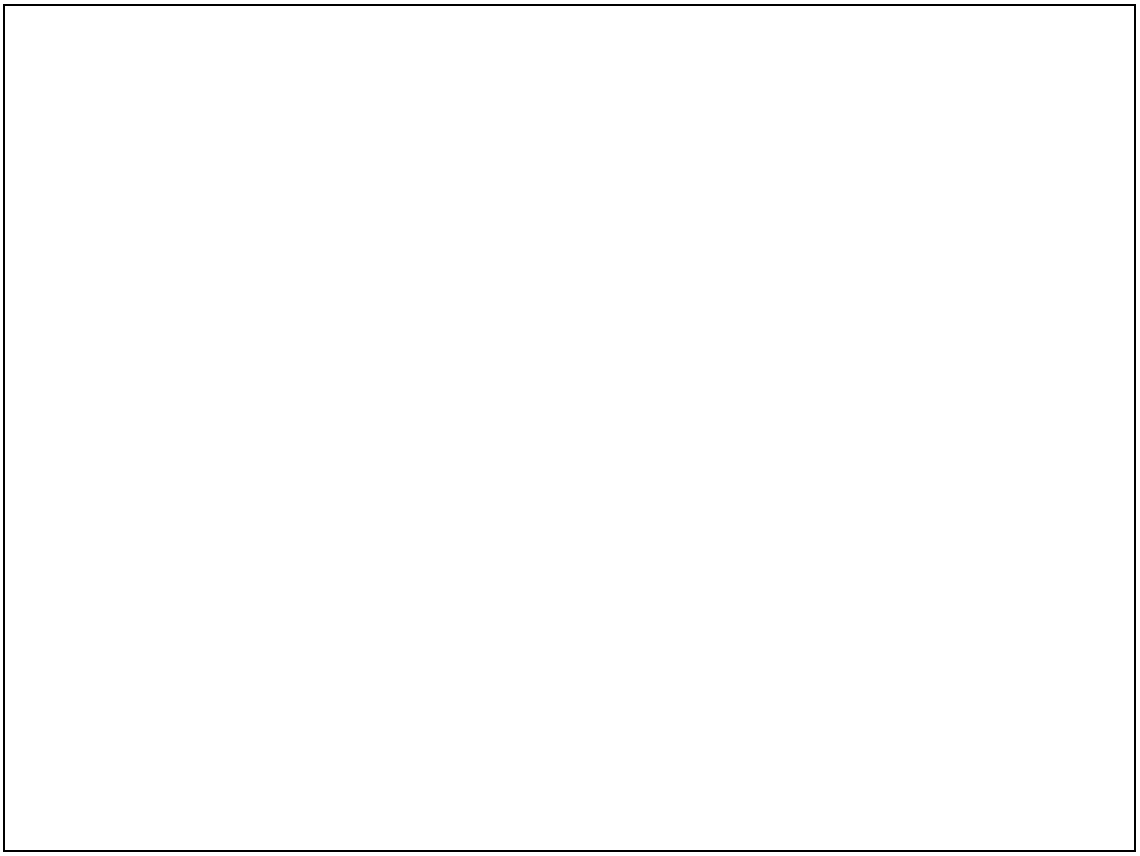

Figure 155. Suggested additional sensors Benicia-Martinez Bridge

7. Conclusion

The monitoring of performance variations of the bridge traditional structural elements as well as of the installed anti-seismic devices is of paramount importance for a comprehensive study of the evolution of the performance of isolated structures.

The complexity of implementation of a SHM procedure required the definition of basic requirements for its validity and potential for in-field deployment.

Among others, a requested main features was the possibility to activate the procedure based on a minimum set of data that allow the assessment of mode shapes. The goal was achieved with the use of optimized modal assessment algorithms tuned with the core of the SHM algorithm and with the numerical implications related to the availability of accelerometric data generally of limited amplitude and duration. The request of simplicity for result interpretation suggested to eliminate any support to the procedure based on F.E. models, used in the present report only for validation purposes. As shown above only a simplified interpretative scheme of the structure is assembled for mainly graphical representation of the results. The procedure is designed with a certain level of modularity that allows to subjectively selected a specific area of the structure of interest. This feature could be useful for damage identification in case a non-complete set of data. In order to respect all the characteristics of a level IV approach to structural health monitoring, the procedure should also be able to indicate the impact of damage on the structure. For this reason is of particular importance the provided mechanism that allows the interpretation of the damage severity index in terms of fundamental performance parameters of the anti-seismic devices as the friction coefficient and the energy dissipation capacity. A companion report, part of this research effort, will provide specific correlations between the device performance changes and the effects on the bridge response.

References

Adina R. & D Inc., (2001), "ADINA (Automatic Dynamic Incremental Nonlinear Analysis)", *Report ARD 019*, Watertown, MA, US.

Aktan, A.E., Catbas, F.N., Grimmelsman, K.A. and Tsikos, C.J. (2000). "Issues in infrastructure health monitoring for management." *Journal of Engineering Mechanics*, 126(7), 711–724.

Aktan, A.E., Farhey, D.N., Helmicki, A.J., Brown, D.L., Hunt, V.J., Lee, K.-L. and Levi, A. (1997). "Structural identification for condition assessment: experimental arts." *Journal of Structural Engineering*, 123(12), 1674–1684.

Alampalli, S. and Fu, G. (1994) "Instrumentation for remote and continuous monitoring of structure conditions. » Transport. Res. Rec. 1432, 59–67.

Almazan J L, De la Llera JC, Inaudi JA. (1998). "Modeling aspects of structures isolated with the friction pendulum system." *Earthquake Eng. Struct. Dyn.*; 27: 845–867.

Bakht, B. and Jaeger, J. G. (1990) "Bridge testing: a surprise every time." *ASCE J. Struct. Eng.* 116, 1370–1383.

Banks, H.T., Inman, D.J., Leo, D.J. and Wang, Y. (1996). "An experimentally validated damage detection theory in smart structures." *Journal of Sound and Vibration*, 191(5), 859–880.

Barai, S. V., and Pandey, P. C. (1997). "Time-delay neural networks in damage detection of railway bridges." *Advances in Engineering Software* 28.1: 1-10.

Benzoni, G. and Seible, F., (1998), "Design of the Caltrans seismic response modification device test System". *Proc. US-Italy Workshop on Seismic Protective System for Bridges* (ed. I.M. Friedland & M.C. Costantinou), pp 173-187.

Benzoni, G. and Seible, F., (2000), "Benicia-Martinez Friction Pendulum bearings-prototype Test Results". *Caltrans SRMD Testing Facility Report, SRMD 2000/4-17*, La Jolla, CA.

Benzoni, G. and Innamorato, D., (2003), “Prototype tests of Sumitomo Co. Dampers Type RDT80 and RDT200”. *Caltrans SRMD Testing Facility Report SRMD 2003/01*, La Jolla, CA, February.

Benzoni, G., Kyler, M. R., Seible, F., (2003), “Richmond-San Rafael, Taylor Dampers Types 1-2 Proof Tests”, *Caltrans SRMD Testing Facility Report, SRMD 2003/05*, La Jolla, Ca, November.

Benzoni G., Casarotti C., (2005), “Continuous Monitoring of Isolated Bridges: Parametric Analysis of the Effects of Damper Characteristics”. *Report SRMD 2005/12*, La Jolla, CA, November.

Benzon,i G., Amaddeo, C., Infanti,S, 2007. “Experimental evaluation of damper performance under simulated damage condition.” *Report SRMD 2007/09*, La Jolla, CA, September.

Biswas, M., A. K. Pandey, and M. M. Samman (1990) "Diagnostic Experimental Spectral/Modal Analysis of a Highway Bridge," *The International Journal of Analytical and Experimental Modal Analysis*, 5, 33-42.

Brincker, R., Andersen, P., and Cantieni, R., (2001). "Identification and level I damage detection of the Z24 highway bridge." *Experimental techniques* 25.6: 51-57.

Brownjohn JMW (2007) “Structural Health Monitoring of Civil Infrastructure.” *Philosophical Transactions of the Royal Society* A, 365 (1851), pp 589-622. ISSN 1471-2946.

Carder, D. S. (1937) “Observed vibrations of bridges”. *Bull. Seismol. Soc. Am.* 27, 267–303.

Cardini, A. J., and De Wolf J. T., (2009). "Long-term structural health monitoring of a multi-girder steel composite bridge using strain data." *Structural Health Monitoring* 8.1: 47-58.

Chang, F.K., 2002. “Ultra reliable and super safe structures for the new century”. *Proceedings of the First European Workshop on Structural Health Monitoring*, Cachan, France, July 10-12, 2002, Lancaster, PA, DEStech Publications, Inc, pp. 3-12.

Computers and Structures, Inc, (2007). “SAP2000, CSI Reference Manual.” Berkeley, California.

Constantinou, M. C., Mokha, A., and Reinhorn A. M. (1990). “Teflon bearings in base isolation II: Modeling.” *J. Struct. Eng*. 116(2): 455–474.

Conte, J., Elgamal, A., El Zarki, M., Fountain, T., Masri, S., Trivedi, M., (2003), “ITR: Collaborative Research: An Integrated Framework for Health Monitoring of Highway Bridges and Civil Infrastructure”. *NSF Annual Report - Activities and Findings 10/02 to 6/03*.

Cross, E., Worden, K., Koo, K. Y., and Brownjohn, J. M. (2011). “Modelling environmental effects on the dynamic characteristics of the Tamar suspension bridge.” *Dynamics of Bridges*, Volume 5 (pp. 21-32). Springer New York.

Doebling, S.W., Farrar, C.R., Prime, M.B. and Shevitz, D.W. (1996). “Damage Identification and Health Monitoring of Structural and Mechanical Systems from Changes in their Vibration Characteristics: A Literature Review.” *Report No. LA-13070-MS*, Los Alamos National Laboratory report, NM (United States).

Doherty, J. E. (1987) “Nondestructive Evaluation,” in *Handbook on Experimental Mechanics*, A. S. Kobayashi Edt., Society for Experimental Mechanics, Chapter 12.

Farrar, C. R., Baker, W. E., Bell, T. M., Cone, K. M., Darling, T. W., Duffey, T. A., and, Migliori, A. (1994). “Dynamic characterization and damage detection in the I-40 bridge over the Rio Grande.” *Report No. LA--12767-MS*, Los Alamos National Lab., NM (United States).

Farrar, C. R., and Cone, K. M. (1995). ‘‘Vibration testing of the I-40 bridge before and after the introduction of damage.’’ *Proc., 13th Int. Modal Anal. Conf., Society of Experimental Mechanics*, Bethel, Conn., 203–209.

Farrar, C., and Jauregui, D. (1996) “Damage detection algorithms applied to experimental modal data from the I-40 Bridge.” *Report No. LA--13074-MS*. Los Alamos National Lab., NM (United States).

Farrar, C. R., and Jauregui D.A. (1999a) "Comparative study of damage identification algorithms applied to a bridge: I. Experiment." *Smart Materials and Structures* 7.5: 704.

Farrar, C. R., and Jauregui D.A. (1999b) "Comparative study of damage identification algorithms applied to a bridge: II. Numerical study." *Smart Materials and Structures* 7.5: 720.

Farrar, C.R. and Doebling, S.W. (1999). "Damage detection II: field applications to large structures". In: Silva, J.M.M. and Maia, N.M.M. (eds.), *Modal Analysis and Testing, Nato Science Series*. Dordrecht, Netherlands: Kluwer Academic Publishers.

Frangopol, D.M. (2003): "New directions and research needs in life-performance and cost of civil infrastructures. Diagnostics & Prognostics to Structural Health Monitoring Management." *Proceedings of the 4th International Workshop on Structural Health Monitoring, Stanford*, CA, September 15-17, 2003, Lancaster, PA, DEStech Publications, Inc, pp. 55-63.

Frangopol D.M. and Liu M. (2007). "Maintenance and management of civil infrastructure based on condition, safety, optimization, and life-cycle cost." *Structure and Infrastructure Engineering: Maintenance, Management, Life-Cycle Design and Performance*, 3:1, 29-41.

Fritzen, C. P., and Bohle K. (1999). "Identification of Damage in Large Scale Structures by Means of Measured FRFs-Procedure and Application to the 140-Highway-Bridge." *Key Engineering Materials* 167: 310-319.

Fu, Y., and DeWolf, J. T. (2001) "Monitoring and analysis of a bridge with partially restrained bearings." *Journal of Bridge Engineering* 6.1: 23-29.

Fujino, Y. (2002) "Vibration, control and monitoring of long-span bridges—recent research, developments and practice in Japan." *Journal of Constructional Steel Research* 58.1: 71-97.

Geier, R. and Wenzel, H. (2002) "Bridge classification based upon ambient vibration monitoring." *Proc. First European conference on structural health monitoring*, Paris, pp. 981–988.

Haritos, N., and Owen., J. S., (2004). "The use of vibration data for damage detection in bridges: a comparison of system identification and pattern recognition approaches." *Structural Health Monitoring* 3.2: 141-163.

Heywood, R. J., Roberts, W., Taylor, R., and Anderson, R. (2000) “Fitness-for-purpose evaluation of bridges using health monitoring technology.” *Transport. Res. Rec*. 1696, 193–201.

Housner, G.W., Bergman, L.A., Caughey, T.K., Chassiakoa, A.G., Claus, R.O., Masri, S.F., Skelton, R.E., Soong, T.T., Spencer, B.F., and Yao, J.T.P. (1997) “Structural Control: Past, Present, and Future”, *ASCE Journal of Engineering Mechanics*, 123[9], pp. 897-971.

Infanti, S., Castellano, M.G., Benzoni, G., (2002), “Non-Linear Viscous Dampers: Testings and Recent Applications”, *ATC-17-2 Seminar on Response Modification Technologies for Performance-Based Seismic Design*, Los Angeles, Ca, May 30-31.

Ingham, T.J., Rodriguez, S., Nader, M., (1997), “Nonlinear analysis of the Vincent Thomas Bridge for seismic retrofit”. *Computer & Structures*, Vol. 64, No. 5/6, pp. 1221-1238.

Jain, B. K. (1991). "Diagnostics Through Experimental Vibration Signature Analysis of Prestressed Concrete Bridges," *International Symposium on Fracture in Steel and Concrete Structures*, 1123-1 136.

Karbhari, V. M., (2005). “Health Monitoring, Damage Prognosis and Service-Life Prediction – Issues Related to Implementation.” Chapter V, *Sensing Issues in Civil Structural Health Monitoring*, ed. F. Ansari, Springer, pp. 301-310, 2005.

Kato, M., and Shimada, S. (1986). “Vibration of PC bridge during failure process.” Journal of Structural Engineering, 112(7), 1692-1703.

Kim J.T. and Stubbs N. (1993). “Assessment of the relative impact of model uncertainty on the accuracy of global nondestructive damage detection in structures”. *Report for New Mexico State University*.

Kim, J.T., Stubbs, N. (2002). “Improved damage identification method based on modal information”. *Journal of Sound and Vibration*; 252(2):223–238.

Kim B.H., Stubbs N., Park T., (2005), “A new method to extract modal parameters using output-only responses”. *Journal of Sound and Vibration* 282, pp. 215-230.

Ko, J. M., Sun, Z. G., and Ni, Y. Q. (2002). “Multi-stage identification scheme for detecting damage in cable-stayed Kap Shui Mun Bridge.” *Engineering Structures*, 24(7), 857-868.

Kullaa, J., (2003). "Damage detection of the Z24 bridge using control charts." *Mechanical Systems and Signal Processing* 17.1: 163-170.

Lee, J. W., Kim, J. D., Yun, C. B., Yi, J. H., & Shim, J. M. (2002). “Health-monitoring method for bridges under ordinary traffic loadings.” *Journal of Sound and Vibration*, 257(2), 247-264.

Li, Z. X., and Chan, T. H. T., (2006). "Fatigue criteria for integrity assessment of long-span steel bridge with health monitoring." *Theoretical and applied fracture mechanics* 46.2: 114-127.

Liang, Z., Lee, G. C. and Kong., F., (1997) "On detection of damage location of bridges." *Proceedings of SPIE, the International Society for Optical Engineering*. Vol. 3089.

Law, S. S., Ward, H. S., Shi, G. B., Chen, R. Z., Waldron, P., & Taylor, C. (1995a). “Dynamic assessment of bridge load-carrying capacities. I.” *Journal of Structural Engineering*, 121(3), 478-487.

Law, S. S., Ward, H. S., Shi, G. B., Chen, R. Z., Waldron, P., & Taylor, C. (1995b). “Dynamic assessment of bridge load-carrying capacities. II.” *Journal of Structural Engineering*, 121(3), 488-495.

Liu, P. L., and Sun, S. J. (2001). "The Health Monitoring of Bridges using Artificial Neural Networks." *Journal of Mechanics* 17.03: 157-166.

Loh, C. H., and Yeh, S. C., (2000). "Application of neural networks to health monitoring of bridge structures." *SPIE's 5th Annual International Symposium on Nondestructive Evaluation and Health Monitoring of Aging Infrastructure*. International Society for Optics and Photonics.

Maeck, J., and De Roeck, G., (1999) "Damage detection on a prestressed concrete bridge and RC beams using dynamic system identification." *Key Engineering Materials* 167: 320-327.

Maeck, J., Peeters, B., and De Roeck, G., (2001). "Damage identification on the Z24 bridge using vibration monitoring." *Smart materials and structures* 10.3: 512.

Mazurek, D. F., and DeWolf, J. T. (1990). “Experimental study of bridge monitoring technique.” J. *Struct. Engrg., ASCE*, 116 (9), 2532–2549.

Mazurek, D. F. (1997) "Modal sensitivity to damage in multigirder bridges." *Proceedings-SPIED the international society for optical engineering*. SPIE international society for optical engineering.

Mevel, L., Goursat, M., and Basseville, M. (2003). "Stochastic subspace-based structural identification and damage detection and localisation—application to the Z24 bridge benchmark." *Mechanical Systems and Signal Processing* 17.1: 143-151.

Nagarajaiah, S., Reinhorn, A. M., Constantinou M. C. (1991). “3D-Basis Non linear Dynamic Analysis of Three Dimensional Base Isolated Structures. Part II.” *Technical Report NCEER-91-0005, National Center for Earth quake Engineering Research*, State University of New York at Buffalo, Buffalo, NY.

Olund, J., & DeWolf, J. (2007). “Passive structural health monitoring of Connecticut’s bridge infrastructure.” *Journal of Infrastructure Systems*, 13(4), 330-339.

Okasha, N. M. and Frangopol, D. M. (2012). “Integration of structural health monitoring in a system performance based life-cycle bridge management framework.” *Structure and Infrastructure Engineering: Maintenance, Management, Life-Cycle Design and Performance*, 8:11, 999-1016.

Pandey, A. K., M. Biswas, and M. M. Samman (1991) "Damage Detection from Changes in Curvature Mode Shapes," *Journal of Sound and Vibration*, 145(2), 32 1-332.

Pandey, A. K. and Biswas, M., (1994). "Damage Detection in Structures using Changes in Flexibility," *Journal of Sound and Vibration*, 169(l), 3- 17.

Pandey, P. C., and Barai, S. V., (1995). "Multilayer perceptron in damage detection of bridge structures." *Computers & Structures* 54.4 (1995): 597-608.

Park, S., Stubbs, N., Bolton, R., Choi, S., and Sikorsky, C. (2001). “Field Verification of the Damage Index Method in a Concrete Box‐Girder Bridge via Visual Inspection.” *Computer Aided Civil and Infrastructure Engineering*, 16(1), 58-70.

Patjawit, A., and Kanok-Nukulchai, W. (2005). "Health monitoring of highway bridges based on a Global Flexibility Index." *Engineering Structures* 27.9: 1385-1391.

Peeters, B., (2000). “System Identification and damage detection in civil engineering.” *Ph.D. thesis Department of Civil Engineering*. K.U. Leuven Belgium.

Raghavendrachar, M. and A. E. Aktan (1992) "Flexibility by Multireference Impact Testing for Bridge Diagnostics," *ASCE Journal of Structural Engineering*, 118, 2 186-2203.

Rytter, A,. (1993), "Vibrational based inspection of civil engineering structure". *PhD dissertation,* University of Aalborg, Denmark.

Salane, H. J., J. W. Baldwin, and R. C. Duffield (1981) "Dynamics Approach for Monitoring Bridge Deterioration," *Transportation Research Record* ,832,2 1-28.

Smyth, A.W., Pei, J.S., Masri, S.F., (2003), "System Identification of the Vincent Thomas suspension bridge using earthquake records". *Earthquake Engineering and Structural Dynamics*, 32, pp. 339-367

Spillman Jr, W. B., Huston, D. R., Fuhr, P. L., & Lord, J. R. (1993). "Neural network damage detection in a bridge element." *Proceedings of the 1993 North American Conference on Smart Structures and Materials* (pp. 288-299). International Society for Optics and Photonics.

Spyrakos, C., Chen, H.L., Stephens, J. and Govindaraj,V., (1990). "Evaluating Structural Deterioration Using Dynamic Response Characterization," *Proceedings of The International Workshop on Intelligent Structures*, Taipei, Taiwan, pp. 137-153.

Stubbs, N. (1985). "A general Theory of non-destructive damage detection in structures." *Proc. Of the 2nd Int. Symposium on Structural Control*, Waterloo, Ontario, Canada; pp. 694-713

Stubbs, N. , Park, S., Choi, S., Sikorsky, C., (2000) A global Non-Destructive Damage Assessment Methodology for Civil Engineering Structures," International Journal of Systems Science, Vol. 31, No 11, pp.1361-1373

Symans, M. D. , and Constantinou, M. C., (1998) "Passive fluid viscous damping systems for seismic energy dissipation." *ISET Journal of Earthquake Technology*, 1998; 35: pp. 185-206.

Tang, J. P. and K.-M. Leu (1991) "Vibration Tests and Damage Detection of P/C Bridges," *Journal of the Chinese Institute of Engineers*, Vol. 14,531-536.

Toksoy, T. and A. E. Aktan (1994) "Bridge-condition Assessment by Modal Flexibility," *Experimental Mechanics*, 27 1-278.

University of Washington, (1954). “Aerodynamic stability of suspension bridges with special reference to the Tacoma Narrows Bridge.” *Bulletin no. 116, University of Washington Engineering Experiment Station*, Seattle, Washington.

Wahab, A. M. M., and De Roeck, G., (1999) "Damage detection in bridges using modal curvatures: application to a real damage scenario." *Journal of Sound and Vibration* 226.2: 217-235.

Wang, M.L., Satpathi, D., Heo, G. (1997). “Damage detection of a model bridge using modal testing”. *Proceedings of the First International Workshop on Structural Health Monitoring, Stanford*, CA, September 18-20, 1997, Lancaster-Basel, Technomic Publishing Co, Inc, pp. 589-600.

Wen YK. (1976) “Method for Random Vibration of Hysteretic Systems.” *Journal of the Engineering Mechanics Division*, ASCE. Vol. 102, No. EM2.

Wong, K. Y. (2003) “Instrumentation and health monitoring of cable-supported bridges.” *Struct. Control Health Monit*. 11, 91–124.

Zayas V, Low S, Mahin SA. “The FPS earthquake resisting system.” *Rep. No. UCB/EERC-87/01, Earthquake Eng. Res. Center*, Univ. of California at Berkeley, Berkeley, Calif. 1987

Zhang, Z. and A. E. Aktan (1995) "The Damage Indices for the Constructed Facilities," *Proceedings of the 13th International Modal Analysis Conference*, 2, 1520- 1529.

Zhao, Z., and Chen, C. (2002). "A fuzzy system for concrete bridge damage diagnosis." Computers & structures 80.7: 629-641.

Zimmerman, D. C. and M. Kaouk (1994) "Structural Damage Detection using a Minimum Rank Update Theory," *Journal of Vibration and Acoustics*, 116, 222-231.